Single-cell characterization of antibody responses in coronavirus infection and COVID-19 vaccination

By

Kevin John Kramer

Dissertation

Submitted to the Faculty of the

Graduate School of Vanderbilt University

in partial fulfillments of the requirements

for the degree of

DOCTOR OF PHILOSOPHY

in

Molecular Pathology & Immunology

September 30th, 2021

Nashville, Tennessee

Approved:

Jeffrey Rathmell, Ph.D.

Borden Lacy, Ph.D.

Jeremy Goettel, Ph.D.

John Wilson, Ph.D.

Ivelin Georgiev, Ph.D.

ACKNOWLEDGEMENTS

First and foremost, I want to thank Dr. Ivelin Georgiev for taking a chance on me as incoming graduate student with very little experience in the field of immunology and more specifically antibodies. Under your guidance, I developed so many technical skills, but I think most importantly you mentored me into an independent scientist. To my committee members Jeff Rathmell, Borden Lacy, Jeremy Goettel, John Wilson, and the late Pierre Massion thank you for all the help and encouragement the past four years.

To the members of the Georgiev lab I will always look back fondly on these years in graduate school and hope to keep life-long friendships with many of you. First to Kelsey Pilewski, also known as lab buddy, who joined the lab the same year I did; I would not be the scientist I am today without your help first year and I will always appreciate our friendship. Andrea Shiakolas our work together helped recover my passion for benchwork and ultimately led to me accepting my dream job. Your kindness and tireless work effort are true inspirations that I plan on carrying with me in my future career. To Lauren Walker, thank you for putting up with me for two plus years sitting next to each other; I always appreciated your sense of humor and your dedication to science. To Nagarajan Raju, your support for all my projects was so instrumental in my success in the lab and I can't thank you enough. To former lab members Allie Greenplate and Ian Setliff, I am so grateful for your examples of thought-provoking scientific discussions and mentorship as a younger graduate student. To Alex Abu-Shmais, Matt Vukovich, Clint Holt, Parker Jamieson, and Steven Wall, it was a pleasure working with you all and helping you onboard into the lab under challenging COVID circumstances and I know you all have a bright future ahead of you. And thank you to Amyn Murji.

Thank you to collaborators that made all the work described in this dissertation a reality. More specifically thank you to Jason McLellan and Daniel Wrapp who first provided us with coronavirus spike constructs and proteins to perform LIBRA-seq as well as Nicole Johnson who

resolved the structure of antibody 54042-4 forming the basis for Chapter III. One of the biggest examples of institutional collaboration resulted in the adapted manuscript in Chapter IV. Thank you to Jeff Rathmell and the Vanderbilt Center for Immunobiology for providing resources to implement a longitudinal, multi-donor study on COVID-19 vaccination. Another special thank you to co-first author Erin Wilfong for drawing donors and assisting with data collection and manuscript writing. Thank you to additional collaborators on this project including Rachel Bonami and Jonathan Irish; this study would not be nearly as impactful without your efforts.

On the more personal side, thank you to my friends who I started graduate school with Clare Laut, Ariana von Lersner, Mike Doyle, Joe Balsamo, Tim Scott, Nate Klopfenstein, Noah Bradley, and Mac Castro. I do not think I make it to my thesis defense without each of you, and I hope that we can continue our friendships as we all move on to the next steps in our careers. Thank you to my sister Katie for always being in my corner for support. Thank you to my brother John and his partner Ashley Harris for putting up with me as a roommate for three years; you all were my rock at times when graduate school was tough, and I'll always be appreciative of our bond moving forward. And finally thank you to my parents Carol and Fred for their unwavering support in everything I do. I would not be in this position earning my Ph.D without your examples of perseverance and dedication.

TABLE OF CONTENTS

Page

LIST OF FIGURES

Figure Page

ABBREVIATIONS

ACE2	Angiotensin converting enzyme 2
BCR	B cell receptor
CD	Cluster of differentiation
CDR	Complementarity determining region
DPP4	Dipeptidyl peptidase 4
ELISA	Enzyme linked immunosorbent assay
Fab	Fragment antigen binding
FACS	Fluorescence activated cell sorting
Fc	Fragment crystallizable
HA	Hemagglutinin
IC_{50}	50% inhibitory concentration
IC_{80}	80% inhibitory concentration
K_D	Dissociation constant
LIBRA-seq	Linking B cell receptor to antigen specificity by sequencing
mAb	Monoclonal antibody
MERS-CoV	Middle eastern respiratory syndrome coronavirus
NGS	Next generation sequencing
PBMC	Peripheral blood mononuclear cells
RNAseq	RNA sequencing
S	Spike
SARS-CoV	Severe acute respiratory syndrome coronavirus
SARS-CoV-2	Severe acute respiratory syndrome coronavirus-2
VH	Variable heavy
VL	Variable light

CHAPTER I

INTRODUCTION

Thesis overview

This dissertation contains my body of primary research focused on the characterization of the human adaptive immune response against coronaviruses, with an emphasis on SARS-CoV-2. In this document, I describe adaptive immunity with an emphasis on the B cell compartment and the role it plays in coronavirus infection and vaccination. One objective of this work was to characterize B cells with reactivity to different pandemic coronavirus strains which can contribute to the development antibody therapeutics as well as rational coronavirus vaccine design. Another goal was to define the changes in healthy, naïve immune repertoires after the vaccination with the first-ever mRNA formulation to counteract COVID-19 infection. A better understanding of both T and B cell subsets elicited by vaccination may provide predictive measures for efficacy and protection against COVID-19 infection but may also translate to other disease indications amenable to mRNA vaccination formulation in the future. To that end, I have divided my dissertation into five chapters to denote different research directions I pursued under the direct mentorship of Dr. Georgiev along with support from numerous Vanderbilt and external collaborators.

In Chapter I, I present fundamental immunology principles behind the adaptive immune response and B cell biology in response to coronavirus infection and vaccination. Chapters II-IV consist of my primary research efforts initially discussed in Chapter I.

Chapter II describes the characterization of cross-reactive coronavirus antibodies isolated from a recovered SARS-CoV donor. I applied LIBRA-seq to a peripheral blood

mononuclear cell (PBMC) sample preserved 12 years after infection onset which resulted in the identification of antibodies with cross-reactivity to spike proteins from both endemic and pandemic coronaviruses. This chapter involved significant effort to adapt the LIBRA-seq workflow to a coronavirus. Experimental analysis included protein labeling quality control, flow cytometric staining, and fluorescence activated cell sorting (FACS) optimization. Additionally, I developed a number of tools to assess these binding profiles including surface display and competition enzyme linked immunosorbent assay (ELISA). External collaborators aided in characterization efforts particularly in Fc effector function and *in vivo* testing of select antibody candidates. A better understanding of the determinants of coronavirus clearance by antibodies may have significant contributions to the design of therapeutic monoclonal antibodies as well as rational vaccine design.

Chapter III is another application of LIBRA-seq, focused on the identification of potent neutralizing antibodies from a recovered COVID-19 individual. I discuss the initial discovery of a panel of neutralizing antibodies with a range of potencies, but the chapter mostly details one candidate, antibody 54042-4, in depth given its potent IC_{50} in a VSV SARS-CoV-2 neutralization assay. Co-first author Nicole Johnson performed cryo-EM to resolve the structural basis for neutralization detailing an epitope footprint on spike that is highly insensitive to mutational selection among currently circulating SARS-CoV-2 lineages. In comparison to other published SARS-CoV-2 antibodies, 54042-4, utilizes an uncommon VH gene and a binding approach to spike protein only shared with a few other antibodies, including two that are under clinical investigation for treating COVID-19 infection. The continual discovery of potently neutralizing SARS-CoV-2 antibodies with different epitope profiles may be critical for therapeutic development in the event of further substitutions that escape from vaccine or therapeutic regimens.

Chapter IV details the application of several different single cell technologies including mass cytometry, single-cell RNA-seq, and LIBRA-seq to characterize the immune response against the Pfizer mRNA BNT162b2 candidate vaccine. From a cohort of 10 healthy individuals, we measured the populations of T and B cells at baseline prior to vaccination and then again 7-10 days post-boost. These paired analyses resulted in the identification of highly enriched T and B cell populations in low abundance prior to mRNA vaccination. I also focus on one donor in depth by performing RNAseq and LIBRA-seq analysis on B cells from longitudinal time points pre-vaccine, day 8, day 14, and day 42. This multiplexed analysis enabled the tracking of evolving B cell subsets into different populations in parallel with the magnitude of antigen specificity, revealing a trend of baseline endemic coronavirus cross-reactivity which transformed into mostly SARS-like antigen-specific repertoire at day 42. In parallel with analysis focusing on single cells, I also measured the serological plasma response from pre-vaccine and post-vaccination which revealed correlations between the frequency of responding T and B cell subsets and with the magnitude of neutralization titer. This collection of work may have a significant impact on the determinants of vaccine efficacy to counteract the COVID-19 pandemic and further provides a comprehensive analysis for the cellular determinants of immunity generated from the first-ever mRNA vaccine formulation to be given to humans at a population level.

Chapter V summarizes the data presented in chapters II-IV. In this section I also discuss some limitations of my work and further propose future research directions to expand on some of the initial observations described in this dissertation. Given the unknown future trajectory of the COVID-19 pandemic, follow-up studies to address further open questions in coronavirus infection and vaccination are critical to the fields of basic and clinical biomedical research.

Adaptive immunity

The human immune response mounted against infection consists of two main arms: the innate immune system and the adaptive immune system (Flajnik and Kasahara, 2010). The innate immune system is initiated by the detection of conserved molecular components shared by a number of different microbial pathogens. These recognition events trigger a quick, targeted response to resolve initial infection which is mediated by innate immune cells such as macrophages, neutrophils, and dendritic cells (Medzhitov and Janeway, 2002). The adaptive immune response in contrast functions by a fundamentally different response mechanism resulting in a recognition recall to pathogens for which a host has previously encountered, also known as immune memory. The adaptive immune response is mediated by two main cell types: T cells and B cells. T cells perform cell-mediated functions whereas B cells function in the humoral immune response (Chaplin, 2010).

Immune memory is generated by extensive genetic diversity enabling the recognition of various pathogens that infect a human host. B and T cells utilize a series of gene recombination events, more generally called V(D)J recombination (Davis and Bjorkman, 1988; Early et al., 2004). The random assembly of Variable (V), diversity (D), and junction (J) genes provides templates for the functional mediators of adaptive immunity immunoglobulins: (Ig) and T cell receptors (TCRs) made by B cells and T cells, respectively. In response to natural infection or vaccination, B and T cells undergo clonal expansion which creates pools of antigen-specific lymphocytes that both counteract a current infection and further develop into memory immune cells to enable a memory-recall response in the event of re-exposure to the same foreign pathogen (Burnet, 1962, 1976). T cells and their role in vaccine-induced immunity will be more thoroughly discussed in Chapter IV, however, the focus of this dissertation is on B cells and their corresponding role in coronavirus infection and vaccination.

Overview of B cell development and antibodies

B cells develop along an extensive hematopoietic cell development scheme producing a steady state of approximately $5e^9$ B cells present in humans (Briney et al., 2019). This number pales in comparison however to the theoretical diversity of the naïve human repertoire of 10^{12} unique antibodies due to gene recombination and further affinity maturation by somatic hypermutation. Recent work detailing ten human naïve antibody repertoires at large sequencing depth suggests the B-cell repertoire may even be as high as 10^{16}-10^{18} unique antibody sequences per individual (Briney et al., 2019).

Antibodies or immunoglobulins secreted by B cells are antigen-binding molecules. Initially membrane bound on the cell surface, immunoglobulins serve as a receptor for antigens also known as the B-cell receptor (BCR) (Blattner and Tucker, 1984). Further B-cell differentiation initiates different surface-bound Ig profiles and antibody secretion by B cells which forms their primary effector role in the arm of adaptive immunity. Antibodies consist of variable and constant domains that each perform different functions. The variable region binds to antigens on pathogens or other molecules while the constant domain recruits other immune cells to promote pathogen clearance through a variety of different mechanisms (Han et al., 1995; Jefferis et al., 1995). The predominant isotype in antibody-mediated immunity is IgG which are “Y” shaped molecules and composed of two heavy chains and two light chains. This orientation enables a bivalent binding mode. The N-terminal end of each heavy and light polypeptide chain form the variable region followed by the beginning of the constant region which spans the rest of the chain until the carboxy-terminus end. This assembly results in the connection of three globular domains: two variable regions and one constant region (Edelman, 1991). Although the general architecture of IgG antibodies is very similar, there is significant variability in amino acid composition in the variable regions thus forming the basis for diverse

molecular recognition and a hallmark of the B-cell repertoire (Saphire et al., 2002). More specifically, the variable region consists of six hypervariable gene segments termed complementary determining regions or CDRs as well as four significantly less variable regions named framework regions. Three CDRs and four framework regions are found in the heavy and light chain of an intact immunoglobulin. The framework regions provide the backbone for the structural basis of IgG, whereas the CDRs orient to the outer edge of the immunoglobulin motif and thus are more implicated in antigen binding (Wu and Kabat, 1970). The contribution of the heavy and light chains in antigen binding allows for significant diversity based on just random gene arrangement and pairing, however B cells can undergo a process called somatic hypermutation in secondary lymphoid organs to increase the affinity of an antibody towards its cognate antigen (McKean et al., 1984). The flexibility enabled by the extensive amino acid variability in the CDRs allows antibodies to adopt theoretically unlimited conformations to bind a specific region of a protein, or an epitope (Davies and Cohen, 1996). Epitopes can be portions of viral coat proteins, polysaccharide cell walls from prokaryotes or less complex soluble proteins.

Coronaviruses

Coronaviruses classify to the *Coronaviridae* family which have positive sense, RNA genomes which span 26-32 kb in length. Despite significant species diversity, coronaviruses share genomic regions critical for survival and host pathogenesis. The 5'-terminal open reading frame 1a/b (ORF1a/b) encodes the proteins replicase polyprotein 1a (pp1a) and pp1ab which are further cleaved into catalytically active non-structural proteins (NSPs) by other genomic elements further downstream papain-like protease (PLpro) and the 3C-like protease (3CL-pro). These NSPs include the essential enzymes RNA-dependent RNA polymerase and helicase which enable viral transcription and replication. Further downstream on the 3' end of the

coronavirus genome are the spike (S), envelope (E), membrane (M), nucleocapsid (N). The E, M, and N structural proteins promote virion assembly within a host cell while S is surface exposed on the coronavirus virion and is thus responsible for host cell engagement. S is divided into the amino-terminal S1 domain and carboxy terminal S2 domain. The S1 domain contains the receptor-binding machinery, namely the receptor binding domain or RBD and the N-terminal domain (NTD). RBD binding to the host cell receptor triggers conformational changes in the S2 domain resulting in cell fusion (Li, 2016; Zumla et al., 2016).

There are seven known coronaviruses to infect humans to date including the endemic viruses HCoV-OC43, HCoV-HKU1, HCoV-NL63, HCoV-229E, as well as the pandemic viruses SARS-CoV, Middle East Respiratory Syndrome coronavirus (MERS-CoV), and SARS-CoV-2 (Chan et al., 2015; Lu et al., 2020). With the exception of HCoV-NL63 and HCoV-229E which are alpha coronaviruses, all other human coronaviruses belong to the beta genus. Endemic coronavirus infections occur on an annual basis resulting in mild clinical illness mostly consistent with symptoms of the common cold (Huang et al., 2020; Pfefferle et al., 2009; Pyrc et al., 2006; Vijgen et al., 2006; Woo et al., 2005). SARS-CoV was the first known pandemic coronavirus to emerge in 2002 resulting in 8439 reported cases and 812 fatalities (Kuiken et al., 2003). The second coronavirus outbreak to achieve pandemic status in 2012, MERS-CoV, resulted in a morality rate of almost 35% (Ramadan and Shaib, 2019). Rare cases of MERS-CoV are still diagnosed each year, although its potential for global spread is limited (Chan et al., 2015). The third coronavirus which eventually developed into a worldwide pandemic, SARS-CoV-2, was detected in December 2019 and continues to circulate among the global population as of this writing (Lu et al., 2020).

The pathogenicity of coronaviruses is highly dependent on the host cell receptor which results in differential tissue tropism and host species reservoirs. For example, the pathogenic SARS-CoV and SARS-CoV-2 viruses share the receptor angiotensin converting enzyme 2

(ACE2) with the annually circulating alpha endemic coronavirus HCoV-NL63 (Wrapp et al., 2020). Other human coronaviruses utilize a spectrum of host cell receptors: MERS-CoV which uses dipeptidyl peptidase 4 (DPP4), aminopeptidase N used by HCoV-229E, and *O*-acetylated sialic acid (utilized by HCoV-OC43 and HCoV-HKU1)(Chan et al., 2015). After cell fusion, coronaviruses enter host cells with the help of endosomal cysteine protease cathepsins and other host proteases such as transmembrane protease serine 2 (TMPRSS2) and TMPRSS11D for the endosomal and cell surface non-endosomal pathways, respectively. Inside the host cell, coronaviruses disassemble and release nucleocapsid and viral RNA into the cytoplasm where ORF1a/b is translated into the proteins pp1a and pp1b and genomic RNA undergoes replication. Non-structural proteins generated from pp1 protein cleavage then assemble to form the replication-transcription complex. From this complex, subgenomic mRNA molecules are synthesized and translated into the structural proteins critical for coronavirus replication and virion formation. After assembly, the virion is transported to the extracellular space through the exocytosis pathway and the cycle is further repeated (Zumla et al., 2016).

Anti-viral antibody mechanisms

B cells and their secreted antibodies can play a variety of roles in the context of coronavirus infection. As a part of the maturation process, B cells in response to different stimuli undergo class-switching which fuses a different constant region domain to the variable region, augmenting cellular function (Jefferis et al., 1995; Sakano et al., 1980). IgM plays a critical role in the early immune response thanks to its pentameric structure and resulting avidity which increases the capture of antigens. After initial response to antigen, IgM B cells traffic to secondary lymphoid organs where they undergo class-switching and affinity maturation by somatic hypermutation which increases the affinity for its cognate antigen (McKean et al., 1984). IgA, a class-switched antibody isotype, plays a significant role in respiratory infections, such as

COVID-19, serving as early responding B cells in mucosal surfaces, where host cell entry occurs through the respiratory tract (Favre et al., 2005). Class-switched IgG is the predominant isotype in circulation and plays an integral role in viral clearance. In the context of SARS-CoV-2, IgG can block viral entry into host cells either by directly or indirectly antagonizing interaction of SARS-CoV-2 spike and angiotensin converting enzyme 2 (ACE2) interaction (Jiang et al., 2020). Antibodies that block viral entry into host cells are known as neutralizing antibodies, and additionally are the focus of monoclonal antibody discovery efforts to combat COVID-19 infection (Brouwer et al., 2020; Pinto et al., 2020; Rogers et al., 2020; Wec et al., 2020b; Zost et al., 2020b). In addition to neutralization, antibodies can also perform other functions such as opsonization and Fc effector functions. These functions include the recruitment of other immune cells to promote viral clearance and are an example of the connection between the adaptive and innate immune response. Antibody dependent cellular phagocytosis (ADCP) functions in the recruitment of macrophages to engulf foreign pathogens such as a virion and stimulate other immune cells such as CD8 T cells (Bournazos et al., 2020; Bournazos et al., 2019). Antibody dependent cellular cytotoxicity or ADCC is another Fc effector function that mobilizes NK cells to bind opsonized cells or virions and release a cytotoxic payload to lyse the targeted cell or virus (Bournazos et al., 2020; Lu et al., 2018). Another function antibodies perform by their Fc domain is complement dependent cytotoxicity. This process initiates the complement cascade with the terminal step producing a membrane attack complex, puncturing an infected cell or virion promoting viral clearance (Lu et al., 2018; van Erp et al., 2019).

Similar to antibodies elicited by natural infection or vaccination, monoclonal antibody candidates are designed to neutralize virus and additionally recruit other immune cells (Chen et al., 2021b; Hansen et al., 2020). Recent evidence supporting the importance of Fc effector functions is demonstrated particularly in the context of therapeutic monoclonal antibody

administration, where the abolishment of Fc effector function significantly decreases survival benefit to animals in a murine infection model (Winkler et al., 2021).

Human antibody response against coronaviruses

Although coronaviruses encode a number of different proteins to replicate in a host, the main target of the human immune system is the spike protein. Decorating the surface of virions, spike is also the sole target of neutralizing antibodies (Jiang et al., 2020). The predominant neutralizing epitope on spike is the receptor binding domain, although a collection of antibodies have been discovered against the NTD (Suryadevara et al., 2021). Virus neutralization is predominantly mediated by antagonism with its host cell receptor. In the context of SARS-CoV and SARS-CoV-2 that is inhibition of binding to ACE2 (Jiang et al., 2020), whereas in MERS-CoV, it is the disruption of interaction with its receptor dipeptidyl peptidase 4 (DPP4) (Chan et al., 2015). The kinetics of the immune response against SARS-CoV-2 is well-documented. Studies report recovered individuals maintaining neutralizing antibody titer as long as a year out, although continued longitudinal studies are needed to better understand SARS-CoV-2 immunity. Neutralizing antibody responses typically peak at 3-5 weeks post infection (Roltgen et al., 2020), however, these levels commonly decay with studies reporting 70 and 90 day half-lives (Dan et al., 2021; Iyer et al., 2020; Wheatley et al., 2021). Importantly, studies of immune memory have shown SARS-CoV-2 RBD reactive memory B cells to increase in frequency among a recovered COVID-19 cohort as far as 8 months post infection (Dan et al., 2021). In agreement with this report, longer term studies up to one year post infection show durable neutralization titer and the maintenance of SARS-CoV-2 memory B cells (Wang et al., 2021b).

The human immune response against the endemic circulating variants HCoV-OC43, HCoV-HKU1, HCoV-229E, and HCoV-NL63 is not as well understood because symptomatic

individuals present with only mild clinical symptoms and thus have not posed a significant public health threat. Evidence for cross-reactivity and the influence of existing coronavirus immunity especially in relation to SARS-CoV-2 immunity is developing space of research. In support of a protective role in heterologous immunity a longitudinal study in newborn infants reported that acute HCoV-NL63 infection provides short term immunity against the related human alpha coronavirus HCoV-229E. Interestingly, HCoV-229E infection did not elicit the same pattern of immunity when tested against HCoV-NL63 (Dijkman et al., 2008). Another study reported seroconversion against HCoV-HKU1 often occurred prior to HCoV-OC43, but rarely after, suggesting infection with the prior confers immunity against the latter (Dijkman et al., 2012). Studies detailing higher cross-reactive coronavirus responses in younger individuals suggest that this phenomenon may be responsible for the lower incidence in COVID-19 cases and correspondingly lower disease severity, however, these observations need to be further investigated (Ng et al., 2020). Further, the correlation of IgG and IgA responses to endemic coronaviruses and corresponding response to SARS-CoV-2 in uninfected children, adolescents and adults points to a beneficial role of pre-existing coronavirus immunity particularly in response to a novel pandemic coronavirus (Ng et al., 2020). Consistent with this notion, pre-existing immunity to HCoV-OC43 significantly correlated with survival from COVID-19 infection. The higher sequence homology in the S2 domain between endemic coronaviruses and SARS-CoV-2, compared to the S1 subunit which mediates cell entry, may therefore stimulate a resting pool of memory B cells that can mount a response against a novel coronavirus more quickly (Kaplonek et al., 2021a). In contrast to studies reporting a survival benefit, an elaborate investigation of pre-existing coronavirus immunity in individuals prior to contracting SARS-CoV-2 revealed an increase in serological titer against the endemic beta coronavirus HCoV-OC43 and not against the more distantly related alpha coronaviruses HCoV-229E and HCoV-NL63. The increase in titer against a heterologous coronavirus or the magnitude of seropositivity

before infection, however, did not correlate with any survival advantage against COVID-19 (Anderson et al., 2021).

The emergence of SARS-CoV-2 variants of concerns (VOCs) poses another consideration for the plasticity of the human immune response to a mutating pathogen. Numerous divergent lineages have arisen across the globe, denoted as alpha, beta, gamma, and delta according to World Health Organization nomenclature (Hoffmann et al., 2021; McCallum et al., 2021; Wang et al., 2021a). The most troubling substitutions reside in the receptor binding domain, most notably N501Y and E484K/Q, and L452R. Current data support that these variants are more transmissible, rather than more lethal however there are detectable reductions in neutralizing antibody titer among individuals surviving infection suggesting that previous exposure to a wild-type strain may not permit as strong of an immune response against circulating VOCs (Chen et al., 2021c; McCallum et al., 2021; Wang et al., 2021a). Geographic areas with high SARS-CoV-2 vaccination rates do not appear to be at high risk for these variants, however, the rampant infection rates in poorly vaccinated populations highlights the need to continue genomic surveillance and continually monitor vaccine- and infection-induced human immune responses, particularly against circulating VOCs (Lopez Bernal et al., 2021).

COVID-19 vaccine immune responses

The development of vaccines to counteract SARS-CoV-2 and COVID-19 infection was achieved at an unprecedented speed. The first candidates to reach emergency use authorization (EUA) by the Federal Drug Administration (FDA) were both mRNA formulations of the pre-fusion stabilized SARS-CoV-2 spike protein (Baden et al., 2021; Frenck et al., 2021; Polack et al., 2020; Wrapp et al., 2020). Additional vaccine candidates including adenovirus formulations from Johnson & Johnson (Sadoff et al., 2021b) and Astra Zeneca (Voysey et al.,

2021) have also been approved across different parts of the world, albeit at lower rates of effectiveness (Madhi et al., 2021; Sadoff et al., 2021b). Early phase clinical trials for the Moderna mRNA-1273 and Pfizer BNT162b2 vaccines showed a robust cellular and antibody response with kinetics consistent with historical vaccination schemes (Frenck et al., 2021; Polack et al., 2020) along with tolerable safety profiles. EUA for a number of different formulations has resulted in a large-scale vaccination effort most notably in the U.S. with varied rates across the globe (Dagan et al., 2021; Madhi et al., 2021; Sadoff et al., 2021b).

Inoculation with BNT162b2 vaccine stimulates a robust response from the adaptive immune system. In a two-dose scheme spaced 21 days apart, SARS-CoV-2 IgG titer develops to approximately half-maximal at day 21, which peaks at day 28 (Walsh et al., 2020). Serological neutralization follows similar kinetics with titer developing at day 21, which declines slightly when measured at 85 days post-vaccination (Sahin et al., 2021). The development of COVID-19 immunity from the mRNA-1273 formulation follows a similar time course for the development of IgG and neutralization titers (Baden et al., 2021). More extended longitudinal analysis has importantly shown that neutralization is still maintained as far out as day 119 in adolescent, adult, and elderly patient cohorts (Widge et al., 2021). SARS-CoV-2 specific CD4 and CD8 T cells are also elicited in a majority of vaccinees. In the BNT162b2 formulation, CD4 T cells exhibited high expression of IFN-γ and IL-2 while SARS-CoV-2 peptide specific CD8 T cells displayed co-expression of CD27 and CD28, suggesting a surface cell expression phenotype amenable for response to infection (Sahin et al., 2021). Recent studies investigating the B cell memory response elicited against vaccination interestingly report a plateau of antigen-specific memory B cells after just one injection (Goel et al., 2021). This observation supports the vaccination design of the Johnson & Johnson candidate which only requires one injection however, levels of protection have been shown to be approximately 30% lower in effectiveness in comparison to BNT162b2 and mRNA-1273 (Sadoff et al., 2021a).

Given the currently EUA vaccine candidates were designed against the original circulating strain, Wuhan-1, studies have focused on the effectiveness of vaccines against the circulating VOCs. Similar to the reduction of neutralizer titer in convalescent individuals, vaccine-induced neutralization titer is diminished against the alpha, beta, gamma, delta, and epsilon variants (Collier et al., 2021; McCallum et al., 2021; Wang et al., 2021a). To address these deficiencies and the emerging breakthrough infections in vaccinated individuals (Hacisuleyman et al., 2021), next-generation vaccines designed with the substitutions in current VOCs are currently under investigation in clinical trials in the event of booster shots becoming necessary to maintain immunity to the mutated lineages of SARS-CoV-2 at a population level (Clinical Trial #NCT04713553). Although cell-mediated immunity is against VOCs is not as well-studied as the antibody response, importantly T cell epitopes mapped by MHC multimers are found to target peptide residues conserved among VOCs in vaccinated individuals (Sahin et al., 2021).

Single cell technologies

The size and sheer diversity of the antibody repertoire makes comprehensive characterization a significant challenge. Traditional approaches to probe antigen-specific B cells capture only a fraction of the total repertoire and thus may not fully represent the B cell response mounted against infection. Techniques such as antigen-specific B cell sorting (Scheid et al., 2009; Wu et al., 2010), immortalized B cell screens (Stiegler et al., 2001), and B cell culture (Bonsignori et al., 2018) are low in throughput and are commonly limited to screening single antigen specificities. The advent of Next Generation Sequencing (NGS) has helped the advance the level of throughput, albeit with the limitations of heavy and light chain pairing and lack of functional information. Furthermore, NGS-based approaches require the labor-intensive process of recombinant gene synthesis, expression, purification, and characterization of hundreds of antibodies only to result in a select number of lead candidates. To address these

limitations, the Georgiev lab developed a technology that enables the simultaneous recovery of paired heavy and light chain sequences with an associated antigen specificity readout (Setliff et al., 2019a). The technology, LIBRA-seq, or Linking B cell Receptor to Antigen Specificity by Sequencing, is analogous to antigen-specific B cell sorting with the added component of oligo-labeled antigen probes. Antigen-specific B cells are enriched by fluorescence activated cell sorting (FACS) which are further generated into cDNA libraries using the 10X Chromium single cell V(D)J profiling kit. After bioinformatic processing LIBRA-seq yields a set of up to tens of thousands B cells each associated with its paired heavy and light chain sequence as well as a LIBRA-seq score, a product of a Z-score transformation of the incorporated oligos bound to antigens that were captured with single cell processing. This approach to antibody discovery allows for expedited lead generation selection compared to previous workflows that require the antibody transfection and purification process of up to thousands of antibodies only resulting in the identification of a small set of lead molecules. The application of LIBRA-seq to recovered coronavirus donors as well as longitudinal SARS-CoV-2 vaccination samples forms the basis of this dissertation.

CHAPTER II

CROSS-REACTIVE CORONAVIRUS ANTIBODIES WITH DIVERSE EPITOPE SPECIFICITIES AND FC EFFECTOR FUNCTIONS

This chapter is adapted from the published manuscript:

Shiakolas AR*, **Kramer KJ*** et al. Cross-reactive coronavirus antibodies with diverse epitope specificities and fc effector functions. *Cell Reports Medicine*. 2021. (*equal contributions)

Contributions: Daniel Wrapp provided initial proteins for LIBRA-seq screen, Simone Richardson and Nelia Manamela performed Fc effector function assays, Alexandra Schafer performed *in vivo* murine prophylaxis models, Steven Wall expressed, purified and characterized initial lead candidate antibodies, Nianshuang Wang provided support with initial spike protein constructs, Kataryzna Janowska characterized quantitative antibody binding by SPR, Kelsey Pilewski tested lead candidate antibodies in mannose competition assays, Rohit Venkat and Nagarajan Raju contributed bioinformatic sequencing data support, Robert Parks tested candidate antibodies in auto-reactivity assays, Emilee Friedman Fechter expressed and purified candidate antibodies, Clinton Holt provided support in resolving computational epitopes across spike proteins, Naveen Suryadevara performed ACE2 inhibition assays, Rita Chen tested antibodies in RTCA SARS-CoV-2 neutralization screens, David Martinez tested antibodies in authentic SARS-CoV-2, SARS-CoV, and MERS-CoV neutralization assays, Rachel Nargi and Rachel Sutton performed high-throughput expression and purification assays of lead candidate antibodies. Julia Ledgerwood and Barney Graham generously provided PBMCs from which the cross-reactive antibodies were derived from. Andrea Shiakolas performed competition assays, ELISAs, as well as cell-surface display assays. I expressed and purified recombinant proteins, and performed ELISAs. Andrea Shiakolas, Ivelin Georgiev, and I wrote the manuscript.

INTRODUCTION

The emergence of a novel coronavirus (CoV) SARS-CoV-2, the causative agent of COVID-19, has resulted in a worldwide pandemic, threatening the lives of billions and imposing an immense burden on healthcare systems and the global economy. SARS-CoV-2, the seventh coronavirus known to infect humans, is a member of the *Betacoronavirus* genus which includes the highly pathogenic SARS-CoV and MERS-CoV, as well as endemic variants HCoV-OC43 and HCoV-HKU1 (Lu et al., 2020). Recent coronavirus outbreaks and the threat of future emerging zoonotic strains highlight the need for broadly applicable coronavirus therapeutic interventions and vaccine design approaches (Graham and Baric, 2010).

Coronaviruses utilize the homotrimeric Spike (S) protein to engage with cell-surface receptors and enter host cells. S consists of two functional subunits: S1 and S2. S1 facilitates attachment to target cells and is composed of the N-terminal domain (NTD) and the receptor-binding domain (RBD), whereas S2, which encodes the fusion peptide and heptad repeats, promotes viral fusion(Bosch et al., 2003; Tortorici and Veesler, 2019). To facilitate cell entry, human coronaviruses employ different host factors; however, SARS-CoV and SARS-CoV-2 both utilize the cell-surface receptor angiotensin converting enzyme 2 (ACE2) (Wrapp et al., 2020). Additionally, SARS-CoV-2 S shares 76% amino acid identity with SARS-CoV S (Lu et al., 2020). Furthermore, S serves as a dominant antibody target and is a focus of countermeasure development for the treatment and prevention of COVID-19 infection (Jiang et al., 2020; Krammer, 2020). S proteins from the *Betacoronavirus* genus share multiple regions of structural homology and thus could serve as targets for a cross-reactive antibody response (Li, 2016). Identifying cross-reactive antibody epitopes can inform rational design strategies for vaccines and therapies that target multiple highly pathogenic coronaviruses.

Numerous potent neutralizing antibodies against SARS-CoV-2 have been discovered, including multiple candidates currently in clinical trials or approved for emergency use for prophylactic and acute treatment of COVID-19 (Brouwer et al., 2020; Chen et al., 2021b; Chi et al., 2020; Cohen, 2021; Pinto et al., 2020; Rogers et al., 2020; Weinreich et al., 2021; Zost et al., 2020b). Investigation of SARS-CoV-2/SARS-CoV cross-reactive antibodies has focused primarily on the RBD epitope, which has resulted in the identification of a number of SARS-CoV-2/SARS-CoV cross-reactive antibody candidates(Liu et al., 2020; Pinto et al., 2020; Wec et al., 2020b) However, the diversity of epitopes and functions beyond virus neutralization have not been extensively explored for cross-reactive antibodies (Lv et al., 2020; Ng et al., 2020; Zohar and Alter, 2020). Evidence of Fc effector function contributing to protection *in vivo* against SARS-CoV (Yasui et al., 2014) and SARS-CoV-2 (Schafer et al., 2021) suggests that the role of antibodies beyond neutralization may be a crucial component of protection and an important consideration in vaccine design strategies for coronaviruses (Atyeo et al., 2020; Loos et al., 2020; Ou et al., 2020; Zohar and Alter, 2020).

In this study, we investigated antibody cross-reactivity across the *Betacoronavirus* genus at monoclonal resolution. To do this, we applied LIBRA-seq (Linking B Cell receptor to antigen specificity through sequencing (Setliff et al., 2019a) to a recovered SARS-CoV donor sample from more than ten years after infection. We identified and characterized SARS-CoV-2/SARS-CoV cross-reactive human antibodies that target multiple, distinct structural domains of S, mediate phagocytosis and trogocytosis, and mitigate pathological burden *in vivo*. A better understanding of the genetic features, epitope specificities, and functional characteristics of cross-reactive coronavirus antibodies may translate into strategies for current vaccine design efforts and additional measures to counteract potential future pandemic strains.

RESULTS

LIBRA-seq characterization of a SARS-CoV recovered donor

To identify cross-reactive antibodies to multiple coronavirus antigens, LIBRA-seq was applied to a PBMC sample from a donor infected with SARS-CoV over ten years prior to sample collection. The antigen screening library consisted of eight oligo-tagged recombinant soluble antigens: six coronavirus trimer antigens (SARS-CoV-2 S, SARS-CoV S, MERS-CoV S, MERS-CoV S1 (with foldon domain), HCoV-OC43 S, HCoV-HKU1 S) and two HIV trimer antigens from strains ZM197 and CZA97 as negative controls (**Figure 2-1A**). After the antigen screening library was mixed with donor PBMCs, antigen positive B cells were enriched by fluorescence activated cell sorting and processed for single-cell sequencing (**Figure 2-1B**). After bioinformatic processing, we recovered 2625 cells with paired heavy/light chain sequences and antigen reactivity information (**Figure 2-1C**), and from these cells, there were 2368 unique VDJ sequences. Overall, LIBRA-seq enabled rapid screening of PBMCs from a patient sample, with recovery of

A

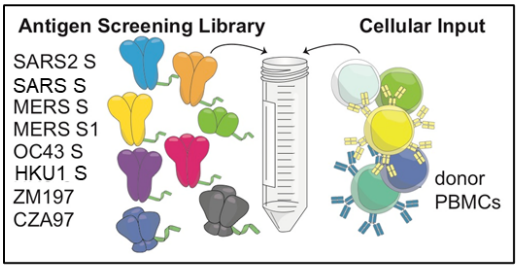

B

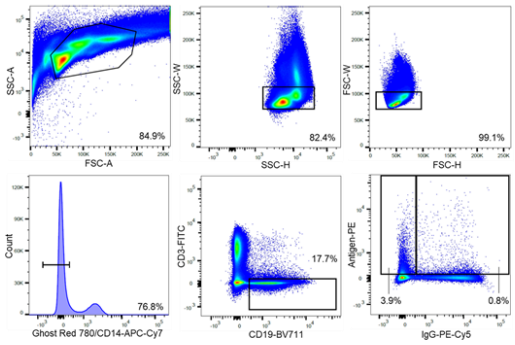

C

	4647-2 Processing
Unique Heavy Chain Barcodes	5113
Unique Heavy Chain Barcodes With Functional Heavy Chains	5072
Unique Heavy Chain Barcodes Without Cells With Multiple Heavy Chains	4875
Unique Light Chain Barcodes	7593
Unique Light Chain Barcodes With Functional Light Chains	7586
Unique Light Chain Barcodes Without Cells With Multiple Light Chains	5914
Unique Paired Heavy-Light Chain Barcodes	3813
Overlapping Barcodes Between Paired Heavy-Light Chains and Antigen Counts	2625

Figure 2-1: Identification of coronavirus cross-reactive antibodies from a SARS-CoV recovered PBMC sample using LIBRA-seq. (**A**) Schematic of DNA-barcoded antigens used to probe a SARS-CoV donor PBMC sample. (**B**) Gating scheme for fluorescent-activated cell sorting of recovered SARS-CoV donor. Cells were initially stained with Ghost Red 780, CD14-APC-Cy7, CD3-FITC, CD19-BV711, and IgG-PE-Cy5 along with a DNA-barcoded antigen screening library. To detect antigen-positive B cells, cells were washed and treated with a streptavidin-PE secondary stain. Gates as drawn are based on gates used during the sort, and percentages from the sort are listed. (**C**) The categorization of processing of Cell Ranger identified cells after sequencing is shown.

paired heavy/light chain sequences and antigen reactivity for thousands of B cells at the single-cell level.

Identification of SARS-CoV-2 and SARS-CoV cross-reactive antibodies

With a goal of identifying antibodies that were cross-reactive to multiple coronavirus S proteins, we prioritized lead candidates based on their sequence features and LIBRA-seq scores (**Figure 2-2A, 2-2B**). We selected 15 antibody candidates that exhibited diverse sequence features and utilized a number of different variable genes for expression and characterization (**Figure 2-2C**). These antibodies displayed a broad range of percent identity to germline (83-98%) and a variety of CDRH3 and CDRL3 lengths (6-24 and 5-13 amino acids, respectively) (**Figure 2-2C**). By ELISA, SARS-CoV-2 S and SARS-CoV S binding was confirmed for 6/15 of the tested antibodies (46472-1, 46472-2, 46472-3, 46472-4, 46472-6, and 46472-12), indicating LIBRA-seq could successfully identify SARS-CoV-2 reactive B cells, but also suggesting potential differences in antigen binding detection for primary B cells with a sequencing readout vs. recombinant IgG by ELISA (**Figure 2-2D-F**). Further, antibodies 46472-6 and 46472-12 bound to S proteins from endemic HCoV-OC43 and HCoV-HKU1, albeit generally at lower levels (**Figure 2-2D-F**). Although the six monoclonal antibodies showed reactivity by ELISA to the MERS-CoV antigen probe used in the LIBRA-seq screening library, antibody binding to other independent preparations of this protein was inconsistent, so MERS-CoV S reactivity could not be confirmed definitively (**Figure 2-3A, 2-3B**). Overall, the application of the LIBRA-seq technology enabled the identification of a panel of cross-reactive antibodies that recognize the S antigen from multiple coronaviruses.

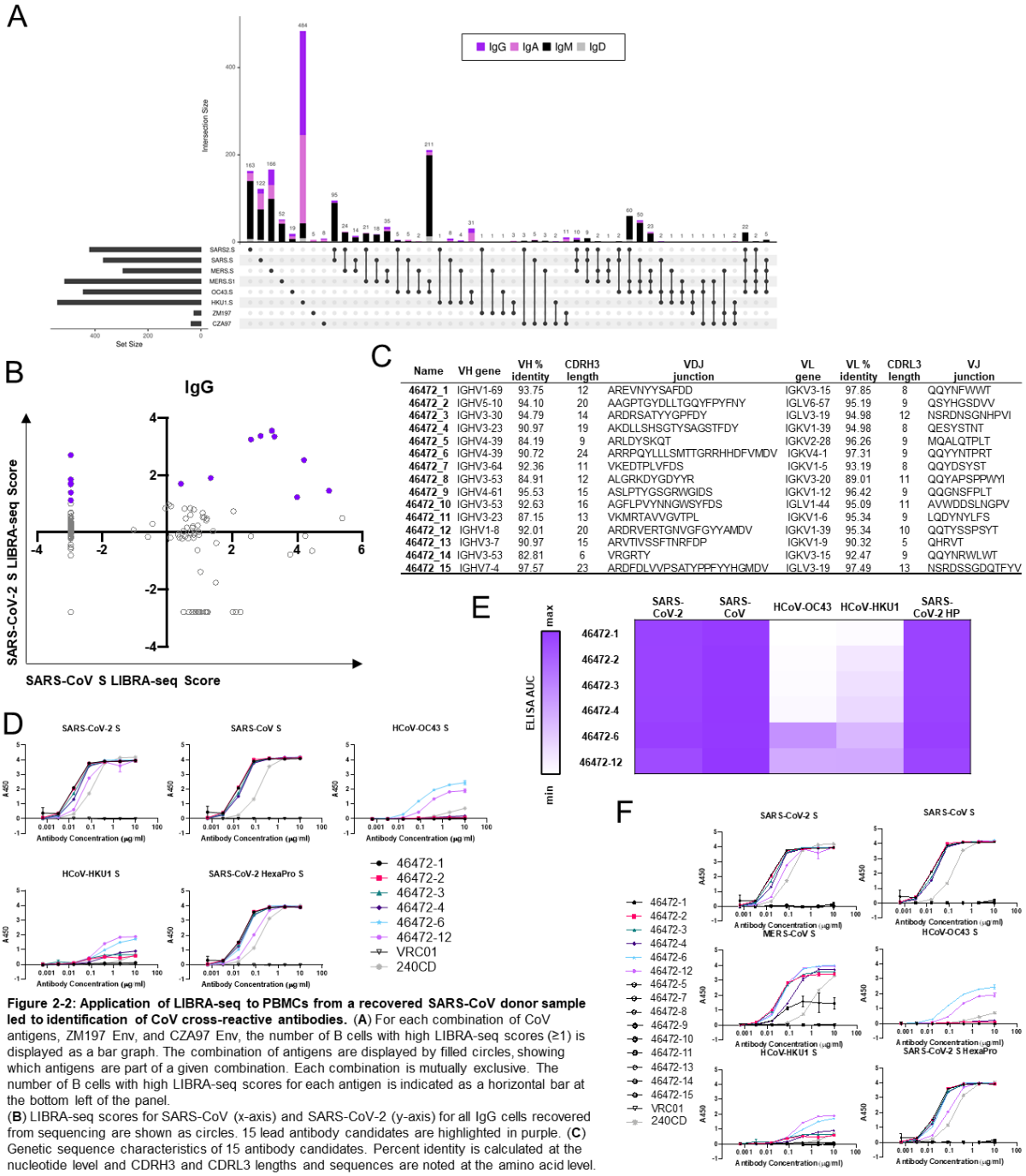

Name	VH gene	VH % identity	CDRH3 length	VDJ junction	VL gene	VL % identity	CDRL3 length	VJ junction
46472_1	IGHV1-69	93.75	12	AREVNYYSAFDD	IGKV3-15	97.85	8	QQYNFWWT
46472_2	IGHV5-10	94.10	20	AAGPTGYDLLTGQYFPYFNY	IGLV6-57	95.19	9	QSYHGSDVV
46472_3	IGHV3-30	94.79	14	ARDRSATYYGPFDY	IGLV3-19	94.98	12	NSRDNSGNHPVI
46472_4	IGHV3-23	90.97	19	AKDLLSHSGTYSAGSTFDY	IGKV1-39	94.98	8	QESYSTNT
46472_5	IGHV4-39	84.19	9	ARLDYSKQT	IGKV2-28	96.26	9	MQALQTPLT
46472_6	IGHV4-39	90.72	24	ARRPQYLLLSMTTGRRHHDFVMDV	IGKV4-1	97.31	9	QQYYNTPRT
46472_7	IGHV3-64	92.36	11	VKEDTPLVFDS	IGKV1-5	93.19	8	QQYDSYST
46472_8	IGHV3-53	84.91	12	ALGRKDYGDYYR	IGKV3-20	89.01	11	QQYAPSPPWYI
46472_9	IGHV4-61	95.53	15	ASLPTYGSGRWGIDS	IGKV1-12	96.42	9	QQGNSFPLT
46472_10	IGHV3-53	92.63	16	AGFLPVYNNGWSYFDS	IGLV1-44	95.09	11	AVWDDSLNGPV
46472_11	IGHV3-23	87.15	13	VKMRTAVVGVTPL	IGKV1-6	95.34	9	LQDYNYLFS
46472_12	IGHV1-8	92.01	20	ARDRVERTGNVGFGYYAMDV	IGKV1-39	95.34	10	QQTYSSPSYT
46472_13	IGHV3-7	90.97	15	ARVTIVSSFTNRFDP	IGKV1-9	90.32	5	QHRVT
46472_14	IGHV3-53	82.81	6	VRGRTY	IGKV3-15	92.47	9	QQYNRWLWT
46472_15	IGHV7-4	97.57	23	ARDFDLVVPSATYPPFYYHGMDV	IGLV3-19	97.49	13	NSRDSSGDQTFYV

Figure 2-2: Application of LIBRA-seq to PBMCs from a recovered SARS-CoV donor sample led to identification of CoV cross-reactive antibodies. (**A**) For each combination of CoV antigens, ZM197 Env, and CZA97 Env, the number of B cells with high LIBRA-seq scores (≥1) is displayed as a bar graph. The combination of antigens are displayed by filled circles, showing which antigens are part of a given combination. Each combination is mutually exclusive. The number of B cells with high LIBRA-seq scores for each antigen is indicated as a horizontal bar at the bottom left of the panel.
(**B**) LIBRA-seq scores for SARS-CoV (x-axis) and SARS-CoV-2 (y-axis) for all IgG cells recovered from sequencing are shown as circles. 15 lead antibody candidates are highlighted in purple. (**C**) Genetic sequence characteristics of 15 antibody candidates. Percent identity is calculated at the nucleotide level and CDRH3 and CDRL3 lengths and sequences are noted at the amino acid level. (**D**) Antibodies were tested for binding to CoV antigens by ELISA. HIV-specific antibody VRC01 was used as a negative control. Anti-SARS-CoV mouse antibody 240CD was also used. ELISAs were performed in technical duplicates with at least two biological duplicates. Data are represented as mean ± SEM. (**E**) ELISA binding data are displayed as a heatmap of the AUC values calculated from data in Figure 1C, with AUC of 0 as white, and maximum AUC as purple. (**F**) ELISA binding data against coronavirus S antigens. HIV-specific antibody VRC01 was used as a negative control and anti-SARS-CoV mouse antibody 240CD was used as a positive control (BEI Resources). ELISAs were performed in technical duplicates with at least two biological duplicates. Data are represented as mean ± SEM.

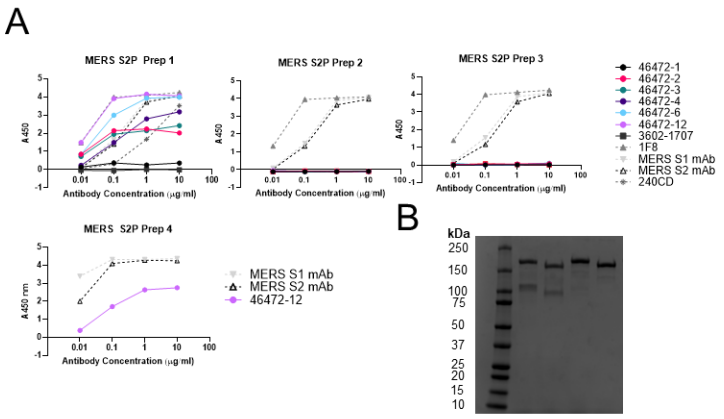

Figure 2-3: MERS-CoV Antigen Quality control. (**A**) ELISA binding data to independent preparations of MERS-CoV S protein. An influenza HA-specific mAb 3502-1707 was used as a negative control along with positive control antibodies 1F8 (expressed and purified recombinantly) and MERS S1 mAb and MERS S2 mAbs (Sino Biological). (**B**) SDS-PAGE gels of MERS-CoV S2P S preparations are shown (preparation 1 – lane 1 & 2, preparation 2 – lane 3 & 4) under both non-reducing conditions (lanes 1 & 3) and reducing conditions (lanes 2 & 4).

Cross-reactive coronavirus antibodies target diverse epitopes on S

To elucidate the epitopes targeted by the cross-reactive antibodies, we performed binding assays to various structural domains of S as well as binding-competition experiments. First, we assessed antibody binding to the S1 and S2 subdomains of SARS-CoV-2. Antibodies 46472-1, 46472-2, 46472-3, and 46472-4 bound to the S2 domain, whereas 46472-6 and 46472-12 recognized the S1 domain but targeted different epitopes, the NTD and RBD, respectively (**Figure 2-4A-E**). Although 46472-12 bound to the RBD, it did not compete with ACE2 for binding to SARS-CoV-2 S and showed partial competition with RBD-directed antibody CR3022 (**Figure 2-4F-G**).

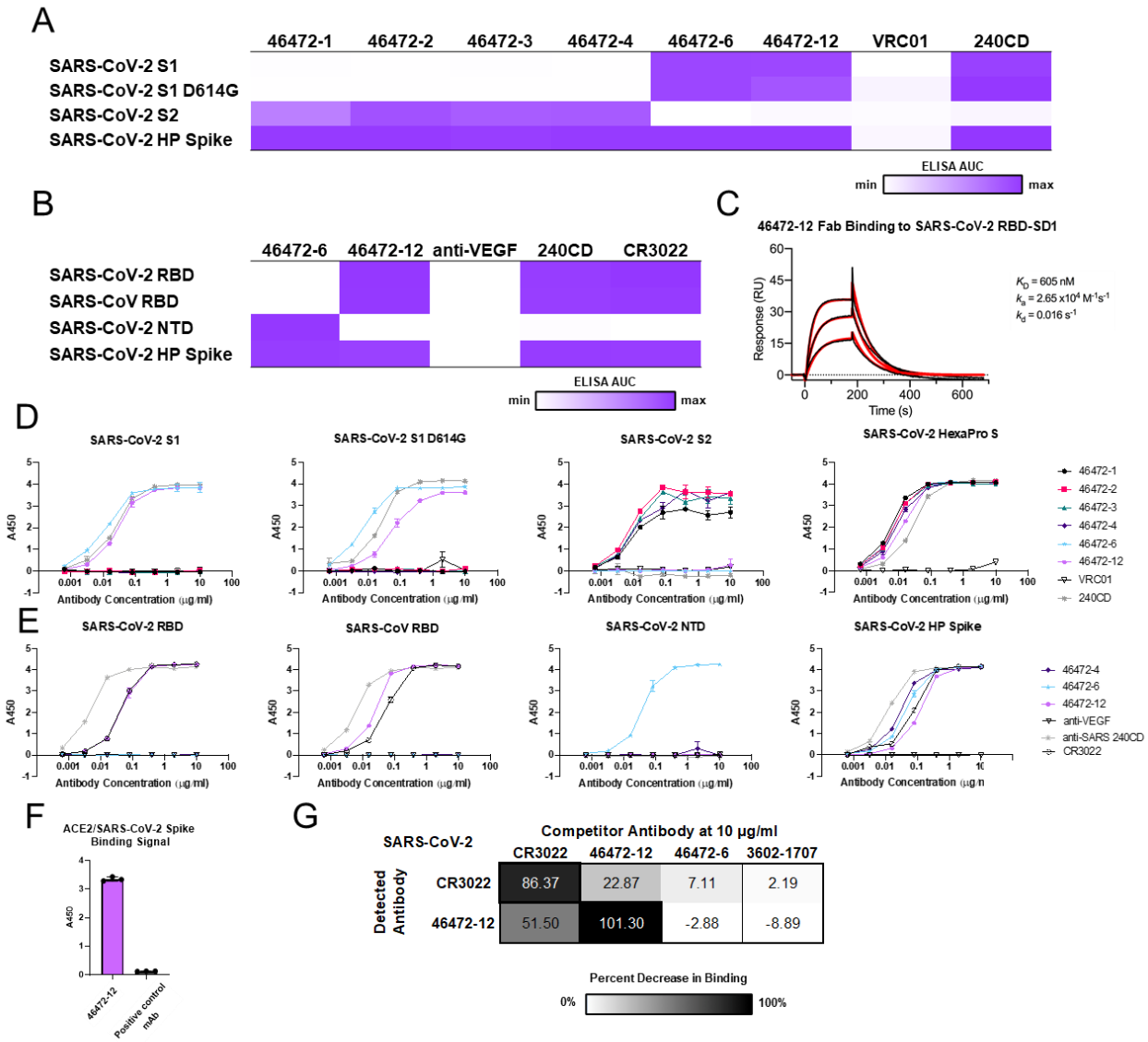

Figure 2-4: Epitope mapping of cross-reactive antibodies. (**A**) For cross-reactive coronavirus antibodies, ELISA data against the antigens are displayed as a heatmap of the AUC values calculated from the data in Figure S2A. (**B**) For SARS-CoV-2 S1 reactive antibodies, ELISA data against the RBD and NTD are displayed as a heatmap of the AUC values calculated from the data in Figure S2B. AUC of 0 is displayed as white and maximum AUC as purple. ELISA data are representative of at least two independent experiments. Anti-HIV antibody VRC01 and anti-VEGF antibody are shown as a negative control, and anti-SARS-CoV antibody 240CD is shown as a positive control. (**C**) Surface plasmon resonance binding of 46472-12 Fab to SARS-CoV-2 RBD. Affinity measurements are shown to the right of the graph. (**D**) Cross-reactive antibodies were tested for binding to SARS-CoV-2 S1 domain, SARS-CoV-2 S1 domain D614G, SARS-CoV-2 S2 domain, and SARS-CoV-2 S (HexaPro). Anti-HIV antibody VRC01 is shown as a negative control and anti-SARS-CoV antibody 240CD is shown as a positive control. Data are represented as mean ± SEM. (**E**) S1-directed antibodies 46472-6 and 46472-12 were tested for binding against SARS-CoV-2 RBD, SARS-CoV RBD, SARS-CoV-2 NTD, and SARS-CoV-2 S (HexaPro). Anti-HIV antibody VRC01 is shown as a negative control and anti-SARS-CoV antibody 240CD is shown as positive control. Data are represented as mean ± SEM. (**F**) 46472-12 was tested for its ability to block ACE2 binding to SARS-CoV-2 S. Signal shown is anti-Flag tag detection of an ACE2-Flag tag protein construct. All values are measured by absorbance at 450 nm and denoted as A_{450}. ACE2 blocking was determined by measuring amount of ACE2 with FLAG tag binding in the presence of each antibody (concentration 10µg/mL), measured by binding of an anti-FLAG secondary antibody. Experiment was done in biological replicate and technical triplicates; shown is representative of one replicate with positive control mAb COV2-2196. Data are represented as mean ± SEM.(**G**) A competition ELISA experiment between antibodies 46472-6, 46472-12 and CR3022 was performed to determine if binding of one antibody to SARS-CoV-2 S affected binding of another. Competitor antibodies were added at 10 µg/ml, and then detected antibodies were added at 0.1 µg/ml. The percent reduction in binding compared to binding without a competitor is shown. Influenza HA-specific antibody 3602-1707 was used as a negative control. ELISAs were performed in technical duplicates with at least two biological duplicates.

To determine whether the antibodies targeted overlapping or distinct epitopes, we performed competition ELISA experiments and found that the S2-directed antibodies 46472-1, 46472-2, and 46472-4 competed for binding to S (**Figure 2-5A**). This pattern was observed for both SARS-CoV-2 and SARS-CoV S. Of note, this competition group did not include S2-directed antibody 46472-3, revealing the identification of multiple cross-reactive epitope targets on S2 (**Figure 2-5A**). Further, antibody binding was not affected by two glycan knockout mutants (N165A or N709A) or mannose competition (**Figure 2-5B-C**). Lastly, we measured antibody autoreactivity, and found that with the exception of 46472-6 binding to Jo-1, none of the antibodies showed autoreactivity against the tested antigens (**Figure 2-5D**). Together, these data suggest that the identified cross-reactive antibodies are coronavirus-specific and target multiple, diverse epitopes on the S protein (**Figure 2-5E**).

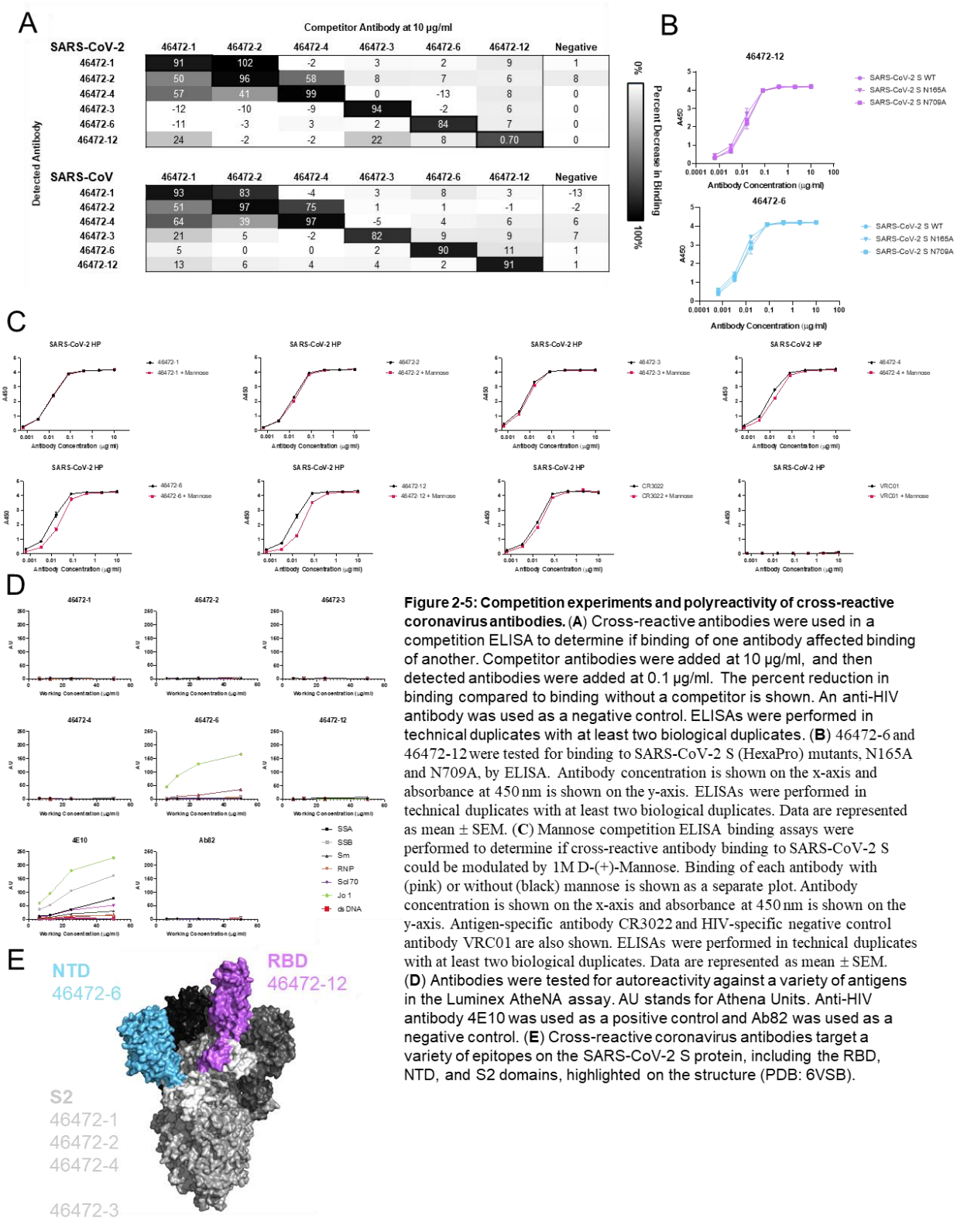

Figure 2-5: Competition experiments and polyreactivity of cross-reactive coronavirus antibodies. (**A**) Cross-reactive antibodies were used in a competition ELISA to determine if binding of one antibody affected binding of another. Competitor antibodies were added at 10 µg/ml, and then detected antibodies were added at 0.1 µg/ml. The percent reduction in binding compared to binding without a competitor is shown. An anti-HIV antibody was used as a negative control. ELISAs were performed in technical duplicates with at least two biological duplicates. (**B**) 46472-6 and 46472-12 were tested for binding to SARS-CoV-2 S (HexaPro) mutants, N165A and N709A, by ELISA. Antibody concentration is shown on the x-axis and absorbance at 450 nm is shown on the y-axis. ELISAs were performed in technical duplicates with at least two biological duplicates. Data are represented as mean ± SEM. (**C**) Mannose competition ELISA binding assays were performed to determine if cross-reactive antibody binding to SARS-CoV-2 S could be modulated by 1M D-(+)-Mannose. Binding of each antibody with (pink) or without (black) mannose is shown as a separate plot. Antibody concentration is shown on the x-axis and absorbance at 450 nm is shown on the y-axis. Antigen-specific antibody CR3022 and HIV-specific negative control antibody VRC01 are also shown. ELISAs were performed in technical duplicates with at least two biological duplicates. Data are represented as mean ± SEM. (**D**) Antibodies were tested for autoreactivity against a variety of antigens in the Luminex AtheNA assay. AU stands for Athena Units. Anti-HIV antibody 4E10 was used as a positive control and Ab82 was used as a negative control. (**E**) Cross-reactive coronavirus antibodies target a variety of epitopes on the SARS-CoV-2 S protein, including the RBD, NTD, and S2 domains, highlighted on the structure (PDB: 6VSB).

Functional characterization of cross-reactive coronavirus antibodies

Next, we characterized our cross-reactive antibody panel for functional activity. Although none of the antibodies neutralized SARS-CoV or SARS-CoV-2 (**Figure 2-6A-B**), all antibodies showed antibody-dependent cellular phagocytosis (ADCP) *in vitro* for SARS-CoV-2 S (**Figure 2-6C**). In particular, the RBD-reactive antibody 46472-12 showed greater ADCP activity compared to the other cross-reactive antibodies and the SARS-CoV/SARS-CoV-2 cross-reactive RBD antibody control, CR3022 (Yuan et al., 2020b) (**Figure 2-6C-D**). Further, we tested and confirmed ADCP activity against SARS-CoV for two antibodies that mediated the highest phagocytotic activity against SARS-CoV-2, 46472-4 and 46472-12, illustrating that these antibodies have cross-coronavirus phagocytic ability (**Figure 2-6E-F**).

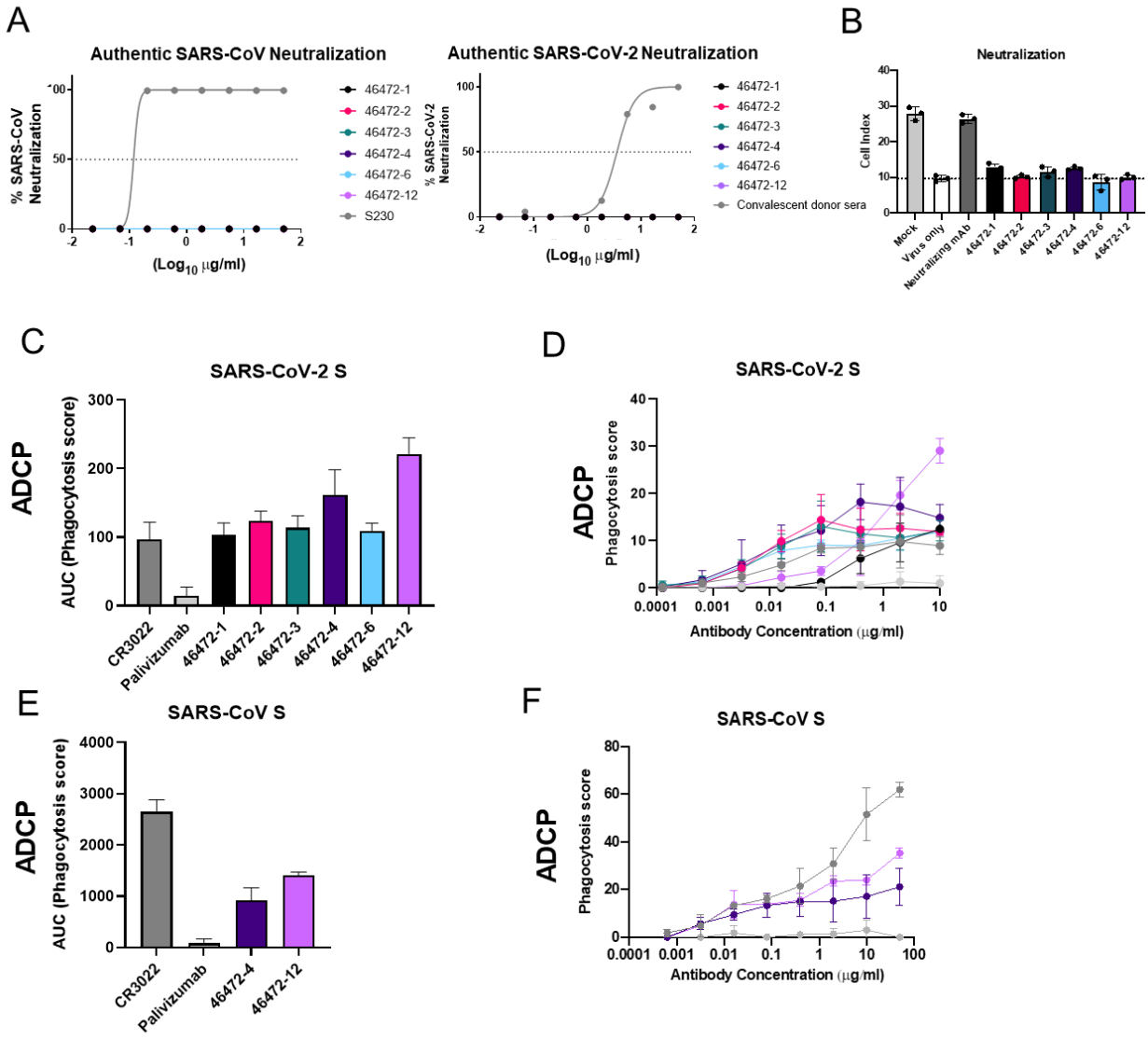

Figure 2-6: Functional characterization of cross-reactive coronavirus antibodies. (**A**) Antibodies were tested for neutralization in authentic SARS-CoV and SARS-CoV-2 nanoluciferase-based assays. Antibody and serum neutralization were measured by relative light units (RLU) via the Nano-Glo Luciferase System (Promega) compared to virus only control wells. (**B**) Antibodies were tested in SARS-CoV-2 RTCA assay. The adhesion of target Vero-furin cells were measured by electronic sensograms of each antibody and control-treated well and converted into Cell Index values by xCelligence software. Neutralization was assessed by comparison to virus only and media only controls. (**C**) Cross-reactive coronavirus antibodies were tested for antibody-dependent cellular phagocytosis activity (ADCP) against SARS-CoV-2 S, compared to positive control CR3022 and negative control Palivizumab, an anti-RSV antibody. AUC of the phagocytosis score is shown, calculated from data in Figure S3C. Data are represented as mean ± SD. (**D**) Cross-reactive coronavirus antibodies were tested for ability to mediate antibody-dependent cellular phagocytosis (ADCP) against SARS-CoV-2 S, compared to antigen-specific control antibody CR3022 and negative control Palivizumab, an anti-RSV antibody. Phagocytosis score (see Methods) is shown on the y-axis and antibody concentration is shown on the x-axis. Experiments were performed at least twice, and data is shown as mean +/- the standard deviation. (**E**) 46472-4 and 46472-12 were tested for ADCP activity against SARS-CoV S, compared to CR3022 and anti-RSV Palivizumab. AUC of the phagocytosis score is shown, calculated from data in Figure S3D. Data are represented as mean ± SD. (**F**) 46472-4 and 46472-12 were tested for antibody-dependent cellular phagocytosis activity against SARS-CoV S, compared to antigen-specific CR3022 antibody and anti-RSV antibody Palivizumab. Phagocytosis score (see Methods) is shown on the y-axis and antibody concentration is shown on the x-axis. Experiments were performed at least twice, and data is shown as mean +/- the standard deviation.

We next tested the antibodies in a trogocytosis assay (Richardson et al., 2018) and found that four antibodies in our panel (46472-1, 46472-2, 46472-3, and 46472-4) mediated trogocytosis (**Figure 3C, Supplemental Figure 3E**). This warrants further investigation as this is the first description of trogocytosis performed by SARS-CoV-2 specific mAbs. Lastly, none of the antibodies promoted complement deposition (ADCD) (**Figure 3D, Supplemental Figure 3F**). Together, these results revealed different profiles of Fc effector functionality within the panel of cross-reactive antibodies.

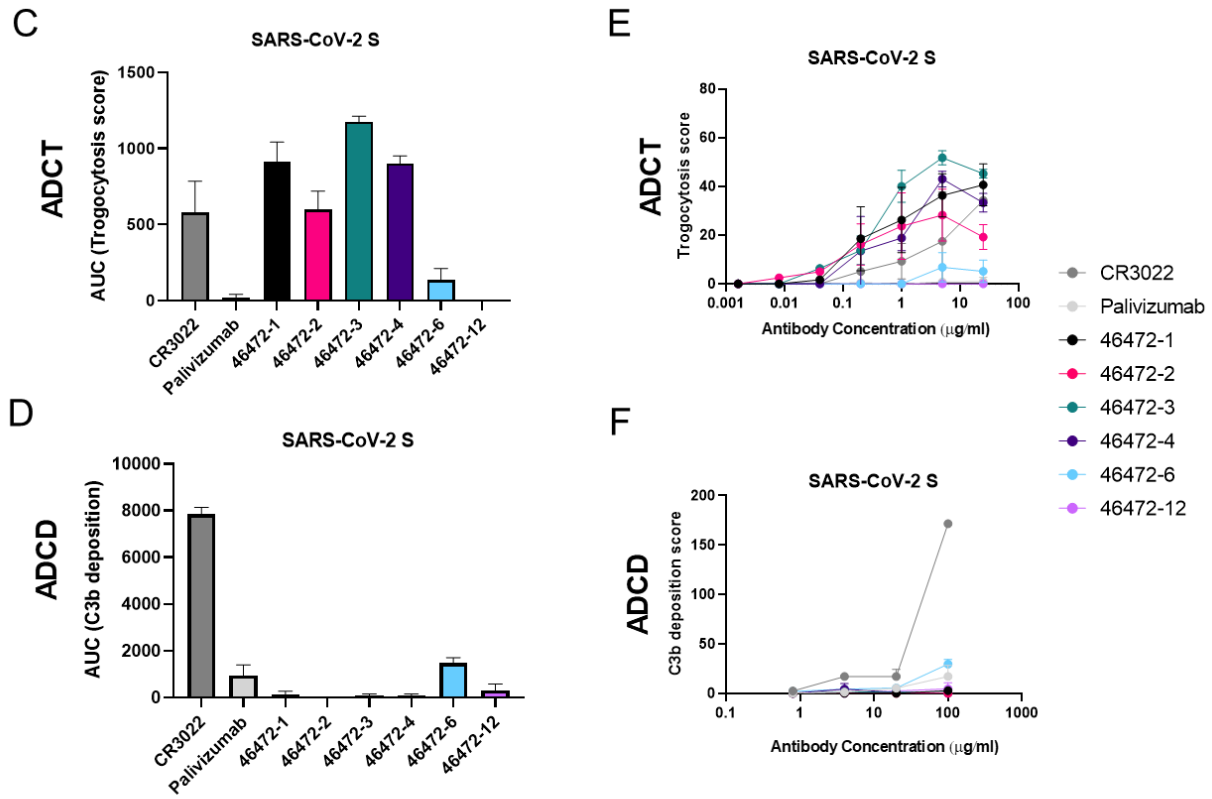

Figure 2-7: Functional characterization of cross-reactive coronavirus antibodies. (**A**) Cross-reactive coronavirus antibodies were tested for antibody-dependent cellular trogocytosis (ADCT) activity against SARS-CoV-2 S displayed on transfected cells, compared to positive control CR3022 and anti-RSV Palivizumab. AUC of the trogocytosis score is shown, calculated from data in Figure S3E. Data are represented as mean ± SD. (**B**) Cross-reactive coronavirus antibodies were tested for antibody-dependent cellular trogocytosis activity against SARS-CoV-2 S displayed on transfected cells, compared to antigen-specific control CR3022 and anti-RSV antibody Palivizumab. Trogocytosis score (see Methods) is shown on the y-axis and antibody concentration is shown on the x-axis. Experiments were performed at least twice, and data is shown as mean +/- the standard deviation. (**C**) Cross-reactive coronavirus antibodies were tested for antibody-dependent complement deposition (ADCD) activity against SARS-CoV-2 S, compared to positive control CR3022 and anti-RSV Palivizumab. AUC of the C3b deposition score is shown, calculated from data in Figure S3F. Data are represented as mean ± SD. (**E**) Cross-reactive coronavirus antibodies were tested for antibody-dependent complement deposition (ADCD) activity against SARS-CoV-2 S, compared to antigen-specific control CR3022 and anti-RSV antibody Palivizumab. Complement deposition score (see Methods) is shown on the y-axis and antibody concentration is shown on the x-axis. Experiments were performed at least twice, and data is shown as mean +/- the standard deviation.

Since non-neutralizing SARS-CoV-2 antibodies with Fc effector function activity have not been extensively characterized *in vivo*, these results prompted us to test antibodies 46472-4 and 46472-12 for prophylaxis in a murine infection model using a mouse-adapted virus strain (SARS-CoV-2 MA) (Dinnon et al., 2020; Leist et al., 2020) at a non-lethal dose of $1x10^3$ PFU (**Figure 2-8A**). Although there were no differences in survival and viral load between experimental and control groups, the lung hemorrhage scores (see Methods) for 46472-4 and 46472-12 were similar to antigen-specific control CR3022, and all three groups were significantly lower than the scores for isotype control DENV-2D22 ($p<0.01$, ordinary one-way ANOVA with multiple comparisons) (**Figure 2-8B-C**).

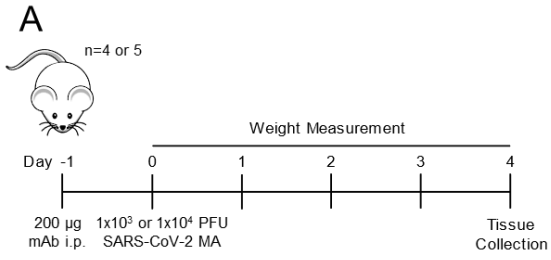

C

	SARS-CoV-2 MA 10^3 PFU				
	Animal Survival, Days Post Infection				
Antibody	0	1	2	3	4
46472-12	4/4	4/4	4/4	4/4	4/4
46472-4	5/5	5/5	5/5	5/5	5/5
CR3022	5/5	5/5	5/5	5/5	5/5
DENV-2D22	5/5	5/5	5/5	5/5	4/5

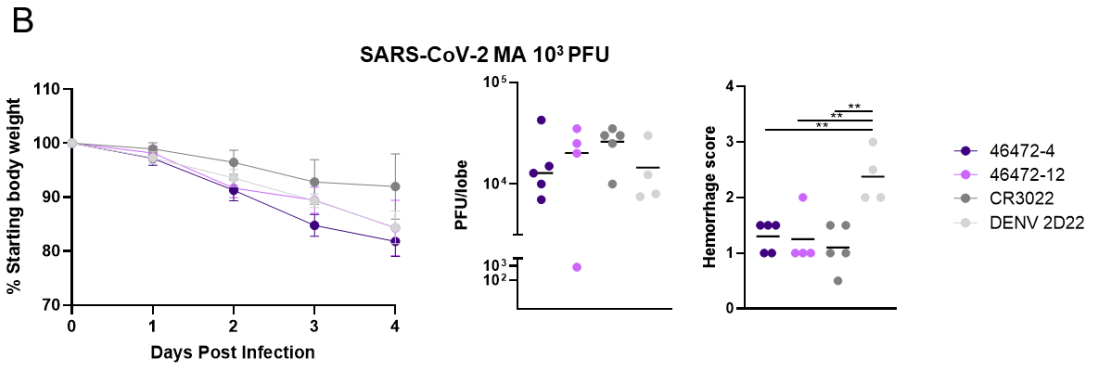

Figure 2-8: In vivo characterization of cross-reactive coronavirus antibodies. (**A**) Timeline of the prophylactic antibody experiment in SARS-CoV-2 mouse adapted (MA) *in vivo* infection model. (**B**) Antibody treatment group for the experiment utilizing $1x10^3$ PFU of SARS-CoV-2 MA, shown are daily body weight progression, and terminal RT-qPCR quantification of lung viral titer and lung hemorrhage scores of gross pathology. For viral titer values and the lung hemorrhage scores, an ordinary one-way ANOVA test with multiple comparisons was performed. (**C**) For each antibody treatment group for the experiment utilizing $1x10^3$ PFU of SARS-CoV-2 MA, a table showing the number of animals to survive per group per day is shown.

To evaluate the *in vivo* effect of these antibodies in a more stringent challenge model in 12-month old female BALB/c mice, we increased the viral dose from $1x10^3$ to $1x10^4$ PFU. In this experiment, mice that received antibody 46472-12 exhibited the best survival rate (4/5 at day 4), compared to the other treatment groups that included CR3022 as an antigen-specific control and DENV-2D22 as a negative control, although statistical significance was not achieved (**Figure 2-9A-C**). There were no significant differences in viral load between groups; however, the surviving animals from the 46472-4 and 46472-12 groups showed significantly lower hemorrhagic pathology scores in harvested mouse lungs compared to the negative control treatment group ($p<0.001$, ordinary one-way ANOVA with multiple comparisons) (**Figure 2-9A**). Animals treated with the antigen-specific control, CR3022, had significantly higher hemorrhage scores than animals treated with 46472-4 and 46472-12 ($p<0.001$, ordinary one-way ANOVA with multiple comparisons), although the statistical analysis may be limited by the small numbers of surviving animals for some of the groups (**Figure 2-9A**). While definitive evidence for protection is limited, the data from the *in vivo* experiments suggests that these cross-reactive antibodies could contribute to counteracting coronavirus infection in prophylaxis.

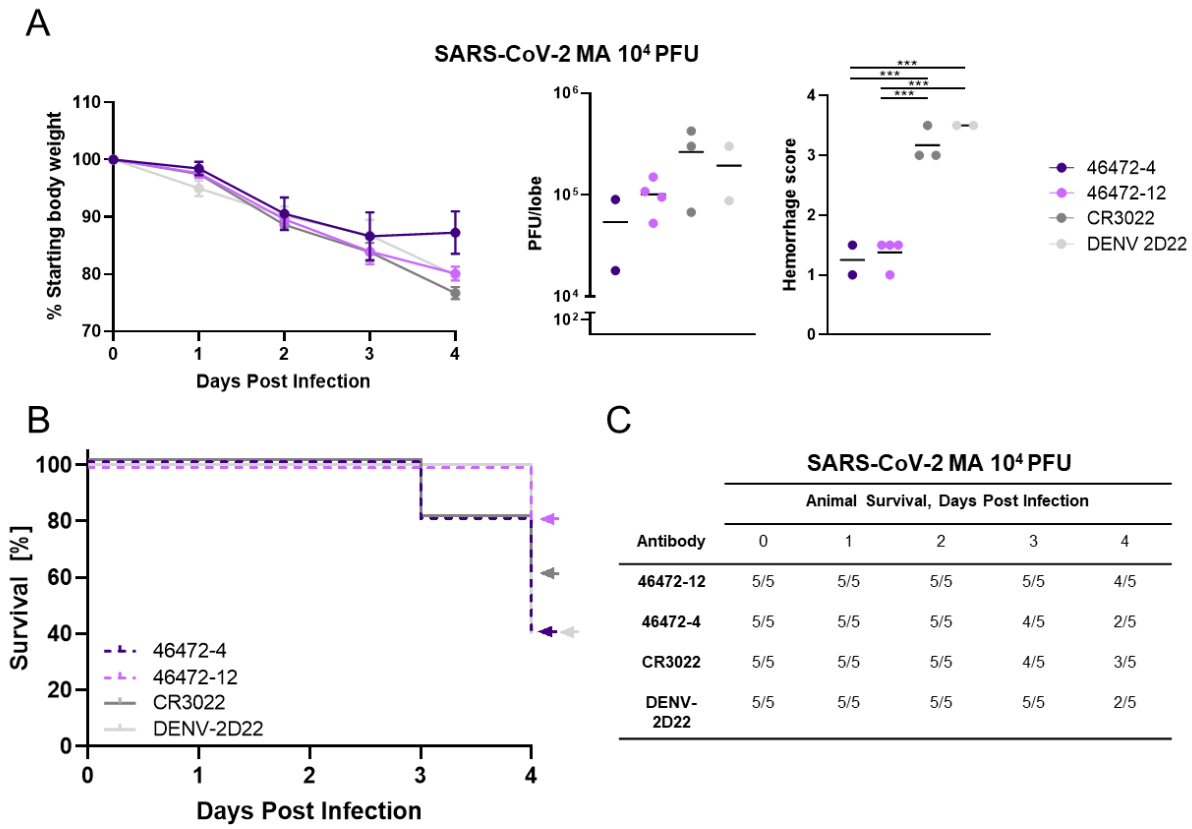

SARS-CoV-2 MA 10^4 PFU

	Animal Survival, Days Post Infection				
Antibody	0	1	2	3	4
46472-12	5/5	5/5	5/5	5/5	4/5
46472-4	5/5	5/5	5/5	4/5	2/5
CR3022	5/5	5/5	5/5	4/5	3/5
DENV-2D22	5/5	5/5	5/5	5/5	2/5

Figure 2-9: In vivo characterization of cross-reactive coronavirus antibodies. (**A**)) Antibody treatment group for the experiment utilizing 1x10^4 PFU of SARS-CoV-2 MA, shown are daily body weight progression, and terminal RT-qPCR quantification of lung viral titer and lung hemorrhage scores of gross pathology. For viral titer values and the lung hemorrhage scores, an ordinary one-way ANOVA test with multiple comparisons was performed. (**B**) For the experiment with 1x10^4 PFU of SARS-CoV-2 MA, percent survival for each antibody group is shown. (**C**) For each antibody treatment group for the experiment utilizing 1x10^4 PFU of SARS-CoV-2 MA, a table showing the number of animals to survive per group, per day is shown (survival curves shown in **Figure 2-9B**). 2/5, 4/5, 3/5, and 2/5 mice survived to day 4 for antibodies 46472-4, 46472-12, CR3022 and isotype control DENV-2D22, respectively.

DISCUSSION

Here, we described a set of cross-reactive *Betacoronavirus* antibodies isolated from a recovered SARS-CoV donor. The antibodies targeted diverse epitopes on S, including the S2 subdomain as well as the RBD and NTD on S1, and demonstrated Fc effector function *in vitro*. Additionally, two of these antibodies were tested *in vivo*, and displayed a reduction in lung hemorrhage score, while effects on viral load were not definitive.

Given the similar effect of 46472-4 and 46472-12 on severe disease in the mouse model, their phagocytotic ability along with the inability to mediate neutralization suggests that the former may be a mechanism through which they function, and additional studies are underway to further assess this hypothesis. Phagocytosis has been shown to be associated with protection in a SARS-CoV-2 DNA vaccination in non-human primates as well as survival in natural infection (Yu et al., 2020) and as such could be an important mechanism for protection by monoclonal antibodies. The role of trogocytosis in COVID-19 is unknown as are the targets that may be important for this function. 46472-4 was able to mediate this membrane nibbling in contrast to 46472-12, suggesting that this function in addition to complement activity was not responsible for the *in vivo* effect on severe disease mediated by these antibodies. Although the precise *in vivo* effects of these antibodies have not been elucidated, the identification of multiple, cross-reactive antibodies highlights a potential role for Fc effector function activity, specifically phagocytosis, in coronavirus infection. Evidence of protection associated with Fc effector function in SARS-CoV (Yasui et al., 2014), SARS-CoV-2 (Atyeo et al., 2020; Atyeo et al., 2021; Schafer et al., 2021), and other infectious diseases including influenza, Ebola, and HIV, motivates further investigation into its contribution for the treatment of COVID-19 (Bournazos et al., 2019; Bournazos et al., 2014; DiLillo et al., 2016; Lu et al., 2018). Furthermore, the importance of Fc effector functionality of potently neutralizing candidate clinical SARS-CoV-2 mAbs in a therapeutic setting rather than prophylaxis highlights the potential benefit for investigation into non-neutralizing antibodies with phagocytic activity and their administration after infection onset (Winkler et al., 2021). Elucidation of the functional roles of cross-reactive but non-neutralizing antibodies could have implications for understanding the factors involved in protection or enhancement of disease.

Given the ongoing SARS-CoV-2 pandemic and the potential for future zoonotic coronavirus pathogens to emerge, coronavirus vaccine and therapeutic development is of paramount

importance (Edwards et al., 2020; Menachery et al., 2015; Menachery et al., 2016; Song et al., 2019). Antibodies that can cross-react with multiple coronavirus strains are primary targets as potential broadly reactive therapies. Such antibodies can further reveal cross-reactive epitopes that could serve as templates for the development of broadly protective vaccines. Understanding the spectrum of cross-reactive epitopes targeted by human antibodies, as well as the functional role that such antibodies have within coronavirus infection, are therefore a vital element of medical countermeasure development.

LIMITATIONS OF THE STUDY

The current study focuses on the characterization of cross-reactive coronavirus antibodies, mostly in the context of SARS-CoV-2. Further characterization of this panel of antibodies against circulating endemic coronavirus strains would enhance the clinical relevance to less severe coronavirus-associated respiratory infections.

The current study utilized a dosing regimen in a prophylactic setting and given the emerging evidence of survival benefit with effector function in antibodies given after infection onset(Winkler et al., 2021), antibody administration in a therapeutic setting may provide further insight into *in vivo* properties. Furthermore, additional effector function characterization such as ADCC and ADNP would strengthen the profile of this panel of non-neutralizing antibodies given their role in both human (Zohar et al., 2020) and mouse SARS-CoV-2 infection studies.

ACKNOWLEDGEMENTS

We thank Angela Jones, Latha Raju, and Jamie Roberson of Vanderbilt Technologies for Advanced Genomics for their expertise regarding NGS and library preparation; David Flaherty and Brittany Matlock of the Vanderbilt Flow Cytometry Shared Resource for help with flow panel optimization; and members of the Georgiev laboratory for comments on the manuscript. The

Vanderbilt VANTAGE Core provided technical assistance for this work. VANTAGE is supported in part by CTSA grant 5UL1 RR024975-03, the Vanderbilt Ingram Cancer Center (P30 CA68485), the Vanderbilt Vision Center (P30 EY08126), and NIH/NCRR (G20 RR030956). This work was conducted in part using the resources of the Advanced Computing Center for Research and Education at Vanderbilt University (Nashville, TN). Flow cytometry experiments were performed in the VUMC Flow Cytometry Shared Resource. The VUMC Flow Cytometry Shared Resource is supported by the Vanderbilt Ingram Cancer Center (P30 CA68485) and the Vanderbilt Digestive Disease Research Center (DK058404).

For work described in this manuscript, I.S.G., A.R.S., K.J.K., S.W., K.A.P., R.V., N.R., E.F.F., C.M.H. were supported in part by NIH NIAID award R01AI131722-S1, the Hays Foundation COVID-19 Research Fund, Fast Grants, and *CTSA award No.* UL1 TR002243 *from the National Center for Advancing Translational Sciences*. J.S.M and D.W. were supported in part by a National Institutes of Health (NIH)/National Institute of Allergy and Infectious Diseases (NIAID) grant awarded to J.S.M. (R01-AI127521). L.M. and S.I.R. acknowledge research funding from the South African Medical Research Council (MRC) Extramural Unit and SHIP-COVID19 programs and an H3 Africa grant (U01A136677). S.I.R. is supported by the South African Research Chairs Initiative of the Department of Science and Technology and the NRF (Grant No 98341) and is a L'Oreal/UNESCO South Africa Young Talents Awardee. R.B., A.S., D.R.M., were supported by NIH grants (U54CA260543, R01AI157155). P.A. and K.J. were supported by NIH grant R01 AI14567. J.E.C., R.H.C., N.S., R.N.S., and R.E.S., were supported by Defense Advanced Research Projects Agency (DARPA) grants HR0011-18-2-0001 and HR00 11-18-3-0001; NIH contracts 75N93019C00074 and 75N93019C00062; NIH grants U01 AI150739, R01 AI130591 and R35 HL145242; the Dolly Parton COVID-19 Research Fund at Vanderbilt; and NIH grant S10 RR028106 for the Next Generation Nucleic Acid Sequencer, housed in VANTAGE. M.S.D. and R.E.C. were supported by grants from NIH (R01 AI157155) and the

Defense Advanced Research Project Agency (HR001117S0019). B.F.H. and R.P. were supported by NC State funding for COVID research. B.S.G. was supported by intramural funding from the NIAID. C.M.H. was supported in part by NIH grant T32 GM008320-30. D.R.M. was supported by an NIH F32 AI152296, a Burroughs Wellcome Fund Postdoctoral Enrichment Program Award, and was previously supported by an NIH NIAID T32 AI007151.

AUTHOR CONTRIBUTIONS

Methodology, A.R.S., K.J.K., and I.S.G.; Investigation, A.R.S., K.J.K., D.W., S.I.R., A.S., S.W., N.W., K.J., K.A.P., R.V., R.P., N.P.M., N.R., E.F.F., C.M.H., N.S., R.E.C., D.R.M., R.S.N., R.E.S., J.E.L., B.S.G., M.S.D., B.F.H., P.A., R.H.C., J.E.C., R.S.B., L.M., J.S.M., and I.S.G.; Software, A.R.S., R.V., N.R.; Validation, A.R.S., K.J.K.; Writing - Original Draft, A.R.S., and K.J.K.; Writing -Review & Editing, all authors; Funding Acquisition, I.S.G., B.S.G., M.S.D., B.F.H., P.A., R.H.C., J.E.C., R.S.B., L.M., J.S.M., and A.R.S, and K.J.K.; Resources, B.S.G., M.S.D., B.F.H., P.A., R.H.C., J.E.C., R.S.B., L.M., J.S.M., and I.S.G.; Supervision, I.S.G.

DECLARATION OF INTERESTS

A.R.S. and I.S.G are co-founders of AbSeek Bio. A.R.S., K.J.K, I.S.G., D.W., N.W., and J.S.M are listed as inventors on patents filed describing the antibodies described here. D.W., J.S.M, B.S.G, and N.W. are also listed as inventors on U.S. patent application no. 62/972,886 (2019-nCoV Vaccine). M.S.D. is a consultant for Inbios, Vir Biotechnology, NGM Biopharmaceuticals, and Carnival Corporation and on the Scientific Advisory Boards of Moderna and Immunome. The Diamond laboratory has unrelated sponsored research agreements from Emergent BioSolutions, Moderna and Vir Biotechnology. J.E.C. has served as a consultant for Eli Lilly, GlaxoSmithKline and Luna Biologics, is a member of the Scientific Advisory Boards of CompuVax and Meissa Vaccines and is Founder of IDBiologics. The Crowe laboratory at

Vanderbilt University Medical Center has received sponsored research agreements from IDBiologics and AstraZeneca. R.S.B. has competing interests associated with Eli Lily, Takeda and Pfizer. The Georgiev laboratory at Vanderbilt University Medical Center has received unrelated funding from Takeda Pharmaceuticals.

METHODS

Antigen purification

A variety of recombinant soluble protein antigens were used in the LIBRA-seq experiment and other experimental assays.

Plasmids encoding residues 1–1208 of the SARS-CoV-2 spike with a mutated S1/S2 cleavage site, proline substitutions at positions 986 and 987, and a C-terminal T4-fibritin trimerization motif, an 8x HisTag, and a TwinStrepTag (SARS-CoV-2 S-2P); residues 1-1190 of the SARS-CoV spike with proline substitutions at positions 968 and 969, and a C-terminal T4-fibritin trimerization motif, an 8x HisTag, and a TwinStrepTag (SARS-CoV S-2P); residues 1-1291 of the MERS-CoV spike with a mutated S1/S2 cleavage site, proline substitutions at positions 1060 and 1061, and a C-terminal T4-fibritin trimerization motif, an AviTag, an 8x HisTag, and a TwinStrepTag (MERS-CoV S-2P Avi); residues 1-751 of the MERS-CoV spike with a C-terminal T4-fibritin trimerization motif, 8x HisTag, and a TwinStrepTag (MERS-CoV S1); residues 1-1277 of the HCoV-HKU1 spike with a mutated S1/S2 cleavage site, proline substitutions at positions 1067 and 1068, and a C-terminal T4-fibritin trimerization motif, an 8x HisTag, and a TwinStrepTag (HCoV-HKU1 S-2P); residues 1-1278 of the HCoV-OC43 spike with proline substitutions at positions 1070 and 1071, and a C-terminal T4-fibritin trimerization motif, an 8x HisTag, and a TwinStrepTag (HCoV-OC43 S-2P); or residues 319–591 of SARS-CoV-2 S with a C-terminal monomeric human IgG Fc-tag and an 8x HisTag (SARS-CoV-2 RBD-SD1) were transiently transfected into FreeStyle293F cells (Thermo Fisher) using polyethylenimine. The

coronavirus trimer spike antigens were in a prefusion-stabilized (S-2P) conformation that better represents neutralization-sensitive epitopes in comparison to their wild-type forms (Pallesen et al., 2017). Two hours post-transfection, cells were treated with kifunensine to ensure uniform glycosylation. Transfected supernatants were harvested after 6 days of expression. SARS-CoV-2 RBD-SD1 was purified using Protein A resin (Pierce), SARS-CoV-2 S-2P, SARS-CoV S-2P, MERS-CoV S-2P Avi, MERS-CoV S1, HCoV-HKU1 S-2P and HCoV-OC43 S-2P were purified using StrepTactin resin (IBA). Affinity-purified SARS-CoV-2 RBD-SD1 was further purified over a Superdex75 column (GE Life Sciences). MERS-CoV S1 was purified over a Superdex200 Increase column (GE Life Sciences). SARS-CoV-2 S-2P, SARS-CoV S-2P, MERS-CoV S-2P Avi, HCoV-HKU1 S-2P and HCoV-OC43 S-2P were purified over a Superose6 Increase column (GE Life Sciences).

For the HIV-1 gp140 SOSIP variant from strain ZM197 (clade C) and CZA97 (clade C), recombinant, soluble antigens contained an AviTag and were expressed in Expi293F cells using polyethylenimine transfection reagent and cultured. FreeStyle F17 expression medium supplemented with pluronic acid and glutamine was used. The cells were cultured at 37°C with 8% CO_2 saturation and shaking. After 5-7 days, cultures were centrifuged and supernatant was filtered and run over an affinity column of agarose bound *Galanthus nivalis* lectin. The column was washed with PBS and antigens were eluted with 30 mL of 1M methyl-a-D-mannopyranoside. Protein elutions were buffer exchanged into PBS, concentrated, and run on a Superdex 200 Increase 10/300 GL Sizing column on the AKTA FPLC system. Fractions corresponding to correctly folded protein were collected, analyzed by SDS-PAGE and antigenicity was characterized by ELISA using known monoclonal antibodies specific to each antigen. Avi-tagged antigens were biotinylated using BirA biotin ligase (Avidity LLC). Non-Avi-

tagged antigens were biotinylated using the EZ-Link Sulfo-NHS-Biotin kits using a 50:1 biotin to protein molar ratio.

For binding studies, SARS-CoV-2 HexaPro S, SARS-CoV S, SARS-CoV-2 RBD, SARS-CoV RBD, and MERS-CoV RBD constructs were expressed in the transient expression system previously mentioned. S proteins were purified using StrepTrap HP columns and RBD constructs were purified over protein A resin, respectively. Each resulting protein was further purified to homogeneity by size-exclusion chromatography on a Superose 6 10/300 GL column.

SARS-CoV-2 S1, SARS-CoV-2 S1 D614G, SARS-CoV-2 S2, and SARS-CoV-2 NTD truncated proteins were purchased from the commercial vendor, Sino Biological.

DNA-barcoding of antigens

We used oligos that possess 15 bp antigen barcode, a sequence capable of annealing to the template switch oligo that is part of the 10X bead-delivered oligos, and contain truncated TruSeq small RNA read 1 sequences in the following structure: 5'-CCTTGGCACCCGAGAATTCCANNNNNNNNNNNNNCCCATATAAGA*A*A-3', where Ns represent the antigen barcode. We used the following antigen barcodes: GCTCCTTTACACGTA (SARS-CoV-2 S), TGACCTTCCTCTCCT (SARS-CoV S), ACAATTTGTCTGCGA (MERS-CoV S), TCCTTTCCTGATAGG (MERS-CoV S1), CAGGTCCCTTATTTC (HCoV-HKU1 S), TAACTCAGGGCCTAT (HCoV-OC43 S), CAGCCCACTGCAATA (CZA97), and ATCGTCGAGAGCTAG (ZM197). Oligos were ordered from IDT with a 5' amino modification and HPLC purified.

For each antigen, a unique DNA barcode was directly conjugated to the antigen itself. In particular, 5'amino-oligonucleotides were conjugated directly to each antigen using the Solulink Protein-Oligonucleotide Conjugation Kit (TriLink cat no. S-9011) according to manufacturer's instructions. Briefly, the oligo and protein were desalted, and then the amino-oligo was modified with the 4FB crosslinker, and the biotinylated antigen protein was modified with S-HyNic. Then, the 4FB-oligo and the HyNic-antigen were mixed together. This causes a stable bond to form between the protein and the oligonucleotide. The concentration of the antigen-oligo conjugates was determined by a BCA assay, and the HyNic molar substitution ratio of the antigen-oligo conjugates was analyzed using the NanoDrop according to the Solulink protocol guidelines. AKTA FPLC was used to remove excess oligonucleotide from the protein-oligo conjugates, which were also verified using SDS-PAGE with a silver stain. Antigen-oligo conjugates were also used in flow cytometry titration experiments.

Antigen specific B cell sorting

Cells were stained and mixed with DNA-barcoded antigens and other antibodies, and then sorted using fluorescence activated cell sorting (FACS). First, cells were counted and viability was assessed using Trypan Blue. Then, cells were washed three times with DPBS supplemented with 0.1% Bovine serum albumin (BSA). Cells were resuspended in DPBS-BSA and stained with cell markers including viability dye (Ghost Red 780), CD14-APC-Cy7, CD3-FITC, CD19-BV711, and IgG-PE-Cy5. Additionally, antigen-oligo conjugates were added to the stain. After staining in the dark for 30 minutes at room temperature, cells were washed three times with DPBS-BSA at 300 g for five minutes. Cells were then incubated for 15 minutes at room temperature with Streptavidin-PE to label cells with bound antigen. Cells were washed

three times with DPBS-BSA, resuspended in DPBS, and sorted by FACS. Antigen positive cells were bulk sorted and delivered to the Vanderbilt Technologies for Advanced Genomics (VANTAGE) sequencing core at an appropriate target concentration for 10X Genomics library preparation and subsequent sequencing. FACS data were analyzed using FlowJo.

Sample and library preparation, and sequencing

Single-cell suspensions were loaded onto the Chromium Controller microfluidics device (10X Genomics) and processed using the B-cell Single Cell V(D)J solution according to manufacturer's suggestions for a target capture of 10,000 B cells per 1/8 10X cassette, with minor modifications in order to intercept, amplify and purify the antigen barcode libraries as previously described (Setliff et al., 2019a).

Sequence processing and bioinformatic analysis

We utilized and modified our previously described pipeline to use paired-end FASTQ files of oligo libraries as input, process and annotate reads for cell barcode, UMI, and antigen barcode, and generate a cell barcode - antigen barcode UMI count matrix (Setliff et al., 2019a). BCR contigs were processed using Cell Ranger (10X Genomics) using GRCh38 as reference. Antigen barcode libraries were also processed using Cell Ranger (10X Genomics). The overlapping cell barcodes between the two libraries were used as the basis of the subsequent analysis. We removed cell barcodes that had only non-functional heavy chain sequences as well as cells with multiple functional heavy chain sequences and/or multiple functional light chain sequences, reasoning that these may be multiplets. Additionally, we aligned the BCR contigs (filtered_contigs.fasta file output by Cell Ranger, 10X Genomics) to IMGT reference genes using HighV-Quest (Alamyar et al., 2012). The output of HighV-Quest was parsed using

ChangeO (Gupta et al., 2015b) and merged with an antigen barcode UMI count matrix. Finally, we determined the LIBRA-seq score for each antigen in the library for every cell as previously described (Setliff et al., 2019a).

Antibody expression and purification

For each antibody, variable genes were inserted into custom plasmids encoding the constant region for the IgG1 heavy chain as well as respective lambda and kappa light chains (pTwist CMV BetaGlobin WPRE Neo vector, Twist Bioscience). Antibodies were expressed in Expi293F mammalian cells (ThermoFisher) by co-transfecting heavy chain and light chain expressing plasmids using polyethylenimine transfection reagent and cultured for 5-7 days. Cells were maintained in FreeStyle F17 expression medium supplemented at final concentrations of 0.1% Pluronic Acid F-68 and 20% 4mM L-Glutamine. These cells were cultured at 37°C with 8% CO_2 saturation and shaking. After transfection and 5-7 days of culture, cell cultures were centrifuged and supernatant was 0.45 µm filtered with Nalgene Rapid Flow Disposable Filter Units with PES membrane. Filtered supernatant was run over a column containing Protein A agarose resin equilibrated with PBS. The column was washed with PBS, and then antibodies were eluted with 100 mM Glycine HCl at 2.7 pH directly into a 1:10 volume of 1M Tris-HCl pH 8.0. Eluted antibodies were buffer exchanged into PBS 3 times using Amicon Ultra centrifugal filter units and concentrated. Antibodies were analyzed by SDS-PAGE. Additionally, antibodies 46472-1, 46472-2, 46472-3, 46472-4, 46472-6 and 46472-12 were assessed by size exclusion chromatography on a Superdex 200 Increase 10/300 GL Sizing column with the AKTA FPLC system.

High-throughput antibody expression

For high-throughput production of recombinant antibodies, approaches were used that are designated as microscale. For antibody expression, microscale transfection were performed (~1 ml per antibody) of CHO cell cultures using the Gibco ExpiCHO Expression System and a protocol for deep 96-well blocks (Thermo Fisher Scientific). In brief, synthesized antibody-encoding DNA (~2 µg per transfection) was added to OptiPro serum free medium (OptiPro SFM), incubated with ExpiFectamine CHO Reagent and added to 800 µl of ExpiCHO cell cultures into 96-deep-well blocks using a ViaFlo 384 liquid handler (Integra Biosciences). The plates were incubated on an orbital shaker at 1,000 r.p.m. with an orbital diameter of 3 mm at 37 °C in 8% CO_2. The next day after transfection, ExpiFectamine CHO Enhancer and ExpiCHO Feed reagents (Thermo Fisher Scientific) were added to the cells, followed by 4 d incubation for a total of 5 d at 37 °C in 8% CO_2. Culture supernatants were collected after centrifuging the blocks at 450*g* for 5 min and were stored at 4°C until use. For high-throughput microscale antibody purification, fritted deep-well plates were used containing 25 µl of settled protein G resin (GE Healthcare Life Sciences) per well. Clarified culture supernatants were incubated with protein G resin for mAb capturing, washed with PBS using a 96-well plate manifold base (Qiagen) connected to the vacuum and eluted into 96-well PCR plates using 86 µl of 0.1 M glycine-HCL buffer pH 2.7. After neutralization with 14 µl of 1 M Tris-HCl pH 8.0, purified mAbs were buffer-exchanged into PBS using Zeba Spin Desalting Plates (Thermo Fisher Scientific) and stored at 4°C until use.

ELISA

To assess antibody binding, soluble protein was plated at 2 µg/ml overnight at 4°C. The next day, plates were washed three times with PBS supplemented with 0.05% Tween-20 (PBS-T) and coated with 5% milk powder in PBS-T. Plates were incubated for one hour at room temperature and then washed three times with PBS-T. Primary antibodies were diluted in 1%

milk in PBS-T, starting at 10 µg/ml with a serial 1:5 dilution and then added to the plate. The plates were incubated at room temperature for one hour and then washed three times in PBS-T. The secondary antibody, goat anti-human IgG conjugated to peroxidase, was added at 1:10,000 dilution in 1% milk in PBS-T to the plates, which were incubated for one hour at room temperature. Goat anti-mouse secondary was used for SARS-CoV specific control antibody 240CD (BEI Resources). Plates were washed three times with PBS-T and then developed by adding TMB substrate to each well. The plates were incubated at room temperature for ten minutes, and then 1N sulfuric acid was added to stop the reaction. Plates were read at 450 nm. Data are represented as mean ± SEM for one ELISA experiment. ELISAs were repeated 2 or more times. The area under the curve (AUC) was calculated using GraphPad Prism 8.0.0. For antibody 240CD, the following reagent was obtained through BEI Resources, NIAID, NIH: Monoclonal Anti-SARS-CoV S Protein (Similar to 240C), NR-616.

Competition ELISA

Competition ELISAs were performed as described above, with some modifications. After coating with antigen and blocking, 25 µl of non-biotinylated competitor antibody was added to each well at 10 µg/ml and incubated at 37°C for 10 minutes. Then, without washing, 75 µl biotinylated antibody (final concentration of 1 µg/ml) was added and incubated at 37°C for 1 hour. After washing three times with PBS-T, streptavidin-HRP was added at 1:10,000 dilution in 1% milk in PBS-T and incubated for 1 hour at room temperature. Plates were washed and substrate and sulfuric acid were added as described above. ELISAs were repeated at least 2 times. Data is shown as the % decrease in binding.

Autoreactivity

Monoclonal antibody reactivity to nine autoantigens (SSA/Ro, SS-B/La, Sm, ribonucleoprotein (RNP), Scl 70, Jo-1, dsDNA, centromere B, and histone) was measured using the AtheNA Multi-Lyte® ANA-II Plus test kit (Zeus scientific, Inc, #A21101). Antibodies were incubated with AtheNA beads for 30min at concentrations of 50, 25, 12.5 and 6.25 µg/mL. Beads were washed, incubated with secondary and read on the Luminex platform as specified in the kit protocol. Data were analyzed using AtheNA software. Positive (+) specimens received a score >120, and negative (-) specimens received a score <100. Samples between 100-120 were considered indeterminate.

Mannose competition

Mannose competition ELISAs were performed as described above with minor modifications. After antigen coating and washing, nonspecific binding was blocked by incubation with 5% FBS diluted in PBS for 1 hour at RT. Primary antibodies were diluted in 5% FBS-PBST +/- 1M D-(+)-Mannose starting at 10 µg/ml with a serial 1:5 dilution and then added to the plate for 1 hour at RT. After washing, antibody binding was detected with goat anti-human IgG conjugated to peroxidase and added at 1:10,000 dilution in 5% FBS in PBS-T to the plates. After 1 hour incubation, plates were washed and substrate and sulfuric acid were added as described above. Data shown is representative of three replicates.

Epitope mapping visualization

SARS-CoV-2 Spike (PDB-6VSB) was visualized using PyMOL software. Antibody epitopes were visualized on the SARS-CoV-2 spike using a structure of the pre-fusion stabilized SARS-

CoV-2 S-2P construct (Wrapp et al. Science. 2020.) modeled in the molecular graphics software PyMOL (The PyMOL Molecular Graphics System, Version 2.3.5 Schrödinger, LLC).

RTCA neutralization assay

To assess for neutralizing activity against SARS-CoV-2 strain 2019 n-CoV/USA_WA1/2020 (obtained from the Centers for Disease Control and Prevention, a gift from N. Thornburg), we used the high-throughput RTCA assay and xCelligence RTCA HT Analyzer (ACEA Biosciences) that has been described previously (Zost et al., 2020b). After obtaining a background reading of a 384-well E-plate, 6,000 Vero-furin cells (Mukherjee et al., 2016) were seeded per well. Sensograms were visualized using RTCA HT software version 1.0.1 (ACEA Biosciences). One day later, equal volumes of virus were added to antibody samples and incubated for 1 h at 37°C in 5% CO_2. mAbs were tested in triplicate with a single (1:20) dilution. Virus–mAb mixtures were then added to Vero-furin cells in 384-well E-plates. Controls were included that had Vero-furin cells with virus only (no mAb) and media only (no virus or mAb). E-plates were read every 8–12 h for 72 h to monitor virus neutralization. At 32 h after virus-mAb mixtures were added to the E-plates, cell index values of antibody samples were compared to those of virus only and media only to determine presence of neutralization.

Nano-luciferase neutralization assay

A full-length SARS-CoV-2 virus based on the Seattle Washington isolate and a full-length SARS-CoV virus based on the Urbani isolate were designed to express luciferase and was recovered via reverse genetics and described previously(Scobey et al., 2013; Yount et al., 2003). Viruses were titered in Vero E6 USAMRID cells to obtain a relative light units (RLU) signal of at least 10X the cell only control background. Vero E6 USAMRID cells were plated at

20,000 cells per well the day prior in clear bottom black walled 96-well plates (Corning 3904). Neutralizing antibody serum samples were tested at a starting dilution of 1:40 and were serially diluted 4-fold up to eight dilution spots. Antibody-virus complexes were incubated at 37C with 5% CO2 for 1 hour. Following incubation, growth media was removed and virus-antibody dilution complexes were added to the cells in duplicate. Virus-only controls and cell-only controls were included in each neutralization assay plate. Following infection, plates were incubated at 37C with 5% CO2 for 48 hours. After the 48 hour incubation, cells were lysed and luciferase activity was measured via Nano-Glo Luciferase Assay System (Promega) according to the manufacturer specifications. SARS-CoV and SARS-CoV-2 neutralization titers were defined as the sample dilution at which a 50% reduction in RLU was observed relative to the average of the virus control wells.

SPR

His-tagged SARS-CoV-2 RBD-SD1 was immobilized to a NiNTA sensorchip to a level of ~150 RUs using a Biacore X100. Serial dilutions of purified Fab 46472-12 were evaluated for binding, ranging in concentration from 1 to 0.25 μM. The resulting data were fit to a 1:1 binding model using Biacore Evaluation Software.

Fc effector function assays

Antibody-dependent cellular phagocytosis (ADCP)

Antibody-dependent cellular phagocytosis (ADCP) was performed using biotinylated SARS-CoV-2 or SARS-CoV S coated fluorescent neutravidin beads as previously described (Ackerman et al., 2011). Briefly, beads were incubated for two hours with antibodies at a starting concentration of 50μg/ml and titrated five fold. CR3022 was used as a positive control while Palivizumab was used as a negative control. Antibodies and beads were incubated with THP-1

cells overnight, fixed and interrogated on the FACSAria II. Phagocytosis score was calculated as the percentage of THP-1 cells that engulfed fluorescent beads multiplied by the geometric mean fluorescence intensity of the population in the FITC channel less the no antibody control.

Antibody-dependent cellular trogocytosis (ADCT)

ADCT was performed as described in and modified from a previously described study(Richardson et al., 2018). HEK293T cells transfected with a SARS-CoV-2 spike pcDNA vector were surface biotinylated with EZ-Link Sulfo-NHS-LC-Biotin as recommended by the manufacturer. Fifty-thousand cells per well were incubated with antibody for 30 minutes starting at 25µg/ml and titrated 5 fold. CR3022 was used as a positive control with Palivizumab as a negative. Following a RPMI media wash, these were then incubated with carboxyfluorescein succinimidyl ester (CFSE) stained THP-1 cells (5 $X10^4$ cells per well) for 1 hour and washed with 15mM EDTA/PBS followed by PBS. Cells were then stained for biotin using Streptavidin-PE and read on a FACSAria II. Trogocytosis score was determined as the proportion of CFSE positive THP-1 cells also positive for streptavidin-PE less the no antibody control.

Antibody-dependent complement deposition (ADCD)

Antibody-dependent complement deposition was performed as previously described (Fischinger et al., 2019). Briefly biotinylated SARS-CoV-2 S protein was coated 1:1 onto fluorescent neutravidin beads for 2 hours at 37 degrees. These beads were incubated with 100ug/ml of antibody for 1 hour and incubated with guinea pig complement diluted 1 in 50 with gelatin/veronal buffer for 15 minutes at 37 degrees. Beads were washed at 2000g twice in PBS and stained with anti-guinea pig C3b-FITC, fixed and interrogated on a FACSAria II. Complement deposition score was calculated as the percentage of C3b-FITC positive beads

multiplied by the geometric mean fluorescent intensity of FITC in this population less the no antibody or heat inactivated controls.

Antibody prophylaxis - murine model of infection

For evaluating the prophylactic efficacy of mAbs, 12-month old female BALB/c mice (BALB/cAnHsd; Envigo, stock number 047) were treated with 200 µg mAb intraperitoneally (i.p.) 12 hours prior to virus inoculation. The next day, mice were administered intranasally with $1x10^3$ PFU or $1x10^4$PFU of SARS-CoV-2 MA10, respectively. Mice were monitored daily for weight loss, morbidity, and mortality, and after four days, mice were sacrificed and lung tissue was harvested for viral titer as measured by plaque assays. One lung lobe was taken for pathological analysis and the other lobe was processed for qPCR and viral load determination as previously described (Leist et al., 2020). For viral plaque assays, the caudal lobe of the right lung was homogenized in PBS, and the tissue homogenate was then serial-diluted onto confluent monolayers of Vero E6 cells, followed by agarose overlay. Plaques were visualized with overlay of Neutral Red dye on day 2 post infection. Gross pulmonary hemorrhage was observed at time of tissue harvest and scored on a scale of 0 (no hemorrhage in any lobe, normal pink healthy lung) to 4 (complete hemorrhage in all lobes of the lung, completely dark red lung).

For viral titer and hemorrhage score comparisons, an ordinary one-way ANOVA test with multiple comparisons was performed using Prism software, GraphPad Prism version 8.0.

ACE2 binding inhibition assay

Wells of 384-well microtiter plates were coated with purified recombinant SARS-CoV-2 S-2P ectoprotein at 4°C overnight. Plates were blocked with 2% non-fat dry milk and 2% normal goat serum in DPBS-T for 1 hr. Purified mAbs were diluted two-fold in blocking buffer starting from 10 µg/mL in triplicate, added to the wells (20 µL/well), and incubated at ambient temperature. Recombinant human ACE2 with a C-terminal FLAG tag protein was added to wells at 2 µg/mL in a 5 µL/well volume (final 0.4 µg/mL concentration of ACE2) without washing of antibody and then incubated for 40 min at ambient temperature. Plates were washed, and bound ACE2 was detected using HRP-conjugated anti-FLAG antibody and TMB substrate. ACE2 binding without antibody served as a control. Experiment was done in biological replicate and technical triplicates, shown is representative of one replicate with positive control mAb COV2-2196 (Zost et al., 2020b).

Identification of residue-level mutants

Potential cross-reactive epitopes were identified based on sequence and structural homology. Reference sequences for each Coronavirus S were obtained either from NCBI for SARS-CoV-2 (YP_009724390.1) and MERS-CoV (YP_009047204.1) or from Uniprot for SARS-CoV (P59594) of the spikes was then obtained using MUSCLE (Madeira et al., 2019) and the amino acid similarity to SARS-CoV-2 at each residue position was calculated using the BLOSUM-62 scoring matrix (Henikoff and Henikoff, 1992). These scores were then used to color each residue position on the SARS-CoV-2 S structure (PDB ID: 6VSB) in PyMOL (Schrodinger, version 2.3.5) in order to visualize surface patches and linear epitopes with structural homology. These conserved regions were then visualized on the other human coronavirus spike structures by retrieving them from the Protein Databank (SARS-CoV: 5X5B, MERS-CoV: 5W9I) and

aligning them to the SARS-CoV-2 S structure. Finally, the residue N165 was part of a conserved surface patches and was mutated to alanine and tested for binding with antibodies. The N709A mutant tested was previously described in Acharya et al., BioRxiv (2020).

CHAPTER III

POTENT NEUTRALIZATION OF SARS-COV-2 VARIANTS OF CONCERN BY AN ANTIBODY WITH AN UNCOMMON GENETIC SIGNATURE AND STRUCTURAL MODE OF SPIKE RECOGNITION

This chapter is adapted from the published manuscript:

Kramer KJ et al. Potent neutralization of SARS-CoV-2 variants of concern by an antibody with an uncommon genetic signature and structural mode of spike recognition. *BioRxiv*. 2021.

Contributions: Nicole Johnson performed cryo-EM grid screening and structural characterization of antibody 54042-4 interaction with SARS-CoV-2 spike. Andrea Shiakolas labeled coronavirus spike antigens with DNA oligo, characterized final purified probes for overstaining by flow cytometry, and performed bioinformatic processing of raw sequencing data. Naveenchandra Suryadevara performed VSV SARS-CoV-2 neutralization assays. Sivakumar Periasamy performed authentic neutralization assays. Nagarajan Raju performed bioinformatic processing as well as structural comparisons between published SARS-CoV-2 antibodies. Jazmean Williams performed shotgun alanine scanning mutagenesis of the SARS-CoV-2 RBD to identify critical residues of 54042-4 antibody binding. Daniel Wrapp performed biolayer interferometry experiments to determine the binding affinity of 54042-4 to the RBD. Seth Zost assisted in the acquisition of GISAID sequencing isolate data as well as oversaw binding competition ELISA experiments. Lauren Walker performed ELISAs of 54042-4 against SARS-CoV-2 S. Steven Wall performed epitope mapping ELISAs against subunit domains as well as RBD domain mutants. Clinton Holt performed structural analysis of the epitope and paratope interactions of SARS-CoV-2 RBD and 54042-4. Ching-Lin Hsieh designed the plasmids for the SARS-CoV-2 Alpha and Beta spike constructs used for ELISA. Rachel Sutton performed competition ELISAs.

Ariana Paulo performed maxiprep DNA isolations as well as purified recombinant 54042-4 antibody. Jason McLellan performed structural characterization of the binding mode of 54042-4 to the RBD. Ivelin Georgiev performed structural comparisons between 54042-4 and published SARS-CoV-2 antibodies. Ivelin Georgiev, Nicole Johnson, Jason McLellan and I wrote the manuscript.

INTRODUCTION

The COVID-19 pandemic caused by a novel coronavirus from the *Sarbecovirus* genus, SARS-CoV-2, spawned an unprecedented global research effort dedicated to therapeutic countermeasure development, resulting in rapid US FDA Emergency Use Authorization (EUA) for vaccines and monoclonal antibodies (Jones et al., 2021; Weinreich et al., 2021). The primary target for vaccine and antibody therapeutic development is the SARS-CoV-2 spike (S) protein, which facilitates host-cell attachment and entry (Wrapp et al., 2020). The emergence of distinct viral lineages that accumulate substitutions in the S protein pose a significant threat to the countermeasures currently approved for clinical use (Chen et al., 2021c; Wang et al., 2021a). Continued genomic surveillance and persistent efforts to identify antibodies with distinct binding modes and mechanisms of action are crucial to maintain availability of therapeutics in the event of further neutralization-escape by SARS-CoV-2 variants of concerns (VOCs).

SARS-CoV-2 spike is a class I viral fusion protein that is a trimer of heterodimers composed of S1 and S2 subunits (Wrapp et al., 2020). S1, which includes both the receptor-binding domain (RBD) and the N-terminal domain (NTD), initiates attachment to the receptor angiotensin-converting enzyme 2 (ACE2), whereas S2 drives membrane fusion by refolding from a prefusion to postfusion conformation (Li, 2016; Tortorici and Veesler, 2019). The primary contact of ACE2 and spike is in the RBD of the S1 subunit, which is composed of a receptor binding motif (RBM) and RBD core. The three RBDs within each spike can adopt an ACE2-accessible “up” conformation and an ACE2-inaccessible “down” conformation via a hinge-like motion (Shang et al., 2020). As a result, the RBD serves as the dominant target of neutralizing antibodies via antagonism of ACE2 binding (Piccoli et al., 2020), although other neutralizing epitopes have been identified (Brouwer et al., 2020; Chi et al., 2020; Suryadevara et al., 2021; Zost et al., 2020b).

Neutralizing antibodies targeting the RBD have been characterized extensively and partition into different classes based on binding mode, ACE2 interface overlap, and cross-reactivity with other *Sarbecoviruses*. For example, neutralizing antibodies predominantly encoded by IGHV3-53 and IGHV3-66 have epitopes directly covering the ACE2 interaction footprint in the RBM (Yuan et al., 2020a). Examples of this class of antibodies are clinical EUA candidates REGN10933 and COV2-2196 (Hansen et al., 2020; Zost et al., 2020b). Antibodies that bind the RBM but are more distal to the ACE2 interface form another distinct class that includes REGN10987 and COV2-2130 (Dong et al., 2021; Hansen et al., 2020). Additionally, antibodies such as S309, CR3022 and ADG-2 that cross-react with other coronaviruses comprise a more diverse group that target conserved residues in the RBD-core (Pinto et al., 2020; Wec et al., 2020a; Yuan et al., 2020b).

The continued transmission of SARS-CoV-2 in the human population has led to the evolution of VOCs with increased transmissibility and resistance to available medical countermeasures, including to some RBD-directed monoclonal antibodies (Alpert et al., 2021; Chen et al., 2021c; Kuzmina et al., 2021). Some of the most consequential amino acid substitutions observed so far have occurred in the RBD, particularly N501Y in the B.1.1.7 (Alpha), B.1.351 (Beta), and P.1 (Gamma) lineages, and the additional combination of K417N/T and E484K in the Gamma and Beta lineages. The L452R substitution, detected in both the B.1.429 (Epsilon) and B.1.617.2 (Delta) variants also permits escape to monoclonal antibodies and a reduction in neutralization titer in comparison to USA-WA1 in vaccinees as well as individuals recovered from COVID-19 infection(McCallum et al., 2021). Notably, the Epsilon lineage also contains substitutions (S13I and W152C) that disrupt the conformation of the NTD, resulting in the loss of numerous published NTD-directed SARS-CoV-2 neutralizing antibodies (McCallum et al., 2021). N501Y is thought to increase affinity for ACE2 (Starr et al., 2020), potentially resulting in increased infectivity, whereas E484K disrupts the antigenic landscape of the RBD that can lead to

substantial decreases in neutralization titers (Hoffmann et al., 2021; Wang et al., 2021a). In some cases, SARS-CoV-2 VOCs also escape neutralization by polyclonal antibodies in the serum from vaccine recipients and individuals previously infected with SARS-CoV-2 (Chen et al., 2021c; McCallum et al., 2021; Wang et al., 2021a). These observations highlight the critical need for a wide range of potently neutralizing antibodies that are not sensitive to substitutions arising in VOCs.

To address this challenge, we applied LIBRA-seq, a recently developed antibody-discovery technology (Setliff et al., 2019a; Shiakolas et al., 2021b), to interrogate the B cell repertoire of an individual who had recovered from COVID-19. Our efforts led to the discovery of a potently neutralizing antibody, designated 54042-4, which uses an uncommon genetic signature and distinct structural mode of SARS-CoV-2 RBD recognition to maintain neutralization potency to known VOCs. Antibody 54042-4 therefore may serve as a viable candidate for further prophylactic or therapeutic development for protection against a broad range of SARS-CoV-2 variants.

RESULTS

Identification of SARS-CoV-2-neutralizing antibodies by LIBRA-seq

To identify SARS-CoV-2 S-directed antibodies, we utilized LIBRA-seq (Linking B Cell receptor to antigen specificity through sequencing), a technology that enables high-throughput simultaneous determination of B cell receptor sequence and antigen reactivity at the single-cell level, expediting the process of lead candidate selection and characterization (Setliff et al., 2019a; Shiakolas et al., 2021b). The LIBRA-seq antigen-screening library included SARS-CoV-2 and SARS-CoV-2 D614G spikes stabilized in a prefusion conformation (Hsieh et al., 2020), along with antigens from other coronaviruses including SARS-CoV S, MERS-CoV S, HCoV-

OC43 S, HCoV-229E S, HCoV-NL63 S, SARS-CoV-2 RBD, SARS-CoV RBD, and MERS-CoV RBD, as well as negative-control antigens ZM197 HIV-1 Env and influenza hemagglutinin (HA) NC99. Antigen-specific B cells were isolated from a donor with potently neutralizing antibodies in serum (1:258 NT_{50}) three months after infection confirmed by nasal swab RT-PCR testing for SARS-CoV-2 (**Figures 3-1A, 1B**). Of the 73 IgG^+ B cells with high LIBRA-seq scores (≥1) for SARS-CoV-2 S (**Figure 3-1D**) we chose nine lead candidates with diverse sequence characteristics, CDRH3 length, and germline V gene usage for characterization as recombinant monoclonal antibodies (**Figure 3-1C, Figure 3-1F**). Binding to SARS-CoV-2 S by ELISA was confirmed for eight of these antibodies, with the only exception being antibody 54042-2, in agreement with its lower LIBRA-seq score (**Figure 3-1F, 3-1C, 3-2A**). Five of these antibodies showed SARS-CoV-2 neutralization activity in a high-throughput neutralization screen using a live chimeric VSV displaying SARS-CoV-2 spike protein (Case et al., 2020) (**Figure 3-1E**). None of the antibodies showed neutralization against VSV SARS-CoV. Further, the five neutralizing antibodies did not show binding cross-reactivity to other coronavirus antigens in the screening panel, with the exception of SARS-CoV (**Figure 3-2B**). Full dose-response neutralization curves in the chimeric VSV assay were obtained for four of these five antibodies, with antibody 54042-4 showing the best potency, at a half-maximal inhibitory concentration (IC_{50}) of 9 ng/mL (**Figure 3-1E**).

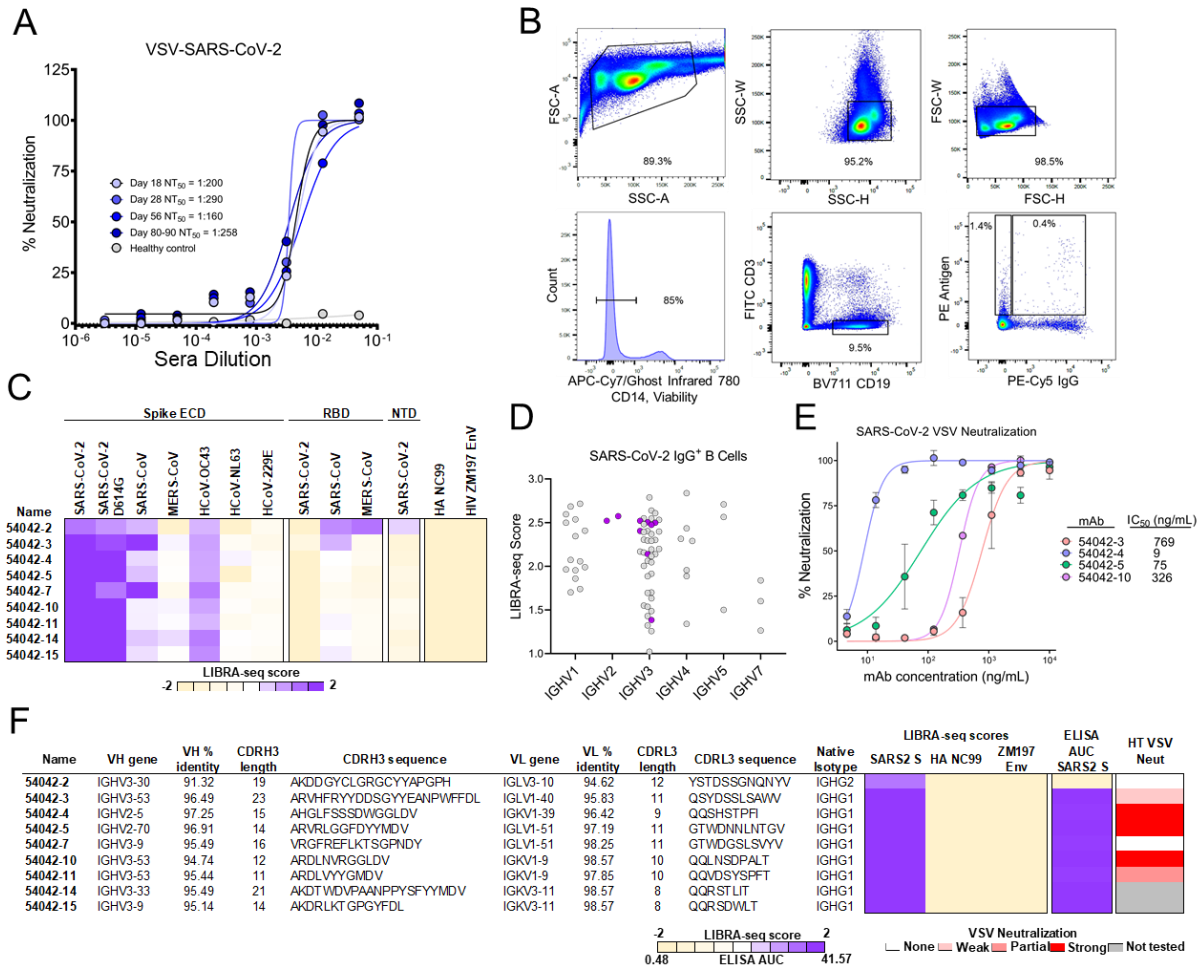

Name	VH gene	VH % identity	CDRH3 length	CDRH3 sequence	VL gene	VL % identity	CDRL3 length	CDRL3 sequence	Native Isotype
54042-2	IGHV3-30	91.32	19	AKDDGYCLGRGCYYAPGPH	IGLV3-10	94.62	12	YSTDSSGNQNYV	IGHG2
54042-3	IGHV3-53	96.49	23	ARVHFRYYDDSGYYEANPWFFDL	IGLV1-40	95.83	11	QSYDSSLSAWV	IGHG1
54042-4	IGHV2-5	97.25	15	AHGLFSSSDWGGLDV	IGKV1-39	96.42	9	QQSHSTPFI	IGHG1
54042-5	IGHV2-70	96.91	14	ARVRLGGFDYYMDV	IGLV1-51	97.19	11	GTWDNNLNTGV	IGHG1
54042-7	IGHV3-9	95.49	16	VRGFREFLKTSGPNDY	IGLV1-51	98.25	11	GTWDGSLSVYV	IGHG1
54042-10	IGHV3-53	94.74	12	ARDLNVRGGLDV	IGKV1-9	98.57	10	QQLNSDPALT	IGHG1
54042-11	IGHV3-53	95.44	11	ARDLVYYGMDV	IGKV1-9	97.85	10	QQVDSYSPFT	IGHG1
54042-14	IGHV3-33	95.49	21	AKDTWDVPAANPPYSFYYMDV	IGKV3-11	98.57	8	QQRSTLIT	IGHG1
54042-15	IGHV3-9	95.14	14	AKDRLKTGPGYFDL	IGKV3-11	98.57	8	QQRSDWLT	IGHG1

Figure 3-1: **Identification and characterization of SARS-CoV-2 antibodies isolated using LIBRA-seq. (A)** VSV-SARS-CoV-2 capacity of serum is displayed from time points at day 18, day 28, day 56, and days 80-90 post-COVID-19 infection. **(B)** Gating scheme for fluorescent-activated cell sorting of recovered COVID-19 individual. Cells were stained with Ghost Red 780, CD14-APC-Cy7, CD3-FITC, CD19-BV711, and IgG-PE-Cy5 along with a DNA-barcoded antigen screening library. To detect antigen-positive B cells, cells were washed and treated with a streptavidin-PE secondary stain. Gates as drawn are based on gates used during the sort, and percentages from the sort are listed. **(C)** LIBRA-seq scores for SARS-CoV-2 S, SARS-CoV-2 S D614G, SARS-CoV S, MERS-CoV S, HCoV-OC43 S, HCoV-229E S, HCoV-NL63 S, SARS-CoV-2 RBD, SARS-CoV RBD, and MERS-CoV RBD, as well as negative-control antigens ZM197 Env and hemagglutinin (HA) NC99 are shown. LIBRA-seq scores for each antigen are displayed as a heatmap with a LIBRA-seq score of -2 displayed as light yellow, 0 as white, and 2 in purple; in this heatmap, scores lower or higher than that range are shown as -2 and 2, respectively. **(D)** Variable heavy gene usage (x-axis) as a function of IgG+ B cells with a SARS-CoV-2 spike LIBRA-seq score (≥1) (y-axis). The nine lead candidates are highlighted in purple. **(E)** RTCA VSV-SARS-CoV-2 neutralization by lead candidate antibodies. IC_{50} values are calculated by non-linear regression analysis by GraphPad Prism software. **(F)** Sequence characteristics and antigen specificity of nine lead candidate antibodies from a recovered COVID-19 donor. Percent identity is calculated at the nucleotide level, and CDR length and sequences are displayed at the amino acid level. LIBRA-seq scores for each antigen are displayed as a heatmap with a LIBRA-seq score of -2 displayed as light yellow, 0 as white, and 2 in purple; in this heatmap scores lower or higher than that range are shown as -2 and 2, respectively. ELISA binding data for SARS-CoV-2 S are displayed as a heatmap of the AUC analysis calculated from (**Figure 3-2A**).

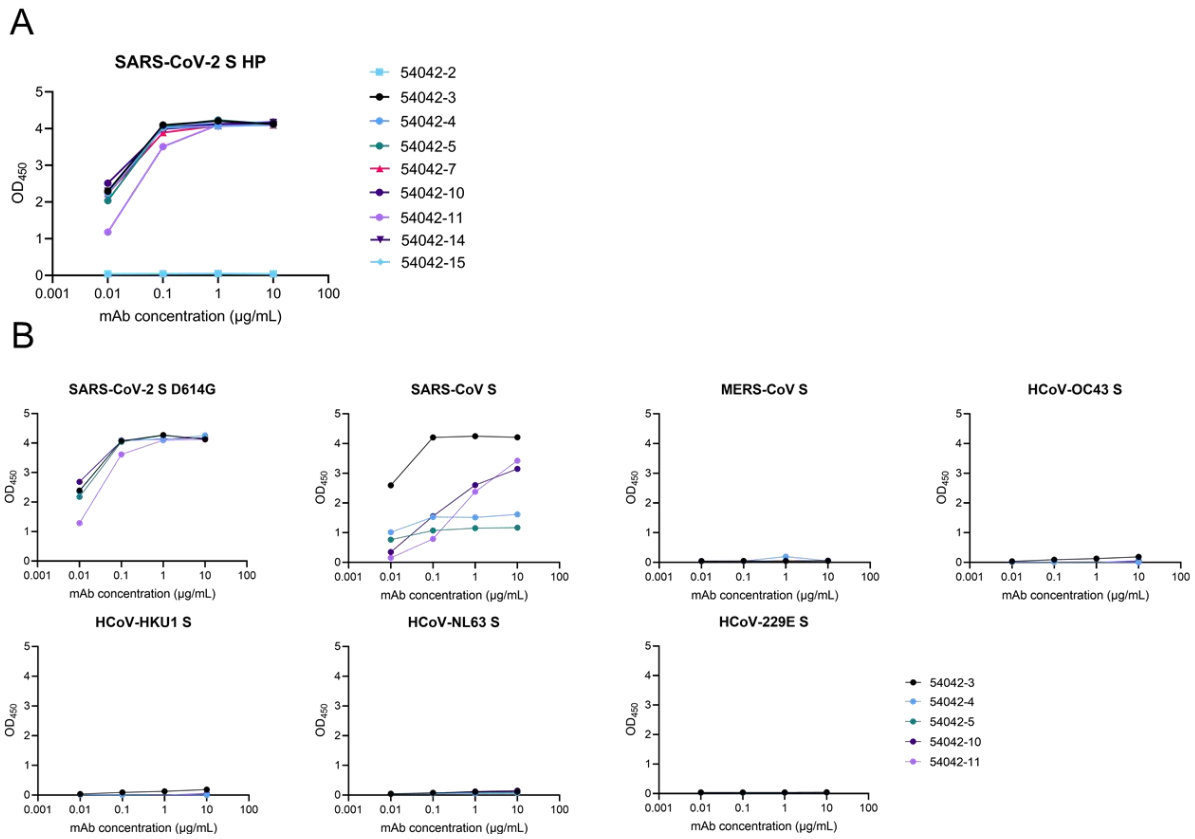

Figure 3-2: Characterization of SARS-CoV-2 antibodies identified by LIBRA-seq. (A) ELISA binding data of candidate antibodies identified by LIBRA-seq against SARS-CoV-2 S HP. The optical density at 450 nm (y-axis) is depicted as a function of antibody concentration (x-axis). **(B)** ELISA binding data of candidate antibodies identified by LIBRA-seq against SARS-CoV-2 S HP. The optical density at 450 nm (y-axis) is depicted as a function of antibody concentration (x-axis).

Antibody 54042-4 targets the SARS-CoV-2 receptor-binding domain

Because of the potent (≤ 10 ng/mL) virus neutralization observed for 54042-4, we selected this antibody for further characterization. ELISAs performed with purified RBD, NTD, S1, and S2 proteins revealed 54042-4 IgG bound to the SARS-CoV-2 S1 subunit as well as the RBD (**Figure 3-3A-3-3B**). To determine the affinity of the antibody-antigen binding interaction, biolayer interferometry experiments were performed by measuring the association and dissociation kinetics of immobilized 54042-4 IgG binding to a soluble protein comprising the RBD and subdomain-1 (SD1) of the SARS-CoV-2 S protein, and curve-fitting resulted in a calculated K_D of 21.8 nM (**Figure 3-3C**). Given the neutralization potency of 9 ng/mL (60 pM), these data suggest that the IgG avidly binds to the S protein on the virion surface. To assess whether 54042-4 neutralizes viral infection by directly competing with ACE2, a receptor-blocking assay was performed by testing competition of 54042-4 with soluble ACE2 for binding to SARS-CoV-2 S. The results demonstrated that 54042-4 inhibits interaction of ACE2 to SARS-CoV-2 S protein, unlike the control antibody CR3022, an extensively characterized SARS-CoV antibody that binds a cryptic epitope in the RBD of both SARS-CoV and SARS-CoV-2 (Yuan et al., 2020b), and the influenza HA-specific 3602-1707 antibody (Setliff et al., 2019a) (**Figure 3-3D**). Next, we performed competition ELISAs to determine if 54042-4 competes for binding with three other RBD-directed antibodies with distinct epitopes. These antibodies included COV2-2196 and COV2-2130, which form the basis of AZD7442, an antibody cocktail currently under investigation in clinical trials for COVID-19 treatment and prevention (ClinicalTrials.gov Identifiers: NCT04625725, NCT04723394, NCT04518410, and NCT04501978) and CR3022. The competition experiment showed that 54042-4 competed for binding to SARS-CoV-2 S protein with COV2-2130 but not COV2-2196 or CR3022 (**Figure 3-3E**). Together, these results suggest that 54042-4 targets an epitope on SARS-CoV-2 RBD that at least partially overlaps with the binding sites for both ACE2 and other potently neutralizing RBD-directed antibodies.

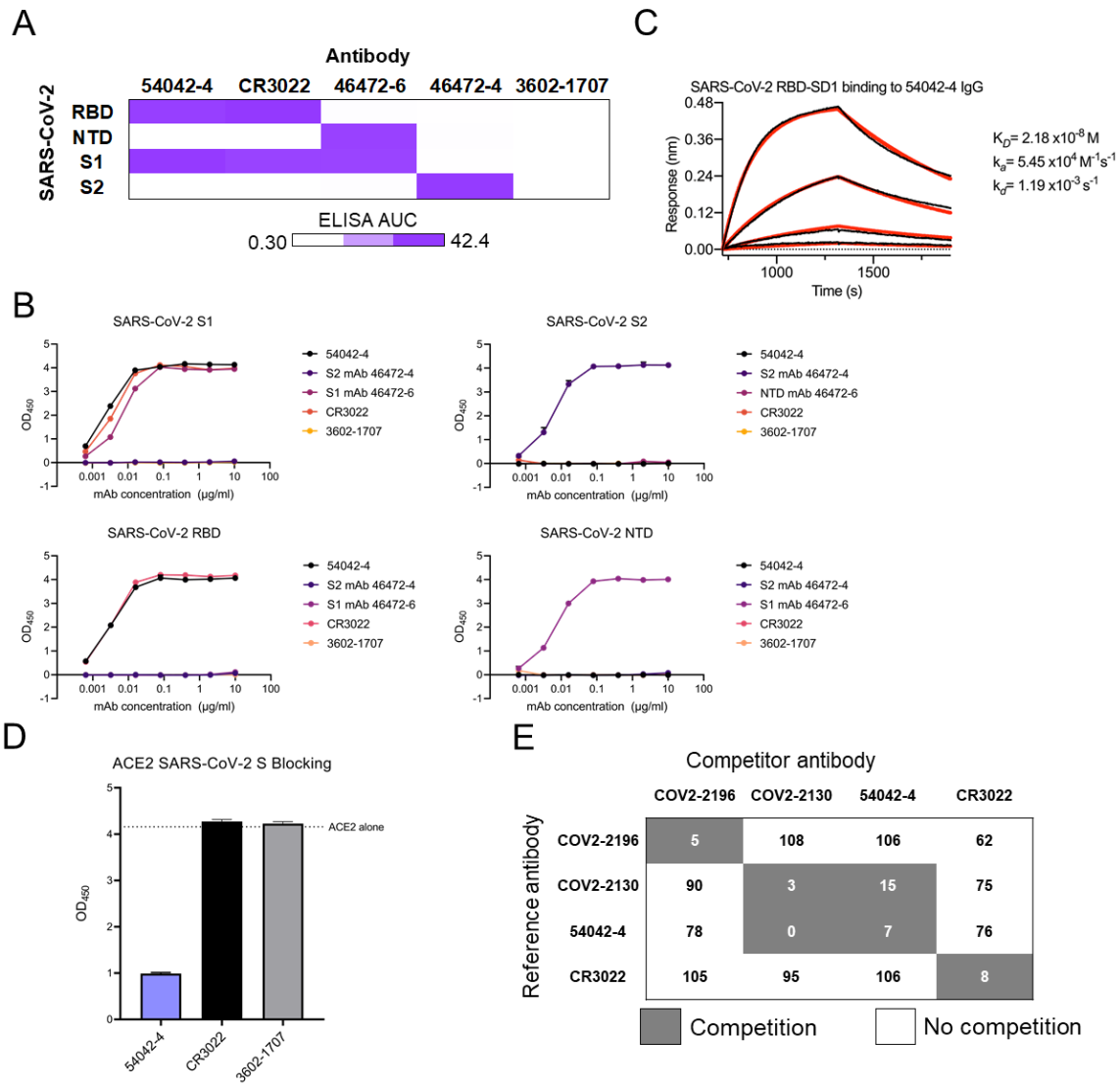

Figure 3-3: **Identification and characterization of SARS-CoV-2 antibodies isolated using LIBRA-seq. (A)** ELISA binding values against SARS-CoV-2 subdomains are displayed as a heatmap of AUC values calculated from the data in (**3-3B**). Antibodies CR3022, 46472-6, 46472-4 were used as positive controls for the RBD, NTD, and S2 antigens, respectively (Shiakolas et al., 2021; Yuan et al., 2020b). 3602-1707 was included as an influenza HA-specific negative control antibody (Setliff et al., 2019). **(B)** ELISA binding data against SARS-CoV-2 subdomains RBD, NTD, S1, and S2 are shown. CR3022 was used as a positive control RBD-directed antibody(Yuan et al., 2020a) whereas 46472-4 and 46472-6 antibodies were used as positive controls for the S2 and NTD, respectively (Shiakolas et al., 2021). The HA-specific 3602-1707 antibody was used as a negative control. **(C)** A biolayer interferometry sensogram that shows binding to recombinant SARS-CoV-2 RBD-SD1. Binding data are depicted by the black lines and the best fit line of the data to a 1:1 binding model is shown in red. **(D)** SARS-CoV-2/ACE2 inhibition ELISA is shown for 54042-4, SARS-CoV-2 antibody CR3022 and negative control HA-specific antibody 3602-1707. For each antibody, the ACE2 binding signal is depicted on the y-axis, in comparison to ACE2-only binding to SARS-COV-2 spike is shown as a dotted line. **(E)** Competition ELISA of 54042-4 with antibodies COV2-2196, COV2-2130, and CR3022. Values in white indicate no competition (presence of competing antibody reduced reference antibody binding by less than 30%) and values in dark grey indicate competition (presence of competing antibody reduced reference antibody binding by more than 60%).

54042-4 binds the apex of the SARS-CoV-2 RBD in the down conformation

To gain a better understanding of the recognition of SARS-CoV-2 S by antibody 54042-4, we determined a 2.7 Å resolution cryo-EM structure of the 54042-4 antigen-binding fragments (Fabs) bound to the SARS-CoV-2 S extracellular domain (ECD) modified so that all three RBDs were disulfide-locked in the down conformation (Henderson et al., 2020) (**Figure 3-4A**). Local refinement of one RBD bound to a 54042-4 Fab was performed to improve the interpretability of the map at the binding interface, resulting in a local 3D reconstruction with a resolution of 2.8 Å (**Figure 3-4B**). The structure revealed that 54042-4 forms an extensive interface with the RBD, making contacts through the complementarity determining regions (CDRs) CDRL1, CDRL3, and all three CDRs of the heavy chain, to form a clamp around the apex of the RBM saddle (**Figure 3-4C, 3-4D, and Figure 3-5A, 3-5B**). The primary interactions involve RBD residues 439–450, with a network of hydrogen bonds between the 54042-4 heavy chain and RBD residues 443–447 (**Figure 3-4C**). From CDRH3, Ser99 forms a hydrogen bond with RBD residue Ser443, and a hydrogen bond is formed between the mainchain atoms of Phe97 and Val445. From CDRH2, Asp56 forms a hydrogen bond and salt bridge with Lys444, whereas Arg58 forms hydrogen bonds with mainchain atoms from Gly446 and Gly447. The CDRH1 contributes a lone residue, Ile32, to the binding interface, forming minor contacts near Leu441. The 54042-4 light chain surrounds the opposite side of this RBD region, mediating interactions primarily through hydrophobic contacts formed by CDRL1 and CDRL3 near RBD residue Val445 (**Figure 3-4D**). Additional light chain contacts are made with residues 498–500 of the RBD, including a hydrogen bond between His92 of CDRL3 and Thr500, and hydrophobic interactions involving CDRL1 Phe30 and Tyr32. Although 54042-4 binds all three RBDs locked in the down position, the epitope region is equally accessible when the RBD is in the up position. Additionally, the epitope lies outside the RBD hinge region, makes no additional contacts with the spike trimer,

and partially overlaps the ACE2 binding site. Therefore, the mechanism of neutralization likely involves inhibition of ACE2 binding rather than locking the RBDs in the down conformation.

Notably, the complex structure indicated that 54042-4 does not make substantial contact with a number of spike substitutions associated with current VOCs. For example, RBD residue Asn501 (present as Tyr501 in several VOCs, including Alpha, Beta, and Gamma) lies just outside of the 54042-4 epitope, whereas the Cα atoms of Glu484 (present as Lys484 or Gln484 in, e.g., Beta, Gamma, and B.1.617 (Kappa)) and Leu452 (present as Arg452 in Epsilon and Delta) are approximately 18 and 14 Å away from the Cα atoms of the nearest 54042-4 residue, respectively (**Figure 3-4B**). Furthermore, the substitution Gly614, which is found in all current VOCs is outside of the RBD, is approximately 75 Å from the nearest 54042-4 residue.

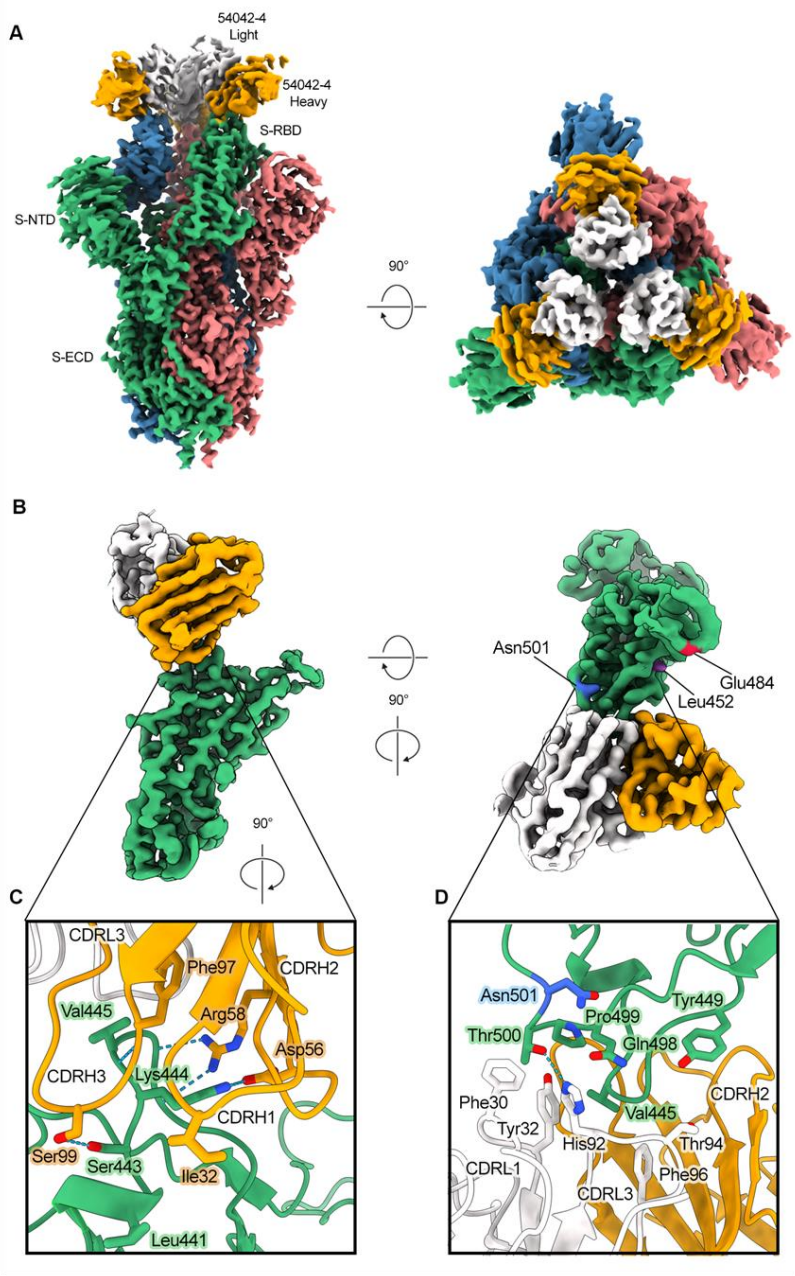

Figure 3-4: **Atomic resolution of 54042-4 binding mode to SARS-CoV-2 S. (A)** 3D reconstructions of side and top views of Fab 54042-4 bound to SARS-CoV-2 spike. **(B)** Focused refinement maps showing the 54042-4 epitope at the apex of the RBM in the down position (left). Top-down view of the 54042-4 epitope showing heavy and light chain contacts, as well as residues outside of the binding interface that are mutated in circulating VOCs (right). **(C)** The 54042-4 heavy chain binds to RBD residues 443–447 primarily through a network of hydrogen bonds involving CDRH2 and CDRH3 and hydrophobic contacts involving Ile32 of CRDH1. **(D)** The 54042-4 light chain contacts RBD residues 498-500 through a hydrogen bond between Thr500 and His92 of CDRL3 and hydrophobic contacts involving Phe30 and Tyr32 of CDRL1

A

54042-4 epitope on SARS-CoV-2 S

S residue #	AA	Buried surface area
346	R	23
439	N	6
440	N	26
441	L	28
443	S	21
444	K	108
445	V	145
446	G	61
447	G	10
448	N	1
449	Y	33
450	N	48
498	Q	34
499	P	35
500	T	82

B

54042-4 paratope on SARS-CoV-2 S

	Ab residue #	AA	Buried surface area
Heavy chain	32	I	12
	52	Y	34
	53	W	42
	54	D	47
	56	D	42
	58	R	61
	97	F	28
	98	S	11
	99	S	99
	100A	D	2
	100B	W	2
	100C	G	2
Light chain	30	F	35
	32	Y	55
	91	S	10
	92	H	73
	93	S	2
	94	T	20
	96	F	6

Figure 3-5: **Epitope and paratope residues of 54042-4 interaction with the SARS-CoV-2 RBD. (A)** SARS-CoV-2 spike residues comprising the epitope of 54042-4 are shown with their associated buried surface area (Å^2). **(B)** 54042-4 residues comprising the antibody paratope against SARS-CoV-2 spike are shown with their associated buried surface area values (Å^2).

Antibody 54042-4 has an uncommon genetic signature and distinct structural mode of RBD recognition

Public clonotype sequence signatures (those shared by multiple individuals recovered from COVID-19 infection) have been identified for potently neutralizing SARS-CoV-2 antibodies, including antibodies currently in clinical trials or approved for emergency use (Nielsen et al., 2020; Yuan et al., 2020a). To investigate whether antibody sequences that are closely related to 54042-4 can be identified among known SARS-CoV-2 antibodies, we searched the CoV-AbDab database that contains paired heavy-light chain sequences of coronavirus antibodies (Raybould et al., 2021). Notably, only 0.5% of antibodies in the database used the same combination of *IGHV2-5* heavy and *IGKV1-39* light chain germline V genes as 54042-4. Further, antibodies with high sequence identity to the 54042-4 CDRH3 and CDRL3 were not identified, whether or not the search was restricted to the *IGHV2-5* heavy chain and *IGKV1-39* light chain genes (**Figure 3-6A**).

Next, we compared the 54042-4 epitope to the epitopes of other known SARS-CoV-2 antibodies by computing pairwise correlations between the antibody-antigen buried surface areas for 54042-4 against a set of 99 publicly available SARS-CoV-2 antibody-antigen structures from the Protein Data Bank, as well as the structure of antibody COV2-2130 in complex with the SARS-CoV-2 RBD (**Figure 3-7**). The results revealed significant positive correlations with only six other antibodies: REGN10987 (Hansen et al., 2020), 2-7 (Liu et al., 2020), C119 (Barnes et al., 2020), COVOX-75 (Dejnirattisai et al., 2021), COV2-2130 (Zost et al., 2020b) (in agreement with the observed binding competition with 54042-4, **Figure 3-3D**), and LY-CoV1404 (Westendorf et al., 2021) (**Figure 3-6B**). However, of these six antibodies, COVOX-75 has been reported as not a potent neutralizer (Dejnirattisai et al., 2021). C119 makes substantial contact with residues Glu484 and Asn501, indicating potential susceptibility of this antibody to substitutions at those positions that are currently associated with relatively high substitution rates (**Figure 3-6C**) and are present in several circulating SARS-CoV-2 VOCs (Alpert et al., 2021; Tegally et al., 2021). Further, both C119 and COVOX-75, as well as COV2-2130, have substantial buried surface area interactions with a number of additional residues compared to those in the epitope of 54042-4 (**Figure 3-6C**), suggesting that these three antibodies could be susceptible to additional potential spike substitutions that would not directly affect antigen interactions with 54042-4.

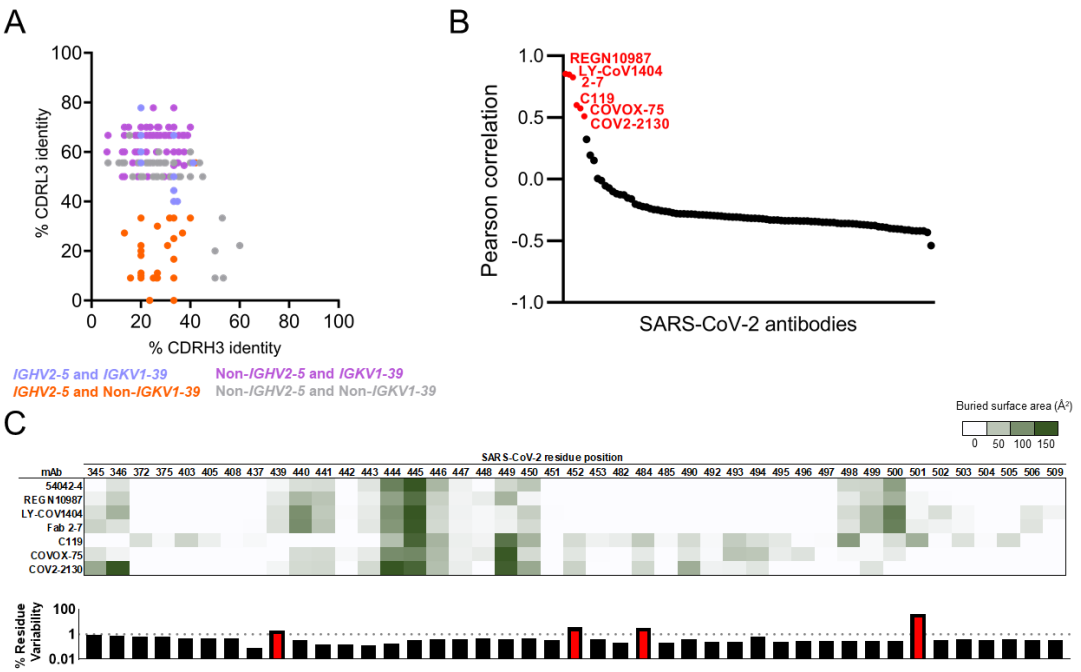

Figure 3-6: **Sequence and structural comparison of 54042-4 to known SARS-CoV-2 antibodies. (A)** Amino acid CDRH3 identity to 54042-4 (x-axis) is plotted against CDRL3 identity to 54042-4 (y-axis) for paired heavy and light chain sequences obtained from the CoV-AbDab database(Raybould et al., 2021). Antibodies using the same heavy and light chain germline gene as 54042-4 (*IGHV2-5* and *IGKV1-39*) are shown in light blue. Antibodies using the *IGHV2-5* heavy chain gene and a non-*IGKV1-39* light chain gene are shown in orange. Additionally, antibodies using a non-*IGHV2-5* heavy chain gene and the *IGKV1-39* light chain gene, with CDRH3 or CDRL3 identity to 54042-4 of at least 50%, are highlighted in purple. Finally, antibodies that do not use *IGHV2-5* or *IGKV1-39*, but that have at least 50% identity to CDRH3 or CDRL3 of 54042-4, are shown in grey. **(B)** Pearson correlation of epitopes of known SARS-CoV-2 antibodies (**Figure 3-7**) in comparison to 54042-4 antibody, with the six antibodies showing a statistically significant ($p<0.05$) positive correlation highlighted in red. **(C)** Heatmap (top) depicting buried surface area (Å^2) at the SARS-CoV-2 RBD interface for the six antibodies with highest epitope correlations with 54042-4. Bar graph (bottom) showing the frequency (%) of substitutions at each given residue position in log scale, with a dashed line at 1% and residue positions with a frequency greater than 1% highlighted in red.

PDB-id	Pearson Correlation	PDB-id	Pearson Correlation	PDB-id	Pearson Correlation
6XDG	0.8543	7JMP	-0.2818	7KLG	-0.3426
7MMO	0.8483	7BEK	-0.2837	6XDG	-0.3436
7LSS	0.8251	7KFV	-0.2853	7BYR	-0.3460
7K8W	0.6007	7JX3	-0.2880	7DEU	-0.3490
7BEN	0.5747	7BEN	-0.2892	7D00	-0.3496
7L7E	0.5098	7BZ5	-0.2911	7CZR	-0.3504
7K8V	0.3231	6XKQ	-0.2918	7CWO	-0.3516
6XKP	0.1940	7BEH	-0.2946	7BEP	-0.3573
7JX3	0.1510	7CJF	-0.2976	7K9Z	-0.3586
7BWJ	0.0041	7CHB	-0.2985	7BEL	-0.3588
7CHH	-0.0111	7CZQ	-0.3023	7K8M	-0.3596
7LS9	-0.0539	7KFY	-0.3058	6XC3	-0.3604
7CZT	-0.0724	7DD8	-0.3063	7EAM	-0.3625
7K8Z	-0.1003	7K45	-0.3076	7CDI	-0.3676
7CZX	-0.1183	7D03	-0.3087	6XE1	-0.3701
7LY2	-0.1263	7B3O	-0.3126	7D0D	-0.3704
7DK4	-0.1278	7BEL	-0.3156	7LM8	-0.3743
7K8Y	-0.1519	7DPM	-0.3161	7KZB	-0.3758
7K8U	-0.1590	7NDB	-0.3172	6XC7	-0.3852
7CDJ	-0.2032	6XC3	-0.3198	7EAN	-0.3875
7K90	-0.2118	7BEI	-0.3200	7KS9	-0.3912
7L56	-0.2217	7KMI	-0.3251	7JX3	-0.3998
7L5B	-0.2261	7JMO	-0.3301	7KMH	-0.4010
7LJR	-0.2380	7CZU	-0.3303	7LAA	-0.4034
7K8S	-0.2471	7CHF	-0.3316	7JVA	-0.4056
7CZP	-0.2475	7CZY	-0.3345	7NX6	-0.4105
7JV2	-0.2565	7LM9	-0.3366	7LD1	-0.4112
7ND7	-0.2600	7NEH	-0.3370	7K9Z	-0.4178
7C01	-0.2652	7KLH	-0.3371	6XCM	-0.4192
7KMG	-0.2725	7CZV	-0.3371	7D0C	-0.4197
7CM4	-0.2796	7KFX	-0.3386	7NX8	-0.4204
6XEY	-0.2803	7ND9	-0.3393	7CH5	-0.4317
7KFW	-0.2814	7CAI	-0.3397	7L58	-0.5379

Figure 3-7: Table of PDB IDs used for pearson correlation comparisons of binding mode to 54042-4.

We also observed that while the epitopes of antibodies 2-7, LY-CoV1404, and REGN10987 correlate well with that of 54042-4, these antibodies have distinct angles of antigen approach (**Figure 3-8A**). To quantify this observation, we aligned the RBDs from the 2-7, LY-CoV1404, and REGN10987 complex structures with the RBD from the 54042-4 structure. Using the

antibody coordinates when the respective RBDs were aligned, we computed the root mean square deviations (RMSD) between the C_α atoms in the FWR1-FWR3 regions of the antibody heavy and light chains. This resulted in RMSDs of 16.4 Å, 16.5Å, and 22 Å between 54042-4 versus 2-7, LY-CoV1404, and REGN10987, respectively, confirming the substantial differences in the structural mode of antigen recognition by 54042-4 compared to 2-7, LY-CoV1404, and REGN10987. Although 54042-4 and 2-7 both originate from the same *IGHV2-5* germline gene and share analogous RBD contacts in the CDRH2 region, these antibodies exhibit different CDRH1 and CDRH3 interactions (**Figure 3-8B**) and use a different light chain germline gene (*VK1-39* for 54042-4, and *VL2-14* for 2-7). Interestingly, antibodies 2-7 and LY-CoV1404 use identical heavy and light chain germline genes, and have virtually indistinguishable structural mode of antigen recognition (RMSD, computed as above, of 1.7Å). Notably, all of 2-7, LY-CoV1404, and REGN10987 have greater interactions with RBD residues 439–441 compared to 54042-4, with buried surface areas of 172, 164, 127, and 60 $Å^2$ for 2-7, LY-CoV1404, REGN10987, and 54042-4, respectively (**Figure 3-6C**), suggesting 2-7, LY-CoV1404, and REGN10987 may be more prone to viral escape in that region. Indeed, the N439K substitution is present in several independent SARS-CoV-2 lineages and has been found to affect binding and neutralization by REGN10987 (Thomson et al., 2021).

Together, these data suggest that antibody 54042-4 utilizes an uncommon genetic signature and a distinct structural mode of antigen recognition compared to other known SARS-CoV-2 antibodies.

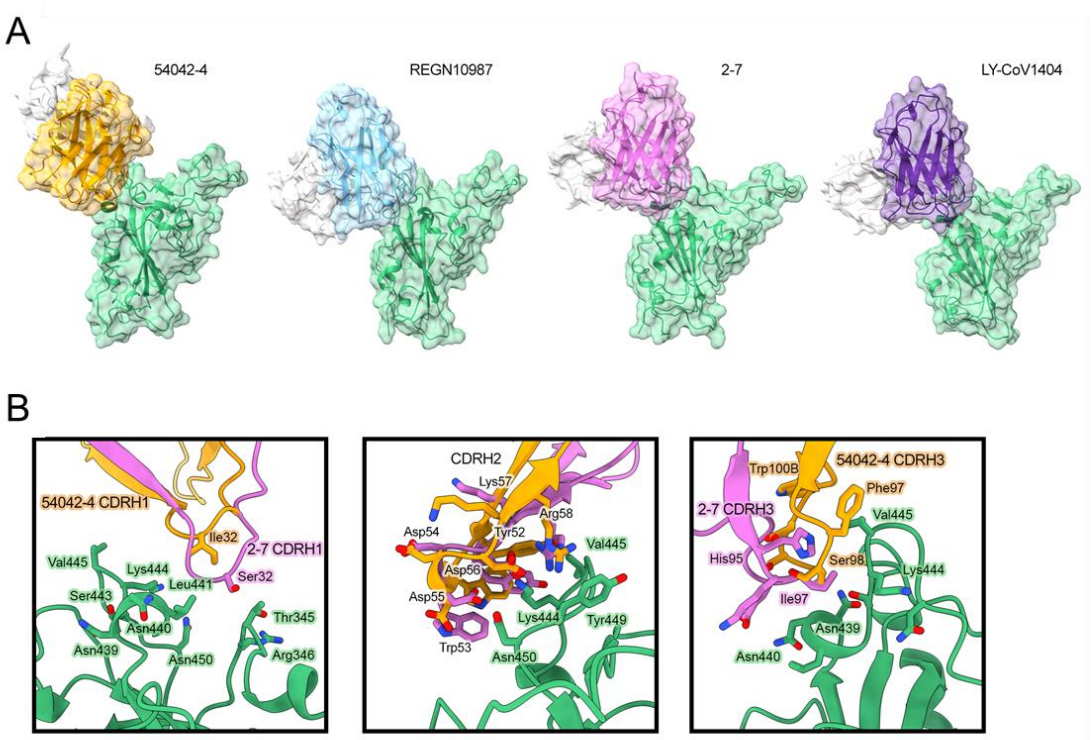

Figure 3-8: **Structural comparison of 54042-4 to known SARS-CoV-2 antibodies. (A)** Distinct angles of approach of antibodies 54042-4 (heavy chain: orange, light chain: white), REGN10987 (heavy chain: blue, light chain: white) (PDB id: 6XDG), 2-7 (heavy chain: pink, light chain: white) (PDB id: 7LSS), and LY-CoV1404 (heavy chain: purple, light chain: white) (PDB id:7MMO) to the SARS-CoV-2 RBD (green). **(B)** Structural comparison of CDRH1, 2, and 3 of antibodies 54042-4 and 2-7. CDRH1 of 2-7 extends further than 54042-4, forming additional contacts with Thr345 and Arg346 of the RBD (left). The CDRH2 region of 2-7 approaches at a different angle, but maintains RBD contacts via Asp56 and Arg58 (center). The CDRH3 contacts of 2-7 and 54042-4 are divergent, with unique CDRH3 residues and RBD interactions (right).

Antibody 54042-4 is not affected by current SARS-CoV-2 VOC substitutions

Next, to identify substitutions capable of disrupting binding to antibody 54042-4, we performed shotgun alanine-scanning mutagenesis of the SARS-CoV-2 RBD (Davidson, 2014). The only tested substitutions that substantially affected binding in comparison to an RBD antibody control were K444A, V445A, G446A, and P499A (**Figure 3-9A)**, which all fall within the 54042-4 epitope (**Figure 3-4C-D, and Figure 3-5**). To assess the functional effect of substitutions within the 54042-4 epitope, we tested neutralization against VSV-SARS-CoV-2 chimeras containing single substitutions at K444R/T/E/N, G446D, or Q498R. These mutants were generated from neutralization escape experiments using saturating concentrations of either COV2-2130

antibody (a 54042-4 competitor, **Figure 3-3E**) or COV2-2499 (a COV2-2130 competitor) (Greaney et al., 2021b). These experiments revealed that the chimeric VSVs with substitutions at Lys444, Gly446, and Gln498 were resistant to neutralization by 54042-4 (**Figure 3-9B**). Together, the alanine-scanning and neutralization experiments indicated that 54042-4 may be sensitive to substitutions at spike residues K444, V445, G446, Q498, and P499. However, analysis of currently circulating SARS-CoV-2 isolates from the GISAID database as of May 6, 2021 (Elbe, 2017) revealed that substitutions at these five residue positions are only present at low levels (**Figure 3-9C**). Further, virtually all of the 54042-4 epitope residues (**Figure 3-5**) are highly conserved in circulating SARS-CoV-2 lineages (**Figure 3-9C**). The only exception is residue N439, which has a substitution frequency of 2.1% (**Figure 3-9C**); however, this residue makes only minimal contacts with antibody 54042-4 (**Figure 3-5**), suggesting that residue N439 may not be critical for 54042-4 recognition of the SARS-CoV-2 spike.

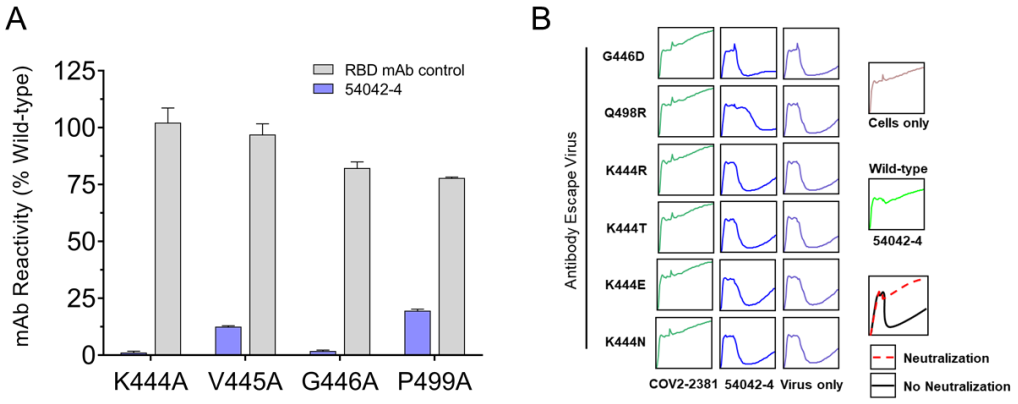

C

54042-4 Epitope Residue	% Conservation
R346	99.183
N439	97.881
N440	99.689
L441	99.846
S443	99.859
K444	99.829
V445	99.676
G446	99.617
G447	99.632
N448	99.564
Y449	99.614
N450	99.570
Q498	99.699
P499	99.693
T500	99.694

Figure 3-9: **Functional characterization of antibody 54042-4. (A)** Binding data of 54042-4 antibody to a shotgun alanine mutagenesis screening library of the SARS-CoV-2 RBD (Wuhan-Hu-1 strain). Residues displayed are the alanine substitutions that resulted in the biggest loss of binding to 54042-4 yet still retained signal with the RBD antibody control. **(B)** Neutralization of VSV SARS-CoV-2 chimera variants harboring specific substitutions. Cell sensograms are shown in boxes corresponding to mutations indicated in each row. Columns (from left to right) are each chimera treated with COV2-2381, 54042-4 and virus only control. Neutralization of 54042-4 of USA-WA1 strain and cells only are indicated on the right. COV2-2381 was chosen as a positive control due to its distinct epitope footprint from the selected mutations. **(C)** 54042-4 epitope residues (non-zero buried surface area on SARS-CoV-2 RBD) with their associated % conservation (the percentage of deposited sequences containing the highest-frequency amino acid at that position) in the GISAID database. The only 54042-4 epitope residue with a % conservation of less than 99%, N439, is highlighted in red.

To investigate the ability of antibody 54042-4 to recognize current SARS-CoV-2 VOCs, we performed ELISAs to test binding of 54042-4 to RBD proteins containing substitutions found in one or more VOCs. These substitutions included K417N found in many isolates in the Beta lineage, as well as E484K (Beta, Gamma), N501Y (Alpha, Beta, Gamma, Delta, Kappa), L452R (Delta, Epsilon) and N439K found in lineages B.1.141 and B.1.258 (Thomson et al., 2021). Notably, antibody 54042-4 bound to these RBD variants at a similar level compared to the binding to the RBD from the Wuhan-1 isolate (**Figure 3-10A, Figure 3-10B**). These results are consistent with the structural observations that 54042-4 makes only minimal contacts with residue N439, and that none of the other RBD substitutions were at residues in the 54042-4 epitope (**Figure 3-5**). Binding of antibody 54042-4 also was not affected in the context of SARS-CoV-2 S ECD proteins that included deletions and substitutions in the S1 domain of the Beta and Alpha VOCs (**Figure 3-10A, Figure 3-10C-D**). Finally, we tested the ability of 54042-4 to neutralize authentic SARS-CoV-2 USA-WA1, Alpha, and Beta, Delta, and Gamma SARS-CoV-2 variants. Consistent with the ELISA data, 54042-4 neutralized each virus potently with IC_{50} values of 3.2, 5.5, 9.7, 1.5, and 3.7, and IC_{80} values of 10, 48, 49, 3.9, and 11.4 ng/mL, respectively (**Figure 3-11A**). Together, these data indicate that 54042-4 can be an effective countermeasure against currently circulating SARS-CoV-2 variants.

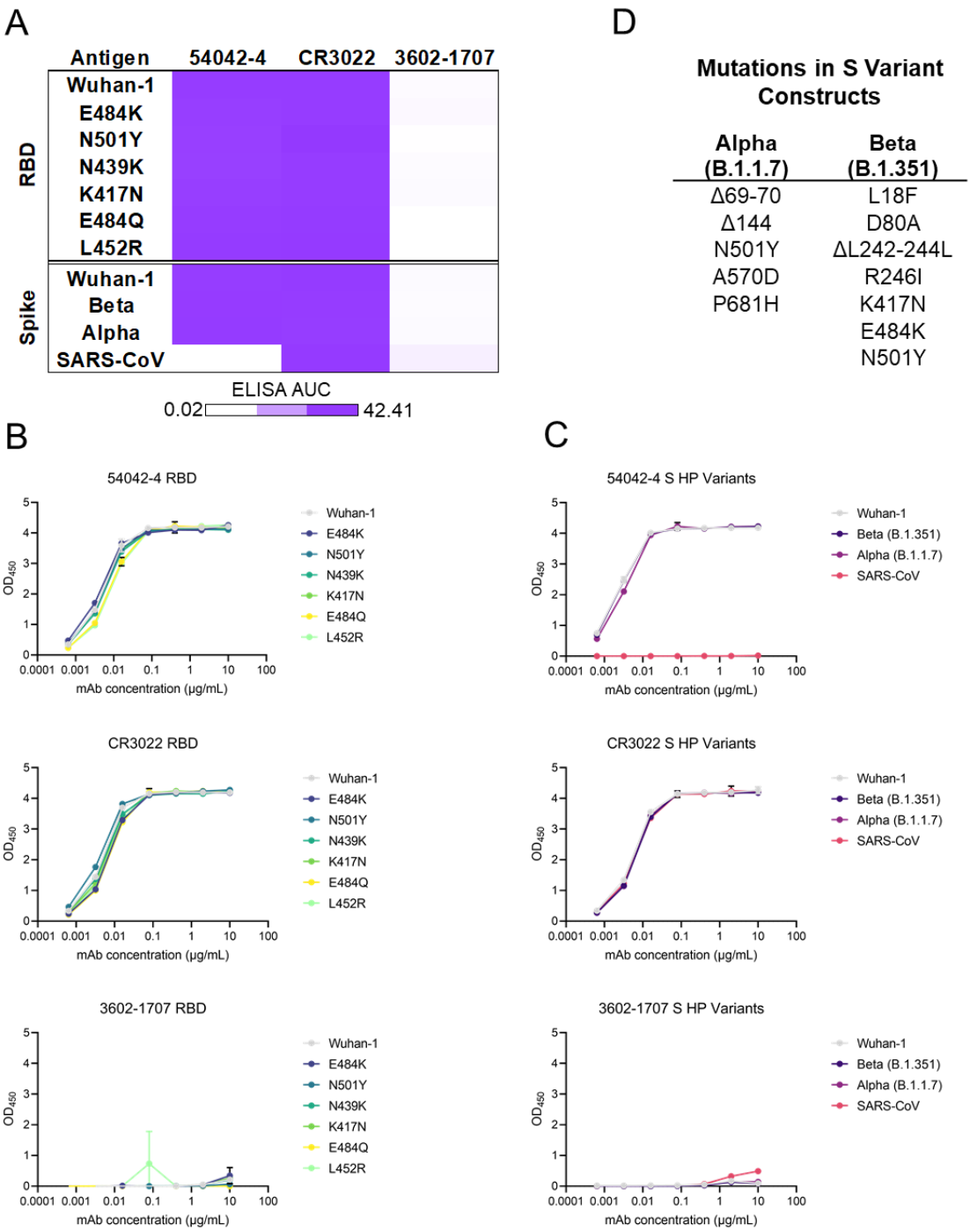

Figure 3-10: **Functional characterization of antibody 54042-4. (A)** ELISA AUC of 54042-4, CR3022, and an influenza HA-specific negative control antibody 3602-1707. AUC is displayed as a heatmap with a value of 0 corresponding to white, 50% maximum as light-purple, and maximum AUC as purple. **(B)** ELISA binding data against SARS-CoV-2 Wuhan-1 RBD and RBDs with substitutions E484K, N501Y, N439K, K417N, E484Q, or L452R. CR3022 was used as a positive control and 3602-1707, an HA-specific antibody, was used as a negative control. **(C)** binding data against SARS-CoV-2 S HP, SARS-CoV S, and SARS-CoV-2 S HP constructs with substitutions in the S1 domain for the Beta, and Alpha variants of concern. CR3022 was used as a positive control and 3602-1707 was used as a negative control antibody. **(D)** The substitutions and deletions present in the Alpha and Beta SARS-CoV-2 S constructs used in the ELISAs depicted in **Figure 3-10C.**

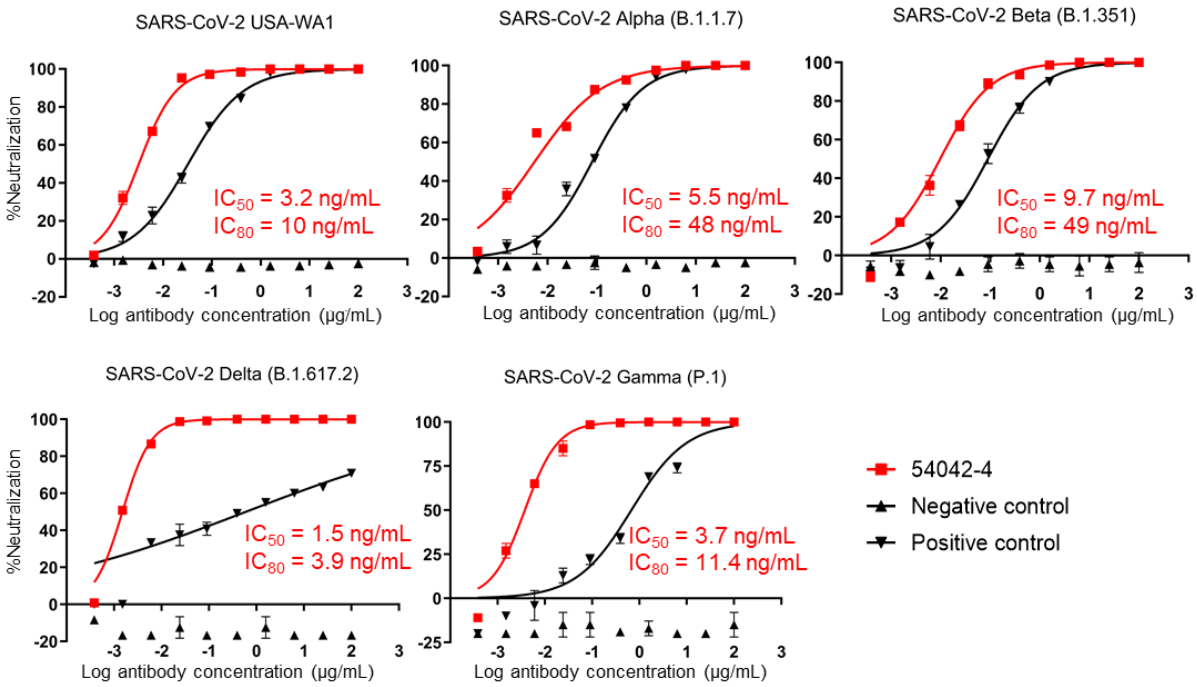

Figure 3-11: **Authentic neutralization by antibody 54042-4.** Authentic SARS-CoV-2 % neutralization of USA-WA1, Alpha, Beta, Delta, and Gamma strains (y-axis) is depicted as a function of antibody concentration (x-axis). Also shown are the respective IC_{50} and IC_{80} values for 54042-4 neutralization against each variant.

DISCUSSION

SARS-CoV-2 neutralizing antibody discovery efforts have produced an extensive panel of antibodies that show a wide range of functional effects, and most antibodies discovered to date cluster into several classes based on RBD-binding orientation, ACE2 antagonism, and cross-reactivity to related SARS-like coronaviruses (Greaney et al., 2021b). Here, we report the identification of 54042-4, an antibody that exhibited potent SARS-CoV-2 neutralization against USA-WA1 as well as the currently circulating Alpha, Beta, Delta, and Gamma VOCs. Interestingly, antibody 54042-4 neutralized virus at comparable IC_{50}s to the clinical candidates LY-CoV1404 and REGN10987, despite having ~10-fold lower affinity for the RBD (Hansen et al., 2020; Westendorf et al., 2021). While the epitope of antibody 54042-4 showed partial overlap with that of several other known RBD-directed antibodies, our findings revealed a distinct mode of SARS-CoV-2 spike recognition, paired with an uncommon genetic signature that distinguishes 54042-4 from other SARS-CoV-2 antibodies. Notably, important differences were observed even for the six antibodies with the highest epitope correlations to 54042-4, with all six of these antibodies exhibiting substantially greater contacts with one or more known residues associated with currently circulating VOCs, as well as with other spike residues (**Figure 3-9C**). While it is not possible to predict what SARS-CoV-2 variants will emerge in the future, having access to antibodies with differences in epitope interactions is critical to broadening the portfolio of countermeasure candidates, should virus variants emerge that are resistant to current therapies. The discovery of antibody 54042-4 is therefore a promising addition to the limited set of antibodies with a high potential for effectively counteracting current SARS-CoV-2 VOCs.

The increased spread of several SARS-CoV-2 VOCs over the past few months has emphasized the need for continued surveillance of vaccine efficacy against the evolving virus targets. The increased transmission rates of the Alpha lineage are likely a product of enhanced ACE2 affinity

for the SARS-CoV-2 RBD (Starr et al., 2020), and not a result of escape from pre-existing antibodies in convalescent or vaccinated individuals (Wang et al., 2021a; Xie et al., 2021). Variants that encode the E484K substitution appear to pose a significantly higher risk of neutralization escape in vaccine recipients and individuals who have recovered from COVID-19 (Wang et al., 2021a). Indeed, the rise of cases associated with the P.1 variant that harbors the E484K substitution (among others) in Manaus, Brazil is on a dangerous trajectory, despite having a 76% population seropositivity rate dating back to March 2020 (Sabino et al., 2021). In the context of vaccination, early vaccine trial data for Novavax against the Beta lineage in South Africa (also encoding the E484K substitution) demonstrated a significant decrease in efficacy (Wadman, 2021). The enhanced transmission profile and recent rise in new infection cases as a result of the Delta variant (Campbell et al., 2021) is another demonstration of the need for SARS-CoV-2 therapeutics. These observations underscore the ongoing need for genomic surveillance to monitor the emergence and spread of new SARS-CoV-2 variants and their effects on population immunity.

In addition to vaccines, antibody therapeutics can play an important role for treating SARS-CoV-2 infections. Given the unknown future trajectory of the pandemic and the potential for emergence of VOCs that may escape neutralization by vaccine-elicited immunity, the development of a wide array of candidate antibody therapeutics that are insensitive to substitutions found in major VOCs may prove critical in the fight against COVID-19. However, current VOCs have already shown an ability to escape neutralization by a number of antibodies in clinical development (Chen et al., 2021c; Wang et al., 2021a). Although the Beta variant or any lineage harboring the Glu484 substitution has yet to propagate in the United States, the nearly complete abrogation of neutralization activity of LY-CoV555 (Bamlinivimab) and REGN10933 against the Beta variant poses a significant risk for the currently available EUA clinical candidates (Wang et al., 2021a). Further, the rise in cases with the L452R substitution

(Epsilon and Delta variants) and the corresponding reduction in neutralization potency associated with the Eli Lilly cocktail (Bamlinivimab and Etesivimab), as well as Regdanivimab (approved for use in Europe), further motivates the continued investigation into antibodies insensitive to currently circulating VOCs (McCallum et al., 2021). In contrast to these clinical candidates, the binding, neutralization, and structural data suggest that antibody 54042-4 maintains functional activity independent of the current major substitutions in circulating VOCs. Combined with those observations, the unique features of 54042-4 in comparison to other SARS-CoV-2 antibodies motivate further clinical development of this antibody to complement the existing pool of therapeutic countermeasures. As SARS-CoV-2 virus evolution continues due to various factors, such as a lack of vaccine access and the associated delayed vaccine rollout to underserved parts of the world, new VOCs are likely to keep emerging, with the potential to decrease or even abrogate protection induced by current vaccines. Antibody therapeutic development, especially focusing on broad protection against diverse SARS-CoV-2 variants, is therefore of continued significance.

METHODS

Donor information

The donor had previous laboratory-confirmed COVID-19, 3 months prior to blood collection. The studies were reviewed and approved by the Institutional Review Board of Vanderbilt University Medical Center. The sample was obtained after written informed consent was obtained.

Antigen purification

A variety of recombinant soluble protein antigens were used in the LIBRA-seq experiment and other experimental assays.

Plasmids encoding residues 1–1208 of the SARS-CoV-2 spike with a mutated S1/S2 cleavage site, proline substitutions at positions 817, 892, 899, 942, 986 and 987, and a C-terminal T4-fibritin trimerization motif, an 8x HisTag, and a TwinStrepTag (SARS-CoV-2 spike HP); 1–1208 of the SARS-CoV-2 spike with a mutated S1/S2 cleavage site, proline substitutions at positions 817, 892, 899, 942, 986 and 987, a glycine mutation at 614, and a C-terminal T4-fibritin trimerization motif, an 8x HisTag, and a TwinStrepTag (SARS-CoV-2 spike HP D614G) 1–1208 of the SARS-CoV-2 spike with a mutated S1/S2 cleavage site, proline substitutions at positions 817, 892, 899, 942, 986 and 987, as well as mutations L18F, D80A, L242-244L del, R246I, K417N, E484K, N501Y, and a C-terminal T4-fibritin trimerization motif, an 8x HisTag, and a TwinStrepTag (SARS-CoV-2 spike HP Beta); 1–1208 of the SARS-CoV-2 spike with a mutated S1/S2 cleavage site, proline substitutions at positions 817, 892, 899, 942, 986 and 987, as well as mutations 69-70del, Y144del, N501Y, A570D, P681H, and a C-terminal T4-fibritin trimerization motif, an 8x HisTag, and a TwinStrepTag (SARS-CoV-2 spike HP Alpha); residues 1-1190 of the SARS-CoV spike with proline substitutions at positions 968 and 969, and a C-terminal T4-fibritin trimerization motif, an 8x HisTag, and a TwinStrepTag (SARS-CoV S-

2P); residues 1-1291 of the MERS-CoV spike with a mutated S1/S2 cleavage site, proline substitutions at positions 1060 and 1061, and a C-terminal T4-fibritin trimerization motif, an AviTag, an 8x HisTag, and a TwinStrepTag (MERS-CoV S-2P Avi); residues 1-1278 of the HCoV-OC43 spike with proline substitutions at positions 1070 and 1071, and a C-terminal T4-fibritin trimerization motif, an 8x HisTag, and a TwinStrepTag (HCoV-OC43 S-2P); residues 319–591 of SARS-CoV-2 S with a C-terminal monomeric human IgG Fc-tag and an 8x HisTag (SARS-CoV-2 RBD-SD1); residues 306−577 of SARS-CoV S (Tor2 strain) were cloned upstream of a C-terminal HRV3C protease cleavage site, a monomeric Fc tag and an 8x HisTag (SARS-CoV RBD-SD1);residues 367–589 of MERS-CoV S with a C-terminal monomeric human IgG Fc-tag and an 8x HisTag (MERS-CoV RBD); residues 306–577 of MERS-CoV S with a C-terminal monomeric human IgG Fc-tag and an 8x HisTag (SARS-CoV RBD-SD1) were transiently transfected into FreeStyle293F cells (Thermo Fisher) using polyethylenimine. For all antigens with the exception of SARS-CoV-2 S HP, transfections were treated with 1 µM kifunensine to ensure uniform glycosylation three hours post-transfection. Transfected supernatants were harvested after 6 days of expression. SARS-CoV-2 RBD-SD1, SARS-CoV RBD-SD1, and MERS-CoV RBD were purified using Protein A resin (Pierce). SARS-CoV-2 S HP, MERS-CoV S-2P Avi, and HCoV-OC43 S-2P were purified using StrepTrap HP columns (Cytiva Life Sciences). Affinity-purified SARS-CoV-2 RBD-SD1, SARS-CoV RBD-SD1, and MERS-CoV RBD were further purified over a Superdex200 column (GE Life Sciences). SARS-CoV-2 S HP, SARS-CoV-2 S HP Beta, SARS-CoV-2 S HP Alpha, SARS-CoV S-2P, MERS-CoV S-2P, and HCoV-OC43 S-2P were purified over a Superose6 Increase column (GE Life Sciences). HCoV-NL63 and HCoV-229E alpha coronavirus spike proteins as well as the SARS-CoV-2 S1, SARS-CoV-2 S2, and SARS-CoV-2 NTD truncated proteins were purchased from the commercial vendor, Sino Biological.

Recombinant, soluble HIV-1 gp140 SOSIP trimer from strain ZM197 (clade) containing an AviTag and recombinant NC99 HA protein consisting of the HA ectodomain with a point mutation at the sialic acid-binding site (Y98F) to abolish non-specific interactions, a T4 fibritin foldon trimerization domain, AviTag, and hexahistidine-tag, were expressed in Expi 293F cells using polyethylenimine transfection reagent and cultured. FreeStyle F17 expression medium supplemented with pluronic acid and glutamine was used. The cells were cultured at 37°C with 8% CO_2 saturation and shaking. After 5-7 days, cultures were centrifuged and supernatant was filtered and run over an affinity column of agarose bound *Galanthus nivalis* lectin. The column was washed with PBS and antigens were eluted with 30 mL of 1M methyl-a-D-mannopyranoside. Protein elutions were buffer exchanged into PBS, concentrated, and run on a Superdex 200 Increase 10/300 GL Sizing column on the AKTA FPLC system. Fractions corresponding to correctly folded protein were collected, analyzed by SDS-PAGE and antigenicity was characterized by ELISA using known monoclonal antibodies specific to each antigen. Avitagged antigens were biotinylated using BirA biotin ligase (Avidity LLC).

Spike protein used for cryo-EM was expressed by transiently transfecting plasmid encoding the HexaPro spike variant (Hsieh et al., 2020) containing additional S383C and D985C substitutions (Henderson et al., 2020) with a C-terminal TwinStrep tag into FreeStyle 293-F cells (Thermo Fisher) using polyethyleneimine. 5 µM kifunensine was added 3h post-transfection. The cell culture was harvested four days after transfection and the spike-containing medium was separated from the cells by centrifugation. Supernatants were passed through a 0.22 µm filter and passaged over StrepTactin resin (IBA). Further purification was achieved by size-exclusion chromatography using a Superose 6 10/300 column (GE Healthcare) in buffer containing 2 mM Tris pH 8.0, 200 mM NaCl and 0.02% NaN3.

DNA-barcoding of antigens

We used oligos that possess 15 bp antigen barcode, a sequence capable of annealing to the template switch oligo that is part of the 10X bead-delivered oligos, and contain truncated TruSeq small RNA read 1 sequences in the following structure: 5'-CCTTGGCACCCGAGAATTCCANNNNNNNNNNNNNCCCATATAAGA*A*A-3', where Ns represent the antigen barcode. We used the following antigen barcodes: We used the following antigen barcodes: GCAGCGTATAAGTCA (SARS-CoV-2 S), AACCCACCGTTGTTA (SARS-CoV-2 S D614G), GCTCCTTTACACGTA (SARS-CoV S), GGTAGCCCTAGAGTA (MERS-CoV S), AGACTAATAGCTGAC (HCoV-OC43 S), GACAAGTGATCTGCA (HCoV-NL63 S), GTGTGTTGTCCTATG (HCoV-229E S), TACGCCTATAACTTG (ZM197 HIV EnV), TCATTTCCTCCGATT (HA NC99), TGGTAACGACAGTCC (SARS-CoV RBD-SD1), TTTCAACGCCCTTTC (SARS-CoV-2 RBD-SD1), GTAAGACGCCTATGC (MERS-CoV RBD), CAGTAAGTTCGGGAC(SARS-CoV-2 NTD), Oligos were ordered from IDT with a 5' amino modification and HPLC purified.

For each antigen, a unique DNA barcode was directly conjugated to the antigen itself. In particular, 5'amino-oligonucleotides were conjugated directly to each antigen using the Solulink Protein-Oligonucleotide Conjugation Kit (TriLink cat no. S-9011) according to manufacturer's instructions. Briefly, the oligo and protein were desalted, and then the amino-oligo was modified with the 4FB crosslinker, and the biotinylated antigen protein was modified with S-HyNic. Then, the 4FB-oligo and the HyNic-antigen were mixed together. This causes a stable bond to form between the protein and the oligonucleotide. The concentration of the antigen-oligo conjugates was determined by a BCA assay, and the HyNic molar substitution ratio of the antigen-oligo conjugates was analyzed using the NanoDrop according to the Solulink protocol guidelines. AKTA FPLC was used to remove excess oligonucleotide from the protein-oligo conjugates,

which were also verified using SDS-PAGE with a silver stain. Antigen-oligo conjugates were also used in flow cytometry titration experiments.

Antigen-specific B cell sorting

Cells were stained and mixed with DNA-barcoded antigens and other antibodies, and then sorted using fluorescence activated cell sorting (FACS). First, cells were counted and viability was assessed using Trypan Blue. Then, cells were washed three times with DPBS supplemented with 0.1% Bovine serum albumin (BSA). Cells were resuspended in DPBS-BSA and stained with cell markers including viability dye (Ghost Red 780), CD14-APC-Cy7, CD3-FITC, CD19-BV711, and IgG-PE-Cy5. Additionally, antigen-oligo conjugates were added to the stain. After staining in the dark for 30 minutes at room temperature, cells were washed three times with DPBS-BSA at 300g for five minutes. Cells were then incubated for 15 minutes at room temperature with Streptavidin-PE to label cells with bound antigen. Cells were washed three times with DPBS-BSA, resuspended in DPBS, and sorted by FACS. Antigen positive cells were bulk sorted and delivered to the Vanderbilt Technologies for Advanced Genomics (VANTAGE) sequencing core at an appropriate target concentration for 10X Genomics library preparation and subsequent sequencing. FACS data were analyzed using FlowJo.

Sample preparation, library preparation, and sequencing

Single-cell suspensions were loaded onto the Chromium Controller microfluidics device (10X Genomics) and processed using the B-cell Single Cell V(D)J solution according to manufacturer's suggestions for a target capture of 10,000 B cells per 1/8 10X cassette, with minor modifications in order to intercept, amplify and purify the antigen barcode libraries as previously described (Setliff et al., 2019a).

Sequence processing and bioinformatics analysis

We utilized and modified our previously described pipeline to use paired-end FASTQ files of oligo libraries as input, process and annotate reads for cell barcode, unique molecular identifier (UMI), and antigen barcode, and generate a cell barcode - antigen barcode UMI count matrix (Setliff et al., 2019a). BCR contigs were processed using Cell Ranger (10X Genomics) using GRCh38 as reference. Antigen barcode libraries were also processed using Cell Ranger (10X Genomics). The overlapping cell barcodes between the two libraries were used as the basis of the subsequent analysis. We removed cell barcodes that had only non-functional heavy chain sequences as well as cells with multiple functional heavy chain sequences and/or multiple functional light chain sequences, reasoning that these may be multiplets. Additionally, we aligned the BCR contigs (filtered_contigs.fasta file output by Cell Ranger, 10X Genomics) to IMGT reference genes using HighV-Quest (Alamyar et al., 2012). The output of HighV-Quest was parsed using ChangeO(Gupta et al., 2015b) and merged with an antigen barcode UMI count matrix. Finally, we determined the LIBRA-seq score for each antigen in the library for every cell as previously described (Setliff et al., 2019a).

Antibody expression and purification

For each antibody, variable genes were inserted into custom plasmids encoding the constant region for the IgG1 heavy chain as well as respective lambda and kappa light chains (pTwist CMV BetaGlobin WPRE Neo vector, Twist Bioscience). Antibody 54042-2 was natively an IGHG2, but was cloned into an IGHG1 Fc backbone vector for monoclonal antibody characterization. Antibodies were expressed in Expi293F mammalian cells (Thermo Fisher Scientific) by co-transfecting heavy chain and light chain expressing plasmids using

polyethylenimine transfection reagent and cultured for 5-7 days. Cells were maintained in FreeStyle F17 expression medium supplemented at final concentrations of 0.1% Pluronic Acid F-68 and 20% 4mM L-Glutamine. These cells were cultured at 37°C with 8% CO_2 saturation and shaking. After transfection and 5-7 days of culture, cell cultures were centrifuged and supernatant was 0.45 µm filtered with Nalgene Rapid Flow Disposable Filter Units with PES membrane. Filtered supernatant was run over a column containing Protein A agarose resin equilibrated with PBS. The column was washed with PBS, and then antibodies were eluted with 100 mM Glycine HCl at 2.7 pH directly into a 1:10 volume of 1M Tris-HCl pH 8.0. Eluted antibodies were buffer exchanged into PBS 3 times using Amicon Ultra centrifugal filter units and concentrated. Antibodies were analyzed by SDS-PAGE.

High-throughput antibody expression

For high-throughput production of recombinant antibodies, approaches were used that are designated as microscale. For antibody expression, microscale transfection were performed (~1 ml per antibody) of CHO cell cultures using the Gibco ExpiCHO Expression System and a protocol for deep 96-well blocks (Thermo Fisher Scientific). In brief, synthesized antibody-encoding DNA (~2 µg per transfection) was added to OptiPro serum free medium (OptiPro SFM), incubated with ExpiFectamine CHO Reagent and added to 800 µl of ExpiCHO cell cultures into 96-deep-well blocks using a ViaFlo 384 liquid handler (Integra Biosciences). The plates were incubated on an orbital shaker at 1,000 r.p.m. with an orbital diameter of 3 mm at 37 °C in 8% CO_2. The next day after transfection, ExpiFectamine CHO Enhancer and ExpiCHO Feed reagents (Thermo Fisher Scientific) were added to the cells, followed by 4 d incubation for a total of 5 d at 37 °C in 8% CO_2. Culture supernatants were collected after centrifuging the blocks at 450*g* for 5 min and were stored at 4°C until use. For high-throughput microscale antibody purification, fritted deep-well plates were used containing 25 µl of settled protein G

resin (GE Healthcare Life Sciences) per well. Clarified culture supernatants were incubated with protein G resin for antibody capturing, washed with PBS using a 96-well plate manifold base (Qiagen) connected to the vacuum and eluted into 96-well PCR plates using 86 µl of 0.1 M glycine-HCL buffer pH 2.7. After neutralization with 14 µl of 1 M Tris-HCl pH 8.0, purified antibodies were buffer-exchanged into PBS using Zeba Spin Desalting Plates (Thermo Fisher Scientific) and stored at 4°C until use.

ELISA

To assess antibody binding, soluble protein was plated at 2 µg/ml overnight at 4°C. The next day, plates were washed three times with PBS supplemented with 0.05% Tween-20 (PBS-T) and coated with 5% milk powder in PBS-T. Plates were incubated for one hour at room temperature and then washed three times with PBS-T. Primary antibodies were diluted in 1% milk in PBS-T, starting at 10 µg/ml with a serial 1:5 dilution and then added to the plate. The plates were incubated at room temperature for one hour and then washed three times in PBS-T. The secondary antibody, goat anti-human IgG conjugated to peroxidase, was added at 1:10,000 dilution in 1% milk in PBS-T to the plates, which were incubated for one hour at room temperature. Plates were washed three times with PBS-T and then developed by adding 3,3′,5,5′-tetramethylbenzidine (TMB) substrate to each well. The plates were incubated at room temperature for ten minutes, and then 1N sulfuric acid was added to stop the reaction. Plates were read at 450 nm. The area under the curve (AUC) was calculated using GraphPad Prism 9.0.1.

Competition ELISA

Competition ELISA was performed as done previously (Zost et al., 2020b). Briefly, antibodies were biotinylated using NHS-PEG4-biotin (Thermo Fisher Scientific, cat# A39259) according to manufacturer protocol. Following biotinylation, specific binding of biotinylated antibodies was confirmed using ELISA. Wells of 384-well microtiter plates were coated with 1 µg/mL SARS-CoV-2 S HP protein at 4ºC overnight. Plates were washed with PBS-T and blocked for 1 h with blocking buffer (1% BSA in PBS-T). Plates were then washed with PBS-T and unlabeled antibodies were added at a concentration of 10 µg/mL in a total volume of 25 µL blocking buffer and incubated 1 h. Without washing, biotinylated antibodies diluted in blocking buffer were added directly to each well in a volume of 5 µL per well (such that the final concentrations of each biotinylated antibody were equal to the respective EC_{90} of each antibody), and then incubated for 30 min at ambient temperature. Plates were then washed with PBS-T and incubated for 1 h with HRP-conjugated avidin (Sigma, 25 µL of a 1:3,500 dilution in blocking buffer). Plates were washed with PBS-T and 25 µL TMB substrate was added to each well. After sufficient development, the reactions were quenched by addition 25 µL 1M HCl and absorbance at 450 nm was quantified using a plate reader. After subtracting the background signal, the signal obtained for binding of the biotin-labeled reference antibody in the presence of the unlabeled tested antibody was expressed as a percentage of the binding of the reference antibody in the presence of 10 µg/mL of the anti-dengue antibody DENV 2D22, which served as a no-competition control. Tested antibodies were considered competing if their presence reduced the reference antibody binding by more than 60% and non-competing if the signal was reduced by less than 30%.

Real-time cell analysis (RTCA) HT neutralization assay screen

To screen for neutralizing activity in the panel of recombinantly expressed antibodies, we used a high-throughput and quantitative RTCA assay and xCelligence RTCA HT Analyzer (ACEA

Biosciences) that assesses kinetic changes in cell physiology, including virus-induced cytopathic effect (CPE). Twenty µl of cell culture medium (DMEM supplemented with 2% FBS) was added to each well of a 384-well E-plate using a ViaFlo384 liquid handler (Integra Biosciences) to obtain background reading. Six thousand (6,000) Vero-furin cells in 20 µl of cell culture medium were seeded per well, and the plate was placed on the analyzer. Sensograms were visualized using RTCA HT software version 1.0.1 (ACEA Biosciences). For a screening neutralization assay, equal amounts of virus were mixed with micro-scale purified antibodies in a total volume of 40 µL using DMEM supplemented with 2% FBS as a diluent and incubated for 1 h at 37 °C in 5% CO2. At ~17–20 h after seeding the cells, the virus–antibody mixtures were added to the cells in 384-well E-plates. Wells containing virus only (in the absence of antibody) and wells containing only Vero cells in medium were included as controls. Plates were measured every 8–12 h for 48–72 h to assess virus neutralization. Micro-scale antibodies were assessed in four 5-fold dilutions (starting from a 1:20 sample dilution), and their concentrations were not normalized. Neutralization was calculated as the percent of maximal cell index in control wells without virus minus cell index in control (virus-only) wells that exhibited maximal CPE at 40–48 h after applying virus–antibody mixture to the cells. An antibody was classified as fully neutralizing if it completely inhibited SARS-CoV-2-induced CPE at the highest tested concentration, while an antibody was classified as partially neutralizing if it delayed but did not fully prevent CPE at the highest tested concentration. Further, if the CPE curve lies between partial and the virus-only control, those mAbs were designated weak (Zost et al., 2020b).

RTCA potency neutralization screening assay

To determine neutralizing activity of IgG and convalescent serum, we used real-time cell analysis (RTCA) assay on an xCELLigence RTCA MP Analyzer (ACEA Biosciences Inc.) that measures virus-induced cytopathic effect (CPE)(Suryadevara et al., 2021). Briefly, 50 µL of cell

culture medium (DMEM supplemented with 2% FBS) was added to each well of a 96-well E-plate using a ViaFlo384 liquid handler (Integra Biosciences) to obtain background reading. A suspension of 18,000 Vero-E6 cells in 50 µL of cell culture medium was seeded in each well, and the plate was placed on the analyzer. Measurements were taken automatically every 15 min, and the sensograms were visualized using RTCA software version 2.1.0 (ACEA Biosciences Inc). VSV-SARS-CoV-2 (0.01 MOI, ~120 PFU per well) was mixed 1:1 with a dilution of antibody in a total volume of 100 µL using DMEM supplemented with 2% FBS as a diluent and incubated for 1 h at 37°C in 5% CO2. At 16 h after seeding the cells, the virus-antibody mixtures were added in replicates to the cells in 96-well E-plates. Triplicate wells containing virus only (maximal CPE in the absence of antibody) and wells containing only Vero cells in medium (no-CPE wells) were included as controls. Plates were measured continuously (every 15 min) for 48 h to assess virus neutralization. Normalized cellular index (CI) values at the endpoint (48 h after incubation with the virus) were determined using the RTCA software version 2.1.0 (ACEA Biosciences Inc.). Results are expressed as percent neutralization in a presence of respective antibody relative to control wells with no CPE minus CI values from control wells with maximum CPE. RTCA IC_{50} and NT_{50} values were determined by nonlinear regression analysis using GraphPad Prism software. A full dose-response neutralization assay was not performed for antibody 54042-11 due to insufficient quantity at the time of experiment. The NT_{50} of the donor sample was comparable to previously reported data for other donors for SARS-CoV-2 antibody discovery efforts (Brouwer et al., 2020; Rogers et al., 2020).

Epitope mapping of antibodies by alanine scanning

Epitope mapping was performed essentially as described previously (Davidson, 2014) using a SARS-CoV-2 (strain Wuhan-Hu-1) spike protein RBD shotgun mutagenesis mutation library, made using an expression construct for full-length spike protein. 184 residues of the RBD (between spike residues

335 and 526) were mutated individually to alanine, and alanine residues to serine and clones arrayed in 384-well plates, one mutant per well. Antibody binding to each mutant clone was determined, in duplicate, by high-throughput flow cytometry. Each spike protein mutant was transfected into HEK-293T cells and allowed to express for 22 hrs. Cells were fixed in 4% (v/v) paraformaldehyde (Electron Microscopy Sciences), and permeabilized with 0.1% (w/v) saponin (Sigma-Aldrich) in PBS plus calcium and magnesium (PBS++) before incubation with antibodies diluted in PBS++, 10% normal goat serum (Sigma), and 0.1% saponin. Antibody screening concentrations were determined using an independent immunofluorescence titration curve against cells expressing wild-type spike protein to ensure that signals were within the linear range of detection. Antibodies were detected using 3.75 µg/mL of AlexaFluor488-conjugated secondary antibody (Jackson ImmunoResearch Laboratories) in 10% normal goat serum with 0.1% saponin. Cells were washed three times with PBS++/0.1% saponin followed by two washes in PBS, and mean cellular fluorescence was detected using a high-throughput Intellicyte iQue flow cytometer (Sartorius). Antibody reactivity against each mutant spike protein clone was calculated relative to wild-type spike protein reactivity by subtracting the signal from mock-transfected controls and normalizing to the signal from wild-type S-transfected controls. Mutations within clones were identified as critical to antibody binding if they did not support reactivity of the test antibody, but supported reactivity of other SARS-CoV-2 antibodies. This counter-screen strategy facilitates the exclusion of spike mutants that are locally misfolded or have an expression defect.

Plaque reduction neutralization test (PRNT)

The virus neutralization with live authentic SARS-CoV-2 virus was performed in the BSL-3 facility of the Galveston National Laboratory using Vero E6 cells (ATCC CRL-1586) following the standard procedure. Briefly, Vero E6 cells were cultured in 96-well plates (10^4 cells/well). Next day, 4-fold serial dilutions of antibodies were made using MEM-2% FBS, as to get an initial

concentration of 100 µg/ml. Equal volume of diluted antibodies (60 µl) were mixed gently with authentic virus (60 µl containing 200 pfu) and incubated for 1 h at 37°C/5% CO_2 atmosphere. The virus-serum mixture (100 µl) was added to cell monolayer in duplicates and incubated for 1 at h 37°C/5% CO2 atmosphere. Later, virus-serum mixture was discarded gently, and cell monolayer was overlaid with 0.6% methylcellulose and incubated for 2 days. The overlay was removed, and the plates were fixed in 4% paraformaldehyde twice following BSL-3 protocol. The plates were stained with 1% crystal violet and virus-induced plaques were counted. The percent neutralization and/or NT_{50} of antibody was calculated by dividing the plaques counted at each dilution with plaques of virus-only control. For antibodies, the inhibitory concentration at 50% (IC_{50}) values were calculated in GraphPad Prism software by plotting the midway point between the upper and lower plateaus of the neutralization curve among dilutions. The Alpha variant virus incorporates the following substitutions: Del 69-70, 144 Del, E484K, N501Y, A570D, D614G, P681H, T716I, S982A, D1118H. The Beta variant incorporates the following substitutions: 24 Del, 242-243 Del, D80A, D215G, K417N, E484K, N501Y, D614G, H665Y, T1027I. The Delta variant incorporates the following substitutions: T19R, G142D, Del 156-157, R158G, L452R, T478K, D614G, P681R, Del 689-691, D950N; the deletion at positions 689-691 has not been observed in nature, and was identified upon one passage of the virus. The Gamma variant incorporates the following substitutions: L18F, T20N, P26S, D138Y, R190S, K417T, E484K, N501Y, D614G, H655Y, T1027I.

BioLayer interferometry (BLI)

Purified 54042-4 IgG was immobilized to AHC sensortips (FortéBio) to a response level of approximately 1.4 nm in a buffer composed of 10 mM HEPES pH 7.5, 150 mM NaCl, 3 mM EDTA, 0.05% Tween 20 and 0.1% (w/v) BSA. Immobilized IgG was then dipped into wells containing four-fold dilutions of SARS-CoV-2 RBD-SD1 ranging in concentration from 100-

1.5625 nM, to measure association. Dissociation was measured by dipping sensortips into wells containing only running buffer. Data were reference subtracted and kinetics were calculated in Octet Data Analysis software v10.0 using a 1:1 binding model.

ACE2 binding inhibition assay

96-well plates were coated with 2 µg/mL purified recombinant SARS-CoV-2 at 4°C overnight. The next day, plates were washed three times with PBS supplemented with 0.05% Tween-20 (PBS-T) and coated with 5% milk powder in PBS-T. Plates were incubated for one hour at room temperature and then washed three times with PBS-T. Purified antibodies were diluted in blocking buffer at 10 µg/mL in triplicate, added to the wells, and incubated at room temperature. Without washing, recombinant human ACE2 protein with a mouse Fc tag was added to wells for a final 0.4 µg/mL concentration of ACE2 and incubated for 40 minutes at room temperature. Plates were washed three times with PBS-T, and bound ACE2 was detected using HRP-conjugated anti-mouse Fc antibody and TMB substrate. The plates were incubated at room temperature for ten minutes, and then 1N sulfuric acid was added to stop the reaction. Plates were read at 450 nm. ACE2 binding without antibody served as a control. Experiment was done in biological replicate and technical triplicates.

RTCA neutralization assay with known antibody escape mutants

We used a real-time cell analysis assay (RTCA) and xCELLigence RTCA MP Analyzer (ACEA Biosciences Inc.) with modification of previously described assays (Greaney et al., 2021a; Greaney et al., 2021b; Suryadevara et al., 2021). Fifty (50) µL of cell culture medium (DMEM supplemented with 2% FBS) was added to each well of a 96-well E-plate to obtain a background reading. Eighteen thousand (18,000) Vero E6 cells in 50 µL of cell culture medium

were seeded per each well, and plates were placed on the analyzer. Measurements were taken automatically every 15 min and the sensograms were visualized using RTCA software version 2.1.0 (ACEA Biosciences Inc). Escape mutant VSV-SARS-CoV-2 or wild-type VSV-SARS-CoV-2 virus (5e3 plaque forming units [PFU] per well, ~0.3 MOI) was mixed with a saturating neutralizing concentration of individual antibody (5 µg/mL) in a total volume of 100 µL and incubated for 1 h at 37°C. At 16-20 h after seeding the cells, the virus-antibody mixtures were added into 8 to 96 replicate wells of 96-well E-plates with cell monolayers. Wells containing only virus in the absence of antibody and wells containing only Vero E6 cells in medium were included on each plate as controls. Plates were measured continuously (every 15 min) for 72 h. The lack of neutralization for the individual escape mutant viruses from 54042-4 was confirmed by delayed CPE in wells containing antibody while COV2-2381 was used as positive control.

EM sample prep and data collection

To form the spike-Fab complex, a final concentration of 0.5 mg/mL spike protein and 5X molar excess of Fab were combined in buffer containing 2mM Tris-Cl pH 8.0, 200 mM NaCl, and 0.02% NaN_3. The complex was incubated on ice for 30 min before 3 µL of the sample was deposited on Au-300 1.2/1.3 grids (UltrAuFoil) that had been plasma cleaned in a Solarus 950 plasma cleaner (Gatan) for 4 minutes using a 4:1 ratio of O_2:H_2. A force of -4 was used to blot excess liquid for 3 s using a Vitrobot Mark IV (Thermo Fisher) followed by plunge-freezing with liquid ethane. 3,762 micrographs were collected from a single grid using a Titan Krios (Thermo Fisher) equipped with a K3 detector (Gatan) with the stage set at a 30° tilt. SerialEM was used to collect movies at 29,000X nominal magnification with a calibrated pixel size of 0.81 Å/pixel.

Cryogenic electron microscopy (Cryo-EM)

Motion correction, CTF estimation, particle picking, and preliminary 2D classification were performed using cryoSPARC v3.2.0 live processing (Punjani et al., 2017). The final iteration of 2D class averaging distributed 374,669 particles into 60 classes using an uncertainty factor of 2. From that, 241,732 particles were used to perform an ab initio reconstruction with four classes followed by heterogeneous refinement of those four classes. Particles from the two highest quality classes were used for homogenous refinement of the best volume with applied C3 symmetry. Non-uniform refinement was performed on the resulting volume using per-particle defocus and per-group CTF optimizations applied (Punjani et al., 2020; Rubinstein and Brubaker, 2015). To improve the 54042-4 Fab-RBD density, C3 symmetry expansion was performed followed by local refinement using a mask created in ChimeraX that encompassed the entire 54042-4 Fab and RBD (Pettersen et al., 2021). Local refinement was performed using a pose/shift gaussian prior during alignment, 3° standard deviation of prior over rotation and 1 Å standard deviation of prior over shifts. Additionally, maximum alignment resolution was limited to 2.8 Å resolution to avoid over-refining. To improve map quality, the focused refinement volumes were processed using the DeepEMhancer(Sanchez-Garcia, 2021) tool via COSMIC^{2}science gateway, which included the use of our refinement mask to help define noise while sharpening (Cianfrocco, 2017a; Cianfrocco, 2017b). An initial model was generated by docking PDBID: 6XKL (Hsieh et al., 2020) and a Fab model based on the 54042-4 sequence built using SAbPred ABodyBuilder (Dunbar et al., 2016) into map density via ChimeraX (Pettersen et al., 2021). The model was iteratively refined and completed using a combination of Phenix, Coot, and ISOLDE (Adams et al., 2002; Croll, 2018; Emsley and Cowtan, 2004).

GISAID mutation frequency calculation

To evaluate the conservation of 54042-4 epitope residues, we utilized the GISAID database (Elbe, 2017) comprising sequences from 1,229,459 SARS-CoV-2 variants (as of May 6th, 2021). The spike glycoprotein sequences were extracted and translated, and pairwise sequence alignment with the reference sequence hCoV-19/Wuhan/WIV04/2019 was then performed. After removing incomplete sequences and sequences with alignment errors, the pairwise alignments for the remaining 1,148,887 spike protein sequences were combined to compute the conservation of each residue position using in-house perl scripts.

RMSD calculation for the differences in angle of antigen approach for different antibodies

The SARS-CoV-2 spike receptor binding domain coordinates present in each antibody-antigen complex were aligned in PyMOL (The PyMOL Molecular Graphics System, Version 2.3.5, Schrödinger, LLC.) using an all-atom alignment with 5 cycles of outlier rejection of atom pairs having an RMSD greater than 2. The alignment was performed for RBD residues 329-529 in antibody 54042-4 (PDB ID: TBD chain A), 329-529 in antibody 2-7 (PDB ID: 7LSS chain B), 333-526 in antibody REGN10987 (PDB ID: 6XDG chain A), and 334-527 in antibody LY-COV1404 (PDB ID: 7MMO chain C). This resulted in RMSD values of 0.751 Å between 54042-4 and REGN10987's RBDs, 1.044 Å between 54042-4 and antibody 2-7's RBDs, 0.632 Å between 54042-4 and LY-COV1404's RBDs, 1.067 Å between REGN10987 and antibody 2-7's RBDs, and 0.751 Å between LY-COV1404 and antibody 2-7's RBDs with well-aligned epitope residues. Next, the residues comprising the N-termini through the end of framework region 3 were determined for the heavy and light chains of all three antibodies using IMGT Domain Gap Align(Alamyar et al., 2012)Each pair of antibodies was aligned using a pairwise sequence alignment of this region in PyMOL. Finally, the alpha carbon root mean square deviation

between antibodies was calculated over this region in the heavy and light chains using residue pairs from the sequence alignment. RMSD values were calculated from 183, 183, and 180 alpha carbon pairs for the 54042-4 vs REGN1087, REGN1087 vs 2-7, and 54042-4 vs 2-7 comparisons respectively.

QUANTIFICATION AND STATISTICAL ANALYSIS

ELISA and neutralization error bars (standard error of the mean) were calculated using GraphPad Prism version 9.0.1.

CHAPTER IV

SINGLE-CELL PROFILING OF THE ANTIGEN-SPECIFIC RESPONSE TO BNT162B2 SARS-COV-2 RNA VACCINE

This chapter is adapted from the published manuscript:

Kramer KJ et al. Single-Cell Profiling of the Antigen-Specific Response to BNT162b2 SARS-CoV-2 RNA Vaccine. *BioRxiv*. 2021.

Contributions: Erin Wilfong drew blood from the ~~ten donor~~ten-donor cohort as well as assisted in mass cytometry and *in vitro* cell assay data analysis. Kelsey Voss performed *in vitro* antigen-specific T cell assays including peptide MHC stimulation as well as characterization of sorted populations treated with SARS-CoV-2 spike protein. Sierra Barone performed computational analysis of mass cytometry data including the development and application of the T-REX machine learning algorithm to identify responding antigen-specific cell subsets. Andrea Shiakolas performed LIBRA-seq including PBMC staining and FACS isolation of antigen-specific B cells from the longitudinal donor samples. Andrea also ran the bioinformatic pipeline to resolve the antigen specificity map associated with the recovered B-cell receptor sequences. Nagarajan Raju performed clonal lineage tracing of the recovered B-cell receptor sequences as well as generated a number of figures for both analysis and publication. Caroline Roe collected the mass cytometry data. Naveenchandra Suryadevara performed the RTCA VSV SARS-CoV-2 plasma neutralization assays. Lauren Walker and Steven Wall performed ELISAs on the antibodies from the expanded cluster 720. Ariana Paulo isolated DNA for recombinant spike proteins. Samuel Schaefer, Camille Westlake and Debolanle Dahunsi processed donor blood samples. Jeff Rathmell oversaw logistics for blood collection as well as provided resources for the study. Rachel Bonami performed the single-cell RNA-sequencing analysis. Jonathan Irish

assisted in the figure making and processing of mass cytometry data. Erin Wilfong, Jeff Rathmell, Rachel Bonami, Jonathan Irish, Ivelin Georgiev, and I wrote the manuscript.

INTRODUCTION

In December 2019, a novel coronavirus strain designated severe respiratory distress syndrome coronavirus 2 (SARS-CoV-2) was identified in Wuhan, China. A global pandemic ensued that has resulted in approximately 200 million cases and over 4 million deaths of coronavirus disease 2019 (COVID-19) to date (Dong et al., 2020). B cells, T cells, and other leukocytes undergo significant shifts upon SARS-CoV-2 infection that may contribute to anti-viral immunity and protective antibodies (Arunachalam et al., 2020; Koutsakos et al., 2021; Mathew et al., 2020; Rodriguez et al., 2020; Schulte-Schrepping et al., 2020). The development of viral neutralizing antibodies following infection has been associated with Th1-like CXCR3+HLADR+PD1+ CD8 and CD4 cells and circulating CXCR3+ CD4 T follicular helper (cTfh) cells and CD4+ CD38+ HLA-DR+ T cell abundance (Koutsakos et al., 2021; Mathew et al., 2020). While therapies, such as dexamethasone (Group et al., 2021), baracitinib (Kalil et al., 2021), tocilizumab (Group, 2021), and neutralizing monoclonal antibodies (Gottlieb et al., 2021; Weinreich et al., 2021) have emerged as treatments for severe COVID-19 disease, preventive measures to develop coronavirus immunity on a population-scale are of upmost importance . To address this need, vaccines formulated with the pre-fusion stabilized SARS-CoV-2 Spike (S) protein were developed to induce protection from COVID-19 infection or development of severe disease (Baden et al., 2021; Dagan et al., 2021; Polack et al., 2020; Sadoff et al., 2021a; Voysey et al., 2021). Globally, nearly 4 billion doses of various COVID-19 vaccines have been administered (Dong et al., 2020).

Messenger RNA (mRNA)-based vaccines represent a promising new class of vaccines that offer protection from COVID-19 as well as potentially a wide range of emerging infectious diseases (Bettini and Locci, 2021; Pardi et al., 2018). These vaccines introduce the minimal genetic information to express viral antigens of interest (Pardi et al., 2018) and mimic natural infection of RNA viruses, such as SARS-CoV-2 (Jeyanathan et al., 2020). Several groups have

explored the immunologic response to SARS-CoV-2 mRNA vaccines using both systems (Arunachalam et al., 2021) and T-cell centric approaches (Sahin et al., 2020; Sattler et al., 2021a; Woldemeskel et al., 2021). From these studies, elevated myeloid and T cell responses have been identified following vaccination and which corresponded to serologic antibody responses. However, antigen-specific cells that respond to vaccination and mechanisms of mRNA-based formulations remain poorly understood. It is also not well established how pre-existing immunity to endemic coronaviruses impacts the B cell and antibody response against SARS-CoV-2 vaccination and how the antibody repertoire may evolve over time

A major challenge to studies of immune responses to emerging diseases is reliable identification of antigen specific cells. While MHC tetramers and other tracking agents can identify pre-determined subsets of antigen-specific cells, a systemic and unbiased view of SARS-CoV-2 antigen responsive cells is needed. Single cell machine learning analysis tools including the Tracking Responders EXpanding (T-REX) algorithm (Barone et al., 2020b) and Linking B cell Receptor to Antigen specificity through sequencing (LIBRA-seq) (Setliff et al., 2019a) combined with whole transcriptome RNA-seq may address this need to reveal immune cells reacting to infection or vaccination. These single-cell approaches identify rare cells that specifically expand following vaccination or infection that can be overlooked when analyzing cellular populations in bulk. Proteomic signatures identified by T-REX can be combined with Marker Enrichment Modeling (MEM) (Diggins et al., 2017) to develop strategies to physically isolate the cell subset using fluorescence activated cell sorting (FACS) enabling *in vitro* validation. LIBRA-seq identifies antigen-binding B cells and their associated B-cell receptor (BCR) sequences, which can be recombinantly expressed as antibody and characterized *in vitro* together with single cell RNA-seq to identify and characterize B cell subsets based on transcriptional profiles *(*Setliff et al., 2019a). Adaptation and evolution of antibody isotypes and

antigen-binding properties provide further insight into the development of B cell responses and antigen-specificity.

To better understand the basis of antigen-specific cells and antibody response in SARS-CoV-2 vaccine-induced immunity, we tracked the development of antigen-specific T and B cells in longitudinal samples collected from healthy donor recipients of the BNT162b2 RNA-based SARS-CoV-2 vaccine, including a donor with a breakthrough SARS-CoV-2 infection. T-REX identified novel expanding and metabolically active S protein-specific, non-canonical memory CD4 and CD8 T cell populations following vaccination that were confirmed as antigen specific. In parallel, coronavirus S protein-binding B cells were characterized with single-cell LIBRA-seq and RNA-seq to establish the evolution of cross-reactive to antigen specific B cells with public antibody sequences over time. These antigen-specific T and B cells correlated and associated with a long-lasting IgG response that was lacking in a donor who subsequently experienced a breakthrough infection. These cell and antibody associations may drive further efforts to predict vaccine effectiveness and identify mechanisms of protection.

RESULTS

Mass cytometry identifies vaccine-induced CD4 and CD8 ICOS+CD38+CXCR5- subsets

The effect of BNT162b2 immunization was first explored on recipient T cell populations in a cohort of ten healthy donors who had not been previously infected with SARS-CoV-2. Donors had an average age of 41.8 ± 6.3 years. Six donors were male, and nine donors identified as having Caucasian ancestry. By collecting longitudinal peripheral blood samples before immunization, one week following booster immunization (day 28), and at an additional time point approximately three months later (day 105), we captured signatures of the initial immune response to BNT162b2 as well as lasting immunity (**Figure 4-1A-B**). T cell populations in the pre-vaccination and post-boost samples were initially examined by mass cytometry using a Helios cytometry by time-of-flight mass spectrometry (CyTOF) instrument and a panel of

antibodies focused on T cell immune and metabolic phenotypes (**Figure 4-2**). Cell density plots of concatenated data of T cells from the pre-vaccination and post-boost samples were first visualized using t-SNE dimensionality reduction (**Figure 4-3A**). Because MHC-peptide tetramer staining reagents were not available to directly identify expanding antigen specific S protein-reactive CD4 and CD8 T cells, data were analyzed using the recently developed T-REX machine learning algorithm (Barone et al., 2020b). By comparing changes in small k-nearest neighbor cell groupings, T-REX specifically identifies populations of cells with the greatest degrees of expansion or contraction from pre- to post- vaccination. In the case of viral infections, these expanding populations were preferentially enriched for virus-specific cells (Barone et al., 2020b). This approach sets aside the majority of peripheral blood T cells, which were unchanged, to instead focus on those populations of T cells in phenotypically distinct regions whose abundance increased or decreased by ≥95% in the initial 7 days following vaccination.

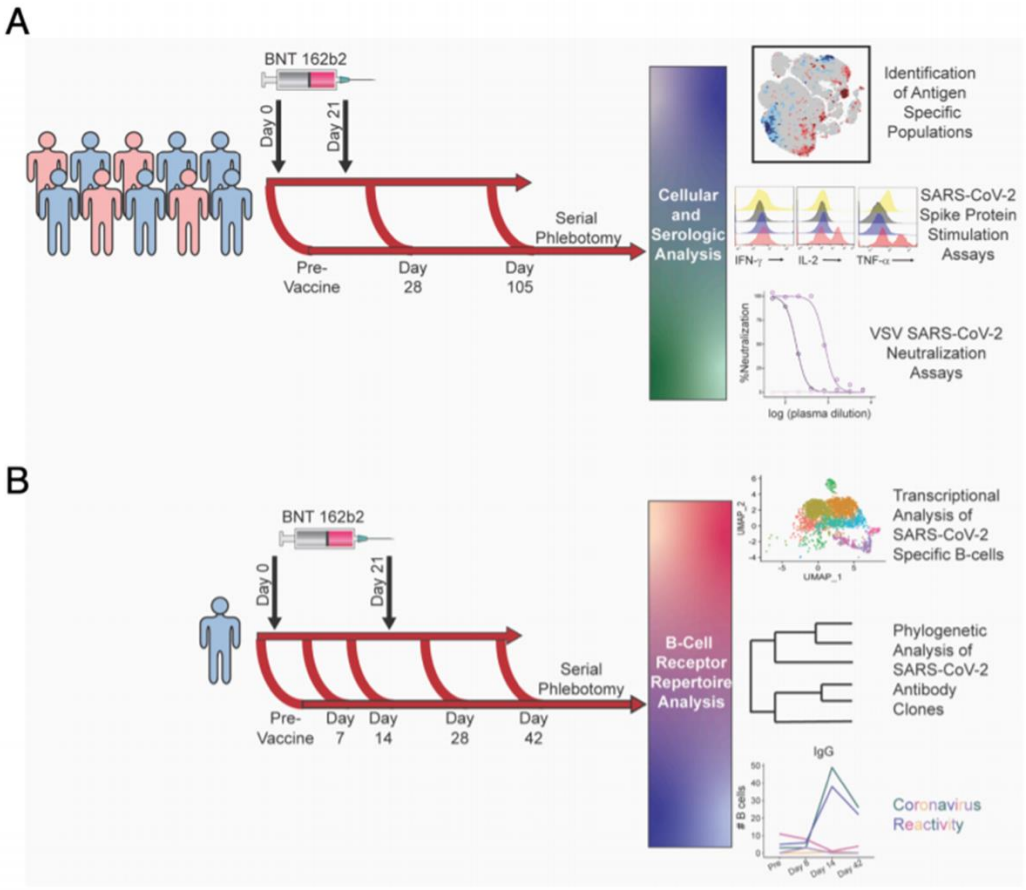

Figure 4-1. Schematic of vaccination schedule and sample collection. All donors were vaccinated with BNT162b2 on days 0 and 21. A. 10 healthy donors underwent serial phlebotomy was performed pre-vaccination (day -3 to 0), on day 28-30, and on day 105- 108. PBMCs were isolated at each time point, and citrated plasma was stored when possible. PBMCs from these donors were utilized for CyTOF and in vitro stimulation studies. Plasma was used both for SARS-CoV-2 ELISAs and vesicular stomatitis virus pseudoneutralization assays. B. A single healthy donor underwent serial phlebotomy prevaccination and on days 7, 14, 28, and 42. PBMCs and citrated plasma were isolated at each time point and used for transcriptional analysis of SARS-CoV-2 specific B cells.

Supplemental Table 1 - Mass cytometry antibody panels and clones					
CIC-HIDI-001 T cells, metabolism			CIC-HIDI-002 B cells, metabolism		
Target	In t-SNE	Mass	Target	In t-SNE	Mass
CD45	√	89	CD45	√	89
Dead Cells		103	Dead Cells		103
CD66B	√	106	CD66B	√	106
CD16	√	110	CD16	√	110
CD8	√	111	CD8	√	111
CD14	√	112	CD14	√	112
CD4	√	113	CD4	√	113
CD3	√	114	CD3	√	114
CD19	√	116	CD19	√	116
CD45R0	√	141	CD45R0	√	141
CPT1A		142	CPT1A		142
CD127	√	143	CD5	√	143
APT5A		144	ATP5A		144
GRIM19		145	GRIM19		145
			IgD	√	146
CD20	√	147	CD20	√	147
CD27	√	148	CD27	√	148
CCR4	√	149			
CD134	√	150	CD43	√	150
ICOS	√	151	IgL	*	151
TCRgd	√	152	CD21	√	152
			CD62L	√	153
GLUT3		154	GLUT3		154
-		155	PD-1	√	155
CXCR3	√	156	CD86	√	156
CD137	√	158			
CCR7	√	159	CD22	√	159
CD98	√	160	CD98	√	160
CTLA4		161	IgK	*	161
Ki67		162	CD79B	√	162
GLUT1		163	GLUT1		163
CD95	√	164			
			CD40	√	165
CD44	√	166	CD44	√	166
CD38	√	167	CD38	√	167
CYTOC		168	CYTOC		168
CD25	√	169	CD24	√	169
CD45RA	√	170	CD45RA	√	170
CXCR5	√	171	CXCR5	√	171
CD57	√	172	IgM	√	172
CXCR4	√	173	CXCR4	√	173
HLA-DR	√	174	HLA-DR	√	174
PD-1	√	175	CD71	√	175
CD56	√	176	CD56	√	176
Cells		191	Cells		191
Cells		193	Cells		193
CD11B	√	209	CD11B	√	209

*Note IgL or IgK was used as a single channel for t-SNE. Rhodium intercalator was used to mark cells without an intact plasma membrane (Dead cells on 103). Metabolism markers (CPT1, APT5A, GRIM19, GLUT1, CYTOC), CTLA4, Ki67, and Iridium intercalator (Cells on 191/193) were stained after fixation and methanol permeabilization.

Figure 4-2. Table of antibodies used for mass cytometry experiments.

T-REX revealed related populations of CD4 and CD8 T cells that expanded by ≥95% following vaccination and one population each that contracted by ≥95% (**Figure 4-3B**). Across the donor cohort, changes in abundance of these cell populations were widely, but not universally, shared in T-REX of individual donor samples (**Figure 4-4A**). Marker Enrichment Modeling (MEM) and specific antibody staining patterns established the protein marker expression patterns characteristic of each population (**Figure 4-3C, 4-3D**). The most expanded populations were CCR7- ~~CD45R0~~CD45RO+ CD4 and CD8 T cell populations that were negative for CXCR5, positive for PD-1, and highly co-expressed CD38 and ICOS (**Figure 4-3E**). Consistent with extensive expansion, these cells were the most proliferative cell subset based on Ki67 positivity, and were highly metabolically active, based on co-expression of transporters for glucose (GLUT1), amino acids (CD98), and lipids (CPT1a). These cells, thus, reflect non-canonical activated memory T cells. The T cell populations with decreasing abundance, in contrast, were CD45RA+ ICOS- and phenotypically characterized as naïve.

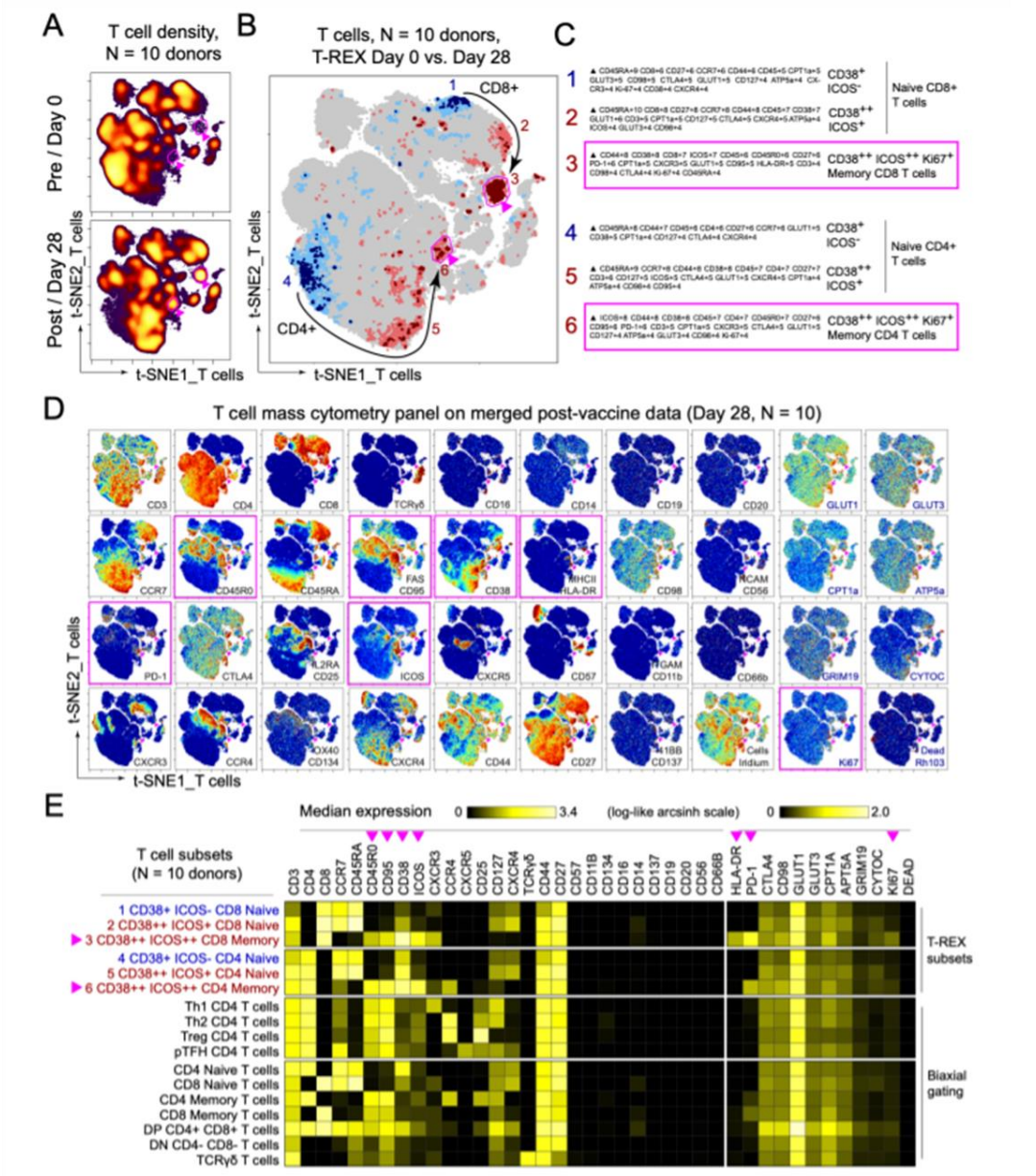

Figure 4-3. Immune phenotyping of BNT162b2 responding T cells. PBMCs collected from study participants pre-vaccination (day 0), day 28 post-vaccination (7 days post-boost) were analyzed by mass cytometry and data were concatenated for analysis. **A.** CD3+ T cells from 10 donors were pooled into two sets, one for pre-vaccination (taken at day 0) and one for post-vaccination (day 28). Cell density for each set is shown on the t-SNE axes. **B.** T-REX analysis of the CD3+ T cells from the 10 donors is shown. A central t-SNE, performed only using cell surface markers, shaded by T-REX change depicts phenotypically similar cells in regions of great expansion (dark red, ≥95% from post-vaccination day 28) or great contraction (dark blue, ≥95% from pre-) over time following SARS-CoV-2 vaccination. Red or blue population interpretations are shown for major expanding or contracting populations identified by T-REX. **C.** MEM labels show enriched protein features for several populations of great expansion or contraction. All measured features were included in MEM enrichment labels, which only show features enriched by at least +4 on a scale from 0 to 10. Pink boxes are around the MEM labels for the CD4+ and CD8+ memory T cell clusters that are greatly enriched for ICOS and CD38 protein and expanded greatly following vaccination. **D.** Each protein marker is shown on t-SNE axes, with proteins that were enriched on CD4+ and CD8+ ICOS+CD38+ cells in pink boxes. A rainbow intensity scale indicates expression levels with red representing high and dark blue representing low expression. Protein names in blue indicate functional features that were not used in t-SNE analysis, including metabolic markers, Rhodium, and Ki67. Surface proteins in black were used in t-SNE analysis. **E**. Heat maps show all markers measured by mass cytometry for cell populations as determined by T-REX or expert gating. Cell labels in red were defined by T-REX as expanding and blue were defined as contracting by T-REX. Black cell labels were expert gated. Protein markers enriched in CD4+ and CD8+ ICOS+CD38+ cells are indicated with pink arrows.

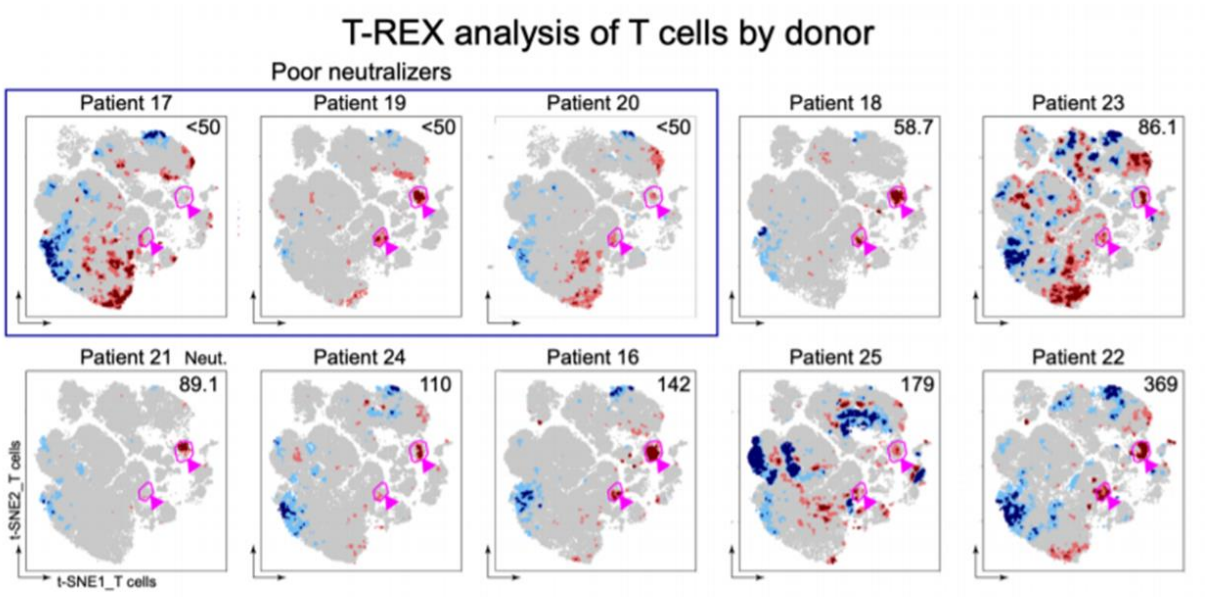

Figure 4-4. T-REX analysis of T cell populations for individual donors. Individual t-SNE MAPS are shown for each donor. T-REX analysis showing contracting populations (blue) and expanding populations (red) for T cells pre- and post-BNT162b2 vaccination. Pink circles denote the antigen-specific CD8+CD38+ICOS+ T cells (right) and CD4+CD38+ICOS+ T cells (middle) identified in Figure 1. Plasma dilution necessary to achieve 50% neutralization in a SARS-CoV-2 vesicular stomatitis virus pseudonormalization assay is shown in the top right of each map. Donors who failed to achieve 50% neutralization with a 50-fold dilution were deemed poor neutralizers.

ICOS+CD38+CXCR5- non-canonical T cell subsets respond specifically to SARS-CoV-2 S protein antigen

The selective enrichment of PD1+ICOS+CD38+CXCR5- CD4 and CD8 T cells following vaccination suggested these cells may specifically recognize viral S protein. To test SARS-CoV-2 specificity and further characterize the CD38+ICOS+ memory T cell populations, fluorescence flow cytometry and FACS were used to characterize cell subsets. Similar to mass cytometry, ICOS+CD38+ CD4 and CD8 cells were present in pre-immunized samples as approximately 1-2% of each T cell subset (**Figure 4-5A**). Importantly, these cell populations expanded in the post-boost sample and returned to initial frequencies at a later sample collection point. The expanded post-boost populations were also enriched for CCR7- cells (**Figure 4-5B**) consistent with mass cytometry findings, but not in $ICOS^{lo}CD38^{lo}$ T cells from the same samples. To investigate the functional capabilities of ICOS+CD38+ T cells, samples were

stimulated with PMA and ionomycin and cytokines were measured. At all collected timepoints, ICOS+CD38+ T cells produced significantly greater levels of IFN-γ and TNFα than ICOS-CD38- cells based on intracellular cytokine flow cytometric staining (**Figure 4-5C**).

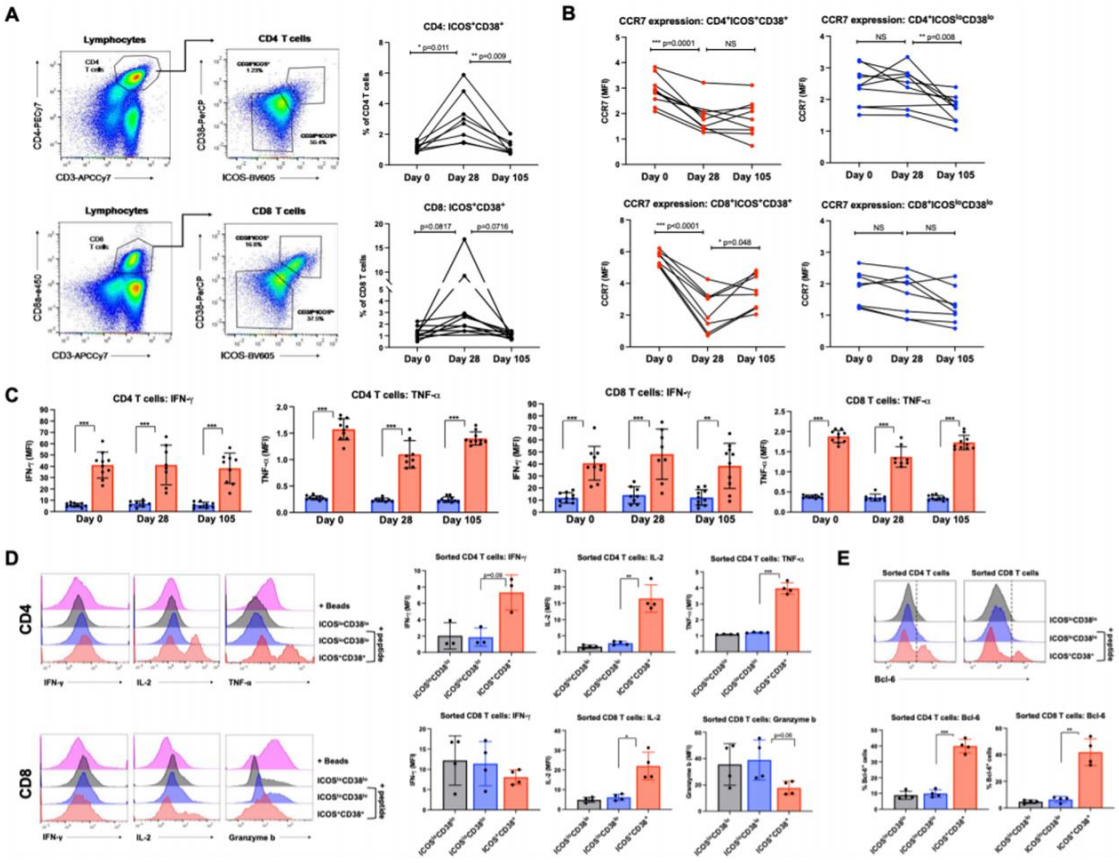

Figure 4-5. Immune phenotyping of BNT162b2 responding T cells. PBMCs collected from study participants pre-vaccination (day 0), day 28 post-vaccination (7 days post-boost) were analyzed by mass cytometry and data were concatenated for analysis. **A.** CD3+ T cells from 10 donors were pooled into two sets, one for pre-vaccination (taken at day 0) and one for post-vaccination (day 28). Cell density for each set is shown on the t-SNE axes. **B.** T-REX analysis of the CD3+ T cells from the 10 donors is shown. A central t-SNE, performed only using cell surface markers, shaded by T-REX change depicts phenotypically similar cells in regions of great expansion (dark red, ≥95% from post-vaccination day 28) or great contraction (dark blue, ≥95% from pre-) over time following SARS-CoV-2 vaccination. Red or blue population interpretations are shown for major expanding or contracting populations identified by T-REX. **C.** MEM labels show enriched protein features for several populations of great expansion or contraction. All measured features were included in MEM enrichment labels, which only show features enriched by at least +4 on a scale from 0 to 10. Pink boxes are around the MEM labels for the CD4+ and CD8+ memory T cell clusters that are greatly enriched for ICOS and CD38 protein and expanded greatly following vaccination. **D.** Each protein marker is shown on t-SNE axes, with proteins that were enriched on CD4+ and CD8+ ICOS+CD38+ cells in pink boxes. A rainbow intensity scale indicates expression levels with red representing high and dark blue representing low expression. Protein names in blue indicate functional features that were not used in t-SNE analysis, including metabolic markers, Rhodium, and Ki67. Surface proteins in black were used in t-SNE analysis. **E.** Heat maps show all markers measured by mass cytometry for cell populations as determined by T-REX or expert gating. Cell labels in red were defined by T-REX as expanding and blue were defined as contracting by T-REX. Black cell labels were expert gated. Protein markers enriched in CD4+ and CD8+ ICOS+CD38+ cells are indicated with pink arrows.

To evaluate the antigen specific T cell response to SARS-CoV-2 S antigen, PBMCs from each time point were incubated with recombinant SARS-CoV-2 S protein or T cell activation beads and cytokine responses were measured in culture supernatant. Interestingly, post-boost samples clustered into responders and non-responders for IFN-γ and TNFα production (**Figure 4-6A, 4-6B**). IL-2, IL-4 and IL-17a were unaffected by stimulation of T cells with S protein (**Figure 4-6C, 4-6E**). Furthermore, a subset of samples from all three time points produced IL-6 in response to S protein, suggesting cross-reactivity with prior coronavirus exposures (**Figure 4-6F**). Especially notable were the late collection time points in which three donor samples produced more IL-6 when incubated with S protein than positive control polyclonal CD3/2/28 bead stimulated samples. Samples from day 105 also showed an increase in the frequency of IL-2 and IFN-γ producing CD8 T cells when restimulated with S protein after 11 days of culture (**Figure 4-6G**).

To directly test antigen specificity and further characterize the expanding T cells identified by T-REX, ICOS+CD38+ and $ICOS^{lo}CD38^{lo}$ cells were isolated from four donor samples using FACS and protein markers from T-REX populations. Cells were then labeled with CellTrace Violet and stimulated with CD3-depleted autologous PBMCs with or without SARS-CoV-2 S peptide pool (**Figure 4-6H**). ICOS+CD38+ CD4 T cells produced IFN-γ, IL-2, and TNFα in response to SARS-CoV-2 S peptide stimulation, while peptide-stimulated $ICOS^{lo}CD38^{lo}$ T cells from the same sample failed to produce cytokines (**Figure 4-5D**). CD8 ICOS+CD38+ T cells also produced significant IL-2 in response to peptide stimulation, but had decreased Granzyme B, suggesting potential post-activation degranulation. Both CD4 and CD8 ICOS+CD38+ populations showed evidence of metabolic reprogramming, as mTORC1 pathway activity as shown by levels of phospho-S6 trended higher in each donor (**Figure 4-6I**). Expression of the glucose transporter GLUT1, however, was unchanged or modestly reduced (**Figure 4-6J**). Although the ICOS+CD38+ CD4 and CD8 T cells lacked CXCR5, the expanding S protein-specific cells shared some characteristics with circulating T follicular helper cells

(cTfh) as a portion of these cells expressed the Tfh characteristic transcription factor BCL6 (**Figure 4-5E**).

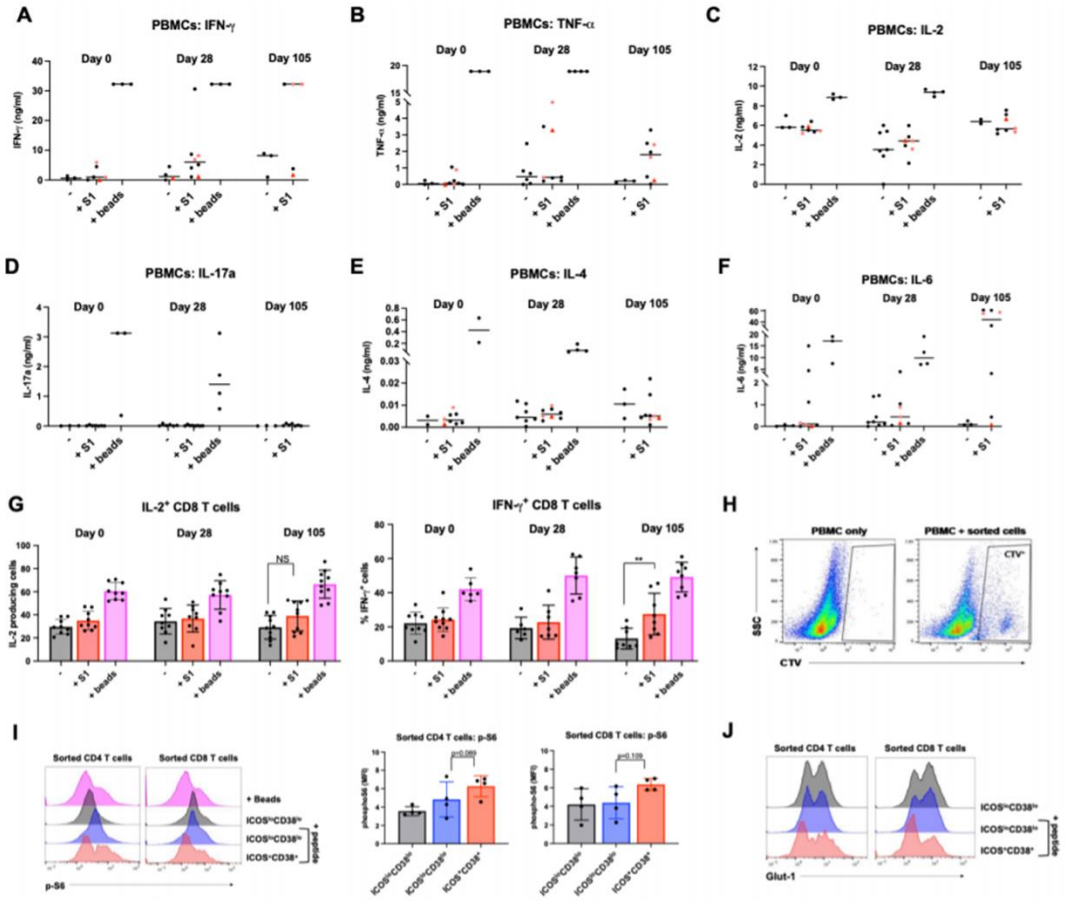

Figure 4-6. Supporting information for cytokine stimulation assays (Figure 4-5). PBMCs collected from study participants pre-vaccination (day 0), day 28 post-vaccination, and day 100 post-vaccination were cultured with no stimulation (-), Spike protein (+S1), or polyclonal anti-CD2/3/28 beads. **A-F.** Supernatants were collected from cultures after 4 days and predicted concentrations of each cytokine was determined by Legendplex bead capture assay. **G.** PBMC Cultures were maintained until day 11 post-stimulation and then subjected to flow cytometry to determine percentages of IL-2 and IFN-y producing T cells. **H.** Representative example of CellTraceViolet (CTV)-labeled samples from FACS, reintroduced to Day 0 autologous unlabeled PBMC cultures. **I.** Sorted CTV+ samples were left unstimulated (black) or stimulated with SARS-CoV-2 peptide (blue and red) for 2 days and phospho-S6 was measured by flow cytometry. Significance was determined by paired ANOVA. **J.** Representative Glut-1 staining in sorted samples as in I.

BNT162b2 induces expansion of CD38+CD43+ plasmablasts

The B cell response to BNT162b2 was next examined using a similar approach as applied to the T cell response. Peripheral blood samples from the same donor cohort were analyzed by mass cytometry using a panel of antibodies focused on B cell populations and metabolism. T-REX analysis of equally sampled B cells from all individuals showed that while

most B cell populations did not change following boost, there were 9 phenotypically-distinct areas of increased or decreased cell abundance (**Figure 4-7**). Of these, seven were populations that expanded and two were populations that contracted. The populations that expanded ≥95% from day 0 to day 28 included activated IgM+ B cells, memory B cells, and plasmablasts, while naïve B cells greatly contracted over this time. While individual donors showed some heterogeneity, these populations remained broadly evident (**Figure 4-8**). Using MEM to characterize cells identified by T-REX, the IgM-IgD- plasmablast population was further defined as CD20-CD38+CD43+ and metabolically active, with high expression of the iron transporter CD71, CD98, and Cytochrome C (**Figure 4-7C-4-7E**).

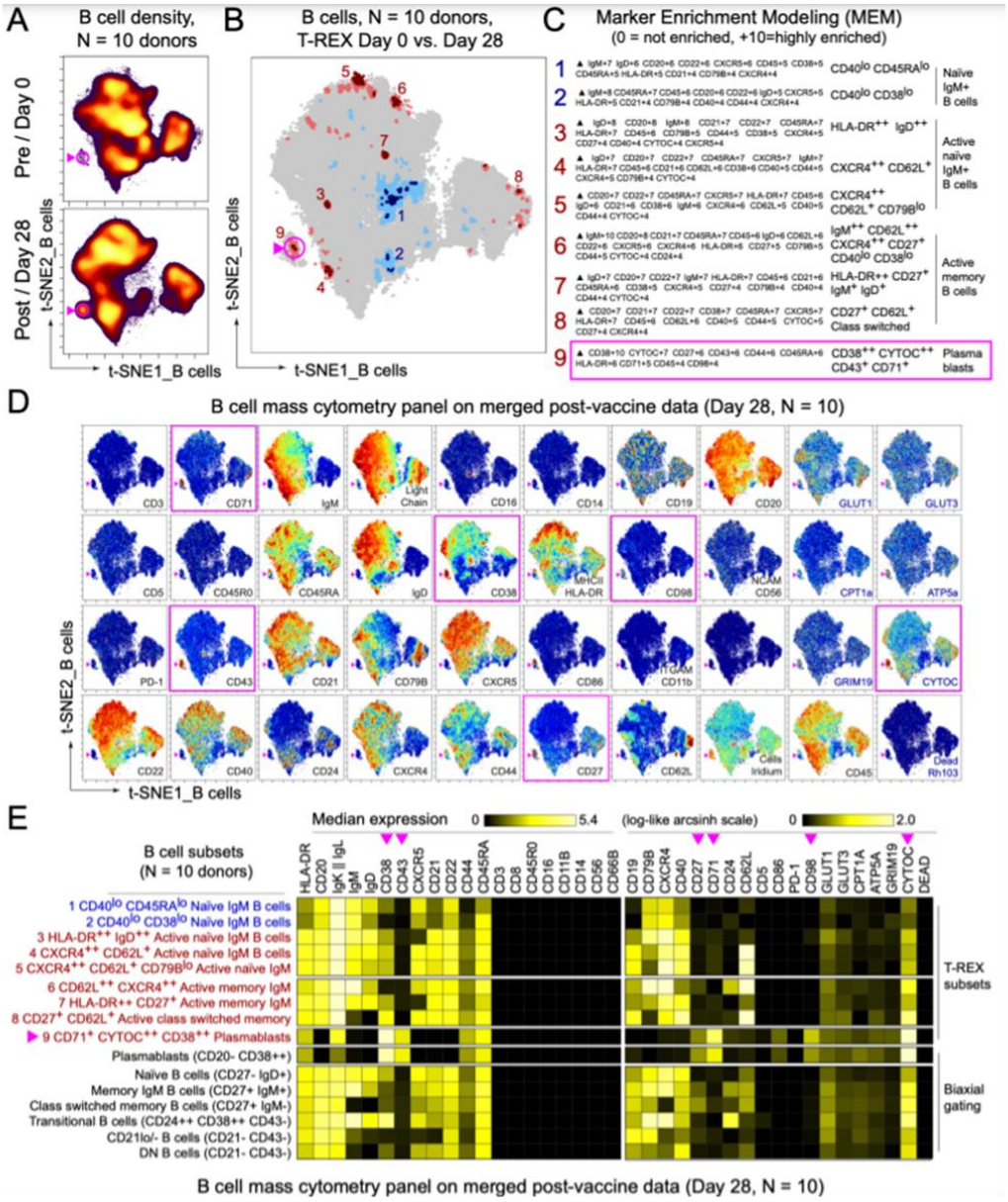

Figure 4-7. Immune phenotyping of BNT162b2 responding B cells. PBMCs collected from study participants pre-vaccination (day 0), day 28 post-vaccination (7 days post-boost) were analyzed by mass cytometry and data were concatenated for analysis of expanded B cell subsets and plasmablasts. **A.** B cells from 10 donors were pooled into two sets, one for pre-vaccination (taken at day 0) and one for post-vaccination (day 28). Cell density for each set is shown on the t-SNE axes. **B.** T-REX analysis of the B cells from the 10 donors is shown. A central t-SNE, performed only using cell surface markers, shaded by T-REX change depicts phenotypically similar cells in regions of great expansion (dark red, ≥95% from post-vaccination day 28) or great contraction (dark blue, ≥95% from pre-) over time following SARS-CoV-2 vaccination. Red or blue population interpretations are shown for major expanding or contracting populations identified by T-REX. **C.** MEM labels show enriched protein features for several populations of great expansion or contraction. All measured features were included in MEM enrichment labels, which only show features enriched by at least +4 on a scale from 0 to 10. A pink box is around the MEM label for the plasmablast cluster that expanded greatly following vaccination. **D.** Each protein marker is shown on t-SNE axes, with proteins that were enriched on the plasmablast population in pink boxes. A rainbow intensity scale indicates expression levels with red representing high and dark blue representing low expression. Protein names in blue indicate functional features that were not used in t-SNE analysis, including metabolic markers, Rhodium, and Ki67. Surface proteins in black were used in t-SNE analysis. **E**. Heat maps show all markers measured by mass cytometry for cell populations as determined by T-REX or expert gating. Cell labels in red were defined by T-REX as expanding and blue were defined as contracting by T-REX. Black cell labels were expert gated. Protein markers enriched in plasmablasts are indicated with pink arrows.

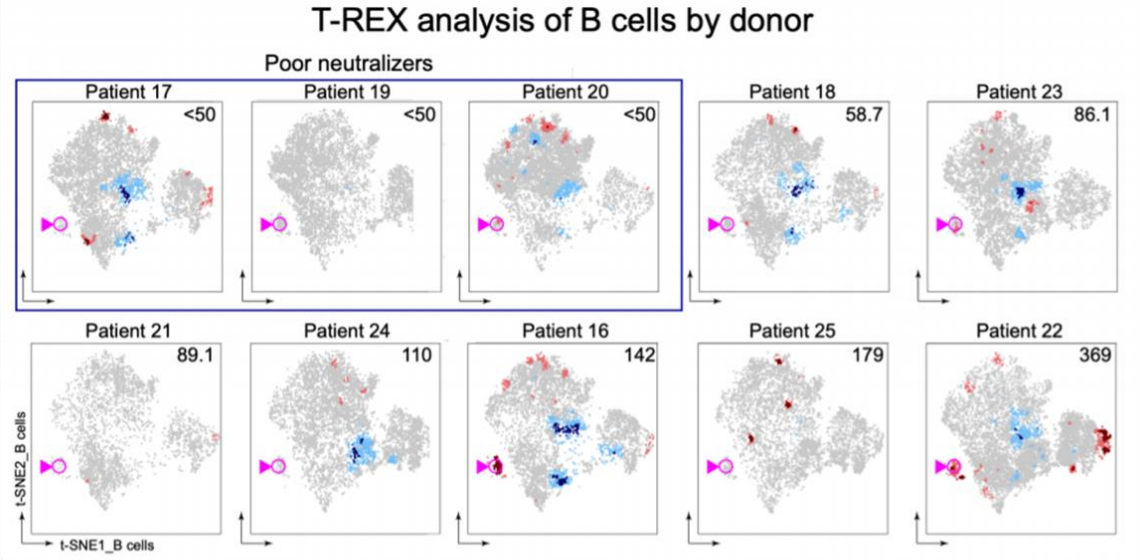

Figure 4-8. T-REX analysis of B cell populations for individual donors. Individual t-SNE MAPS are shown for each donor. T-REX analysis showing contracting populations (blue) and expanding populations (red) for B cells pre- and post- BNT162b2 vaccination. Pink circles denote the activated plasmablast population. Plasma dilution necessary to achieve 50% neutralization in a SARS-CoV-2 vesicular stomatitis virus pseudonormalization assay is shown in the top right of each map. Donors who failed to achieve 50% neutralization with a 50-fold dilution were deemed poor neutralizers.

Serologic response to BNT162b2 does not correlate to pre-existing immunity for endemic coronaviruses

BNT162b2-induced serological responses were measured by testing donor plasma samples from day 0, day 28, and day 105 for reactivity to S proteins from SARS-CoV-2 Wuhan-1, SARS-CoV-2 Beta, SARS-CoV-2 Alpha, HCoV-OC43, and HCoV-HKU1. Robust IgG responses were measured against SARS-CoV-2 Wuhan-1 by ELISA, with more varied IgM responses (**Figure 4-9A, Figure 4-10A**). These patterns were generally consistent across the S proteins from circulating variants of concern (VOCs). Interestingly, an IgA vaccine response was also evident in most donors. Most donors also displayed signatures of pre-existing immunity to the coronaviruses HCoV-OC43 and HCoV-HKU1, consistent with their endemic nature among the human population (Huang et al., 2020). Antibody levels to these endemic strains, however, did not change following BNT162b2 vaccination. Next, using a replication-competent vesicular stomatitis virus (VSV) SARS-CoV-2 (Case et al., 2020), Real Time Cell Analysis assay (Gilchuk et al., 2021) was performed to evaluate the neutralization activity of donor plasma at both pre- and at multiple timepoints post-vaccination. While pre-vaccine samples exhibited no SARS-

CoV-2 neutralization activity, most donors showed some neutralizing activity 3 months post-boost, although 3 of the 10 donors showed only weak neutralization at that timepoint (**Figure 4-9B**). Interestingly, a sharp decline in neutralization potency was observed for samples 3 months post-boost compared to day 7-8 post-boost in 3 of the 4 donors with multiple timepoints post-vaccination. Despite a modest trend for HCoV-HKU1 IgG, pre-existing antibody titers to HCoV-OC43 and HCoV-HKU1 did not correlate with SARS-CoV-2 neutralization potency 3 months post-vaccination (**Figure 4-9C**). Among the serological variables that were tested, SARS-CoV-2 IgG level 3 months post-boost was the only one with a significant correlation with VSV SARS-CoV-2 neutralization potency (**Figures 4-9C, 4-9D)**. Therefore, pre-existing coronavirus antibody did not appear to be a major determinant for defining the antibody response to BNT162b2 vaccination.

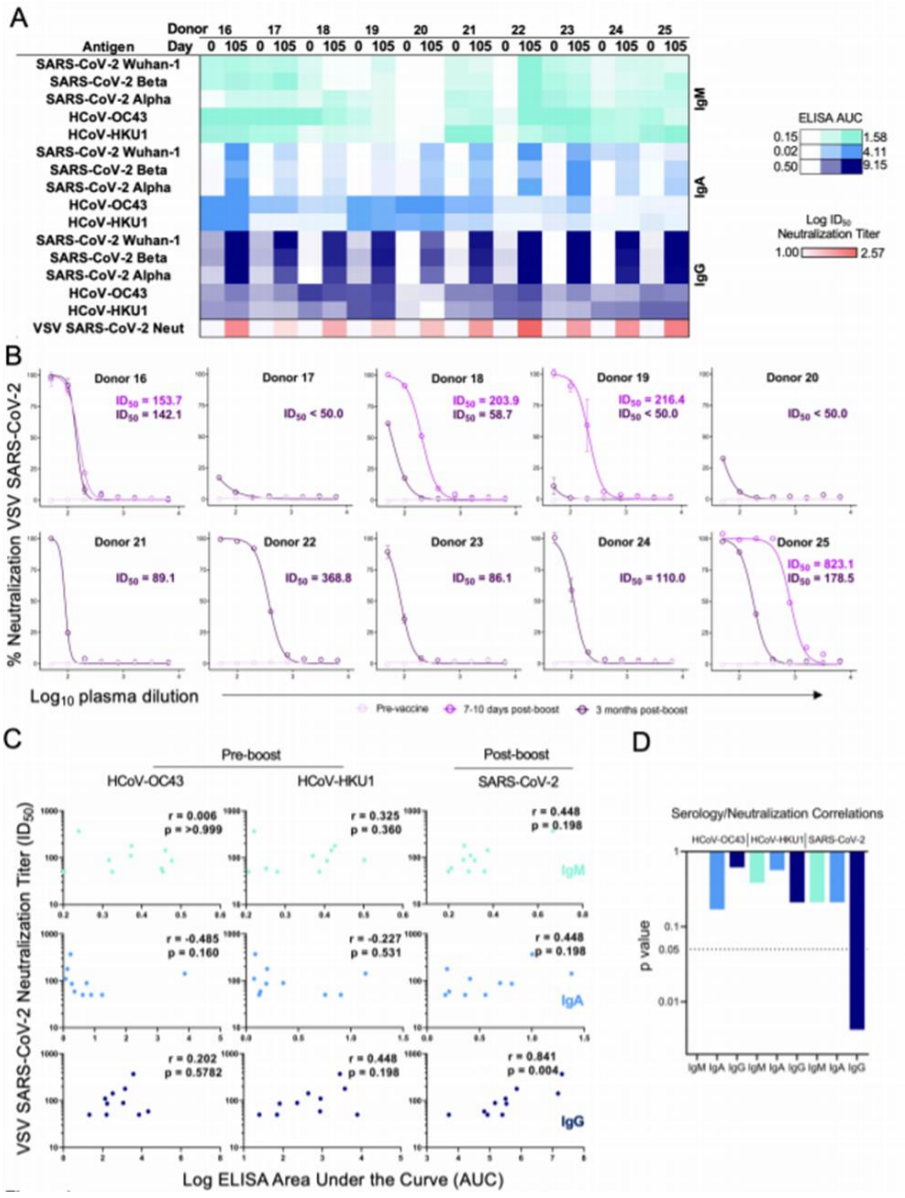

Figure 4-9. Serologic response induced by BNT162b2. Sera were analyzed from healthy donors pre-vaccination and at a late time point. **A.** ELISA area under the curve (AUC) values from vaccine recipient plasma are depicted as a heatmap against spike proteins from SARS-CoV-2 Wuhan-1, SARS-CoV-2 Alpha, SARS-CoV-2 Beta, HCoV-OC43, and HCoV-HKU1 coronaviruses. The minimum signal is represented in white and maximum signal is depicted by teal, blue, and navy blue for IgM, IgA, and IgG, respectively. At the bottom of the serology heatmap, Log ID_{50} neutralization titer is depicted from zero neutralization (white) to the maximum Log ID_{50} value quantified in the donor cohort. **B.** VSV SARS-CoV-2 neutralization curves of vaccine recipient plasma. Pre-vaccine, 7-10 days post-boost (collected only from donors 16, 18, 19, and 25), and 3 months post-boost are depicted in light pink, pink, and purple, respectively. %Neutralization (y-axis) is plotted as a function of plasma dilution (x-axis). **C.** Spearman correlations for serological responses as log ELISA AUC (x-axis) of patient cohort against pre-vaccination HcoV-OC43 (left), HcoV-HKU1 (middle), and post-boost SARS-CoV-2 (right) as a function of neutralization titer expressed as ID50 (y-axis). IgM is depicted in teal (top), IgA is shown in blue (middle), and IgG is shown in navy blue (bottom). The respective rho and p values are shown in the top right of each plot. **D.** Individual statistical significance comparison values are depicted as a bar graph for HCoV-OC43, HCoV-HKU1, and SARS-CoV-2 (left to right). IgM is depicted in teal, IgA is shown in blue, and IgG is shown in navy blue.

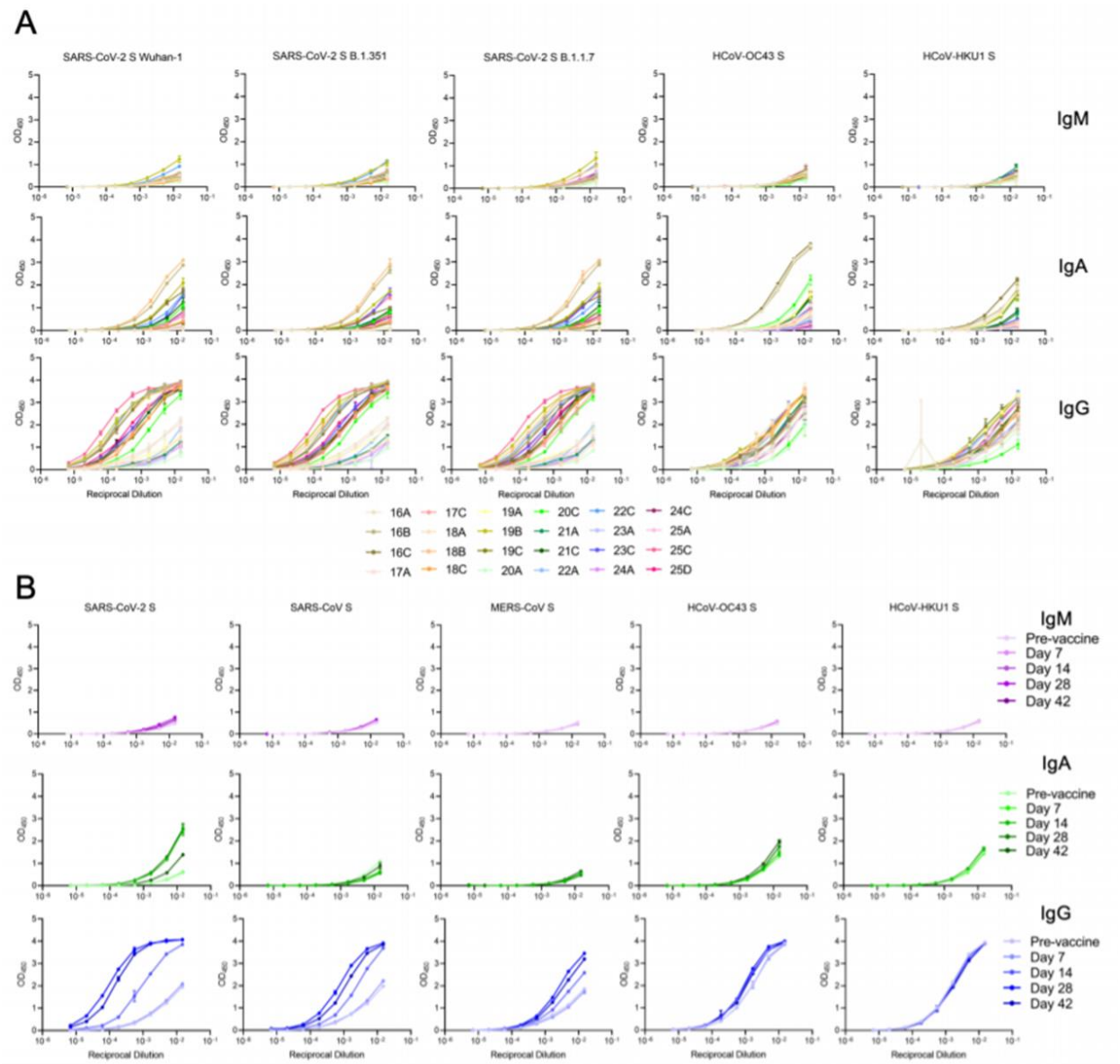

Figure 4-10. ELISA data for individual donors. A. ELISA curves for 10 donor vaccinee plasma for IgM, IgA, and IgG isotypes against spike proteins from SARS-CoV-2, SARS-CoV, MERS-CoV, HCoV-OC43, and HCoV-HKU1. The optical density at 450 nm (y-axis) is plotted as a function of antibody concentration (x-axis). **B.** ELISA curves for longitudinal donor plasma for IgM, IgA, and IgG isotypes against spike proteins from SARS-CoV-2, SARS-CoV, MERS-CoV, HCoV-OC43, and HCoV-HKU1. The optical density at 450 nm (y-axis) is plotted as a function of antibody concentration (x-axis).

Antigen selectivity of the SARS-CoV-2-reactive B cell response to BNT162b2 increases over time

While numerous antigen-specific antibodies have been isolated from SARS-CoV-2 infection (Robbiani et al., 2020; Rogers et al., 2020; Zost et al., 2020a) and more recently from vaccination (Wang et al., 2021c), little is currently known about the antigen specificities of individual B cells within the repertoire of SARS-CoV-2 vaccinees and how these change over time. We thus set out to characterize the evolution of the SARS-CoV-2 specific B cell repertoire by analyzing multiple time points pre- and post-vaccination of a single healthy male Caucasian donor of age 45-50 with no prior history of SARS-CoV-2 infection (**Figure 4-1B**) with LIBRA-seq (Setliff et al., 2019a; Shiakolas et al., 2021b). LIBRA-seq enables high-throughput mapping of B cell receptor sequence to antigen specificity for large numbers of B cells per sample against a diverse set of coronavirus antigens. The antigen specificity of the polyclonal plasma from this donor was largely similar to what was observed for the ten-donor cohort described above, with BNT162b2 immunization leading to the emergence of SARS-CoV-2-reactive IgM, IgA, and IgG antibodies (**Figure 4-10A**). While some reactivity with the closely related coronavirus SARS-CoV was observed, little reactivity was observed against the more distantly related MERS-CoV. Although SARS-CoV-2 S-reactive IgA and IgG were present at day 14 post-vaccine prime, neutralizing antibody titers were first detected at day 28 (7 days post-boost) at levels that remained largely unchanged at day 42 (**Figure 4-10B**).

Using a LIBRA-seq antigen library consisting of DNA oligo-tagged S proteins from SARS-CoV-2, SARS-CoV-2 D614G, SARS-CoV, MERS-CoV, HCoV-HKU1, HCoV-OC43, as well as the negative control proteins, B cells were enriched for antigen-positive cells by FACS (**Figure 4-11A**) and mapped to their antigen reactivity profile utilizing a next-generation sequencing readout. Clonal lineage tracing of BCR sequences from each timepoint identified several clusters containing sequences with high LIBRA-seq scores for SARS-CoV-2 (>1) across multiple timepoints (**Figure 4-11B**). LIBRA-seq identified both B cells that were specific to

SARS-CoV-2 (henceforth referred to as SARS-CoV-2-only B cells) as well as B cells that were cross-reactive between SARS-CoV-2 and other coronaviruses (cross-reactive B cells) (**Figure 4-12**). Both SARS-CoV-2-only and cross-reactive B cells showed a shift from IgM to IgG after vaccination, suggesting antigen-driven class switching (**Figure 4-13C**). IgM remained more prevalent than IgG in the cross-reactive B cell population, suggesting a stronger class-switching potential for SARS-CoV-2-only over cross-reactive B cells in response to vaccination. SARS-CoV-2 cross-reactivity was primarily observed in HCoV-OC43-reactive IgM cells in this donor, although the overall levels of SARS-CoV-2 cross-reactive B cells generally decreased at later timepoints post-vaccination (**Figure 4-13D**). In contrast, the levels of SARS-CoV-2-only IgG+ B cells and IgG+ B cells that cross-reacted between SARS-CoV-2 and the closely related SARS-CoV were substantially increased at days 14 and 42. Interestingly, while the levels of SARS-CoV-2-reactive B cells peaked at day 14 for both the IgG and IgA isotypes, the IgA levels were reduced to near baseline at day 42, while IgG levels at day 42 were decreased but clearly present. Changes in B cell cross-reactivity and isotype abundance were also evident when analyzed at the single-cell level using antigen-specific LIBRA-seq scores as a metric for comparing antigen specificity evolution (**Figure 4-13E**). These results suggest an evolution in SARS-CoV-2 antibody specificity and cross-reactivity in response to BNT162b2 vaccination, supporting a model of immune progression from early prevalence of endemic cross-reactive IgM to more highly selective SARS-CoV-2 IgG production over time.

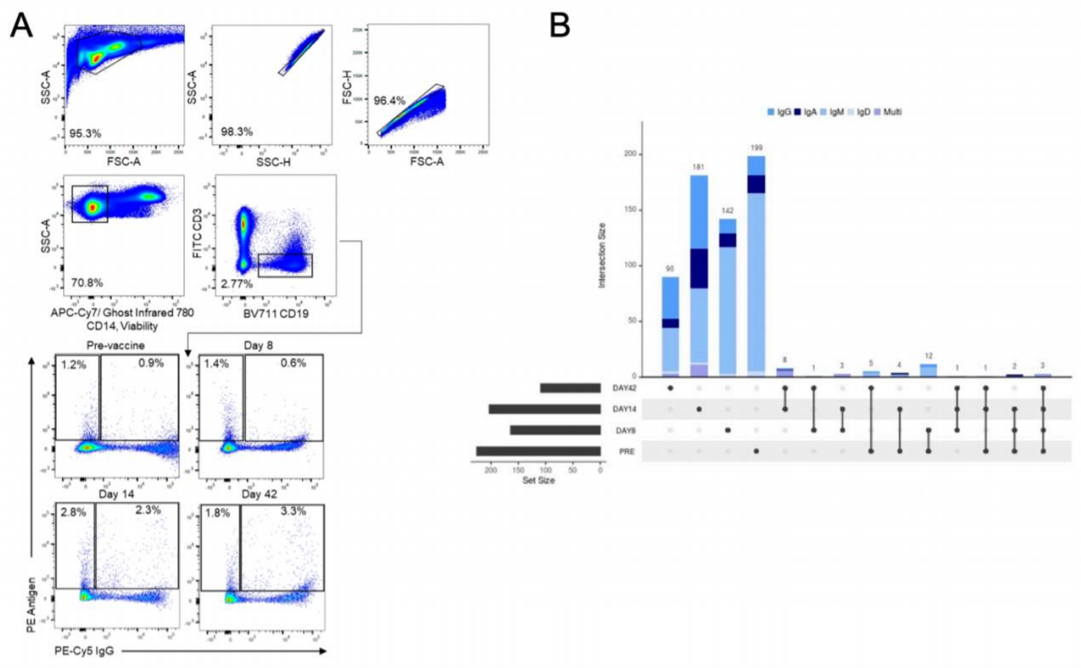

Figure 4-11. Flow cytometry enrichment of coronavirus antigen-binding B cells. A. Gating scheme for fluorescence activated cell sorting (FACS) of PBMCs. Cells were stained with viability dye Ghost Infrared 780, CD14-APC-Cy7, CD3-FITC, BV711-CD19, and IgG-PE-Cy5. Antigen positive B cells were detected by streptavidin-PE binding to biotinylated DNA-oligo tagged antigens. Gates are drawn based on parameters set during cell sorting and percentages are from sort are listed in each plot. The gate for enrichment of CD19+ cells is shown for the pre-vaccine sample; Day 8, Day 14, and Day 42 samples all followed this sorting scheme. **B.** Representation of unique and shared clonotypes between different timepoints. For each individual and combination of timepoints, the number of clonotypes is displayed as a vertical bar graph. Shared clonotypes between timepoints is displayed by filled circles, showing which timepoints are part of a given shared cluster/combination where each combination is mutually exclusive. For each timepoint, the total number unique and shared clonotypes is indicated as a horizontal bar at the bottom left of the panel. Isotypes of clonotypes are represented in different colors in the vertical bar graphs. Clusters with multiple isotypes is shown as "Multi."

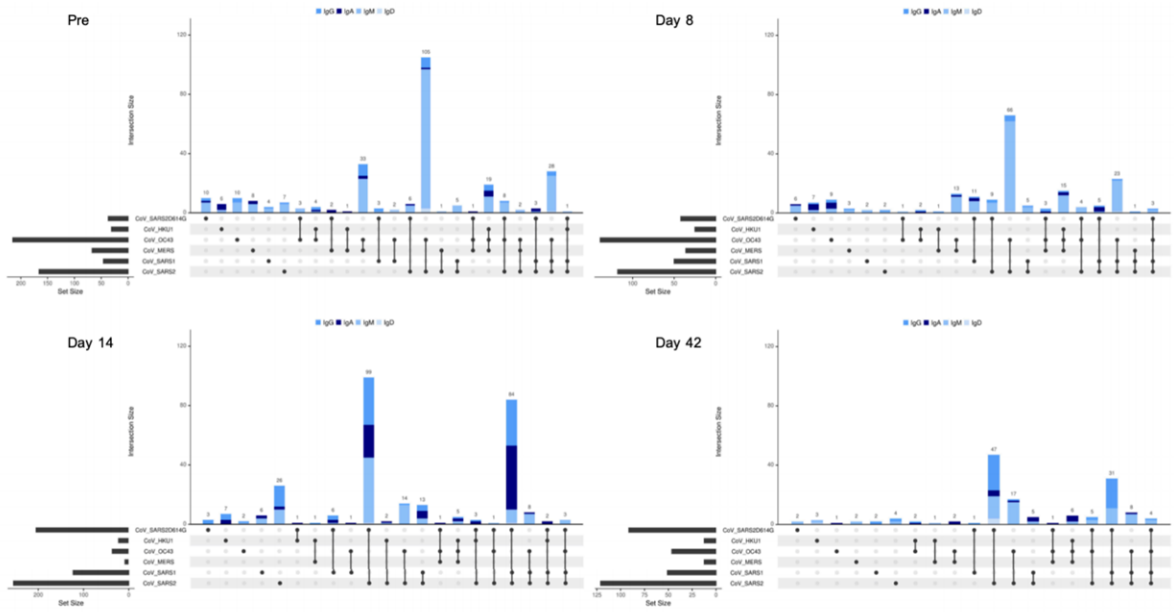

Figure 4-12. B cell clones with cross-reactive LIBRA-seq scores over time. For each combination of CoV antigens, the number of B cells with high LIBRA-seq scores (≥1) is displayed as a bar graph. The combination of antigens is displayed by filled circles, showing which antigens are part of a given combination. Each combination is mutually exclusive. The number of B cells with high LIBRA-seq scores for each antigen is indicated as a horizontal bar at the bottom left of the panel. Isotypes of select B cells are depicted as more intense colors of blue beginning at IgD and following with IgM, IgG, and IgA.

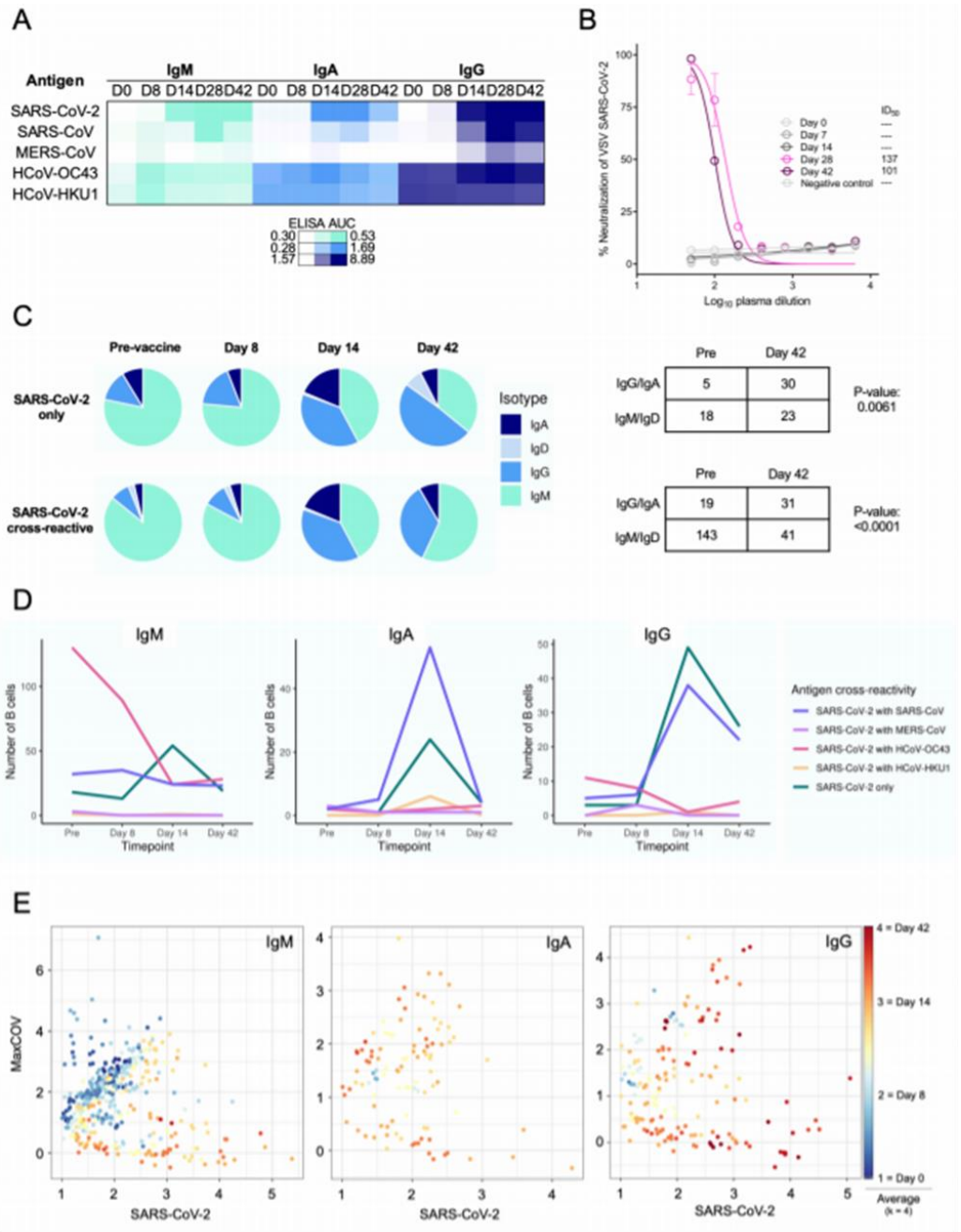

Figure 4-13. LIBRA-seq characterization of the antigen specificity of the SARS-CoV-2-reactive B cell response to BNT162b2. A single donor with multiple longitudinal samples was analyzed serologically and by LIBRA-seq. **A.** Plasma ELISA area under the curve (AUC) values are depicted as a heatmap against spike proteins for SARS-CoV-2, SARS-CoV, MERS-CoV, HCoV-OC43, and HCoV-HKU1. The minimum signal is represented in white and maximum signal is depicted by teal, blue, and navy blue for IgM, IgA, and IgG, respectively. **B.** VSV SARS-CoV-2 neutralization of longitudinal timepoints. % Neutralization (y-axis) is plotted as a function of plasma dilution (x-axis). The negative control sample, Day 0, Day 8, and Day 14 timepoints are depicted in grey, with Day 28 and Day 42 curves shown in pink and purple respectively. The inhibitory dose at 50% neutralization (ID_{50}) values of each timepoint are denoted to the right of graph. **C.** Pie charts representing: (top) SARS-CoV-2 specific B cells with an associated LIBRA-seq score ≥1 for SARS-CoV-2; and (bottom) SARS-CoV-2 cross-reactive B cells (bottom) with an associated LIBRA-seq score ≥1 for SARS-CoV-2 and for at least one other coronavirus antigen (MERS-CoV, SARS-CoV, HCoV-OC43 or HCoV-HKU1). For the pre-vaccine, day 8, day 14, and day 42 timepoints, the segments in each pie chart represent the number of antibody sequences with the isotypes IgD (light blue), IgM (teal), IgG (blue), IgA (navy blue). Also shown is a statistical comparison of isotype distribution of SARS-CoV-2 specific (top) and SARS-CoV-2 cross-reactive (bottom) B cells in the pre-vaccine and day 42 post-vaccination timepoints. The values in each table represent the number of antibody sequences with the designated isotypes. **D.** Evolution of cross-reactive SARS-CoV-2 and SARS-CoV-2-only B cells from each isotype (separate plots) over time. Each line shows the number of B cells (y-axis) for either SARS-CoV-2-only (blue) or SARS-CoV-2 cross-reactive with other coronaviruses (designated colors) B cells at the four timepoints (x-axis). **E.** Individual IgM, IgA, and IgG expressing cells graphed for cumulative cross-reactive (Max COV) and SARS-CoV-2 LIBRA-seq scores shaded based on k=4 nearest neighbor averaging for time of sample collection.

SARS-CoV-2-binding memory B cells and plasmablasts expand following BNT162b2 vaccination

The LIBRA-seq B cell receptor sequence and antigen specificity data was further combined with RNA-seq to identify gene expression patterns and B cell subset identities of SARS-CoV-2-binding B cells over time following vaccination. Seurat and LIBRA-seq analyses were integrated to enable immune repertoire analysis within transcriptionally-defined B cell subsets. Nine clusters were identified by UMAP across all B cells based on gene expression profiles that represented naive, predominantly IgM memory (termed “memory”), predominantly IgA or IgG-switched memory (termed “switched memory”), or plasmablast populations (**Figure 4-14A, 4-14B**). Characteristic gene expression patterns defined each B cell subset (**Figure 4-14C, Figure 4-15A**). Only a modest number of genes were differentially expressed in LIBRA-seq predicted SARS-CoV-2-binding B cells relative to other members of those cell clusters (**Figure 4-15B**). These did include, however, selectively elevated *CCR9*, *IgHM*, and *IGLC1* and decreased Galectin 1 (*LGALS1*) in the SARS-CoV-2-binding plasmablast populations, suggesting active migration and antibody production. When combined with LIBRA-seq scores for putative antigen specificity, predicted SARS-CoV-2-binding B cells expressed a wide range of *IGHV* gene segments (**Figure 4-15C**). Class-switching is associated with protective immune responses, thus further analyses focused on class-switched SARS-CoV-2-binding B cells. Consistent with plasmablast populations identified by T-REX analysis of B cell protein expression (**Figure 4-7**), LIBRA-seq suggested SARS-CoV-2-binding B cells were represented among both switched memory and plasmablast cell clusters (**Figure 4-14D**). Analysis of class-switched, SARS-CoV-2-binding B cells revealed the majority had no or only modest degrees of somatic hypermutation, which did not increase with time (**Figure 4-14E, Figure 4-15D**). By day 14 a robust SARS-CoV-2 binding plasmablast population with limited somatic hypermutation was evident that diminished by day 42 after initial BNT162b2 vaccination (**Figure 4-15F)**. These plasmablasts did not have significant LIBRA-seq cross-reactivity scores for

endemic coronaviruses but included plasmablasts selective for SARS-CoV-2 or with dual selectivity for SARS-CoV-2 and SARS-CoV (**Figure 4-14G**).

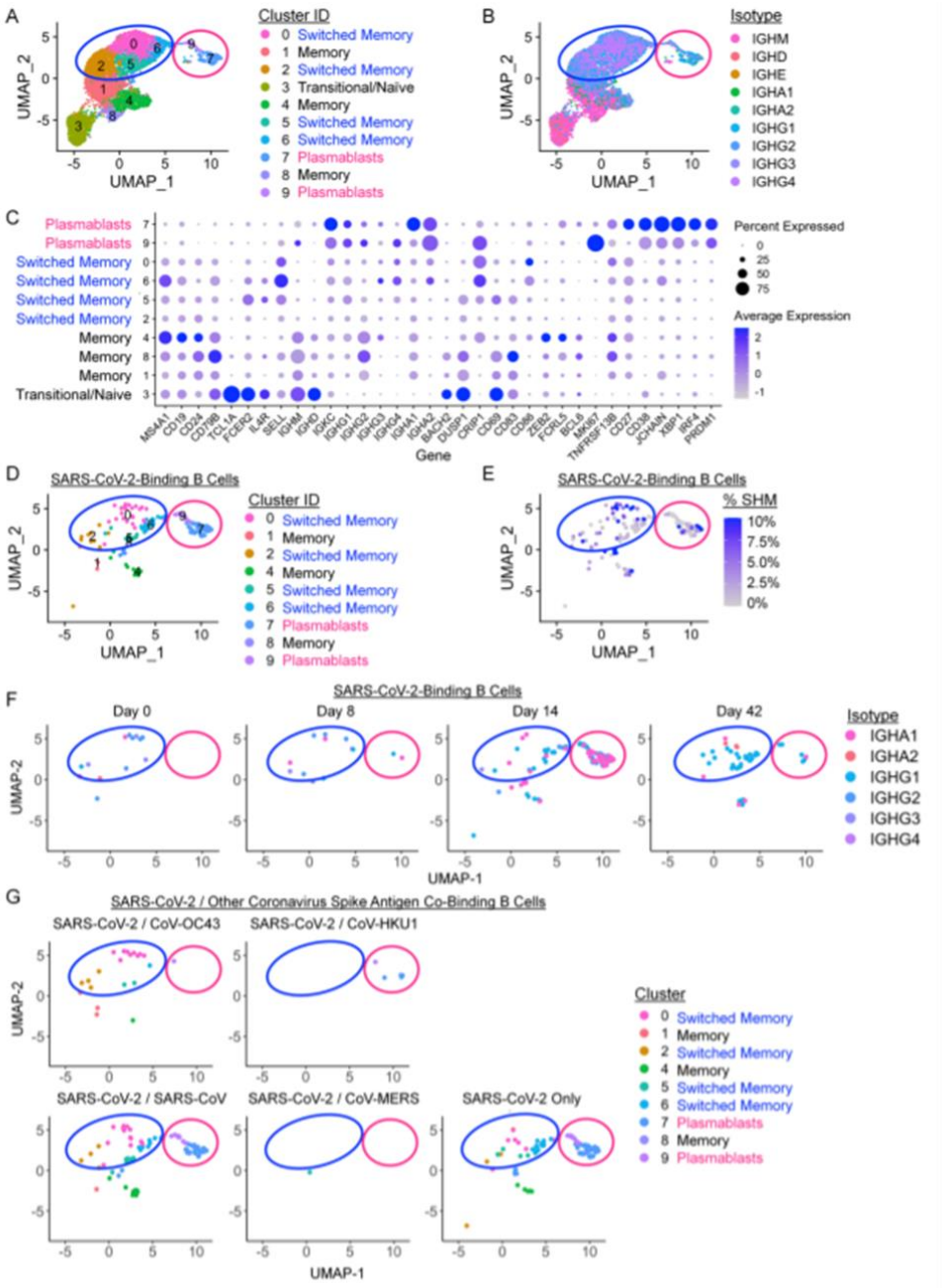

Figure 4-14. BNT162b2 vaccination drives IgG and IgA-switched SARS-CoV-2-binding memory B cell and plasmablast expansion. B cells that bound a panel of LIBRA-seq antigens were purified from peripheral blood samples and single cell RNA-seq/BCR-seq/LIBRA-seq data were integrated. Cells were scored positive for binding a given antigen for LIBRA-seq scores > 1. **A.** UMAP identified clusters of B cells based on transcriptional similarity. Antibody-secreting cells (pink circle encompassing clusters 7 and 9) and isotype-switched memory B cells (blue circle encompassing clusters 0, 2, 5, and 6) are highlighted across all UMAP plots. **B.** BCR isotypes are shown among sorted B cells. **C.** Selected gene expression profiles within each cluster are shown. **D-F.** SARS-CoV-2-binding B cells were identified using LIBRA-seq and non-class-switched B cells were filtered out for detailed analysis. **D.** UMAP identified clusters of SARS-CoV-2-binding B cells based on transcriptional similarity. **E.** IgH somatic hypermutation frequency of SARS-CoV-2-binding B cells is indicated. **F.** SARS-CoV-2-binding B cell isotypes are shown for each time point. **G.** SARS-CoV-2-binding B cells are shown, each panel indicates cells which also bound the indicated coronavirus S antigens.

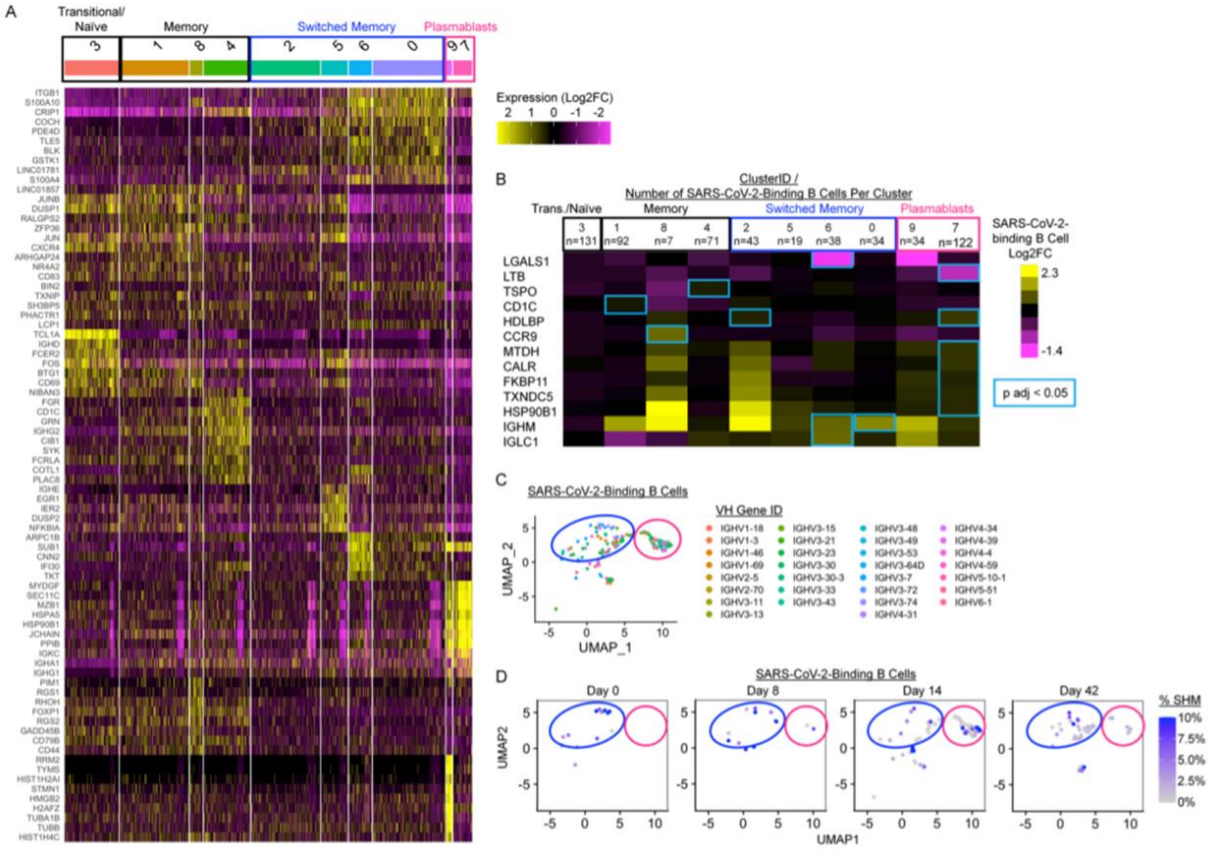

Figure 4-15. Single-cell RNAseq analysis identifies distinct clusters of memory and plasmablast subsets among B cells enriched for coronavirus antigen-binding by LIBRAseq. A. The top 10 differentially expressed genes were identified by Seurat for each cluster identified as in Fig. 5. Heatmap depicts relative expression for each gene, columns are individual cells within each cluster. **B-D.** SARS-CoV-2-binding B cells were identified by LIBRAseq as in Fig. 5. Circles depict switched memory (blue) and plasmablast clusters (pink). **B.**SARS-CoV-2-binding B cells were compared to non-SARS-CoV-2-binding B cells within each cluster identified in panel A. Log2 fold change is shown for differentially-expressed genes that were significantly different between these two groups in at least one cluster (p adj < 0.05, blue rectangles). **C.** VH gene identity is shown among all SARS-CoV-2-binding B cells.**D.** Somatic hypermutation is shown among SARS-CoV-2-binding B cells identified at each time point following vaccination with BNT162b2.

Integrated associations of antigen-specific cell and antibody responses to BNT162b2

To test associations of the antigen-specific CD4, CD8 T and B cell plasmablast populations and the antibody response to BNT162b2, the abundance of ICOS+CD38+ CD4 or CD8 and plasmablast cell populations were compared across donors (**Figure 4-16A**). The CD4, CD8, and plasmablast populations were associated with each other to support a coordinated response. Further, plasmablast frequencies showed a trend towards significance and ICOS+CD38+ CD8 T cells correlated with eventual levels of SARS-CoV-2 specific IgG. The three donors with the lowest levels of neutralizing antibodies (red and pink) also had the lowest numbers of ICOS+CD38+ CD8 cells. Intriguingly, donor 17 (red) had the lowest abundance of

ICOS+CD38+ CD8 cells and plasmablasts and was subsequently infected with SARS-CoV-2. While donor 17 represents a single case, the observation supports the idea that BNT162b2-induced expansion of non-canonical memory ICOS+CD38+ CD4 and CD8 T cells may be critical to drive plasmablast expansion, antibody production, and protective immunity to SARS-CoV-2.

We next examined the antibody sequence relationships of B cells elicited by vaccination from the longitudinally collected donor. Interestingly, a cluster of antibody heavy chain sequences, referred to as cluster 720, was found to exhibit high similarity with public antibody sequences from the CoV AbDab database (Raybould et al., 2021) of individuals with natural COVID-19 infection (**Figure 4-16B**). Consistent with previous studies, this is indicative of a convergent B cell response from natural infection and vaccination (Chen et al., 2021a). Interestingly, however, despite the high similarity in heavy chain sequences, the members of cluster 720 utilized a diversity of light chain V-genes and CDRL3 sequences. The B cells from cluster 720 included sequences with IgM, IgA, and IgG isotypes, and originated from switched memory and plasmablast cell clusters (**Figure 4-16C**) that displayed only low to moderate degrees of somatic hypermutation (**Figure 4-16B**). Day 8 sequences from cluster 720 were an IgM isotype, whereas the sequences from days 14 and 42 appeared as IgG and IgA isotypes (**Figure 4-16B**). To characterize individual antibodies from cluster 720, we expressed heavy- and light- chain pairs as recombinant IgG for two members from diverse branches in the tree, 720-3 (using *IGKV3-15*) and 720-17 (using *IGKV3-20*), and tested for reactivity against coronavirus S proteins. Consistent with their LIBRA-seq scores, these antibodies were cross-reactive to SARS-CoV-2 and the closely related SARS-CoV but showed no reactivity to the endemic coronaviruses HCoV-HKU1 and HCoV-OC43 (**Figure 4-16D)**. Epitope mapping experiments revealed that these two antibodies were specific to the S2 domain of spike (**Figure 4-16E, Figure 4-17**).

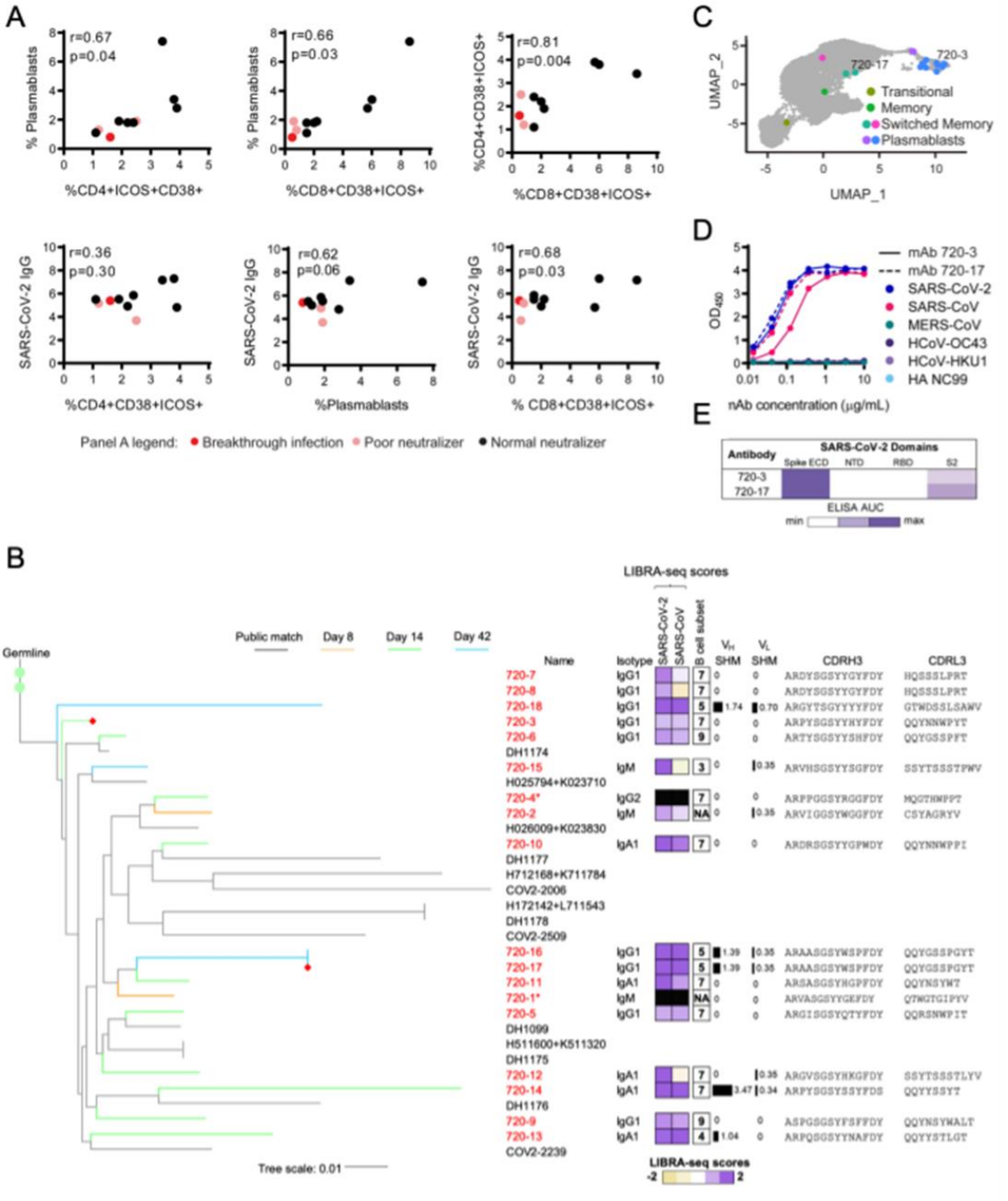

Figure 4-16. Associations of antigen-specific cell populations and antibody responses. A. Correlation of biaxially gated plasmablast and T cell populations with other cellular subsets and SARS-CoV-2 IgG using Pearson correlations. Patients with normal neutralization titers are shown in black, poor neutralizers with no known breakthrough infection are shown in pink, and a poor neutralizer with known breakthrough infection is shown in red. **B.** Phylogenetic tree of a public antibody cluster comprised of LIBRA-seq-identified sequences (antibody names: red; branches: colored by timepoint) and previously published SARS-CoV-2 antibody sequences from the CoV-AbDab database (grey), with recombinantly expressed antibodies 720-3 and 720-17 highlighted with a red diamond at the end of their respective branches. For each sequence from the cluster, sequence features including isotype, LIBRA-seq scores, % SHM of V-gene, and amino acid sequences of CDRH3 and CDRL3 are displayed. Nucleotide level percentage of SHM changes of V-genes of both heavy and light chains were reported as bars with numerical values. LIBRA-seq scores are shown as a range with tan-white-purple representing -2 to 0 to 2. Scores higher or lower than this range are shown as -2 and 2, respectively. The B cell subsets are classified by scRNA-seq analysis. **C.** Location of B cells in cluster 720 including recombinantly expressed monoclonal antibodies (720-3 and 720-17) on UMAP identified clusters of B cells based on transcriptional similarity. **D.** ELISAs for antibodies selected for monoclonal antibody characterization are shown against spike proteins for SARS-CoV-2 (black), SARS-CoV (pink), MERS-CoV (teal), HCoV-OC43 (purple), HCoV-HKU1 (light purple), and HA NC99 (light blue) for antibodies 720-3 (solid lines) and 720-17 (dashed lines). **E.** Epitope mapping ELISA AUC for antibodies 720-3 and 72017 against SARS-CoV-2 spike ECD, and truncated subunit domains NTD, RBD, and S2.

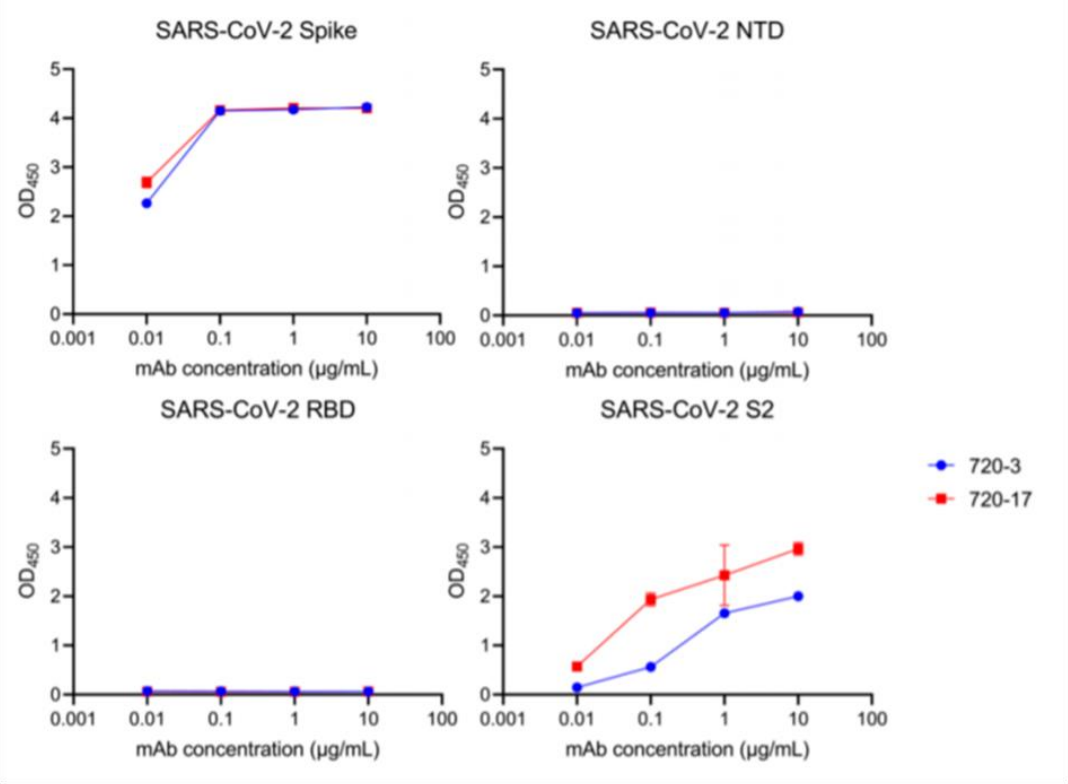

Figure 4-17. Domain mapping of recombinant monoclonal antibodies. ELISA data for the SARS-CoV-2 spike and the truncated SARS-CoV-2 NTD, RBD, and S2 domains. Optical density at 450 nm (y-axis) is depicted as a function of antibody concentration (x-axis).

DISCUSSION

Here we describe the antigen-specific cellular response and development of the specific antibody repertoire over time in a longitudinal cohort of healthy donor recipients of the BNT162b2 vaccine. Machine learning analyses of proteomic mass cytometry data and single cell sequencing of the SARS-CoV-2 S B cell repertoire identified antigen-specific CD4 T cell, CD8 T cell, B cell and plasmablast populations. PD1+CD38+ICOS+CXCR5- CD4 and CD8 T cells produced TNFα and IFN-γ in response to stimulation with SARS-CoV-2 S protein and shared features of memory or Tfh. The B-cell repertoire shifted from initial apparent cross-reactivity with endemic coronavirus prior to immunization to a more SARS-CoV-2-selective response later, marked by expansion of IgA and IgG plasmablasts. Importantly, antigen-specific cell subsets identified early after boost correlated with sustained IgG antibody response at day

105, and both the CD4 and CD8 populations of ICOS+CD38+ T cells were deficient in a donor who later experienced a breakthrough SARS-CoV-2 infection.

Antigen-specific CD4 and CD8 T cells that drive the vaccine response were phenotypically distinct from canonical peripheral blood T cell populations. SARS-CoV-2 S protein specific CD4+ PD1+CD38+ICOS+CXCR5- did resemble CD38+ICOS+CXCR5- T cells previously identified following SARS-CoV-2 infection (Koutsakos et al., 2021) and a prior study of BNT162b2 vaccination (Samanovic et al., 2021), but had several previously undescribed characteristics. A subset of these antigen specific cells did express the Tfh transcription factor BCL6, and PD1+ICOS+ cTfh cells have been previously associated with vaccine responses (Cardeno et al., 2018; Herati et al., 2017; Huber et al., 2020). However, they lacked CXCR5 that is characteristic of Tfh and CD4 T cells produced IL-2 and TNFα when antigen-stimulated. The CD38+ICOS+ antigen specific population resemble rhinovirus-specific tissue homing memory CD4+ T cells that express CCR5 and CD38 and are associated with transcription factor TBET (Muehling et al., 2018) and may reflect extrafollicular PD-1+CXCR5- CD4+ T cells observed following viral infections (Wang et al., 2021d). Alternatively, these cells may include memory Tfh or IFN-γ-producing Thf1 populations that have down regulated CXCR5 in circulation as they enter a memory pool (Fang et al., 2018; Hale and Ahmed, 2015; Zhu and Zhu, 2020). CD38+ICOS+CXCR5- cells thus appear as antigen-experienced memory T cell that may be tissue homing and arise from multiple T cell subtypes, such as Th1 and Tfh CD4 T cells to be poised for long-lived anti-viral memory responses.

In addition to induction of SARS-CoV-2 neutralizing antibodies (Khoury et al., 2021), cytotoxic T cell responses also contribute to vaccine-mediated protection. CD8+ T cells support life-long immunity against influenza (McMichael et al., 1983), EBV (Rickinson and Moss, 1997), and CMV (Currier et al., 2002), and induction of a robust CD8+ T cell response is an emerging focus in vaccine development (Estrada and Schultz-Cherry, 2019; McMichael, 2018). Here, we identified antigen-specific CD8+ PD1+CD38+ICOS+CXCR5- cytotoxic memory T cell population

capable of cytokine production in response to S antigenic peptides. Similar CD8+ T cells are induced by yellow-fever vaccination (Co et al., 2009) that can persist up to 25 years (Fuertes Marraco et al., 2015). CD8+ PD1+CD38+ICOS+CXCR5- T cells described here may, therefore, also provide immunological memory for long-lasting protection against SARS-CoV-2. Interestingly, cellular immunity may provide protection to individuals who mounted a suboptimal humoral antibody response and the donor with breakthrough SARS-CoV-2 infection failed to generate CD8+CD38+ICOS+ T cells. If confirmed in a larger cohort, CD8+CD38+ICOS+ T cells may provide a novel marker of successful immunization and protection following SARS-CoV-2 vaccination.

SARS-CoV-2 S protein-specific B cells identified here exhibited similar phenotypic properties as previous studies. These include expression of the B cell activation marker CD71, an iron transport receptor that is commonly expressed on antigen-specific B cell subsets including in the context of vaccination (Ellebedy et al., 2016; Fuertes Marraco et al., 2015). Reports of CD71 expression after COVID-19 infection (Ahmadizar et al., 2020; Hartley et al., 2020) are consistent with overlap of mRNA vaccination and natural SARS-CoV-2 infection. Limited pre-existing immunity to endemic coronaviruses prior to SARS-CoV-2 vaccination was detected in this study, albeit at varying levels between donors. Although a previous report noted an increased serological response in recovered COVID-19 individuals (Anderson et al., 2021), we noted only modest changes in HCoV-OC43 serology following vaccination. Instead, LIBRA-seq antigen-specificity data showed an initial HCoV-OC43, SARS-CoV-2 cross-reactive IgM-expressing B cell that decreased in frequency over time and evolved to development of IgA- and IgG-expressing B cells with greater SARS-CoV-2 specificity. Given HCoV-OC43 and HCoV-HKU1 utilize different cell receptors for host entry, the lack of correlation between pre-existing coronavirus immunity and SARS-CoV-2 neutralization is not surprising. Instead, antibodies and memory B cells that target the more conserved S2 portion of spike may promote anti-viral function via Fc effector function mechanisms. Indeed, pre-existing immunity to the endemic

coronavirus HCoV-OC43 has been previously reported to associate with survival outcome from COVID-19 infection (Kaplonek et al., 2021b). Further investigation into this potential association is needed, given an independent study reporting no correlation of endemic coronavirus immunity and survival after COVID-19 infection (Anderson et al., 2021).

The longitudinal characterization of the B cell repertoire of a BNT162b2-vaccinated donor revealed the presence of a cluster of public antibody heavy chain sequences with high similarity to antibody sequences observed in natural infection. These public heavy chain sequences were observed at multiple timepoints after vaccination, with IgM members identified at day 8, and IgG/IgA sequences identified at later timepoints, suggesting antigen-driven evolution of a public mode of SARS-CoV-2 spike recognition. Interestingly, despite the high similarity in heavy chain sequences, antibodies from this public cluster utilized a variety of different light chain V-genes and CDRL3 sequences, suggesting that the immune response to SARS-CoV-2 may utilize a combination of common heavy chain sequence characteristics that are important for antigen recognition, paired with a heterogeneous set of light chain sequences that may allow for additional diversification of the fine epitope specificities of responding B cells. The ability to increase the diversity in B cell responses, while retaining critical antigen interactions, may be an important tool that the human immune system utilizes for counteracting virus evasion mechanisms.

Immunization with BNT162b2 in the donor cohort also resulted in a transient SARS-CoV-2 IgA response. While the polysaccharide pneumococcal vaccine can lead to a persistent IgA vaccine response (Parker et al., 2019), robust IgA responses are not generated by either the intramuscular influenza (Cox et al., 2004) or tetanus-diphtheria-acellular pertussis vaccine (Halperin et al., 2011). IgA is critical in the SARS-CoV-2 early neutralizing antibody response (Sterlin et al., 2021) and was previously observed together with IgG in response to the SARS-CoV-2 mRNA vaccine (Wisnewski et al., 2021). Consistent with the development of protective immunity, antigen-binding B cells were IgG and IgA class-switched and primarily observed

among memory B cell and plasmablast subsets. The strong IgA response elicited by the SARS-CoV-2 mRNA vaccines may arise as a consequence of single-stranded RNA directly stimulating B-cells (Meiler et al., 2008; Zheng et al., 2020) or activation of TLR7 on dendritic cells (Bessa et al., 2009). Indeed, addition of a single-stranded RNA adjuvant to a traditional influenza vaccine generated mucosal immunity through a robust IgA response and provided more strain cross-protection (Kim et al., 2020).

This study uses unbiased machine learning and sequencing technologies to identify the antigen-specific cells and evolving antibody response to RNA-based vaccination against SARS-CoV-2. The approach allowed isolation of live, virus-specific T cells that will facilitate further studies and development of new therapies. The multi-compartment vaccine response induced by BNT162b2 may have important ramifications, particularly in immunocompromised populations. Reduced humoral responses have been reported to SARS-CoV-2 infection or BNT162b2 in patients with solid organ transplant (Marinaki et al., 2021; Peled et al., 2021; Sattler et al., 2021b), cancer (Grivas et al., 2021), or immune-mediated inflammatory diseases (Furer et al., 2021; Mahil et al., 2021). The identification of altered proteins or specific cell populations to serve as biomarkers for successful vaccination may provide important insight to monitor development and continued protection of these vulnerable populations. While limited sample sizes here reduce statistical power for population level correlations and detailed outcomes, the unbiased identification of antigen-specific CD4, CD8, and B cell populations provides important insight into general mechanisms of RNA-based vaccines and the cellular basis for vaccine-induced antibodies and protection from SARS-CoV-2.

Acknowledgements

We thank members of the Vanderbilt Center for Immunobiology for input and Summer Brown for administrative assistance. This work was supported by Human Immunology Discovery Initiative of the Vanderbilt Center for Immunobiology (JCR, EMW, RHB, JMI), CTSA award No. UL1TR000445 (EMW, JCR), the National Institutes of Health KL2TR002245 (EMW), K12HD043483 (RHB), R01CA226833 (JMI, SMB, CER), U01AI125056 (JMI, SMB), U54CA217450 (JMI), P30CA68485 (VUMC Flow Cytometry Shared Research), R01AI131722-S1 (ISG), R01AI157155 (JEC), R01DK105550 (JCR), R01CA217987 (JCR), R01AI153167 (JCR), R01AI127521 (JSM); HHSN contracts 75N93019C00074 (JEC), DARPA HR0011-18-2-0001 (JEC), Hays Foundation COVID-19 Research Fund (ISG), Fast Grants Mercatus Center of George Mason University (ISG, JEC), the Dolly Parton COVID-19 Research Fund at Vanderbilt (JEC), Welch Foundation F-0003-19620604 (JSM), and William Paul Distinguished Innovator Award of the Lupus Research Alliance (JCR).

Author contributions

KJK contributed to conceptualization, data curation, formal analysis, investigation, methodology, visualization, and writing the original draft. EMW contributed to conceptualization, formal analysis, project administration, resources, visualization, and writing the original draft. KV contributed to formal analysis, investigation, methodology, visualization, and writing the original draft. SMB contributed to data curation, formal analysis, visualization, software development, and visualization. CER contributed to investigation and data curation, ARS contributed to conceptualization, data curation, formal analysis, methodology, visualization, software development. NR contributed to data curation, formal analysis, methodology, visualization, software development. NS contributed to data curation. LW contributed to data curation. SCW contributed to data curation. AP contributed to data curation. SS and DD contributed to sample acquisition, processing, and management. CSW, CH, JSM, RHC, and

JEC contributed resources. JCR contributed to conceptualization, formal analysis, funding acquisition, methodology, resources, supervision, visualization, and writing the original draft. RHB contributed to conceptualization, data curation, formal analysis, investigation, software, visualization, and writing the original draft. ISG contributed to conceptualization, data curation, funding acquisition, methodology, resources, software, supervision, and visualization. JMI contributed to conceptualization, data curation, formal analysis, funding acquisition, methodology, resources, software, supervision, and visualization.

Competing interests

EMW receives research funding from Boehringer-Ingelheim and is a member of their myositis ILD advisory board. ARS and ISG are co-founders of AbSeek Bio. RHC is an inventor on patents related to other SARS-CoV-2 antibodies. JEC has served as a consultant for Luna Biologics, is a member of the Scientific Advisory Boards of CompuVax and Meissa Vaccines and is Founder of IDBiologics. JEC has received sponsored research agreements from Takeda Vaccines, IDBiologics and AstraZeneca. JMI was a co-founder and a board member of Cytobank Inc. and has engaged in sponsored research with Incyte Corp, Janssen, Pharmacyclics. JCR is a founder, scientific advisory board member, and stockholder of Sitryx Therapeutics, a scientific advisory board member and stockholder of Caribou Biosciences, a member of the scientific advisory board of Nirogy Therapeutics, has consulted for Merck, Pfizer, and Mitobridge within the past three years, and has received research support from Incyte Corp., Calithera Biosciences, and Tempest Therapeutics. No other author reports a competing interest.

Data and materials availability

Materials and data are or will be made available by corresponding authors and deposited in appropriate public databases and materials will be available upon request with

appropriate MTA approval. Mass cytometry datasets in this manuscript have been deposited in FlowRepository (http://flowrepository.org/).

MATERIALS AND METHODS

Human subjects information

IRB approval was obtained (VUMC 191562). Informed consent was obtained, and a baseline health questionnaire was also completed. Simple phlebotomy was performed either pre-vaccine (day 0), day 28-30, and day 95-100 OR pre-vaccine and days 8, 14, and 42 after initial BNT162b2 vaccination using sodium citrate mononuclear cell preparation (CPT) tubes. All participants received two doses of vaccine 21 days apart.

PBMC and plasma isolation

CPT tubes were spun at 1600 RCF for 20 minutes. The plasma layer was carefully removed, transferred to a conical vial, spun at 600g for 10 minutes, and the supernatant transferred to microtubes in 1 mL aliquots. Plasma was stored at -80°C until further use. Buffy coat was divided amongst two clean conical tubes. CPT tubes were rinsed with 1 mL PBS (Gibco), and the total volume in the conical was increased to 15cc. Cells were pelleted at 600g for 10 minutes. Cell pellets were combined and washed with 10cc PBS, and then cells were pelleted again at 600g for 10 minutes. PBS was discarded, and the pellet was re-suspended in 3mL ACK buffer (Gibco) for 5 minutes. 10 mL of PBS was added to the ACK cell suspension, and cells were pelleted for 10 minutes at 600g. Cells were resuspended in PBS, strained through a cell strainer (Falcon) and counted using an ACT Diff hematology analyzer (Beckman Coulter). Cells were pelleted by centrifugation at 600g for 10 minutes and resuspended in heat-inactivated FBS (Gibco) containing 10% DMSO (Sigma-Aldrich) at a concentration of 5 million

cells/mL in cryovials (Nalgene). Cryovials were frozen overnight to -80°C using Mr. Frosty freezing containers (Nalgene) and then transferred to liquid nitrogen for long-term storage.

Mass cytometry PBMC staining

Metal-tagged antibodies were purchased from Fluidigm. Cell labeling and mass cytometry analysis were performed as previously described (Ferrell et al., 2016; Greenplate et al., 2016). Briefly, cells were incubated with a viability reagent (Cell ID Intercalator-Rh; Fluidigm), per the product literature. Then cells were washed in PBS without calcium or magnesium (Gibco, Thermo Fisher Scientific) containing 1% BSA (Thermo Fisher Scientific) and stained in 50 µL PBS and BSA 1%–containing antibody cocktail for extracellular targets. Cells were stained for 30 minutes at room temperature using the antibodies listed in Supplemental Table 3. Cells were washed in PBS and BSA 1% and then fixed with 1.6% paraformaldehyde (Electron Microscopy Sciences). Cells were washed once in PBS and permeabilized by resuspension in ice-cold methanol. After incubation overnight at −20°C, cells were washed with PBS and BSA 1% and stained in 50 µL PBS and BSA 1%–containing antibody cocktail for intracellular targets. Cells were washed in PBS and BSA 1%, then washed with PBS and stained with an iridium DNA intercalator (Fluidigm) for 20 minutes at room temperature. Finally, cells were washed with PBS and with diH2O before being resuspended in 1× EQ Four Element Calibration Beads (Fluidigm) and collected on a Helios mass cytometer (Fluidigm) at the Vanderbilt Flow Cytometry Shared Resource Center. Events were normalized as previously described (Finck et al., 2013).

Mass cytometry data analysis

After normalization, CYTOF data were scaled with an arcsinh transformation, with an appropriate cofactor set for each channel following standard procedures for fluorescence and mass cytometry data (Irish et al., 2010). Data were then manually gated for removal of atypical

events (Roe et al., 2020). After quality control gating, a UMAP analysis was performed on the cleaned-up samples using the surface markers in each panel. Metabolic markers, ki67, iridium, and rhodium were not used to create the UMAP. The resulting common, 2-dimensional embedding of the data was used for visualization and selection of either CD3+ T cells (from T cell panel data) or B cells (from B cell panel data) for further downstream analysis. A common t-SNE analysis was done on all 10 donor samples using the same markers used to create the UMAP on either the CD3+ T cells or B cells extracted from their respective UMAP. After the t-SNE, equally sampling was done on each donor pair. The 10 donor samples were then combined for a T-REX comparison of day 0 and day 28 data (Barone et al., 2020a). MEM was used to quantify enriched features in each region of significant change (Diggins et al., 2017). Comparisons of population frequencies pre- and post-vaccination as well as correlations between post-vaccine cell frequencies and IgG titers were done in GraphPad Prism version 9.0. Populations were compared using Mann-Whitney U tests. Statistical correlations were determined using Pearson correlations. P values less than 0.05 were considered statistically significant.

In vitro characterization of CD38+ICOS+ cells

To quantify CD38+ICOS+ CD4 and CD8 T cells, PBMCs were first resuspended with Human TruStain Fcx (Biolegend) for 10 minutes at room temperature and then stained with the following antibodies in FACS buffer (PBS+ 2% fetal bovine serum): CD8a e450 (Invitrogen 48-0086-42, 1:200) ICOS BV605 (Biolegend 313538, 1:50), CCR7 PE (Biolegend 353204, 1:200), CD38 PerCP (Biolegend 303520, 1:100), CD4 PECy7 (Biolegend 357410, 1:100), and CD3 APCCy7 (Biolegend 300318, 1:200). Cells were analyzed on a Miltenyi MACSQuant16 Analyzer with single-stain control PBMC samples used for compensation conducted in FlowJo v10.6.2.

Stimulation of ICOS+CD38+ and ICOS^{lo}CD38^{lo} populations with SARS-CoV-2 S protein

The same staining procedure was used for FACS of ICOS+CD38+ and ICOSloCD38lo populations on a BD FACSAria III instrument in the Vanderbilt University Medical Center Flow Cytometry Shared Resource Core. Sorted cells were stained with 1uM CellTraceViolet (CTV) (ThermoFisher) for 20 minutes and then cultured with autologous unlabeled PBMC samples from day 0 (pre-vaccination) samples. Before adding CTV-labeled cells to PBMCs for activation, PBMCs were CD3-depleted by positive selection (CD3 Microbeads, Miltenyi Biotec) and purity of CD3 depletions were assessed by flow cytometry. Cells were cultured in Human Plasma-like Media (HPLM) (Cantor et al., 2017) + 1% pen/strep + 5% dialyzed serum (Sigma Aldrich). For SARS-CoV-2 peptide stimulation, cultures were treated with Peptivator SARS-CoV2 Prot_S peptide pool (Miltenyi Biotec #130-126-700) in a 48-well plate format for 2 days.

For cytokine staining, cells were either stimulated with PMA (1ug/ml) and ionomycin (750ng/ml) for 5 hours, or restimulated on day 11 in 96-well plates with 2.5ug/ml recombinant SARS-CoV-S protein S1 (Biolegend 792906, carrier-free) for 8h in the presence of 1ug/ml Golgiplug and 0.7ug/ml Golgistop. Peptivator-stimulated cultures were treated with Golgiplug/Golgistop overnight after 2 days of activation. Cells were surface stained in FACS buffer, fixed with 1.5% paraformaldehyde for 10 minutes, and permeabilized with methanol for 20 minutes on ice. Additional intracellular antibodies were: TNF-a AF488 (Biolegend 502915, 1:100), IFN-g APC (Invitrogen 17-7319-82, 1:100) IL-2 AlexaFluor 700 (Biolegend 500320, 1:150), granzyme b FITC (Biolegend 515403, 1:100), phospho-S6 APC Ser235/236 (Invitrogen 17-9007-42, 1:80), Bcl-6 FITC (Biolegend 358513, 1:100), and Glut-1 AlexaFluor 647 (Abcam ab115730, 1:300). Cytokines measured from PBMC supernatants were collected after 4 days of incubation with S protein and concentrations were predicted using a standard curve in the LEGENDplex assay (Miltenyi Biotec 741028).

Flow cytometric in vitro data analysis

Group comparisons were performed using GraphPad Prism version 9.0. Populations were compared using Mann-Whitney U tests. P values less than 0.05 were considered statistically significant.

Recombinant expression and purification of coronavirus antigens

Plasmids encoding residues 1–1208 of the SARS-CoV-2 spike with a mutated S1/S2 cleavage site, proline substitutions at positions 817, 892, 899, 942, 986 and 987, and a C-terminal T4-fibritin trimerization motif, an 8x HisTag, and a TwinStrepTag (SARS-CoV-2 S HP); 1–1208 of the SARS-CoV-2 spike with a mutated S1/S2 cleavage site, proline substitutions at positions 817, 892, 899, 942, 986 and 987, as well as mutations L18F, D80A, L242-244L del, R246I, K417N, E484K, N501Y, and a C-terminal T4-fibritin trimerization motif, an 8x HisTag, and a TwinStrepTag (SARS-CoV-2 S HP Beta); 1–1208 of the SARS-CoV-2 spike with a mutated S1/S2 cleavage site, proline substitutions at positions 817, 892, 899, 942, 986 and 987, as well as mutations 69-70del, Y144del, N501Y, A570D, P681H, and a C-terminal T4-fibritin trimerization motif, an 8x HisTag, and a TwinStrepTag (SARS-CoV-2 S HP Alpha); residues 1-1190 of the SARS-CoV spike with proline substitutions at positions 968 and 969, and a C-terminal T4-fibritin trimerization motif, an 8x HisTag, and a TwinStrepTag (SARS-CoV S-2P); residues 1-1291 of the MERS-CoV spike with a mutated S1/S2 cleavage site, proline substitutions at positions 1060 and 1061, and a C-terminal T4-fibritin trimerization motif, an AviTag, an 8x HisTag, and a TwinStrepTag (MERS-CoV S-2P Avi); residues 1-1277 of the HCoV-HKU1 spike with a mutated S1/S2 cleavage site, proline substitutions at positions 1067 and 1068, and a C-terminal T4-fibritin trimerization motif, an 8x HisTag, and a TwinStrepTag (HCoV-HKU1 S-2P); residues 1-1278 of the HCoV-OC43 spike with proline substitutions at positions 1070 and 1071, and a C-terminal T4-fibritin trimerization motif, an 8x HisTag, and a TwinStrepTag (HCoV-OC43 S-2P); were transiently transfected into FreeStyle293F cells

(Thermo Fisher) using polyethylenimine. For all antigens with the exception of SARS-CoV-2 S HP, cells were treated with 1 µM kifunensine to ensure uniform glycosylation three hours post-transfection. Transfected supernatants were harvested after five days of expression. SARS-CoV-2 S HP, SARS-CoV S-2P, MERS-CoV S-2P, HCoV-HKU1 S-2P and HCoV-OC43 S-2P were purified using StrepTrap columns. SARS-CoV-2 S HP, SARS-CoV-2 S HP Beta, SARS-CoV-2 S HP Alpha, SARS-CoV S-2P, MERS-CoV S-2P, HCoV-HKU1 S-2P and HCoV-OC43 S-2P were purified over a Superose6 Increase column (GE Life Sciences).

Recombinant expression and purification of ZM197 Env and NC99 Hemagglutinin

Recombinant, soluble HIV-1 gp140 SOSIP trimer from strain ZM197 (clade) containing an AviTag and recombinant NC99 HA protein consisting of the HA ectodomain with a point mutation at the sialic acid-binding site (Y98F) to abolish non-specific interactions, a T4 fibritin foldon trimerization domain, AviTag, and hexahistidine-tag, were expressed in Expi 293F cells using polyethylenimine transfection reagent and cultured. FreeStyle F17 expression medium supplemented with pluronic acid and glutamine was used. The cells were cultured at 37°C with 8% CO2 saturation and shaking. After 5-7 days, cultures were centrifuged and supernatant was filtered and run over an affinity column of agarose bound Galanthus nivalis lectin. The column was washed with PBS and antigens were eluted with 30 mL of 1M methyl-a-D-mannopyranoside. Protein elutions were buffer exchanged into PBS, concentrated, and run on a Superdex 200 Increase 10/300 GL Sizing column on the AKTA FPLC system.

Biotinylation of antigens

Constructs containing an Avi-tag (ZM197 Env and HA NC99) were biotinylated using the site-specific biotinylation kit according to manufacturer instructions (Avidity LLC.) All other antigens not containing an Avi-tag were non-specifically biotinylated using the EZ-Link Sulfo-NHS-Biotin kit at a 50:1 biotin:protein molar ratio.

DNA-barcoding of antigens

We used oligos that possess 15 bp antigen barcode, a sequence capable of annealing to the template switch oligo that is part of the 10X bead-delivered oligos, and contain truncated TruSeq small RNA read 1 sequences in the following structure: 5'-CCTTGGCACCCGAGAATTCCANNNNNNNNNNNNNCCCATATAAGA*A*A-3', where Ns represent the antigen barcode. We used the following antigen barcodes: GCAGCGTATAAGTCA (SARS-CoV-2 S HP), GACAAGTGATCTGCA (SARS-CoV-2 S HP D614G), GCTCCTTTACACGTA (SARS-CoV S), GGTAGCCCTAGAGTA (MERS-CoV S), TGTGTATTCCCTTGT (HCoV-HKU1 S), AGACTAATAGCTGAC (HCoV-OC43 S), TCATTTCCTCCGATT (ZM197 EnV), CTTCACTCTGTCAGG (HA NC99), Oligos were ordered from IDT with a 5' amino modification and HPLC purified.

For each antigen, a unique DNA barcode was directly conjugated to the antigen itself. In particular, 5'amino-oligonucleotides were conjugated directly to each antigen using the Solulink Protein-Oligonucleotide Conjugation Kit (TriLink cat no. S-9011) according to manufacturer's instructions. Briefly, the oligo and protein were desalted, and then the amino-oligo was modified with the 4FB crosslinker, and the biotinylated antigen protein was modified with S-HyNic. Then, the 4FB-oligo and the HyNic-antigen were mixed together. This causes a stable bond to form between the protein and the oligonucleotide. The concentration of the antigen-oligo conjugates was determined by a BCA assay, and the HyNic molar substitution ratio of the antigen-oligo conjugates was analyzed using the NanoDrop according to the Solulink protocol guidelines. AKTA FPLC was used to remove excess oligonucleotide from the protein-oligo conjugates, which were also verified using SDS-PAGE with a silver stain. Antigen-oligo conjugates were also used in flow cytometry titration experiments.

Antigen specific B cell sorting

Cells were stained and mixed with DNA-barcoded antigens and other antibodies, and then sorted using fluorescence activated cell sorting (FACS). First, cells were counted and viability was assessed using Trypan Blue. Then, cells were washed three times with DPBS supplemented with 0.1% Bovine serum albumin (BSA). Cells were resuspended in DPBS-BSA and stained with cell markers including viability dye (Ghost Red 780), CD14-APC-Cy7, CD3-FITC, CD19-BV711, and IgG-PE-Cy5. Additionally, antigen-oligo conjugates were added to the stain (1 µg of every antigen except for HA NC99 and HCoV-HKU1 S which were added at 0.1 µg). After staining in the dark for 30 minutes at room temperature, cells were washed three times with DPBS-BSA at 300 g for five minutes. Cells were then incubated for 15 minutes at room temperature with Streptavidin-PE to label cells with bound antigen. Cells were washed three times with DPBS-BSA, resuspended in DPBS, and sorted by FACS. Antigen positive cells were bulk sorted and delivered to the Vanderbilt Technologies for Advanced Genomics (VANTAGE) sequencing core at an appropriate target concentration for 10X Genomics library preparation and subsequent sequencing. FACS data were analyzed using FlowJo.

Sample preparation, library preparation, and sequencing

Single-cell suspensions were loaded onto the Chromium Controller microfluidics device (10X Genomics) and processed using the B-cell Single Cell V(D)J solution according to manufacturer's suggestions for a target capture of 10,000 B cells per 1/8 10X cassette, with minor modifications in order to intercept, amplify and purify the antigen barcode libraries as previously described (Setliff et al., 2019b).

NGS processing and bioinformatic analysis

We utilized our previously described pipeline to use paired-end FASTQ files of oligo libraries as input, process and annotate reads for cell barcode, UMI, and antigen barcode, and generate a cell barcode - antigen barcode UMI count matrix (Shiakolas et al., 2021b). BCR contigs were processed using Cell Ranger (10X Genomics) using GRCh38 as reference. Antigen barcode libraries were also processed using Cell Ranger (10X Genomics). The overlapping cell barcodes between the two libraries were used as the basis of the subsequent analysis. We removed cell barcodes that had only non-functional heavy chain sequences as well as cells with multiple functional heavy chain sequences. Additionally, we aligned the BCR contigs (filtered_contigs.fasta file output by Cell Ranger, 10X Genomics) to IMGT reference genes using HighV-Quest (Alamyar et al., 2012). The output of HighV-Quest was parsed using Change-O (Gupta et al., 2015a). and merged with an antigen barcode UMI count matrix. Finally, we determined the LIBRA-seq score for each antigen in the library for every cell as previously described (Setliff et al., 2019b).

LIBRA-seq data quality control filtering

Cells were filtered based on multiple criteria for further analysis. Cells were only included if the sum of all antigen UMI counts for a particular cell barcode was greater than 4. All cells that met these criteria from pre, day 8, day 14, and day 42 time points were combined. Then, we removed cells from the dataset that had multiple heavy chains or multiple light chains associated with a single cell barcode. Then, LIBRA-seq scores were generated (8). Briefly, a pseudocount of 1 was added to each antigen UMI count, and then centered-log ratios (CLR) were calculated for each antigen UMI count for each cell. Then, an antigen-wise z-score transformation was applied. After performing the LIBRA-seq score calculation, cells were filtered out if they fulfilled any of the following criteria: (1) Max UMI among all antigens less than or

equal to 30, (2) ZM197 UMI counts greater than or equal to 30, (3) HA UMI counts greater than or equal to 30, (4) MERS UMI counts greater than 10 times the max UMI of other CoV in that cell, or (5) 10 times ZM197 UMI counts greater than the max UMI of non-MERS CoV in that cell. **Figure 4-11B** and **Figure 4-16B** were generated using the pre-filtered data. **Figure 4-12** and **Figure 4-13C-E** used post-filtered data.

Antibody sequence clustering

Using pre-filtered data, cells from multiple timepoints were combined together to identity highly similar antibody sequences between timepoints. Single-linkage clustering was performed using Change-O (Gupta et al., 2015a) with the criteria of same VH- and JH-gene usage, same junction and CDRH3 length and 80% CDRH3 nucleotide sequence identity.

Phylogenetic tree visualization

For the selected cluster 720, phylogenetic analysis was performed to understand the heavy chain sequence similarities. The sequences from cluster 720 used IGHV3-30-3 and IGHJ4 genes and included 18 members from 3 different post-vaccination timepoints. The cluster 720 heavy chain sequences were compared to sequences from the Coronavirus antibody database (CoV-AbDab) to identify antibodies with high sequence similarity (based on same VH-and JH-gene usage and 70% CDRH3 amino acid sequence identity) to at least one member of cluster 720. This resulted in the identification of 14 antibody sequences that fulfilled the similarity criteria with the cluster 720 sequences. To generate a phylogenetic tree of these public sequences, the tree was rooted on a putative germline sequence that was generated using the IGHV3-30-3 gene, a consensus CDRH3 sequence based on the cluster 720 members with

100% germline gene identity, and the IGHJ4 J-gene for framework 4. The tree was visualized using the Dendroscope tool (Huson and Scornavacca, 2012).

Plasma serology ELISAs

100 µL of antigen was plated at a concentration of 500 ng/µL in PBS overnight at 4ºC. The following day plates are washed with 1X PBS and 0.1% Tween-20 (PBS-T) and then blocked with 5% non-fat dry milk (NFDM). After an hour blocking at 1 hour at RT, plates are washed 3X with PBS-T and plasma is diluted in 1% NFDM PBS-T at a top concentration of 1:67 followed by 7 3-fold dilutions. The plates were incubated at RT for 1 hour and then washed three times in PBST. The secondary antibody was added in 1% NFDM in PBS-T to the plates, which were incubated for one hour at RT. Plates were washed three times with PBS-T and then developed by adding TMB substrate to each well. The plates were incubated at room temperature for ten minutes, and then 1N sulfuric acid was added to stop the reaction. Plates were read at 450 nm.

Plasma VSV SARS-CoV-2 neutralization assay

In brief, 100uL of plasma samples are heat inactivated at 570C for 1hr and starting at 1:25 dilution eight 2-fold serial dilutions were made with DMEM supplemented with 2% FBS. To determine neutralizing activity of plasma/serum , we used real-time cell analysis (RTCA) assay on an xCELLigence RTCA MP Analyzer (ACEA Biosciences Inc.) that measures virus-induced cytopathic effect (CPE). Briefly, 50 µL of cell culture medium (DMEM supplemented with 2% FBS) was added to each well of a 96-well E-plate using a ViaFlo384 liquid handler (Integra Biosciences) to obtain background reading. A suspension of 18,000 Vero cells in 50 µL of cell culture medium was seeded in each well, and the plate was placed on the analyzer. Measurements were taken automatically every 15 min, and the sensograms were visualized using RTCA software version 2.1.0 (ACEA Biosciences Inc). VSV-SARS-CoV-2 (0.01 MOI, ~120 PFU per well) was mixed 1:1 with a dilution of plasma/serum in a total volume of 100 µL

using DMEM supplemented with 2% FBS as a diluent and incubated for 1 h at 37°C in 5% CO2. At 16 h after seeding the cells, the virus-plasma/serum mixtures were added in replicates to the cells in 96-well E-plates. Triplicate wells containing virus only (maximal CPE in the absence of mAb) and wells containing only Vero cells in medium (no-CPE wells) were included as controls. Plates were measured continuously (every 15 min) for 48 h to assess virus neutralization. Normalized cellular index (CI) values at the endpoint (48 h after incubation with the virus) were determined using the RTCA software version 2.1.0 (ACEA Biosciences Inc.). Results are expressed as percent neutralization in a presence of respective plasma/serum relative to control wells with no CPE minus CI values from control wells with maximum CPE. RTCA IC50 values were determined by nonlinear regression analysis using Prism software.

Single-cell RNA-seq analysis

Single-cell analysis was performed using Seurat v4.0.0 (Satija et al., 2015). Cells with fewer than 200 RNA features that contained greater than 10% mitochondrial genes were removed. Immunoglobulin VH, Vκ, and Vλ genes were removed prior to UMAP clustering of RNAseq data to prevent them from driving transcriptionally-defined clusters. LIBRA-seq scores were used to identify SARS-CoV-2-binding B cells. B cell subset identities were assigned to clusters based on transcriptional profiles that were consistent with other studies defining these populations. The Seurat FindMarkers function, which uses a non-parametric Wilcoxon rank sum test, was used to identify differentially expressed genes between SARS-CoV-2-binding B cells and non-SARS-CoV-2-binding B cells within each transcriptionally-defined cluster. VDJ data were processed via CellRanger, IMGT/HighV-QUEST, and CHANGE-O, as outlined above to assign V genes, isotypes, and calculate percent VH somatic hypermutation.

THESIS SUMMARY

The emergence and continued development of SARS-CoV-2 since its original identification in December 2019 poses a significant threat until herd immunity is established whether that be from vaccination, natural infection or the combination of both. Despite a broad collection of medical countermeasures as well as highly efficacious vaccines, the currently circulating VOCs loom large, particularly their potential to escape coronavirus immune mechanisms. The continued investigation of monoclonal antibodies insensitive to mutation pressure is one critical direction to have a pool of existing medical countermeasures in the event of more transmissible variants. Further investigation into the vaccine response generated by novel mRNA formulations as well as the impact of endemic coronaviruses and their implications for the design of pan-coronavirus vaccine templates are other significant areas of research to enhance coronavirus global pandemic preparedness. In this dissertation, I sought to study the B-cell human response to coronavirus infection investigating both the cross-reactive repertoire with multiple coronaviruses as well as SARS-CoV-2 specificity for the development of potential therapeutic molecules. Additionally, in response to a global vaccination effort I aimed to characterize the B and T cell mounted vaccine response against the first of its kind mRNA-based formulation.

First, I pioneered an antibody discovery effort to characterize the implications of coronavirus cross-reactivity from a donor who survived SARS-CoV infection. I utilized LIBRA-seq to deconvolute monoclonal specificity of B cells from this donor using spike antigens from both endemic and pandemic coronaviruses. This resulted in a set of lead candidates that displayed a broad cross-reactivity profile to a number of different coronaviruses. Epitope mapping experiments revealed these antibodies bound to distinct domains of the spike protein and performed a spectrum of Fc effector functions *in vitro*. Additionally, two select candidates reduced pathological burden of mice in a SARS-CoV-2 mouse adapted strain infection model.

Although these antibodies likely do not make suitable clinical candidates, the basis for the cross-reactivity profile conserved across different coronaviruses could have profound implications for pan-coronavirus vaccine design.

In another direction of this dissertation, I used LIBRA-seq to identity potently neutralizing SARS-CoV-2 antibodies which may be applicable to clinical therapeutic development efforts. To perform this campaign, I screened donor PBMCs from a survivor of COVID-19 80 days after infection onset. From this effort, I identified and characterized a small panel of antibodies with a high LIBRA-seq score for SARS-CoV-2 spike. Neutralization assays revealed a spectrum of potency for a subset of the monoclonal antibodies including one, 54042-4, that displayed potently neutralizing activity in a VSV SARS-CoV-2 system at 9 ng/mL. Given this value is consistent with antibody therapeutics authorized for emergency use by the FDA, we decided to characterize the structural and functional properties in more detail. Binding and structural data, including a 2.7 angstrom cryo-EM structure revealed an epitope on SARS-CoV-2 spike insensitive to substitutions in currently circulating variants of concern. Consistent with our structural data, antibody 54042-4 neutralizes the alpha, beta, gamma, and delta VOCs further motivating its development as a therapeutic countermeasure against SARS-CoV-2.

In another application of LIBRA-seq, I tracked the development of coronavirus B cell immunity at monoclonal resolution across longitudinal time points of SARS-CoV-2 mRNA vaccination. Along with repertoire level analysis by sequencing, I also employed whole transcriptome analysis of vaccine-induced B cells as well as proteomic characterization of both T and B cells using mass cytometry. Systems level repertoire analysis revealed a change in pre-existing coronavirus immunity from endemic coronaviruses to mostly SARS-like coronavirus immunity including both SARS-CoV and SARS-CoV-2 across the time course of vaccination. At the cell surface expression level, mass cytometry revealed notable enrichment of cell subsets particularly ICOS+ CD38+ CD8 and CD4 and CD8 T cells as well as CD38+, CD71+ B cell

plasmablast populations. We noted a varied frequency of these cell subsets in the studied donor cohort, however, interestingly one donor who did not develop neutralizing titer or a robust cellular response encountered a breakthrough infection despite being fully vaccinated. Although this study is derived from a small patient cohort, the study implications have the potential to inform future vaccine-induced immune responses or future mRNA formulations for other disease indications.

CAVEATS

Cross-reactive antibody characterization

In the context of cross-reactive coronavirus antibodies, we missed a key element of this phenomenon in relation to MERS-CoV. Unfortunately, due to an expedited experimental timeline because of laboratory shutdowns during the beginning of the pandemic, we were not able to perform as rigorous of quality control on our LIBRA-seq antigen probes and we had to disregard MERS-CoV as well as MERS-CoV S1 proteins from our downstream analysis due to atypical reactivity patterns. Cross-reactivity patterns between pandemic coronaviruses that do not share significant sequence homology or utilize the same host cell receptor such as MERS-CoV would be of enormous value to the field. A better understanding of conserved elements shared among coronaviruses with severe clinical pathologies has the potential to further inform pan-coronavirus vaccine efforts.

In vivo animal model study design

In Chapter II detailing the characterization of non-neutralizing coronavirus antibodies with effector functions, the animal study design is a large limitation. Intact Fc effector function has been demonstrated to be critical in animal studies when given in a therapeutic setting, rather than prophylaxis preceding viral challenge (Winkler et al., 2021). These observations suggest

that we missed a window to observe a benefit in the mouse adapted SARS-CoV-2 *in vivo* model when tested in prophylaxis rather than in a therapeutic setting.

B cell subtype selection

Antigen specific B cell sorting is a powerful tool to isolate B cells from infection or vaccination donors for both systems level and monoclonal antibody characterization. One caveat of this approach, however, is the reliance on surface-bound immunoglobulin. In the context of chronic infections such as HIV-1 or influenza, long-lived memory B cells which retain surface IgG can be readily isolated to track the immune compartment in response to infection and further find interesting potential therapeutic antibodies (Setliff et al., 2018; Setliff et al., 2019a). In response to recent infection or vaccination, however, other B cell subsets lacking surface Ig such as plasmablasts and plasma cells are not captured in antigen-specific sorting schemes. Even in the context of chronic infection, enrichment for antigen positive cells by FACS may lose resolution of long-lived plasmablasts and plasma cells which are critical mediators of the durable immune response against invading pathogens (Brynjolfsson et al., 2018; Hammarlund et al., 2017) due to the low amount of surface Ig rendering it unable to be sorted due to surface bound fluorescent antigen. A potential solution to this limitation would be splitting samples in two and utilizing one portion for antigen-specific B cell sorting and the other for paired NGS which can resolve clonally related cells at a much larger sequencing depth providing information on all populations of B cells. Another method to achieve the same goal could utilize whole transcriptomic analysis with paired heavy and light chain NGS sequencing to acquire B cell subset information and determine its relation to a memory B cell identified from antigen-specific sorting.

FUTURE DIRECTIONS

Further characterization of antibody 54042-4

Chapter III details significant structural and functional characterization of antibody 54042-4, but to fully motivate its further development as a therapeutic animal studies testing protection must be assessed. Plans are currently underway to investigate the administration of 54042-4 in a therapeutic setting against viral challenge with a mouse adapted strain of SARS-CoV-2. Challenge studies using VOC viruses would also be of high interest given the neutralization profile, however, given the comparable potencies for 54042-4 against each variant *in vitro*, the demonstration of protection against the USA-WA1 ancestral strain may be sufficient. Another crucial characterization piece for antibody 54042-4 is neutralization escape experiments. Jesse Bloom's lab developed an elegant escape mutant selection system to treat wild-type virus with saturating concentrations of antibody and after rounds of replication, viruses encoding specific mutations can be tracked via a sequencing readout (Starr et al., 2020). Knowledge of mutations that reduce the effectiveness of 54042-4 would guide efforts for clinical utility as well as inform decisions to include as a cocktail of antibodies targeting distinct epitopes and producing non-overlapping escape mutations as previously done with clinical EUA candidates (Greaney et al, 2021; Hansen et al., 2020).

LIBRA-seq antibody discovery technology development

Antibody discovery efforts continually raise the bar for efficiency and productive campaigns to save both time and precious resources. To that end, I contributed a significant effort to an adaptation of LIBRA-seq which involves a functional readout of antigen-specific B cells rather than just antigen specificity (Shiakolas et al., 2021a). We used SARS-CoV-2 spike and ACE2 as a model system to resolve ligand blocking antibodies at the single-cell level. This effort resulted

in a substantial increase in the identification rate for neutralizing antibodies by prioritizing antibodies predicted to block ACE2 from the LIBRA-seq readout. To take this application a step further, I propose to expand the antigen-screening library to include six “SARS-like” coronaviruses (all of which utilize ACE2 for their host receptor) to screen for broadly-reactive neutralizing antibodies. A small collection of these antibodies has been described in the field, including a few currently being investigated in clinical trials (Pinto et al., 2020; Rappazzo et al., 2021; Starr et al., 2021; Tortorici et al., 2021). This technology adaptation would not only produce antibodies with clinical relevance given the possibility of another SARS-like coronavirus emergence, but the discovered antibodies could also inform vaccine design efforts to generate pan-coronavirus immunity.

Another application of LIBRA-seq that could be applied to any antibody/antigen target, rather than just coronavirus, is the identification of competitor molecules. This would involve a target antigen and antibody of interest each labeled with a DNA oligo and then applied to B cell source of interest. Antigen-specific B cells identified by LIBRA-seq that display an enrichment for the antibody barcode would suggest a non-competitive antibody, but a B cell with a lower barcode score for the target antibody may identify an antibody with a competitive epitope. This LIBRA-seq adaptation has the potential to further increase the efficiency of lead identification particularly in the context of the pharmaceutical industry where biosimilar molecules are now replacing billion dollar antibody therapies going off patent such as anti-VEGF Bevacizumab (Thatcher et al., 2019) and anti-TNF-α Adalimumab (Frampton, 2018).

Longitudinal screening of COVID-19 vaccinees

One of the biggest outstanding questions in not only the scientific community, but also society is the efficacy and long-term immunity generated by SARS-CoV-2 vaccination. Recent evidence supports the durability of SARS-CoV-2 IgG and neutralization titer as far as 119 days post-vaccination. Characterization of the B cell memory compartment post-vaccination remain

understudied, however the demonstrated longevity of RBD-specific memory B cells 8 months post COVID-19 infection (Dan et al., 2021) is encouraging for long term vaccine-based immunity. To this end I propose to utilize the same donor cohort studied a in chapter IV to better understand the memory contributions from both B and T cells. From pre-vaccine and post boost aliquots, I would perform B and T cell NGS to resolve the baseline post-boost repertoires for comparison to time points collected 9-12 months post vaccination. As outlined in the caveats section above, the use of NGS may resolve plasmablasts and plasma cells that are not captured during antigen-specific B cell sorting. Utilizing these samples, I would perform SARS-CoV-2 antigen-specific B cell sorting and SARS-CoV-2 peptide pool MHC tetramer staining to study the immune repertoire post-vaccination. Further, using computational tools I would measure the sequence relatedness in each population shared among each donor. The "publicness" of an immune response as studied in multiple disease indications as well as vaccination (Jackson et al., 2014; Parameswaran et al., 2013; Setliff et al., 2018) can inform population-level data of the direction of antigen-specific immunity. Further application of this effort would be the characterization of shared clonotypes in B cells and T cells and their reactivity against circulating variants of concern. Shared clonotypes in the context of COVID-19 infection and vaccination have been studied previously (Sahin et al., 2021; Wang et al., 2021b) however, not with the comparison of pre-vaccination to understand baseline repertoire and germline targeting. A better understanding of the genetic determinants of vaccine responses may have further the understanding of the development or lack thereof for immunity against COVID-19.

Post-vaccination break-through infection

In chapter IV, I described a donor who did not develop a neutralizing antibody response nor had a minimal expansion of responding CD4 or CD8 T cells who interestingly developed a breakthrough SARS-CoV-2 infection two months post-vaccination. These cases are beginning

to be characterized more in depth including viral load quantification, and neutralization response (Hacisuleyman et al., 2021) could prove crucial for identifying the underlying deficiencies behind a poor immune response against mRNA vaccines. Repertoire-level T and B cell characterization could explain a poor response; however, whole exome sequencing or HLA-typing, previously shown to predict vaccine responses in other disease indications (Yao et al., 2019) may also elucidate mechanisms for non-responder vaccinees.

Cross-reactive coronavirus antibody discovery campaigns

Reverse vaccinology and structure-based vaccine design efforts or the design of vaccines based on the epitopes of broadly neutralizing antibodies, have been met with success in the production of a meningococcal vaccine (Masignani et al., 2019) as well as considerable progress in other indications. For example, the epitope of the anti-RSV F antibody motavizumab when mounted on a multivalent immunogen elicited neutralizing antibodies in mice (Zuniga et al., 2021). In the context of the extraordinarily challenging vaccine target HIV, significant progress in vaccine design has been made including the screening of neutralizing antibodies from humans to define the best epitopes to target in a candidate immunogen (Walker and Burton, 2018). Taken a step further, recent work has further optimized immunogens to target germline genes in HIV naïve individuals to better elicit the sequential development of a broadly neutralizing antibodies (Jardine et al., 2016). These principles can also be applied to coronaviruses with the goal of achieving pan-coronavirus immunity. Indeed, significant research has been devoted to this concept since SARS-CoV-2 emerged including a mosaic nanoparticle consisting of a collection of SARS-like RBD subunits generating cross-neutralizing polyclonal responses against each strain included in the formulation (Cohen et al., 2021). A limitation of this approach, however, is this immunity is likely only to confer protection against coronaviruses similar to SARS-CoV-2. MERS-CoV, a much more distant relative, only shares 50% amino acid

identity, including utilizing a different host cell receptor, which also presents with much more severe pathologies including a 33% mortality rate (Chan et al., 2015; Lu et al., 2020). Furthermore, zoonotic leap from the alpha coronavirus genus which shares much lower amino acid identity to SARS-CoV-2, yet can still infect humans, could result in another pandemic outbreak (Chan et al., 2015). To combat this challenge, I propose to utilize LIBRA-seq to identify cross-reactive antibodies against every human coronavirus spike protein, as well as spike proteins from coronaviruses that infect bats such as HKU9-CoV (Hammond et al., 2017) as well as pigs (PEDV-CoV) (Lee, 2015). The output would be two-fold: potential antibody candidates to serve as therapeutic in the event of a future zoonotic outbreak and more importantly the rational design of vaccines to target the epitopes of these conserved regions of spike for the elicitation of pan-coronavirus immunity. A small collection of broad coronavirus antibodies has been discovered, including pan-Beta coronavirus antibodies against the more conserved S2 domain (Sauer et al., 2021; Tortorici et al., 2021; Zhou et al., 2021) although none have been resolved to bind distinct coronaviruses outside of the Beta subgenus. Because these antibodies are likely exceedingly rare, I propose to utilize an alternative B cell source to enrich for cross-reactive antibodies. Adolescent and young children have recently been shown to have significantly higher cross-reactive antibody responses to viral targets, including coronaviruses (Ng et al., 2020) and thus this subset of donors may serve as a pool of B cells enriched for broadly-reactive coronavirus antibodies.

Impact of endemic coronaviruses on SARS-CoV-2 immunity

An important consideration for the field of public health moving forward will be the surveillance of the mutational patterns of SARS-CoV-2. Given the widespread nature of COVID-19 infection as well as several re-infection cases suggests society may be living with COVID-19 for the foreseeable future. Another factor that may have an impact on the development of the pandemic

is the effect of endemic coronavirus infections. Although HCoV-HKU1, HCoV-OC43, HCoV-NL63, and HCoV-229E do not cause severe clinical illness, their impact on immunity to a pandemic coronavirus may have more severe clinical consequences. Despite only sharing limited sequence homology and utilizing distinct host cell receptors, all coronaviruses share a similar globular structure of their respective spike proteins. Furthermore, coronaviruses do share limited, highly conserved domains, particularly in the S2 subunit responsible for cell-fusion such as the heptad repeat region (Chan et al., 2015; Lu et al., 2020; Wrapp et al., 2020). The impact of pre-existing endemic coronavirus immunity and the effect on COVID-19 infection outcome has been explored previously, albeit at a very preliminary level. One study reports an increase in serological titer against HCoV-OC43 upon infection with SARS-CoV-2, however, the magnitude of increase or pre-existing level serological response did not associate with a survival benefit in donors who survived COVID-19 infection (Anderson et al., 2021). In contrast to this observation, another study reported that higher titer against HCoV-OC43 associated with better survival outcomes in patients admitted to the hospital for COVID-19 (Kaplonek et al., 2021a). The effect of these endemic coronavirus infections occurring after COVID-19 infection or vaccination, however, has not been explored to date yet. One limitation to approaching this study is the lack of a widely available PCR test to confirm infection with a non-pandemic coronavirus, however, this may change given some overlap in clinical symptoms with SARS-CoV-2, albeit at lower disease severity. To study this phenomenon, I would advertise for a donor cohort of convalescent COVID-19 donors as well as COVID-19 vaccinees and monitor respiratory infections over the course of a year. From any donor who contracts an endemic coronavirus infection, I propose to perform LIBRA-seq to dissect the changes at the monoclonal level as well as serological titer and neutralization activity in comparison to the baseline sample collected prior to cohort collection. The observed changes, whether beneficial, detrimental, or static to SARS-CoV-2 immunity, would have a profound impact for the continued treatment of COVID-19 as it continues to circulate and develop into more transmissible VOCs.

Next-generation SARS-CoV-2 vaccination design

The RBD of SARS-CoV-2 S serves as the dominant target of neutralizing antibodies (Jiang et al., 2020), and unsurprisingly was a main consideration for COVID-19 vaccine design. In fact, Pfizer and BioNTech co-developed an RBD-only mRNA vaccine formulation, BNT162b1, which showed promising efficacy (Mulligan et al., 2020). However, the full-length spike candidate, BNT162b2, was prioritized likely due to thoughts of including T cell epitopes and domains of spike that may not be neutralizing, but that could enhance immune Fc effector function. On trimeric SARS-CoV-2 S, the RBD adopts an equilibrium of an up and down conformation (Wrapp et al., 2020). To engage with the receptor ACE2, the RBD must be in the up conformation; in the down position the RBD interaction residues are not surface accessible (Wrapp et al., 2020). Given this inherent flexibility and association with cell infectivity, computational protein design efforts were undertaken to introduce substitutions in the SARS-CoV-2 S protein which enforce different orientations of the RBD. One construct design enabled a higher frequency of RBD-up spikes and an additional construct utilized cysteines to covalently lock spike in all-RBD down conformation (Henderson et al., 2020). Given the functional consequences of the RBD, these formulations may warrant consideration for vaccination strategies. For example, utilizing a SARS-CoV-2 S antigen with more RBDs in the up conformation may stimulate a more potent neutralizing antibody response resulting in better vaccine efficacy. An all RBD-down construct may also be useful in the investigation as a vaccine candidate, particularly because it may expose residues in the RBD ridge more highly conserved across SARS-like coronavirus family aiding in the development of a more broad immune response (Henderson et al., 2020). Another consideration for vaccine design is validation of the pre-fusion stabilized form of SARS-CoV-2 spike used in both mRNA1273 and BNT162b2 (Baden et al., 2021; Polack et al., 2020) among other vaccine candidates. The pre-fusion stabilizing mutations (S-2P) in coronavirus spikes have resulted in significantly stable

molecules which enables more efficient drug design strategies as well as candidacy for immunogens because they express more robustly in a mammalian system (Pallesen et al., 2017; Wrapp et al., 2020). While these stabilizing mutations may be beneficial for vaccine production and exposure of neutralizing epitopes, there is evidence that these stabilizing mutations in SARS-CoV-2 S could contribute to instability resulting in non-native conformation (Cai et al., 2020). Another drawback of pre-fusion stabilizing mutations is the lack of post-fusion conformation exposure to the immune system which have been shown to yield neutralizing epitopes in other viruses such as HIV-1 and RSV (Frey et al., 2010; McLellan et al., 2013). However, given the outstanding efficacy of COVID-19 vaccines designed in the S-2P conformation, these considerations may be irrelevant. In favor of further protein stability, an independent effort in computational protein design resulted in a SARS-CoV-2 spike construct, denoted HexaPro, with higher thermostability and enhanced recombinant protein expression yields potentially motivating its use as a vaccine candidate (Hsieh et al., 2020). Indeed, this construct is being explored for use as a vaccine candidate in Thailand (Clinical Trial #NCT04764422). LIBRA-seq is a technology uniquely suited to test the immunogenicity of potential vaccine candidates. Rationale for continual vaccine design is imperative to not only address the current pandemic, but potential future pandemic viruses. To test the differences of the conformations of SARS-CoV-2 S described above, LIBRA-seq could be applied to COVID-19 vaccine and infection naïve samples to elucidate the reactive B cells as well as the frequencies of antibodies directed to different functional domains. A direct comparison of multiple antigen constructs at a time, a unique component of LIBRA-seq, would be an important pre-clinical experiment to rationalize development and further characterization of different constructs of spike as clinical vaccine candidates.

REFERENCES

Ackerman, M.E., Moldt, B., Wyatt, R.T., Dugast, A.S., McAndrew, E., Tsoukas, S., Jost, S., Berger, C.T., Sciaranghella, G., Liu, Q.*, et al.* (2011). A robust, high-throughput assay to determine the phagocytic activity of clinical antibody samples. J Immunol Methods *366*, 8-19.

Adams, P.D., Grosse-Kunstleve, R.W., Hung, L.W., Ioerger, T.R., McCoy, A.J., Moriarty, N.W., Read, R.J., Sacchettini, J.C., Sauter, N.K., and Terwilliger, T.C. (2002). PHENIX: building new software for automated crystallographic structure determination. Acta Crystallogr D Biol Crystallogr *58*, 1948-1954.

Ahmadizar, F., Soroush, N., Ikram, M.A., Kors, J.A., Kavousi, M., and Stricker, B.H. (2020). QTc-interval prolongation and increased risk of sudden cardiac death associated with hydroxychloroquine. Eur J Prev Cardiol, zwaa118.

Alamyar, E., Duroux, P., Lefranc, M.P., and Giudicelli, V. (2012). IMGT((R)) tools for the nucleotide analysis of immunoglobulin (IG) and T cell receptor (TR) V-(D)-J repertoires, polymorphisms, and IG mutations: IMGT/V-QUEST and IMGT/HighV-QUEST for NGS. Methods Mol Biol *882*, 569-604.

Alpert, T., Brito, A.F., Lasek-Nesselquist, E., Rothman, J., Valesano, A.L., MacKay, M.J., Petrone, M.E., Breban, M.I., Watkins, A.E., Vogels, C.B.F.*, et al.* (2021). Early introductions and transmission of SARS-CoV-2 variant B.1.1.7 in the United States. Cell.

Anderson, E.M., Goodwin, E.C., Verma, A., Arevalo, C.P., Bolton, M.J., Weirick, M.E., Gouma, S., McAllister, C.M., Christensen, S.R., Weaver, J.*, et al.* (2021). Seasonal human coronavirus antibodies are boosted upon SARS-CoV-2 infection but not associated with protection. Cell *184*, 1858-1864 e1810.

Arunachalam, P.S., Scott, M.K.D., Hagan, T., Li, C., Feng, Y., Wimmers, F., Grigoryan, L., Trisal, M., Edara, V.V., Lai, L.*, et al.* (2021). Systems vaccinology of the BNT162b2 mRNA vaccine in humans. Nature, doi: 10.1038/s41586-41021-03791-x.

Arunachalam, P.S., Wimmers, F., Mok, C.K.P., Perera, R., Scott, M., Hagan, T., Sigal, N., Feng, Y., Bristow, L., Tak-Yin Tsang, O.*, et al.* (2020). Systems biological assessment of immunity to mild versus severe COVID-19 infection in humans. Science *369*, 1210-1220.

Atyeo, C., Fischinger, S., Zohar, T., Slein, M.D., Burke, J., Loos, C., McCulloch, D.J., Newman, K.L., Wolf, C., Yu, J.*, et al.* (2020). Distinct Early Serological Signatures Track with SARS-CoV-2 Survival. Immunity *53*, 524-532 e524.

Atyeo, C., Slein, M.D., Fischinger, S., Burke, J., Schafer, A., Leist, S.R., Kuzmina, N.A., Mire, C., Honko, A., Johnson, R.*, et al.* (2021). Dissecting strategies to tune the therapeutic potential of SARS-CoV-2-specific monoclonal antibody CR3022. JCI Insight *6*.

Baden, L.R., El Sahly, H.M., Essink, B., Kotloff, K., Frey, S., Novak, R., Diemert, D., Spector, S.A., Rouphael, N., Creech, C.B.*, et al.* (2021). Efficacy and Safety of the mRNA-1273 SARS-CoV-2 Vaccine. N Engl J Med *384*, 403-416.

Barnes, C.O., Jette, C.A., Abernathy, M.E., Dam, K.A., Esswein, S.R., Gristick, H.B., Malyutin, A.G., Sharaf, N.G., Huey-Tubman, K.E., Lee, Y.E.*, et al.* (2020). SARS-CoV-2 neutralizing antibody structures inform therapeutic strategies. Nature *588*, 682-687.

Barone, S.M., Paul, A.G.A., Muehling, L.M., Lannigan, J.A., Kwok, W.W., Turner, R.B., Woodfolk, J.A., and Irish, J.M. (2020a). Unsupervised machine learning reveals key immune cell subsets in COVID-19, rhinovirus infection, and cancer therapy. bioRxiv, 2020.2007.2031.190454.

Barone, S.M., Paul, A.G.A., Muehling, L.M., Lannigan, J.A., Kwok, W.W., Turner, R.B., Woodfolk, J.A., and Irish, J.M. (2020b). Unsupervised machine learning reveals key immune cell subsets in COVID-19, rhinovirus infection, and cancer therapy. bioRxiv, DOI: 10.1101/2020.1107.1131.190454.

Bessa, J., Jegerlehner, A., Hinton, H.J., Pumpens, P., Saudan, P., Schneider, P., and Bachmann, M.F. (2009). Alveolar macrophages and lung dendritic cells sense RNA and drive mucosal IgA responses. J Immunol *183*, 3788-3799.

Bettini, E., and Locci, M. (2021). SARS-CoV-2 mRNA Vaccines: Immunological Mechanism and Beyond. Vaccines (Basel) *9*, 147.

Blattner, F.R., and Tucker, P.W. (1984). The molecular biology of immunoglobulin D. Nature *307*, 417-422.

Bonsignori, M., Scott, E., Wiehe, K., Easterhoff, D., Alam, S.M., Hwang, K.K., Cooper, M., Xia, S.M., Zhang, R., Montefiori, D.C.*, et al.* (2018). Inference of the HIV-1 VRC01 Antibody Lineage Unmutated Common Ancestor Reveals Alternative Pathways to Overcome a Key Glycan Barrier. Immunity *49*, 1162-1174 e1168.

Bosch, B.J., van der Zee, R., de Haan, C.A., and Rottier, P.J. (2003). The coronavirus spike protein is a class I virus fusion protein: structural and functional characterization of the fusion core complex. J Virol *77*, 8801-8811.

Bournazos, S., Corti, D., Virgin, H.W., and Ravetch, J.V. (2020). Fc-optimized antibodies elicit CD8 immunity to viral respiratory infection. Nature *588*, 485-490.

Bournazos, S., DiLillo, D.J., Goff, A.J., Glass, P.J., and Ravetch, J.V. (2019). Differential requirements for FcgammaR engagement by protective antibodies against Ebola virus. Proc Natl Acad Sci U S A *116*, 20054-20062.

Bournazos, S., Klein, F., Pietzsch, J., Seaman, M.S., Nussenzweig, M.C., and Ravetch, J.V. (2014). Broadly neutralizing anti-HIV-1 antibodies require Fc effector functions for in vivo activity. Cell *158*, 1243-1253.

Briney, B., Inderbitzin, A., Joyce, C., and Burton, D.R. (2019). Commonality despite exceptional diversity in the baseline human antibody repertoire. Nature *566*, 393-397.

Brouwer, P.J.M., Caniels, T.G., van der Straten, K., Snitselaar, J.L., Aldon, Y., Bangaru, S., Torres, J.L., Okba, N.M.A., Claireaux, M., Kerster, G.*, et al.* (2020). Potent neutralizing antibodies from COVID-19 patients define multiple targets of vulnerability. Science *369*, 643-650.

Brynjolfsson, S.F., Persson Berg, L., Olsen Ekerhult, T., Rimkute, I., Wick, M.J., Martensson, I.L., and Grimsholm, O. (2018). Long-Lived Plasma Cells in Mice and Men. Front Immunol *9*, 2673.

Burnet, F.M. (1962). The immunological significance of the thymus: an extension of the clonal selection theory of immunity. Australas Ann Med *11*, 79-91.

Burnet, F.M. (1976). A modification of Jerne's theory of antibody production using the concept of clonal selection. CA Cancer J Clin *26*, 119-121.

Cai, Y., Zhang, J., Xiao, T., Peng, H., Sterling, S.M., Walsh, R.M., Jr., Rawson, S., Rits-Volloch, S., and Chen, B. (2020). Distinct conformational states of SARS-CoV-2 spike protein. Science *369*, 1586-1592.

Campbell, F., Archer, B., Laurenson-Schafer, H., Jinnai, Y., Konings, F., Batra, N., Pavlin, B., Vandemaele, K., Van Kerkhove, M.D., Jombart, T.*, et al.* (2021). Increased transmissibility and global spread of SARS-CoV-2 variants of concern as at June 2021. Euro Surveill *26*.

Cantor, J.R., Abu-Remaileh, M., Kanarek, N., Freinkman, E., Gao, X., Louissaint, A., Jr., Lewis, C.A., and Sabatini, D.M. (2017). Physiologic Medium Rewires Cellular Metabolism and Reveals Uric Acid as an Endogenous Inhibitor of UMP Synthase. Cell *169*, 258-272 e217.

Cardeno, A., Magnusson, M.K., Quiding-Jarbrink, M., and Lundgren, A. (2018). Activated T follicular helper-like cells are released into blood after oral vaccination and correlate with vaccine specific mucosal B-cell memory. Sci Rep *8*, 2729.

Case, J.B., Rothlauf, P.W., Chen, R.E., Liu, Z., Zhao, H., Kim, A.S., Bloyet, L.M., Zeng, Q., Tahan, S., Droit, L.*, et al.* (2020). Neutralizing Antibody and Soluble ACE2 Inhibition of a Replication-Competent VSV-SARS-CoV-2 and a Clinical Isolate of SARS-CoV-2. Cell Host Microbe *28*, 475-485 e475.

Chan, J.F., Lau, S.K., To, K.K., Cheng, V.C., Woo, P.C., and Yuen, K.Y. (2015). Middle East respiratory syndrome coronavirus: another zoonotic betacoronavirus causing SARS-like disease. Clin Microbiol Rev *28*, 465-522.

Chaplin, D.D. (2010). Overview of the immune response. J Allergy Clin Immunol *125*, S3-23.
Chen, E.C., Gilchuk, P., Zost, S.J., Suryadevara, N., Winkler, E.S., Cabel, C.R., Binshtein, E., Sutton, R.E., Rodriguez, J., Day, S.*, et al.* (2021a). Convergent antibody responses to the SARS-CoV-2 spike protein in convalescent and vaccinated individuals. bioRxiv, DOI:10.1101/2021.1105.1102.442326.

Chen, P., Nirula, A., Heller, B., Gottlieb, R.L., Boscia, J., Morris, J., Huhn, G., Cardona, J., Mocherla, B., Stosor, V.*, et al.* (2021b). SARS-CoV-2 Neutralizing Antibody LY-CoV555 in Outpatients with Covid-19. N Engl J Med *384*, 229-237.

Chen, R.E., Zhang, X., Case, J.B., Winkler, E.S., Liu, Y., VanBlargan, L.A., Liu, J., Errico, J.M., Xie, X., Suryadevara, N.*, et al.* (2021c). Resistance of SARS-CoV-2 variants to neutralization by monoclonal and serum-derived polyclonal antibodies. Nat Med *27*, 717-726.

Chi, X., Yan, R., Zhang, J., Zhang, G., Zhang, Y., Hao, M., Zhang, Z., Fan, P., Dong, Y., Yang, Y.*, et al.* (2020). A neutralizing human antibody binds to the N-terminal domain of the Spike protein of SARS-CoV-2. Science *369*, 650-655.

Cianfrocco, M., Wong, M., Youn, C. COSMIC2 (2017a). COSMIC2 - A Science gateway for cryo-electron microscopy.

Cianfrocco, M.A., Wong-Barnum, M., Youn, C., Wagner, R. & Leschzinger, A (2017b). COSMIC2: A Science Gateway for Cryo-Electron Microscopy Structure Determination in Proceedings of the Practice and Experience in Advanced Research Computing 2017 on Sustainability, Success, and Impact 1-5. Association for Computing Machinery.

Co, M.D., Kilpatrick, E.D., and Rothman, A.L. (2009). Dynamics of the CD8 T-cell response following yellow fever virus 17D immunization. Immunology *128*, e718-727.

Cohen, A.A., Gnanapragasam, P.N.P., Lee, Y.E., Hoffman, P.R., Ou, S., Kakutani, L.M., Keeffe, J.R., Wu, H.J., Howarth, M., West, A.P.*, et al.* (2021). Mosaic nanoparticles elicit cross-reactive immune responses to zoonotic coronaviruses in mice. Science *371*, 735-741.

Cohen, M.S. (2021). Monoclonal Antibodies to Disrupt Progression of Early Covid-19 Infection. N Engl J Med *384*, 289-291.

Collier, D.A., De Marco, A., Ferreira, I., Meng, B., Datir, R.P., Walls, A.C., Kemp, S.A., Bassi, J., Pinto, D., Silacci-Fregni, C.*, et al.* (2021). Sensitivity of SARS-CoV-2 B.1.1.7 to mRNA vaccine-elicited antibodies. Nature *593*, 136-141.

Cox, R.J., Brokstad, K.A., and Ogra, P. (2004). Influenza virus: immunity and vaccination strategies. Comparison of the immune response to inactivated and live, attenuated influenza vaccines. Scand J Immunol *59*, 1-15.

Croll, T.I. (2018). ISOLDE: a physically realistic environment for model building into low-resolution electron-density maps. Acta Crystallogr D Struct Biol *74*, 519-530.

Currier, J.R., Kuta, E.G., Turk, E., Earhart, L.B., Loomis-Price, L., Janetzki, S., Ferrari, G., Birx, D.L., and Cox, J.H. (2002). A panel of MHC class I restricted viral peptides for use as a quality control for vaccine trial ELISPOT assays. J Immunol Methods *260*, 157-172.

Dagan, N., Barda, N., Kepten, E., Miron, O., Perchik, S., Katz, M.A., Hernan, M.A., Lipsitch, M., Reis, B., and Balicer, R.D. (2021). BNT162b2 mRNA Covid-19 Vaccine in a Nationwide Mass Vaccination Setting. N Engl J Med *384*, 1412-1423.

Dan, J.M., Mateus, J., Kato, Y., Hastie, K.M., Yu, E.D., Faliti, C.E., Grifoni, A., Ramirez, S.I., Haupt, S., Frazier, A.*, et al.* (2021). Immunological memory to SARS-CoV-2 assessed for up to 8 months after infection. Science *371*.

Davidson, E.D., B. J. (2014). A high-throughput shotgun mutagenesis approach to mapping B-cell antibody epitopes. Immunology *143*, 13-20.

Davies, D.R., and Cohen, G.H. (1996). Interactions of protein antigens with antibodies. Proc Natl Acad Sci U S A *93*, 7-12.

Davis, M.M., and Bjorkman, P.J. (1988). T-cell antigen receptor genes and T-cell recognition. Nature *334*, 395-402.

Dejnirattisai, W., Zhou, D., Ginn, H.M., Duyvesteyn, H.M.E., Supasa, P., Case, J.B., Zhao, Y., Walter, T.S., Mentzer, A.J., Liu, C.*, et al.* (2021). The antigenic anatomy of SARS-CoV-2 receptor binding domain. Cell *184*, 2183-2200 e2122.

Diggins, K.E., Greenplate, A.R., Leelatian, N., Wogsland, C.E., and Irish, J.M. (2017). Characterizing cell subsets using marker enrichment modeling. Nat Methods *14*, 275-278.

Dijkman, R., Jebbink, M.F., El Idrissi, N.B., Pyrc, K., Muller, M.A., Kuijpers, T.W., Zaaijer, H.L., and van der Hoek, L. (2008). Human coronavirus NL63 and 229E seroconversion in children. J Clin Microbiol *46*, 2368-2373.

Dijkman, R., Jebbink, M.F., Gaunt, E., Rossen, J.W., Templeton, K.E., Kuijpers, T.W., and van der Hoek, L. (2012). The dominance of human coronavirus OC43 and NL63 infections in infants. J Clin Virol *53*, 135-139.

DiLillo, D.J., Palese, P., Wilson, P.C., and Ravetch, J.V. (2016). Broadly neutralizing anti-influenza antibodies require Fc receptor engagement for in vivo protection. J Clin Invest *126*, 605-610.

Dinnon, K.H., 3rd, Leist, S.R., Schafer, A., Edwards, C.E., Martinez, D.R., Montgomery, S.A., West, A., Yount, B.L., Jr., Hou, Y.J., Adams, L.E.*, et al.* (2020). A mouse-adapted model of SARS-CoV-2 to test COVID-19 countermeasures. Nature *586*, 560-566.

Dong, E., Du, H., and Gardner, L. (2020). An interactive web-based dashboard to track COVID-19 in real time. Lancet Infect Dis *20*, 533-534.

Dong, J., Zost, S.J., Greaney, A.J., Starr, T.N., Dingens, A.S., Chen, E.C., Chen, R.E., Case, J.B., Sutton, R.E., Gilchuk, P.*, et al.* (2021). Genetic and structural basis for recognition of SARS-CoV-2 spike protein by a two-antibody cocktail. bioRxiv.

Dunbar, J., Krawczyk, K., Leem, J., Marks, C., Nowak, J., Regep, C., Georges, G., Kelm, S., Popovic, B., and Deane, C.M. (2016). SAbPred: a structure-based antibody prediction server. Nucleic Acids Res *44*, W474-478.

Early, P., Huang, H., Davis, M., Calame, K., and Hood, L. (2004). An immunoglobulin heavy chain variable region gene is generated from three segments of DNA: VH, D and JH. 1980. J Immunol *173*, 6503-6514.

Edelman, G.M. (1991). Antibody structure and molecular immunology. Scand J Immunol *34*, 1-22.

Edwards, C.E., Yount, B.L., Graham, R.L., Leist, S.R., Hou, Y.J., Dinnon, K.H., 3rd, Sims, A.C., Swanstrom, J., Gully, K., Scobey, T.D.*, et al.* (2020). Swine acute diarrhea syndrome coronavirus replication in primary human cells reveals potential susceptibility to infection. Proc Natl Acad Sci U S A *117*, 26915-26925.

Elbe, S.B.-M., G. (2017). Data, disease and diplomacy: GISAID's innovative contribution to global health. Glob Chall *1*, 33-46.

Ellebedy, A.H., Jackson, K.J., Kissick, H.T., Nakaya, H.I., Davis, C.W., Roskin, K.M., McElroy, A.K., Oshansky, C.M., Elbein, R., Thomas, S.*, et al.* (2016). Defining antigen-specific plasmablast and memory B cell subsets in human blood after viral infection or vaccination. Nat Immunol *17*, 1226-1234.

Emsley, P., and Cowtan, K. (2004). Coot: model-building tools for molecular graphics. Acta Crystallogr D Biol Crystallogr *60*, 2126-2132.

Estrada, L.D., and Schultz-Cherry, S. (2019). Development of a Universal Influenza Vaccine. J Immunol *202*, 392-398.

Fang, D., Cui, K., Mao, K., Hu, G., Li, R., Zheng, M., Riteau, N., Reiner, S.L., Sher, A., Zhao, K.*, et al.* (2018). Transient T-bet expression functionally specifies a distinct T follicular helper subset. J Exp Med *215*, 2705-2714.

Favre, L., Spertini, F., and Corthesy, B. (2005). Secretory IgA possesses intrinsic modulatory properties stimulating mucosal and systemic immune responses. J Immunol *175*, 2793-2800.

Ferrell, P.B., Jr., Diggins, K.E., Polikowsky, H.G., Mohan, S.R., Seegmiller, A.C., and Irish, J.M. (2016). High-Dimensional Analysis of Acute Myeloid Leukemia Reveals Phenotypic Changes in Persistent Cells during Induction Therapy. PLoS One *11*, e0153207.

Finck, R., Simonds, E.F., Jager, A., Krishnaswamy, S., Sachs, K., Fantl, W., Pe'er, D., Nolan, G.P., and Bendall, S.C. (2013). Normalization of mass cytometry data with bead standards. Cytometry Part A *83A*, 483-494.

Fischinger, S., Fallon, J.K., Michell, A.R., Broge, T., Suscovich, T.J., Streeck, H., and Alter, G. (2019). A high-throughput, bead-based, antigen-specific assay to assess the ability of antibodies to induce complement activation. J Immunol Methods *473*, 112630.

Flajnik, M.F., and Kasahara, M. (2010). Origin and evolution of the adaptive immune system: genetic events and selective pressures. Nat Rev Genet *11*, 47-59.

Frampton, J.E. (2018). SB5: An Adalimumab Biosimilar. BioDrugs *32*, 507-510.

Frenck, R.W., Jr., Klein, N.P., Kitchin, N., Gurtman, A., Absalon, J., Lockhart, S., Perez, J.L., Walter, E.B., Senders, S., Bailey, R.*, et al.* (2021). Safety, Immunogenicity, and Efficacy of the BNT162b2 Covid-19 Vaccine in Adolescents. N Engl J Med.

Frey, G., Chen, J., Rits-Volloch, S., Freeman, M.M., Zolla-Pazner, S., and Chen, B. (2010). Distinct conformational states of HIV-1 gp41 are recognized by neutralizing and non-neutralizing antibodies. Nat Struct Mol Biol *17*, 1486-1491.

Fuertes Marraco, S.A., Soneson, C., Cagnon, L., Gannon, P.O., Allard, M., Abed Maillard, S., Montandon, N., Rufer, N., Waldvogel, S., Delorenzi, M.*, et al.* (2015). Long-lasting stem cell-like memory CD8+ T cells with a naive-like profile upon yellow fever vaccination. Sci Transl Med *7*, 282ra248.

Furer, V., Eviatar, T., Zisman, D., Peleg, H., Paran, D., Levartovsky, D., Zisapel, M., Elalouf, O., Kaufman, I., Meidan, R.*, et al.* (2021). Immunogenicity and safety of the BNT162b2 mRNA COVID-19 vaccine in adult patients with autoimmune inflammatory rheumatic diseases and in

the general population: a multicentre study. Ann Rheum Dis, DOI: 10.1136/annrheumdis-2021-220647.

Gilchuk, P., Thomsen, I., Yoder, S., Brady, E., Chappell, J.D., Stevens, L.J., Denison, M.R., Sutton, R.E., Chen, R.E., Suryadevara, N.*, et al.* (2021). Standardized Two-Step Testing of Antibody Activity in COVID-19 Convalescent Plasma. . Cell Rep Med *https://ssrn.com/abstract=3878407* DOI: 10.2139/ssrn.3878407.

Goel, R.R., Apostolidis, S.A., Painter, M.M., Mathew, D., Pattekar, A., Kuthuru, O., Gouma, S., Hicks, P., Meng, W., Rosenfeld, A.M.*, et al.* (2021). Distinct antibody and memory B cell responses in SARS-CoV-2 naive and recovered individuals following mRNA vaccination. Sci Immunol *6*.

Gottlieb, R.L., Nirula, A., Chen, P., Boscia, J., Heller, B., Morris, J., Huhn, G., Cardona, J., Mocherla, B., Stosor, V.*, et al.* (2021). Effect of Bamlanivimab as Monotherapy or in Combination With Etesevimab on Viral Load in Patients With Mild to Moderate COVID-19: A Randomized Clinical Trial. JAMA *325*, 632-644.

Graham, R.L., and Baric, R.S. (2010). Recombination, reservoirs, and the modular spike: mechanisms of coronavirus cross-species transmission. J Virol *84*, 3134-3146.

Greaney, A.J., Loes, A.N., Crawford, K.H.D., Starr, T.N., Malone, K.D., Chu, H.Y., and Bloom, J.D. (2021a). Comprehensive mapping of mutations in the SARS-CoV-2 receptor-binding domain that affect recognition by polyclonal human plasma antibodies. Cell Host Microbe *29*, 463-476 e466.

Greaney, A.J., Starr, T.N., Barnes, C.O., Weisblum, Y., Schmidt, F., Caskey, M., Gaebler, C., Cho, A., Agudelo, M., Finkin, S.*, et al.* (2021b). Mapping mutations to the SARS-CoV-2 RBD that escape binding by different classes of antibodies. Nat Commun *12*, 4196.

Greaney et al, T.N.S., Christopher O. Barnes, Yiska Weisblum, Fabian Schmidt, Marina Caskey, Christian Gaebler, Alice Cho, Marianna Agudelo, Shlomo Finkin, Zijun Wang, Daniel Poston, Frauke Muecksch, Theodora Hatziioannou, Paul D. Bieniasz, Davide F. Robbiani, Michel C. Nussenzweig, Pamela J. Bjorkman, Jesse D. Bloom (2021). Mutational escape from the polyclonal antibody response to SARS-CoV-2 infection is largely shaped by a single class of antibodies. BioRxiv.

Greenplate, A.R., Johnson, D.B., Roussel, M., Savona, M.R., Sosman, J.A., Puzanov, I., Ferrell, P.B., and Irish, J.M. (2016). Myelodysplastic Syndrome Revealed by Systems Immunology in a Melanoma Patient Undergoing Anti-PD-1 Therapy. Cancer Immunol Res *4*, 474-480.

Grivas, P., Khaki, A.R., Wise-Draper, T.M., French, B., Hennessy, C., Hsu, C.Y., Shyr, Y., Li, X., Choueiri, T.K., Painter, C.A.*, et al.* (2021). Association of clinical factors and recent anticancer therapy with COVID-19 severity among patients with cancer: a report from the COVID-19 and Cancer Consortium. Ann Oncol *32*, 787-800.

Group, R.C. (2021). Tocilizumab in patients admitted to hospital with COVID-19 (RECOVERY): a randomised, controlled, open-label, platform trial. Lancet *397*, 1637-1645.

Group, R.C., Horby, P., Lim, W.S., Emberson, J.R., Mafham, M., Bell, J.L., Linsell, L., Staplin, N., Brightling, C., Ustianowski, A.*, et al.* (2021). Dexamethasone in Hospitalized Patients with Covid-19. N Engl J Med *384*, 693-704.

Gupta, N.T., Vander Heiden, J.A., Uduman, M., Gadala-Maria, D., Yaari, G., and Kleinstein, S.H. (2015a). Change-O: a toolkit for analyzing large-scale B cell immunoglobulin repertoire sequencing data. Bioinformatics *31*, 3356-3358.

Gupta, N.T., Vander Heiden, J.A., Uduman, M., Gadala-Maria, D., Yaari, G., and Kleinstein, S.H. (2015b). Change-O: a toolkit for analyzing large-scale B cell immunoglobulin repertoire sequencing data. Bioinformatics *31*, 3356-3358.

Hacisuleyman, E., Hale, C., Saito, Y., Blachere, N.E., Bergh, M., Conlon, E.G., Schaefer-Babajew, D.J., DaSilva, J., Muecksch, F., Gaebler, C.*, et al.* (2021). Vaccine Breakthrough Infections with SARS-CoV-2 Variants. N Engl J Med *384*, 2212-2218.

Hale, J.S., and Ahmed, R. (2015). Memory T follicular helper CD4 T cells. Front Immunol *6*, 16.
Halperin, B.A., Morris, A., Mackinnon-Cameron, D., Mutch, J., Langley, J.M., McNeil, S.A., Macdougall, D., and Halperin, S.A. (2011). Kinetics of the antibody response to tetanus-diphtheria-acellular pertussis vaccine in women of childbearing age and postpartum women. Clin Infect Dis *53*, 885-892.

Hammarlund, E., Thomas, A., Amanna, I.J., Holden, L.A., Slayden, O.D., Park, B., Gao, L., and Slifka, M.K. (2017). Plasma cell survival in the absence of B cell memory. Nat Commun *8*, 1781.

Hammond, R.G., Tan, X., and Johnson, M.A. (2017). SARS-unique fold in the Rousettus bat coronavirus HKU9. Protein Sci *26*, 1726-1737.

Han, W., Mou, J., Sheng, J., Yang, J., and Shao, Z. (1995). Cryo atomic force microscopy: a new approach for biological imaging at high resolution. Biochemistry *34*, 8215-8220.
Hansen, J., Baum, A., Pascal, K.E., Russo, V., Giordano, S., Wloga, E., Fulton, B.O., Yan, Y., Koon, K., Patel, K.*, et al.* (2020). Studies in humanized mice and convalescent humans yield a SARS-CoV-2 antibody cocktail. Science *369*, 1010-1014.

Hartley, G.E., Edwards, E.S.J., Aui, P.M., Varese, N., Stojanovic, S., McMahon, J., Peleg, A.Y., Boo, I., Drummer, H.E., Hogarth, P.M.*, et al.* (2020). Rapid generation of durable B cell memory to SARS-CoV-2 spike and nucleocapsid proteins in COVID-19 and convalescence. Sci Immunol *5*, eabf8891.

Henderson, R., Edwards, R.J., Mansouri, K., Janowska, K., Stalls, V., Gobeil, S.M.C., Kopp, M., Li, D., Parks, R., Hsu, A.L.*, et al.* (2020). Controlling the SARS-CoV-2 spike glycoprotein conformation. Nat Struct Mol Biol *27*, 925-933.

Henikoff, S., and Henikoff, J.G. (1992). Amino acid substitution matrices from protein blocks. Proc Natl Acad Sci U S A *89*, 10915-10919.

Herati, R.S., Muselman, A., Vella, L., Bengsch, B., Parkhous
e, K., Del Alcazar, D., Kotzin, J., Doyle, S.A., Tebas, P., Hensley, S.E.*, et al.* (2017). Successive annual influenza vaccination induces a recurrent oligoclonotypic memory response in circulating T follicular helper cells. Sci Immunol *2*, eaag2152.

Hoffmann, M., Arora, P., Gross, R., Seidel, A., Hornich, B.F., Hahn, A.S., Kruger, N., Graichen, L., Hofmann-Winkler, H., Kempf, A.*, et al.* (2021). SARS-CoV-2 variants B.1.351 and P.1 escape from neutralizing antibodies. Cell *184*, 2384-2393 e2312.

Hsieh, C.L., Goldsmith, J.A., Schaub, J.M., DiVenere, A.M., Kuo, H.C., Javanmardi, K., Le, K.C., Wrapp, D., Lee, A.G., Liu, Y.*, et al.* (2020). Structure-based design of prefusion-stabilized SARS-CoV-2 spikes. Science *369*, 1501-1505.

Huang, A.T., Garcia-Carreras, B., Hitchings, M.D.T., Yang, B., Katzelnick, L.C., Rattigan, S.M., Borgert, B.A., Moreno, C.A., Solomon, B.D., Trimmer-Smith, L.*, et al.* (2020). A systematic review of antibody mediated immunity to coronaviruses: kinetics, correlates of protection, and association with severity. Nat Commun *11*, 4704.

Huber, J.E., Ahlfeld, J., Scheck, M.K., Zaucha, M., Witter, K., Lehmann, L., Karimzadeh, H., Pritsch, M., Hoelscher, M., von Sonnenburg, F.*, et al.* (2020). Dynamic changes in circulating T follicular helper cell composition predict neutralising antibody responses after yellow fever vaccination. Clin Transl Immunology *9*, e1129.

Huson, D.H., and Scornavacca, C. (2012). Dendroscope 3: an interactive tool for rooted phylogenetic trees and networks. Syst Biol *61*, 1061-1067.

Irish, J.M., Myklebust, J.H., Alizadeh, A.A., Houot, R., Sharman, J.P., Czerwinski, D.K., Nolan, G.P., and Levy, R. (2010). B-cell signaling networks reveal a negative prognostic human lymphoma cell subset that emerges during tumor progression. Proceedings of the National Academy of Sciences *107*, 12747.

Iyer, A.S., Jones, F.K., Nodoushani, A., Kelly, M., Becker, M., Slater, D., Mills, R., Teng, E., Kamruzzaman, M., Garcia-Beltran, W.F.*, et al.* (2020). Persistence and decay of human antibody responses to the receptor binding domain of SARS-CoV-2 spike protein in COVID-19 patients. Sci Immunol *5*.

Jackson, K.J., Liu, Y., Roskin, K.M., Glanville, J., Hoh, R.A., Seo, K., Marshall, E.L., Gurley, T.C., Moody, M.A., Haynes, B.F.*, et al.* (2014). Human responses to influenza vaccination show seroconversion signatures and convergent antibody rearrangements. Cell Host Microbe *16*, 105-114.

Jardine, J.G., Kulp, D.W., Havenar-Daughton, C., Sarkar, A., Briney, B., Sok, D., Sesterhenn, F., Ereno-Orbea, J., Kalyuzhniy, O., Deresa, I.*, et al.* (2016). HIV-1 broadly neutralizing antibody precursor B cells revealed by germline-targeting immunogen. Science *351*, 1458-1463.
Jefferis, R., Lund, J., and Goodall, M. (1995). Recognition sites on human IgG for Fc gamma receptors: the role of glycosylation. Immunol Lett *44*, 111-117.

Jeyanathan, M., Afkhami, S., Smaill, F., Miller, M.S., Lichty, B.D., and Xing, Z. (2020). Immunological considerations for COVID-19 vaccine strategies. Nat Rev Immunol *20*, 615-632.
Jiang, S., Hillyer, C., and Du, L. (2020). Neutralizing Antibodies against SARS-CoV-2 and Other Human Coronaviruses. Trends Immunol *41*, 355-359.

Jones, B.E., Brown-Augsburger, P.L., Corbett, K.S., Westendorf, K., Davies, J., Cujec, T.P., Wiethoff, C.M., Blackbourne, J.L., Heinz, B.A., Foster, D.*, et al.* (2021). The neutralizing antibody, LY-CoV555, protects against SARS-CoV-2 infection in non-human primates. Sci Transl Med.

Kalil, A.C., Patterson, T.F., Mehta, A.K., Tomashek, K.M., Wolfe, C.R., Ghazaryan, V., Marconi, V.C., Ruiz-Palacios, G.M., Hsieh, L., Kline, S.*, et al.* (2021). Baricitinib plus Remdesivir for Hospitalized Adults with Covid-19. N Engl J Med *384*, 795-807.

Kaplonek, P., Wang, C., Bartsch, Y., Fischinger, S., Gorman, M.J., Bowman, K., Kang, J., Dayal, D., Martin, P., Nowak, R.*, et al.* (2021a). Early cross-coronavirus reactive signatures of protective humoral immunity against COVID-19. bioRxiv.

Kaplonek, P., Wang, C., Bartsch, Y., Fischinger, S., Gorman, M.J., Bowman, K., Kang, J., Dayal, D., Martin, P., Nowak, R.*, et al.* (2021b). Early cross-coronavirus reactive signatures of protective humoral immunity against COVID-19. bioRxiv, DOI:10.1101/2021.1105.1111.443609.

Khoury, D.S., Cromer, D., Reynaldi, A., Schlub, T.E., Wheatley, A.K., Juno, J.A., Subbarao, K., Kent, S.J., Triccas, J.A., and Davenport, M.P. (2021). Neutralizing antibody levels are highly predictive of immune protection from symptomatic SARS-CoV-2 infection. Nat Med *27*, 1205-1211.

Kim, Y.H., Bang, Y.J., Park, H.J., Li Ko, H., Park, S.I., Hwang, K.A., Kim, H., and Nam, J.H. (2020). Inactivated influenza vaccine formulated with single-stranded RNA-based adjuvant confers mucosal immunity and cross-protection against influenza virus infection. Vaccine *38*, 6141-6152.

Koutsakos, M., Rowntree, L.C., Hensen, L., Chua, B.Y., van de Sandt, C.E., Habel, J.R., Zhang, W., Jia, X., Kedzierski, L., Ashhurst, T.M.*, et al.* (2021). Integrated immune dynamics define correlates of COVID-19 severity and antibody responses. Cell Rep Med *2*, 100208.

Krammer, F. (2020). SARS-CoV-2 vaccines in development. Nature *586*, 516-527.

Kuiken, T., Fouchier, R.A., Schutten, M., Rimmelzwaan, G.F., van Amerongen, G., van Riel, D., Laman, J.D., de Jong, T., van Doornum, G., Lim, W.*, et al.* (2003). Newly discovered coronavirus as the primary cause of severe acute respiratory syndrome. Lancet *362*, 263-270.

Kuzmina, A., Khalaila, Y., Voloshin, O., Keren-Naus, A., Boehm-Cohen, L., Raviv, Y., Shemer-Avni, Y., Rosenberg, E., and Taube, R. (2021). SARS-CoV-2 spike variants exhibit differential infectivity and neutralization resistance to convalescent or post-vaccination sera. Cell Host Microbe *29*, 522-528 e522.

Lee, C. (2015). Porcine epidemic diarrhea virus: An emerging and re-emerging epizootic swine virus. Virol J *12*, 193.

Leist, S.R., Dinnon, K.H., 3rd, Schafer, A., Tse, L.V., Okuda, K., Hou, Y.J., West, A., Edwards, C.E., Sanders, W., Fritch, E.J.*, et al.* (2020). A Mouse-Adapted SARS-CoV-2 Induces Acute Lung Injury and Mortality in Standard Laboratory Mice. Cell *183*, 1070-1085 e1012.
Li, F. (2016). Structure, Function, and Evolution of Coronavirus Spike Proteins. Annu Rev Virol *3*, 237-261.

Liu, L., Wang, P., Nair, M.S., Yu, J., Rapp, M., Wang, Q., Luo, Y., Chan, J.F., Sahi, V., Figueroa, A.*, et al.* (2020). Potent neutralizing antibodies against multiple epitopes on SARS-CoV-2 spike. Nature *584*, 450-456.

Loos, C., Atyeo, C., Fischinger, S., Burke, J., Slein, M.D., Streeck, H., Lauffenburger, D., Ryan, E.T., Charles, R.C., and Alter, G. (2020). Evolution of Early SARS-CoV-2 and Cross-Coronavirus Immunity. mSphere *5*.

Lopez Bernal, J., Andrews, N., Gower, C., Gallagher, E., Simmons, R., Thelwall, S., Stowe, J., Tessier, E., Groves, N., Dabrera, G.*, et al.* (2021). Effectiveness of Covid-19 Vaccines against the B.1.617.2 (Delta) Variant. N Engl J Med.

Lu, L.L., Suscovich, T.J., Fortune, S.M., and Alter, G. (2018). Beyond binding: antibody effector functions in infectious diseases. Nat Rev Immunol *18*, 46-61.

Lu, R., Zhao, X., Li, J., Niu, P., Yang, B., Wu, H., Wang, W., Song, H., Huang, B., Zhu, N.*, et al.* (2020). Genomic characterisation and epidemiology of 2019 novel coronavirus: implications for virus origins and receptor binding. Lancet *395*, 565-574.

Lv, H., Wu, N.C., Tsang, O.T., Yuan, M., Perera, R., Leung, W.S., So, R.T.Y., Chan, J.M.C., Yip, G.K., Chik, T.S.H.*, et al.* (2020). Cross-reactive Antibody Response between SARS-CoV-2 and SARS-CoV Infections. Cell Rep *31*, 107725.

Madeira, F., Park, Y.M., Lee, J., Buso, N., Gur, T., Madhusoodanan, N., Basutkar, P., Tivey, A.R.N., Potter, S.C., Finn, R.D.*, et al.* (2019). The EMBL-EBI search and sequence analysis tools APIs in 2019. Nucleic Acids Res *47*, W636-W641.

Madhi, S.A., Baillie, V., Cutland, C.L., Voysey, M., Koen, A.L., Fairlie, L., Padayachee, S.D., Dheda, K., Barnabas, S.L., Bhorat, Q.E.*, et al.* (2021). Efficacy of the ChAdOx1 nCoV-19 Covid-19 Vaccine against the B.1.351 Variant. N Engl J Med *384*, 1885-1898.

Mahil, S.K., Bechman, K., Raharja, A., Domingo-Vila, C., Baudry, D., Brown, M.A., Cope, A.P., Dasandi, T., Graham, C., Lechmere, T.*, et al.* (2021). The effect of methotrexate and targeted immunosuppression on humoral and cellular immune responses to the COVID-19 vaccine BNT162b2: a cohort study. Lancet Rheumatol, DOI: 10.1016/S2665-9913(1021)00212-00215.

Marinaki, S., Adamopoulos, S., Degiannis, D., Roussos, S., Pavlopoulou, I.D., Hatzakis, A., and Boletis, I.N. (2021). Immunogenicity of SARS-CoV-2 BNT162b2 vaccine in solid organ transplant recipients. Am J Transplant, DOI: 10.1111/ajt.16607.

Masignani, V., Pizza, M., and Moxon, E.R. (2019). The Development of a Vaccine Against Meningococcus B Using Reverse Vaccinology. Front Immunol *10*, 751.

Mathew, D., Giles, J.R., Baxter, A.E., Oldridge, D.A., Greenplate, A.R., Wu, J.E., Alanio, C., Kuri-Cervantes, L., Pampena, M.B., D'Andrea, K.*, et al.* (2020). Deep immune profiling of COVID-19 patients reveals distinct immunotypes with therapeutic implications. Science *369*, eabc8511.

McCallum, M., Bassi, J., De Marco, A., Chen, A., Walls, A.C., Di Iulio, J., Tortorici, M.A., Navarro, M.J., Silacci-Fregni, C., Saliba, C.*, et al.* (2021). SARS-CoV-2 immune evasion by the B.1.427/B.1.429 variant of concern. Science.

McKean, D., Huppi, K., Bell, M., Staudt, L., Gerhard, W., and Weigert, M. (1984). Generation of antibody diversity in the immune response of BALB/c mice to influenza virus hemagglutinin. Proc Natl Acad Sci U S A *81*, 3180-3184.

McLellan, J.S., Chen, M., Joyce, M.G., Sastry, M., Stewart-Jones, G.B., Yang, Y., Zhang, B., Chen, L., Srivatsan, S., Zheng, A.*, et al.* (2013). Structure-based design of a fusion glycoprotein vaccine for respiratory syncytial virus. Science *342*, 592-598.

McMichael, A.J. (2018). Is a Human CD8 T-Cell Vaccine Possible, and if So, What Would It Take? Could a CD8(+) T-Cell Vaccine Prevent Persistent HIV Infection? Cold Spring Harb Perspect Biol *10*, a029124.

McMichael, A.J., Gotch, F.M., Noble, G.R., and Beare, P.A. (1983). Cytotoxic T-cell immunity to influenza. N Engl J Med *309*, 13-17.

Medzhitov, R., and Janeway, C.A., Jr. (2002). Decoding the patterns of self and nonself by the innate immune system. Science *296*, 298-300.

Meiler, F., Klunker, S., Zimmermann, M., Akdis, C.A., and Akdis, M. (2008). Distinct regulation of IgE, IgG4 and IgA by T regulatory cells and toll-like receptors. Allergy *63*, 1455-1463.

Menachery, V.D., Yount, B.L., Jr., Debbink, K., Agnihothram, S., Gralinski, L.E., Plante, J.A., Graham, R.L., Scobey, T., Ge, X.Y., Donaldson, E.F.*, et al.* (2015). A SARS-like cluster of circulating bat coronaviruses shows potential for human emergence. Nat Med *21*, 1508-1513.

Menachery, V.D., Yount, B.L., Jr., Sims, A.C., Debbink, K., Agnihothram, S.S., Gralinski, L.E., Graham, R.L., Scobey, T., Plante, J.A., Royal, S.R.*, et al.* (2016). SARS-like WIV1-CoV poised for human emergence. Proc Natl Acad Sci U S A *113*, 3048-3053.

Muehling, L.M., Turner, R.B., Brown, K.B., Wright, P.W., Patrie, J.T., Lahtinen, S.J., Lehtinen, M.J., Kwok, W.W., and Woodfolk, J.A. (2018). Single-Cell Tracking Reveals a Role for Pre-Existing CCR5+ Memory Th1 Cells in the Control of Rhinovirus-A39 After Experimental Challenge in Humans. J Infect Dis *217*, 381-392.

Mukherjee, S., Sirohi, D., Dowd, K.A., Chen, Z., Diamond, M.S., Kuhn, R.J., and Pierson, T.C. (2016). Enhancing dengue virus maturation using a stable furin over-expressing cell line. Virology *497*, 33-40.

Mulligan, M.J., Lyke, K.E., Kitchin, N., Absalon, J., Gurtman, A., Lockhart, S., Neuzil, K., Raabe, V., Bailey, R., Swanson, K.A.*, et al.* (2020). Phase I/II study of COVID-19 RNA vaccine BNT162b1 in adults. Nature *586*, 589-593.

Ng, K.W., Faulkner, N., Cornish, G.H., Rosa, A., Harvey, R., Hussain, S., Ulferts, R., Earl, C., Wrobel, A.G., Benton, D.J.*, et al.* (2020). Preexisting and de novo humoral immunity to SARS-CoV-2 in humans. Science *370*, 1339-1343.

Nielsen, S.C.A., Yang, F., Jackson, K.J.L., Hoh, R.A., Roltgen, K., Jean, G.H., Stevens, B.A., Lee, J.Y., Rustagi, A., Rogers, A.J.*, et al.* (2020). Human B Cell Clonal Expansion and Convergent Antibody Responses to SARS-CoV-2. Cell Host Microbe *28*, 516-525 e515.
Ou, X., Liu, Y., Lei, X., Li, P., Mi, D., Ren, L., Guo, L., Guo, R., Chen, T., Hu, J.*, et al.* (2020). Characterization of spike glycoprotein of SARS-CoV-2 on virus entry and its immune cross-reactivity with SARS-CoV. Nat Commun *11*, 1620.

Pallesen, J., Wang, N., Corbett, K.S., Wrapp, D., Kirchdoerfer, R.N., Turner, H.L., Cottrell, C.A., Becker, M.M., Wang, L., Shi, W.*, et al.* (2017). Immunogenicity and structures of a rationally designed prefusion MERS-CoV spike antigen. Proc Natl Acad Sci U S A *114*, E7348-E7357.
Parameswaran, P., Liu, Y., Roskin, K.M., Jackson, K.K., Dixit, V.P., Lee, J.Y., Artiles, K.L., Zompi, S., Vargas, M.J., Simen, B.B.*, et al.* (2013). Convergent antibody signatures in human dengue. Cell Host Microbe *13*, 691-700.

Pardi, N., Hogan, M.J., Porter, F.W., and Weissman, D. (2018). mRNA vaccines - a new era in vaccinology. Nat Rev Drug Discov *17*, 261-279.

Parker, A.R., Park, M.A., Harding, S., and Abraham, R.S. (2019). The total IgM, IgA and IgG antibody responses to pneumococcal polysaccharide vaccination (Pneumovax(R)23) in a healthy adult population and patients diagnosed with primary immunodeficiencies. Vaccine *37*, 1350-1355.

Peled, Y., Ram, E., Lavee, J., Sternik, L., Segev, A., Wieder-Finesod, A., Mandelboim, M., Indenbaum, V., Levy, I., Raanani, E.*, et al.* (2021). BNT162b2 vaccination in heart transplant recipients: Clinical experience and antibody response. J Heart Lung Transplant *S1053-2498*, 02274-02279.

Pettersen, E.F., Goddard, T.D., Huang, C.C., Meng, E.C., Couch, G.S., Croll, T.I., Morris, J.H., and Ferrin, T.E. (2021). UCSF ChimeraX: Structure visualization for researchers, educators, and developers. Protein Sci *30*, 70-82.

Pfefferle, S., Oppong, S., Drexler, J.F., Gloza-Rausch, F., Ipsen, A., Seebens, A., Muller, M.A., Annan, A., Vallo, P., Adu-Sarkodie, Y.*, et al.* (2009). Distant relatives of severe acute respiratory syndrome coronavirus and close relatives of human coronavirus 229E in bats, Ghana. Emerg Infect Dis *15*, 1377-1384.

Piccoli, L., Park, Y.J., Tortorici, M.A., Czudnochowski, N., Walls, A.C., Beltramello, M., Silacci-Fregni, C., Pinto, D., Rosen, L.E., Bowen, J.E.*, et al.* (2020). Mapping Neutralizing and Immunodominant Sites on the SARS-CoV-2 Spike Receptor-Binding Domain by Structure-Guided High-Resolution Serology. Cell *183*, 1024-1042 e1021.

Pinto, D., Park, Y.J., Beltramello, M., Walls, A.C., Tortorici, M.A., Bianchi, S., Jaconi, S., Culap, K., Zatta, F., De Marco, A.*, et al.* (2020). Cross-neutralization of SARS-CoV-2 by a human monoclonal SARS-CoV antibody. Nature *583*, 290-295.

Polack, F.P., Thomas, S.J., Kitchin, N., Absalon, J., Gurtman, A., Lockhart, S., Perez, J.L., Perez Marc, G., Moreira, E.D., Zerbini, C.*, et al.* (2020). Safety and Efficacy of the BNT162b2 mRNA Covid-19 Vaccine. N Engl J Med *383*, 2603-2615.

Punjani, A., Rubinstein, J.L., Fleet, D.J., and Brubaker, M.A. (2017). cryoSPARC: algorithms for rapid unsupervised cryo-EM structure determination. Nat Methods *14*, 290-296.

Punjani, A., Zhang, H., and Fleet, D.J. (2020). Non-uniform refinement: adaptive regularization improves single-particle cryo-EM reconstruction. Nat Methods *17*, 1214-1221.

Pyrc, K., Dijkman, R., Deng, L., Jebbink, M.F., Ross, H.A., Berkhout, B., and van der Hoek, L. (2006). Mosaic structure of human coronavirus NL63, one thousand years of evolution. J Mol Biol *364*, 964-973.

Ramadan, N., and Shaib, H. (2019). Middle East respiratory syndrome coronavirus (MERS-CoV): A review. Germs *9*, 35-42.

Rappazzo, C.G., Tse, L.V., Kaku, C.I., Wrapp, D., Sakharkar, M., Huang, D., Deveau, L.M., Yockachonis, T.J., Herbert, A.S., Battles, M.B.*, et al.* (2021). Broad and potent activity against SARS-like viruses by an engineered human monoclonal antibody. Science *371*, 823-829.

Raybould, M.I.J., Kovaltsuk, A., Marks, C., and Deane, C.M. (2021). CoV-AbDab: the coronavirus antibody database. Bioinformatics *37*, 734-735.

Richardson, S.I., Crowther, C., Mkhize, N.N., and Morris, L. (2018). Measuring the ability of HIV-specific antibodies to mediate trogocytosis. J Immunol Methods *463*, 71-83.

Rickinson, A.B., and Moss, D.J. (1997). Human cytotoxic T lymphocyte responses to Epstein-Barr virus infection. Annu Rev Immunol *15*, 405-431.

Robbiani, D.F., Gaebler, C., Muecksch, F., Lorenzi, J.C.C., Wang, Z., Cho, A., Agudelo, M., Barnes, C.O., Gazumyan, A., Finkin, S.*, et al.* (2020). Convergent antibody responses to SARS-CoV-2 in convalescent individuals. Nature *584*, 437-442.

Rodriguez, L., Pekkarinen, P.T., Lakshmikanth, T., Tan, Z., Consiglio, C.R., Pou, C., Chen, Y., Mugabo, C.H., Nguyen, N.A., Nowlan, K.*, et al.* (2020). Systems-Level Immunomonitoring from Acute to Recovery Phase of Severe COVID-19. Cell Rep Med *1*, 100078.

Roe, C.E., Hayes, M.J., Barone, S.M., and Irish, J.M. (2020). Training Novices in Generation and Analysis of High-Dimensional Human Cell Phospho-Flow Cytometry Data. Current Protocols in Cytometry *93*, e71.

Rogers, T.F., Zhao, F., Huang, D., Beutler, N., Burns, A., He, W.T., Limbo, O., Smith, C., Song, G., Woehl, J.*, et al.* (2020). Isolation of potent SARS-CoV-2 neutralizing antibodies and protection from disease in a small animal model. Science *369*, 956-963.

Roltgen, K., Powell, A.E., Wirz, O.F., Stevens, B.A., Hogan, C.A., Najeeb, J., Hunter, M., Wang, H., Sahoo, M.K., Huang, C.*, et al.* (2020). Defining the features and duration of antibody responses to SARS-CoV-2 infection associated with disease severity and outcome. Sci Immunol *5*.

Rubinstein, J.L., and Brubaker, M.A. (2015). Alignment of cryo-EM movies of individual particles by optimization of image translations. J Struct Biol *192*, 188-195.

Sabino, E.C., Buss, L.F., Carvalho, M.P.S., Prete, C.A., Jr., Crispim, M.A.E., Fraiji, N.A., Pereira, R.H.M., Parag, K.V., da Silva Peixoto, P., Kraemer, M.U.G.*, et al.* (2021). Resurgence of COVID-19 in Manaus, Brazil, despite high seroprevalence. Lancet *397*, 452-455.

Sadoff, J., Gray, G., Vandebosch, A., Cardenas, V., Shukarev, G., Grinsztejn, B., Goepfert, P.A., Truyers, C., Fennema, H., Spiessens, B.*, et al.* (2021a). Safety and Efficacy of Single-Dose Ad26.COV2.S Vaccine against Covid-19. N Engl J Med *384*, 2187-2201.

Sadoff, J., Le Gars, M., Shukarev, G., Heerwegh, D., Truyers, C., de Groot, A.M., Stoop, J., Tete, S., Van Damme, W., Leroux-Roels, I.*, et al.* (2021b). Interim Results of a Phase 1-2a Trial of Ad26.COV2.S Covid-19 Vaccine. N Engl J Med *384*, 1824-1835.

Sahin, U., Muik, A., Derhovanessian, E., Vogler, I., Kranz, L.M., Vormehr, M., Baum, A., Pascal, K., Quandt, J., Maurus, D.*, et al.* (2020). COVID-19 vaccine BNT162b1 elicits human antibody and TH1 T cell responses. Nature *586*, 594-599.

Sahin, U., Muik, A., Vogler, I., Derhovanessian, E., Kranz, L.M., Vormehr, M., Quandt, J., Bidmon, N., Ulges, A., Baum, A.*, et al.* (2021). BNT162b2 vaccine induces neutralizing antibodies and poly-specific T cells in humans. Nature.

Sakano, H., Maki, R., Kurosawa, Y., Roeder, W., and Tonegawa, S. (1980). Two types of somatic recombination are necessary for the generation of complete immunoglobulin heavy-chain genes. Nature *286*, 676-683.

Samanovic, M.I., Cornelius, A.R., Gray-Gaillard, S.L., Allen, J.R., Karmacharya, T., Wilson, J.P., Hyman, S.W., Tuen, M., Koralov, S.B., Mulligan, M.J.*, et al.* (2021). Poor antigen-specific responses to the second BNT162b2 mRNA vaccine dose in SARS-CoV-2-experienced individuals. medRxiv, DOI:10.1101/2021.1102.1107.21251311.

Sanchez-Garcia, J.G.-B., A Cuervo, JM Carazo, COS Sorzano, J Vargas (2021). DeepEMhancer: a deep learning solution for cryo-EM volume post-processing. BioRXiv.

Saphire, E.O., Stanfield, R.L., Crispin, M.D., Parren, P.W., Rudd, P.M., Dwek, R.A., Burton, D.R., and Wilson, I.A. (2002). Contrasting IgG structures reveal extreme asymmetry and flexibility. J Mol Biol *319*, 9-18.

Satija, R., Farrell, J.A., Gennert, D., Schier, A.F., and Regev, A. (2015). Spatial reconstruction of single-cell gene expression data. Nat Biotechnol *33*, 495-502.

Sattler, A., Schrezenmeier, E., Weber, U., Potekhin, A., Bachmann, F., Budde, K., Storz, E., Proß, V., Bergmann, Y., Thole, L.*, et al.* (2021a). Impaired Humoral and Cellular Immunity after SARS-CoV2 BNT162b2 (Tozinameran) Prime-Boost Vaccination in Kidney Transplant Recipients. medRxiv, 2021.2004.2006.21254963.

Sattler, A., Schrezenmeier, E., Weber, U.A., Potekhin, A., Bachmann, F., Straub-Hohenbleicher, H., Budde, K., Storz, E., Pross, V., Bergmann, Y.*, et al.* (2021b). Impaired humoral and cellular immunity after SARS-CoV-2 BNT162b2 (tozinameran) prime-boost vaccination in kidney transplant recipients. J Clin Invest *131*, e150175.

Sauer, M.M., Tortorici, M.A., Park, Y.J., Walls, A.C., Homad, L., Acton, O.J., Bowen, J.E., Wang, C., Xiong, X., de van der Schueren, W.*, et al.* (2021). Structural basis for broad coronavirus neutralization. Nat Struct Mol Biol *28*, 478-486.

Schafer, A., Muecksch, F., Lorenzi, J.C.C., Leist, S.R., Cipolla, M., Bournazos, S., Schmidt, F., Maison, R.M., Gazumyan, A., Martinez, D.R.*, et al.* (2021). Antibody potency, effector function, and combinations in protection and therapy for SARS-CoV-2 infection in vivo. J Exp Med *218*.

Scheid, J.F., Mouquet, H., Feldhahn, N., Seaman, M.S., Velinzon, K., Pietzsch, J., Ott, R.G., Anthony, R.M., Zebroski, H., Hurley, A.*, et al.* (2009). Broad diversity of neutralizing antibodies isolated from memory B cells in HIV-infected individuals. Nature *458*, 636-640.

Schulte-Schrepping, J., Reusch, N., Paclik, D., Bassler, K., Schlickeiser, S., Zhang, B., Kramer, B., Krammer, T., Brumhard, S., Bonaguro, L.*, et al.* (2020). Severe COVID-19 Is Marked by a Dysregulated Myeloid Cell Compartment. Cell *182*, 1419-1440 e1423.

Scobey, T., Yount, B.L., Sims, A.C., Donaldson, E.F., Agnihothram, S.S., Menachery, V.D., Graham, R.L., Swanstrom, J., Bove, P.F., Kim, J.D.*, et al.* (2013). Reverse genetics with a full-length infectious cDNA of the Middle East respiratory syndrome coronavirus. Proc Natl Acad Sci U S A *110*, 16157-16162.

Setliff, I., McDonnell, W.J., Raju, N., Bombardi, R.G., Murji, A.A., Scheepers, C., Ziki, R., Mynhardt, C., Shepherd, B.E., Mamchak, A.A.*, et al.* (2018). Multi-Donor Longitudinal Antibody Repertoire Sequencing Reveals the Existence of Public Antibody Clonotypes in HIV-1 Infection. Cell Host Microbe *23*, 845-854 e846.

Setliff, I., Shiakolas, A.R., Pilewski, K.A., Murji, A.A., Mapengo, R.E., Janowska, K., Richardson, S., Oosthuysen, C., Raju, N., Ronsard, L.*, et al.* (2019a). High-Throughput Mapping of B Cell Receptor Sequences to Antigen Specificity. Cell *179*, 1636-1646 e1615.

Setliff, I., Shiakolas, A.R., Pilewski, K.A., Murji, A.A., Mapengo, R.E., Janowska, K., Richardson, S., Oosthuysen, C., Raju, N., Ronsard, L.*, et al.* (2019b). High-Throughput Mapping of B Cell Receptor Sequences to Antigen Specificity. Cell *179*, 1636-1646.e1615.

Shang, J., Ye, G., Shi, K., Wan, Y., Luo, C., Aihara, H., Geng, Q., Auerbach, A., and Li, F. (2020). Structural basis of receptor recognition by SARS-CoV-2. Nature *581*, 221-224.

Shiakolas, A.R., Johnson, N., Kramer, K.J., Suryadevara, N., Wrapp, D., Periasamy, S., Pilewski, K.A., Raju, N., Nargi, R., Sutton, R.E.*, et al.* (2021a). Efficient discovery of potently neutralizing SARS-CoV-2 antibodies using LIBRA-seq with ligand blocking. bioRxiv.

Shiakolas, A.R., Kramer, K.J., Wrapp, D., Richardson, S.I., Schafer, A., Wall, S., Wang, N., Janowska, K., Pilewski, K.A., Venkat, R.*, et al.* (2021b). Cross-reactive coronavirus antibodies with diverse epitope specificities and Fc effector functions. Cell Rep Med *2*, 100313.

Song, Z., Xu, Y., Bao, L., Zhang, L., Yu, P., Qu, Y., Zhu, H., Zhao, W., Han, Y., and Qin, C. (2019). From SARS to MERS, Thrusting Coronaviruses into the Spotlight. Viruses *11*.

Starr, T.N., Czudnochowski, N., Liu, Z., Zatta, F., Park, Y.J., Addetia, A., Pinto, D., Beltramello, M., Hernandez, P., Greaney, A.J.*, et al.* (2021). SARS-CoV-2 RBD antibodies that maximize breadth and resistance to escape. Nature.

Starr, T.N., Greaney, A.J., Hilton, S.K., Ellis, D., Crawford, K.H.D., Dingens, A.S., Navarro, M.J., Bowen, J.E., Tortorici, M.A., Walls, A.C.*, et al.* (2020). Deep Mutational Scanning of SARS-CoV-2 Receptor Binding Domain Reveals Constraints on Folding and ACE2 Binding. Cell *182*, 1295-1310 e1220.

Sterlin, D., Mathian, A., Miyara, M., Mohr, A., Anna, F., Claer, L., Quentric, P., Fadlallah, J., Devilliers, H., Ghillani, P.*, et al.* (2021). IgA dominates the early neutralizing antibody response to SARS-CoV-2. Sci Transl Med *13*, eabd2223.

Stiegler, G., Kunert, R., Purtscher, M., Wolbank, S., Voglauer, R., Steindl, F., and Katinger, H. (2001). A potent cross-clade neutralizing human monoclonal antibody against a novel epitope on gp41 of human immunodeficiency virus type 1. AIDS Res Hum Retroviruses *17*, 1757-1765.

Suryadevara, N., Shrihari, S., Gilchuk, P., VanBlargan, L.A., Binshtein, E., Zost, S.J., Nargi, R.S., Sutton, R.E., Winkler, E.S., Chen, E.C.*, et al.* (2021). Neutralizing and protective human monoclonal antibodies recognizing the N-terminal domain of the SARS-CoV-2 spike protein. Cell *184*, 2316-2331 e2315.

Tegally, H., Wilkinson, E., Giovanetti, M., Iranzadeh, A., Fonseca, V., Giandhari, J., Doolabh, D., Pillay, S., San, E.J., Msomi, N.*, et al.* (2021). Detection of a SARS-CoV-2 variant of concern in South Africa. Nature *592*, 438-443.

Thatcher, N., Goldschmidt, J.H., Thomas, M., Schenker, M., Pan, Z., Paz-Ares Rodriguez, L., Breder, V., Ostoros, G., and Hanes, V. (2019). Efficacy and Safety of the Biosimilar ABP 215 Compared with Bevacizumab in Patients with Advanced Nonsquamous Non-small Cell Lung Cancer (MAPLE): A Randomized, Double-blind, Phase III Study. Clin Cancer Res *25*, 2088-2095.

Thomson, E.C., Rosen, L.E., Shepherd, J.G., Spreafico, R., da Silva Filipe, A., Wojcechowskyj, J.A., Davis, C., Piccoli, L., Pascall, D.J., Dillen, J.*, et al.* (2021). Circulating SARS-CoV-2 spike N439K variants maintain fitness while evading antibody-mediated immunity. Cell *184*, 1171-1187 e1120.

Tortorici, M.A., Czudnochowski, N., Starr, T.N., Marzi, R., Walls, A.C., Zatta, F., Bowen, J.E., Jaconi, S., Di Iulio, J., Wang, Z.*, et al.* (2021). Broad sarbecovirus neutralization by a human monoclonal antibody. Nature.

Tortorici, M.A., and Veesler, D. (2019). Structural insights into coronavirus entry. Adv Virus Res *105*, 93-116.

van Erp, E.A., Luytjes, W., Ferwerda, G., and van Kasteren, P.B. (2019). Fc-Mediated Antibody Effector Functions During Respiratory Syncytial Virus Infection and Disease. Front Immunol *10*, 548.

Vijgen, L., Keyaerts, E., Lemey, P., Maes, P., Van Reeth, K., Nauwynck, H., Pensaert, M., and Van Ranst, M. (2006). Evolutionary history of the closely related group 2 coronaviruses: porcine hemagglutinating encephalomyelitis virus, bovine coronavirus, and human coronavirus OC43. J Virol *80*, 7270-7274.

Voysey, M., Clemens, S.A.C., Madhi, S.A., Weckx, L.Y., Folegatti, P.M., Aley, P.K., Angus, B., Baillie, V.L., Barnabas, S.L., Bhorat, Q.E.*, et al.* (2021). Safety and efficacy of the ChAdOx1 nCoV-19 vaccine (AZD1222) against SARS-CoV-2: an interim analysis of four randomised controlled trials in Brazil, South Africa, and the UK. Lancet *397*, 99-111.

Wadman, J.C. (2021). Novavax vaccine delivers 89% efficacy against COVID-19 in U.K.—but is less potent in South Africa. Science.

Walker, L.M., and Burton, D.R. (2018). Passive immunotherapy of viral infections: 'super-antibodies' enter the fray. Nat Rev Immunol *18*, 297-308.

Walsh, E.E., Frenck, R.W., Jr., Falsey, A.R., Kitchin, N., Absalon, J., Gurtman, A., Lockhart, S., Neuzil, K., Mulligan, M.J., Bailey, R.*, et al.* (2020). Safety and Immunogenicity of Two RNA-Based Covid-19 Vaccine Candidates. N Engl J Med *383*, 2439-2450.

Wang, P., Nair, M.S., Liu, L., Iketani, S., Luo, Y., Guo, Y., Wang, M., Yu, J., Zhang, B., Kwong, P.D.*, et al.* (2021a). Antibody resistance of SARS-CoV-2 variants B.1.351 and B.1.1.7. Nature *593*, 130-135.

Wang, Z., Muecksch, F., Schaefer-Babajew, D., Finkin, S., Viant, C., Gaebler, C., Hoffmann, H.H., Barnes, C.O., Cipolla, M., Ramos, V.*, et al.* (2021b). Naturally enhanced neutralizing breadth against SARS-CoV-2 one year after infection. Nature.

Wang, Z., Schmidt, F., Weisblum, Y., Muecksch, F., Barnes, C.O., Finkin, S., Schaefer-Babajew, D., Cipolla, M., Gaebler, C., Lieberman, J.A.*, et al.* (2021c). mRNA vaccine-elicited antibodies to SARS-CoV-2 and circulating variants. Nature *592*, 616-622.

Wang, Z.C., Yao, Y., Chen, C.L., Guo, C.L., Ding, H.X., Song, J., Wang, Z.Z., Wang, N., Li, X.L., Liao, B.*, et al.* (2021d). Extrafollicular PD-1(high)CXCR5(-)CD4(+) T cells participate in local immunoglobulin production in nasal polyps. J Allergy Clin Immunol *S0091-6749*, 01050-01052.

Wec, A.Z., Wrapp, D., Herbert, A.S., Maurer, D., Haslwanter, D., Sakharkar, M., Jangra, R.K., Dieterle, M.E., Lilov, A., Huang, D.*, et al.* (2020a). Broad sarbecovirus neutralizing antibodies define a key site of vulnerability on the SARS-CoV-2 spike protein. bioRxiv.

Wec, A.Z., Wrapp, D., Herbert, A.S., Maurer, D.P., Haslwanter, D., Sakharkar, M., Jangra, R.K., Dieterle, M.E., Lilov, A., Huang, D.*, et al.* (2020b). Broad neutralization of SARS-related viruses by human monoclonal antibodies. Science *369*, 731-736.

Weinreich, D.M., Sivapalasingam, S., Norton, T., Ali, S., Gao, H., Bhore, R., Musser, B.J., Soo, Y., Rofail, D., Im, J.*, et al.* (2021). REGN-COV2, a Neutralizing Antibody Cocktail, in Outpatients with Covid-19. N Engl J Med *384*, 238-251.

Westendorf, K., Zentelis, S., Foster, D., Vaillancourt, P., Wiggin, M., Lovett, E., Hendle, J., Pustilnik, A., Sauder, J.M., Kraft, L.*, et al.* (2021). LY-CoV1404 potently neutralizes SARS-CoV-2 variants. bioRxiv.

Wheatley, A.K., Juno, J.A., Wang, J.J., Selva, K.J., Reynaldi, A., Tan, H.X., Lee, W.S., Wragg, K.M., Kelly, H.G., Esterbauer, R.*, et al.* (2021). Evolution of immune responses to SARS-CoV-2 in mild-moderate COVID-19. Nat Commun *12*, 1162.

Widge, A.T., Rouphael, N.G., Jackson, L.A., Anderson, E.J., Roberts, P.C., Makhene, M., Chappell, J.D., Denison, M.R., Stevens, L.J., Pruijssers, A.J.*, et al.* (2021). Durability of Responses after SARS-CoV-2 mRNA-1273 Vaccination. N Engl J Med *384*, 80-82.

Winkler, E.S., Gilchuk, P., Yu, J., Bailey, A.L., Chen, R.E., Chong, Z., Zost, S.J., Jang, H., Huang, Y., Allen, J.D.*, et al.* (2021). Human neutralizing antibodies against SARS-CoV-2 require intact Fc effector functions for optimal therapeutic protection. Cell *184*, 1804-1820 e1816.

Wisnewski, A.V., Campillo Luna, J., and Redlich, C.A. (2021). Human IgG and IgA responses to COVID-19 mRNA vaccines. PLoS One *16*, e0249499.

Woldemeskel, B.A., Garliss, C.C., and Blankson, J.N. (2021). SARS-CoV-2 mRNA vaccines induce broad CD4+ T cell responses that recognize SARS-CoV-2 variants and HCoV-NL63. J Clin Invest *131*, e149335.

Woo, P.C., Lau, S.K., Chu, C.M., Chan, K.H., Tsoi, H.W., Huang, Y., Wong, B.H., Poon, R.W., Cai, J.J., Luk, W.K.*, et al.* (2005). Characterization and complete genome sequence of a novel coronavirus, coronavirus HKU1, from patients with pneumonia. J Virol *79*, 884-895.

Wrapp, D., Wang, N., Corbett, K.S., Goldsmith, J.A., Hsieh, C.L., Abiona, O., Graham, B.S., and McLellan, J.S. (2020). Cryo-EM structure of the 2019-nCoV spike in the prefusion conformation. Science *367*, 1260-1263.

Wu, T.T., and Kabat, E.A. (1970). An analysis of the sequences of the variable regions of Bence Jones proteins and myeloma light chains and their implications for antibody complementarity. J Exp Med *132*, 211-250.

Wu, X., Yang, Z.Y., Li, Y., Hogerkorp, C.M., Schief, W.R., Seaman, M.S., Zhou, T., Schmidt, S.D., Wu, L., Xu, L.*, et al.* (2010). Rational design of envelope identifies broadly neutralizing human monoclonal antibodies to HIV-1. Science *329*, 856-861.

Xie, X., Liu, Y., Liu, J., Zhang, X., Zou, J., Fontes-Garfias, C.R., Xia, H., Swanson, K.A., Cutler, M., Cooper, D.*, et al.* (2021). Neutralization of SARS-CoV-2 spike 69/70 deletion, E484K and N501Y variants by BNT162b2 vaccine-elicited sera. Nat Med *27*, 620-621.

Yao, Y., Yang, H., Shi, L., Liu, S., Li, C., Chen, J., Zhou, Z., Sun, M., and Shi, L. (2019). HLA Class II Genes HLA-DRB1, HLA-DPB1, and HLA-DQB1 Are Associated With the Antibody Response to Inactivated Japanese Encephalitis Vaccine. Front Immunol *10*, 428.

Yasui, F., Kohara, M., Kitabatake, M., Nishiwaki, T., Fujii, H., Tateno, C., Yoneda, M., Morita, K., Matsushima, K., Koyasu, S.*, et al.* (2014). Phagocytic cells contribute to the antibody-mediated elimination of pulmonary-infected SARS coronavirus. Virology *454-455*, 157-168.

Yount, B., Curtis, K.M., Fritz, E.A., Hensley, L.E., Jahrling, P.B., Prentice, E., Denison, M.R., Geisbert, T.W., and Baric, R.S. (2003). Reverse genetics with a full-length infectious cDNA of severe acute respiratory syndrome coronavirus. Proc Natl Acad Sci U S A *100*, 12995-13000.
Yu, J., Tostanoski, L.H., Peter, L., Mercado, N.B., McMahan, K., Mahrokhian, S.H., Nkolola, J.P., Liu, J., Li, Z., Chandrashekar, A.*, et al.* (2020). DNA vaccine protection against SARS-CoV-2 in rhesus macaques. Science *369*, 806-811.

Yuan, M., Liu, H., Wu, N.C., Lee, C.D., Zhu, X., Zhao, F., Huang, D., Yu, W., Hua, Y., Tien, H.*, et al.* (2020a). Structural basis of a shared antibody response to SARS-CoV-2. Science *369*, 1119-1123.

Yuan, M., Wu, N.C., Zhu, X., Lee, C.D., So, R.T.Y., Lv, H., Mok, C.K.P., and Wilson, I.A. (2020b). A highly conserved cryptic epitope in the receptor binding domains of SARS-CoV-2 and SARS-CoV. Science *368*, 630-633.

Zheng, N., Xie, K., Ye, H., Dong, Y., Wang, B., Luo, N., Fan, J., Tan, J., Chen, W., and Yu, X. (2020). TLR7 in B cells promotes renal inflammation and Gd-IgA1 synthesis in IgA nephropathy. JCI Insight *5*, e136965.

Zhou, P., Yuan, M., Song, G., Beutler, N., Shaabani, N., Huang, D., He, W.T., Zhu, X., Callaghan, S., Yong, P.*, et al.* (2021). A protective broadly cross-reactive human antibody defines a conserved site of vulnerability on beta-coronavirus spikes. bioRxiv.

Zhu, X., and Zhu, J. (2020). CD4 T Helper Cell Subsets and Related Human Immunological Disorders. Int J Mol Sci *21*, 8011.

Zohar, T., and Alter, G. (2020). Dissecting antibody-mediated protection against SARS-CoV-2. Nat Rev Immunol *20*, 392-394.

Zohar, T., Loos, C., Fischinger, S., Atyeo, C., Wang, C., Slein, M.D., Burke, J., Yu, J., Feldman, J., Hauser, B.M.*, et al.* (2020). Compromised Humoral Functional Evolution Tracks with SARS-CoV-2 Mortality. Cell *183*, 1508-1519 e1512.

Zost, S.J., Gilchuk, P., Case, J.B., Binshtein, E., Chen, R.E., Nkolola, J.P., Schafer, A., Reidy, J.X., Trivette, A., Nargi, R.S.*, et al.* (2020a). Potently neutralizing and protective human antibodies against SARS-CoV-2. Nature *584*, 443-449.

Zost, S.J., Gilchuk, P., Chen, R.E., Case, J.B., Reidy, J.X., Trivette, A., Nargi, R.S., Sutton, R.E., Suryadevara, N., Chen, E.C.*, et al.* (2020b). Rapid isolation and profiling of a diverse panel of human monoclonal antibodies targeting the SARS-CoV-2 spike protein. Nat Med *26*, 1422-1427.

Zumla, A., Chan, J.F., Azhar, E.I., Hui, D.S., and Yuen, K.Y. (2016). Coronaviruses - drug discovery and therapeutic options. Nat Rev Drug Discov *15*, 327-347.

Zuniga, A., Rassek, O., Vrohlings, M., Marrero-Nodarse, A., Moehle, K., Robinson, J.A., and Ghasparian, A. (2021). An epitope-specific chemically defined nanoparticle vaccine for respiratory syncytial virus. NPJ Vaccines *6*, 85.